MINERALOGY OF THE PERALUMINOUS SPRUCE PINE PLUTONIC SUITE, MITCHELL, AVERY, AND YANCEY COUNTIES, NORTH CAROLINA

by

William Brian Veal

(Under the Direction of Samuel E. Swanson)

ABSTRACT

The Spruce Pine plutonic suite consists of numerous Devonian (390-410 ma) peraluminous granitic plutons, dikes, sills, and associated pegmatites. The mineralogy of pegmatites and host granodiorites from seven locations was studied to determine the extent of fractionation of the pegmatites relative to the granodiorite. Garnets in the plutons are almandine-spessartine and some display epitaxial overgrowths of grossular garnet. Similar garnets are found in the pegmatites. Pegmatitic muscovite contains several percent iron and is compositionally similar to muscovite from the host granodiorite. Feldspars in the granodiorites and pegmatites are compositionally similar (plagioclase Ab_{69-98}; k-feldspar Or_{95-98}). The lack of compositional variation between minerals in pegmatites and host granodiorites indicates the pegmatites were not the result of extreme fractionation and indicates that pegmatite mineralogy can be used to characterize the mineralogy of an entire granodiorite body.

INDEX WORDS: Spruce Pine, Pegmatites, Granodiorite, Garnet, Muscovite, Feldspar

MINERALOGY OF THE PERALUMINOUS SPRUCE PINE PLUTONIC SUITE, MITCHELL, AVERY, AND YANCEY COUNTIES, NORTH CAROLINA

by

WILLIAM BRIAN VEAL

B.S., Georgia Southwestern State University, 2002

A Thesis Submitted to the Graduate Faculty of The University of Georgia in Partial Fulfillment of the Requirements for the Degree

MASTER OF SCIENCE

ATHENS, GEORGIA

2004

MINERALOGY OF THE PERALUMINOUS SPRUCE PINE PLUTONIC SUITE, MITCHELL, AVERY, AND YANCEY COUNTIES, NORTH CAROLINA

by

WILLIAM BRIAN VEAL

Major Professor:	Samual E. Swanson
Committee:	Michael F. Roden
	Paul A. Schroeder

Electronic Version Approved:

Maureen Grasso
Dean of the Graduate School
The University of Georgia
August 2004

ACKNOWLEGEMENTS

Many people have helped me along my educational path. I thank my parents for giving me a sense of right and wrong and for their never-ending support in everything I do. I thank my brother for the fun in the mudpits and drives to the mountains. I thank my wife for understanding the long hours and tolerating the incessant geology references I make in everyday speech. At the University of Georgia, I would like to thank my major advisor, Dr. Samuel E. Swanson, and my committee members, Dr. Michael Roden and Dr. Paul Schroeder, for generous help and guidance needed to complete this project. I thank all of my committee members for their patience with me as I strove to complete this project. Many thanks to Chris Fleischer for assistance with the many microprobe riddles that came my way. I thank the UGA Department of Geology for financial support through the Wheeler-Watts and Allard Funds. Through the department's generous help, I was able to complete my field work and present my data at the Northeastern/Southeastern joint meeting of the Geological Society of America. In Spruce Pine, Mr. Alex Glover proved to be a valuable contact and provided me with much information on the Spruce Pine mining district that helped to guide my research. Mr. Bob Schabilion was gracious enough to give me access and allow me to sample Hootowl Mine and Bon Ami Mine. Mr. Alex Glover allowed access and permission to sample from the Pete Lawson Mine. Many thanks to all of them, without which this project would be much smaller in scale. Most of all, thanks to God for standing beside me when I face the challenges of my life, for carrying me when I cannot stand, and for Allison.

TABLE OF CONTENTS

Page

ACKNOWLEDGEMENTS iv

LIST OF TABLES viii

LIST OF FIGURES ix

CHAPTER

1 INTRODUCTION 1

History of Mining in the Spruce Pine District 1

Purpose of Project 4

2 PEGMATITE PETROGENESIS 5

Types of Pegmatites 5

Crystallization of Pegmatites 7

3 GEOLOGIC BACKGROUND 16

Tectonic Setting 16

Ages of Spruce Pine Granitoid Rocks 20

Geology of Spruce Pine Granites and Pegmatites 20

Intrusions 20

Petrology of the Spruce Pine Intrusions 24

Geochemistry of Granitoid Rocks and Pegmatites 24

Bulk Elemental Analysis 24

Mineralogy of Spruce Pine Granitoid Rocks 25

Crystallization History of Spruce Pine Pegmatites 33

4 METHODS 37

Field Mapping and Sampling 37

Microprobe Procedures 40

5 BODIES STUDIED 41

Crabtree Creek Exposure 41

Field Mine 45

Bon Ami Mine 45

Hootowl Mine 54

Exposure on Roan Road 59

6 RESULTS 65

Mineralogy of the Pegmatites 65

7 DISCUSSION 115

Pegmatite Zones 115

Granodiorite Mineralogy 115

Pegmatite Mineralogy 117

Post-Magmatic Recrystallization 125

8 CONCLUSIONS 129

Recommendations for Future Work 130

REFERENCES CITED 131

APPENDICES 134

A ELECTRON MICROPROBE ANALYSIS ROUTINES FOR GARNET, MUSCOVITE, AND FELDSPAR 134

B MINERAL ASSEMBLAGES IN GRANODIORITE AND PEGMATITE SAMPLES FROM SPRUCE PINE, NORTH CAROLINA.....138

C ELECTRON MUCROPROBE ANALYSES OF GARNETS FROM SPRUCE PINE GRANODIORITES AND PEGMATITES.....144

D ELECTRON MICROPROBE ANALYSES OF MUSCOVITE AND BIOTITE FROM SPRUCE PINE GRANODIORITES AND PEGMATITES 160

E ELECTRON MICROPROBE ANALYSES OF PLAGIOCLASE AND ALKALI FELDSPAR FROM SPRUCE PINE GRANODIORITES AND PEGMATITES.....189

F ELECTRON MICROPROBE ANALYSES OF EPIDOTE FROM SPRUCE PINE GRANODIORITES AND PEGMATITES.....209

LIST OF TABLES

Page

Table 1: Estimated metamorphic conditions of Spruce Pine Thrust Sheet.....18

Table 2: Radiometric dates of selected Spruce Pine materials. 21

Table 3: Chemical compositions of Spruce Pine granitoid rocks and pegmatites. 26

Table 4: Comparison of pegmatite zones.....116

LIST OF FIGURES

Page

Figure 1: Geologic Map of Spruce Pine District. 2

Figure 2: Phase assemblage diagram for Spruce Pine pegmatite at 5 kbar. 13

Figure 3: Phase equilibria for the Spruce Pine pegmatite composition modified from Fenn (1986). 14

Figure 4: Tectonic map of western North Carolina with Spruce Pine District. 17

Figure 5: A typical zoned Spruce Pine pegmatite. 23

Figure 6: Classification of Spruce Pine granitoids based on normative mineralogy. 27

Figure 7: Variation in Mn:Fe:Mg ratios of garnets from peraluminous granitoid rocks. 29

Figure 8: Compositional range of igneous muscovite. 31

Figure 9: Normative composition of aqueous phase in equilibrium with Spruce Pine pegmatite 35

Figure 10: Photograph of stained pegmatite and granodiorite slabs. 39

Figure 11: Map of Spruce Pine area with locations of bodies studied 42

Figure 12: Photograph of Crabtree Creek exposure. 43

Figure 13: Geologic map of Crabtree Creek exposure 44

Figure 14: Photograph of Field Mine pegmatite and granodiorite. 46

Figure 15: Geologic map of Field Mine pegmatite. 47

Figure 16: Location of sampled pegmatite areas in Bon Ami mine. 49

Figure 17: Zoned pegmatite in Bon Ami A area 50

Figure 18: Geologic map of Bon Ami A area. 51
Figure 19: Pegmatite outcrop sampled at Bon Ami B. 52
Figure 20: Geologic map of Bon Ami B area. 53
Figure 21: Pegmatite outcrop sampled at Bon Ami C area. 55
Figure 22: Geologic map of Bon Ami C area. 56
Figure 23: Map of Hootowl Mine with sampled pegmatite locations. 57
Figure 24: Pegmatite exposure in Northwest Hootowl study area. 58
Figure 25: Geologic map of pegmatite exposure at Northwest Hootowl study area. 60
Figure 26: Pegmatite exposure at Southeast Hootowl study area. 61
Figure 27: Geologic map of pegmatite exposed at Southeast Hootowl study area. 62
Figure 28: Roan Road granodiorite outcrop. 64
Figure 29: Backscatter electron image of grossular growths on rim of almandine-spessartine garnet from granotiorite in Bon Ami Ca area.. 66
Figure 30: Pegmatitic garnet compositions from Field Mine. 68
Figure 31: Pegmatitic garnets from Bon Ami B area. 69
Figure 32: Composition of garnet from Bon Ami C area. 71
Figure 33: Composition of garnet from Crabtree Creek exposure. 72
Figure 34: Garnet compositions from Northwest Hootowl study area. 73
Figure 35: Pegmatitic garnet compositions from the Southeast Hootowl study area. 74
Figure 36: Summary of all garnet compositions. 75
Figure 37: Backscatter electron image of grossular garnet between fragments of Almandine-spessartine garnets from the Southeast Hootowl study area. 77
Figure 38: Backscatter electron image of small muscovite crystals in a spray pattern. 78

Figure 39: Celadonitic substitution in Field Mine muscovite.....81
Figure 40: Paragonitic substitution in Field Mine muscovite.....82
Figure 41: Celadonitic substitution in Bon Ami A muscovite.....83
Figure 42: Paragonitic substitution in Bon Ami A muscovite.....84
Figure 43: Celadonitic substitution in Bon Ami B muscovite.....85
Figure 44: Paragonitic substitution in Bon Ami B muscovite.....86
Figure 45: Celadonitic substitution in Bon Ami C muscovite.....88
Figure 46: Paragonitic substitution in Bon Ami C muscovite.....89
Figure 47: Celadonitic substitution in Northwest Hootowl muscovite.....90
Figure 48: Paragonitic substitution in Northwest Hootowl muscovite.....91
Figure 49: Celadonitic substitution in Southeast Hootowl muscovite.....93
Figure 50: Paragonitic substitution in Southeast Hootowl muscovite.....94
Figure 51: Celadonitic substitution in Crabtree Creek muscovite.....95
Figure 52: Paragonitic substitution in Crabtree Creek muscovite.....96
Figure 53: Celadonitic substitution in Roan Road muscovite.....98
Figure 54: Paragonitic substitution in Roan Road muscovite.....99
Figure 55: Summary of celadonitic substitution in all white mica analyses.....100
Figure 56: Summary of paragonitic substitution in all white mica analyses.....101
Figure 57: Field Mine feldspar compositions.....105
Figure 58: Bon Ami B feldspar compositions.....106
Figure 59: Bon Ami C feldspar compositions.....107
Figure 60: Northwest Hootowl feldspar compositions.....108
Figure 61: Southeast Hootowl feldspar compositions.....109

Figure 62: Crabtree Creek feldspar compositions. 110

Figure 63: Roan Road feldspar compositions. 111

Figure 64: Summary of feldspar compositions from all bodies studied. 113

Figure 65: Backscatter electron image of epidote in muscovite. 114

Figure 66: Chart of decreasing microprobe totals with increasing grossular component in garnet. 119

Figure 67: Chart of weight percent fluorine in muscovite versus weight percent calcium in garnet rims. 121

CHAPTER 1

INTRODUCTION

History of Mining in Spruce Pine District

The Spruce Pine area of Mitchell, Avery, and Yancey counties, North Carolina (Figure 1), contains thousands of Silurian-Devonian pegmatites and associated granitoid intrusions with economically valuable industrial minerals (Brobst, 1962; McSween et al., 1991). The Spruce Pine plutonic suite is the source of potassium feldspar, plagioclase, silica, and mica (Brobst, 1962). Although originally (and still) mined for feldspar and mica, the Spruce Pine granitoid rocks currently also supply high purity quartz for the electronics industry.

Mining in the Spruce Pine area dates back to the pre-historic mining of muscovite by native Americans (Parker, 1952). Mica mined by these natives, used for grave decoration and wampum (money), made its way as far as the Ohio Valley (A. Glover, personal communication). Legends of this silvery, shiny mica led Hernando Desoto to the Spruce Pine area in search of gold and silver (A. Glover, personal communication). Traces of old mining pits and trenches dig by native Americans were still evident when mica mining was begun in 1867 (Sterrett, 1923). Large sheets of muscovite discovered in mounds built by the mound building native Americans probably came from the Spruce Pine region of North Carolina (Sterrett, 1923).

More advanced mining began about 1868 with the removal of sheet mica (Parker, 1952). This mining was started by Mr. L. E. Pearson, after a friend in Philadelphia directed his attention to Jackson County, North Carolina, after viewing a crystal of mica at the State Fair in Columbia, North Carolina (Sterrett, 1923). Pearson went to Jackson County and opened several

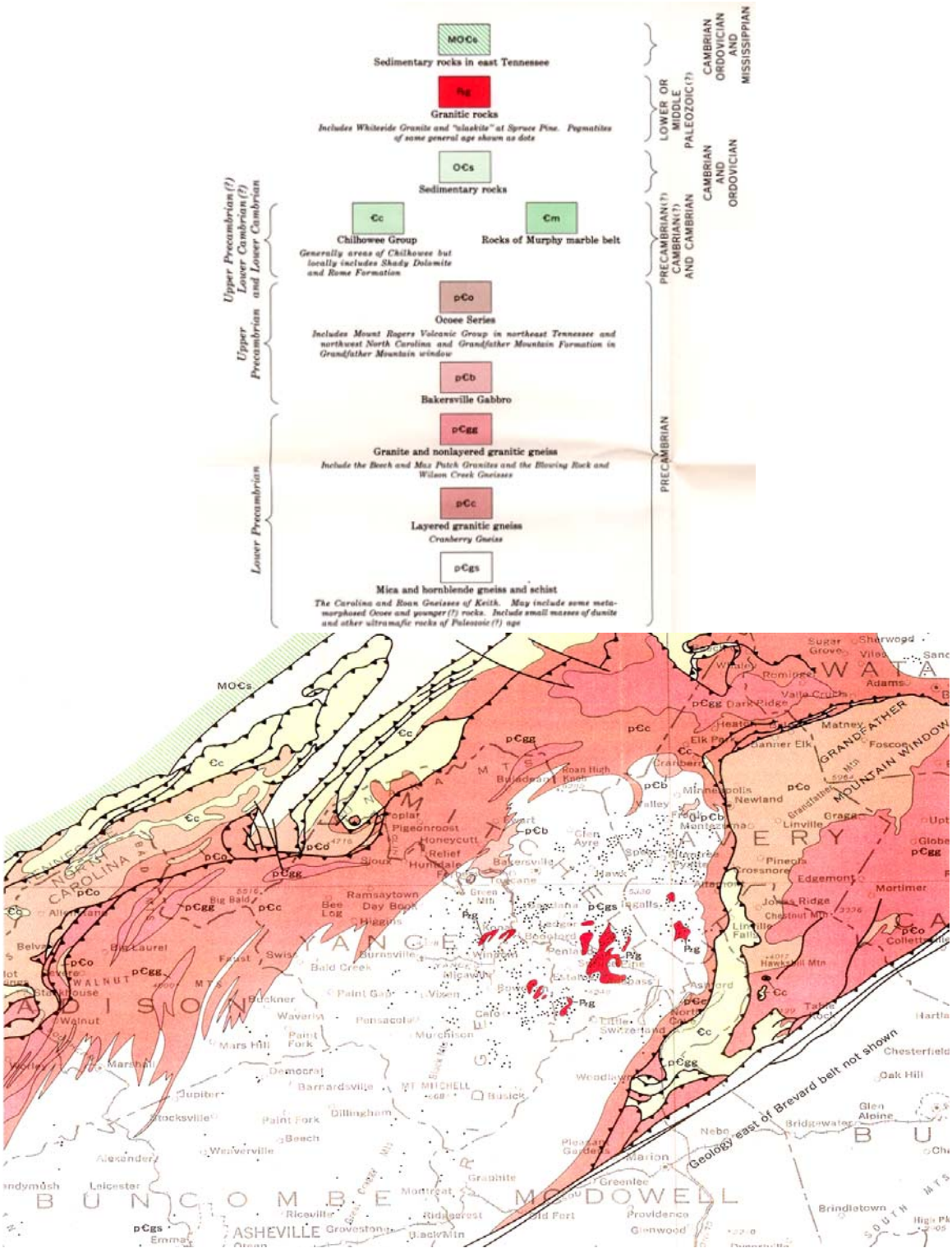

Figure 1 Geologic map of Spruce Pine District. Spruce Pine plutonic suite intrudes the biotite schists and amphibolites of the Ashe Metamorphic Suite. Red fields are granitoid plutons and black dots are individual known pegmatites. Map view is 60 km wide.

favorable prospects as mica mines and, shortly after, mica mining began in several other counties in North Carolina (Sterrett, 1923). Uses for sheet mica included windows for wood and coal burning stoves and, later, radio tube capacitors (A. Glover, personal communication). Starting in 1893, scrap mica became an ever increasing part of mining production in the Spruce Pine area (Parker, 1952). Scrap mica is finely ground for use currently in sheetrock mud and joint compounds (A. Glover, personal communication).

Spruce Pine feldspar was first shipped in 1911 from the Deer Park mine, and by 1917, North Carolina ranked first in feldspar production in the United States (Parker, 1952). Feldspar mined from the Spruce Pine area was shipped to Golding Sons Ceramic Plants in Trenton, NJ, Wilmington, DE, and East Liverpool, OH (A. Glover, personal communication). Three years after feldspar mining began in the Spruce Pine area, feldspar grinding plants were built in Erwin, Tennessee (A. Glover, personal communication). The two main feldspar products are potash spar from perthitic microcline for pottery and soda spar from plagioclase (mostly plagioclase) for glassmaking (Parker, 1952). Early mica and feldspar mines were opened up into very coarse grained pegmatites whose large crystal sizes allowed hand separation of minerals. Quartz was discarded as an unusable byproduct of feldspar and mica mining. After World War II, mineral processing technology advanced and flotation using heavy liquids came into use making it possible to separate feldspar and quartz. The mechanical separation of feldspars and quartz permitted a shift from hand-mining pegmatites to bulk mining of all granitoid rocks (including pegmatites). Quartz is now a major product mined from the Spruce Pine pegmatites and separated using froth flotation. This quartz is particularly valuable because its minor impurities can be leached out leaving a very pure silica product. This pure silica is used to make glass rods and crucibles. The crucibles are used for the growth of silicon boules for silicon chips and the

glass rods support silicon chips in high temperature furnaces. High purity quartz is also used for lamp covers in halogen light bulbs.

Purpose of Project

Not all bodies of Spruce Pine granitoid rocks yield quartz of suitable quality for making high-purity silica for use in industry. Spruce Pine quartz of suitable quality can be refined into a silica glass with impurities measured in the parts per million (A. Glover, personal communication). Several bodies are currently mined for this high-purity quartz, but more bodies in the Spruce Pine district seem to lack this type of quartz. The current method of identifying a body with valuable quartz is to mine a bulk sample to determine in a suitable quartz can be produced. A tool is needed to guide the identification of bodies with economically valuable quartz prior to mining. Mineralogy of a Spruce Pine granitoid body may be a valuable indicator of the economic potential of its quartz. The purpose of this project is to find a useful mineralogic/petrologic indicator that can be used to characterize different granitic bodies.

CHAPTER 2

PEGMATITE PETROGENESIS

Types of Pegmatites

Granitic pegmatites are characterized by at least some mineral phases of very coarse grain size, but through usage the grain size that distinguishes pegmatite from granite is more relative than quantitative (London, 1996). Pegmatites are distinguished from other intrusive equivalents (granite, diorite, etc.) by internal heterogeneity in the pegmatites; abrupt variations in grain size or in mineralogy, anisotropy in fabric and a wide range of crystal morphologies, such as skeletal, graphic, and euhedral (London 1996). Most granitic pegmatites deviate from average granitic composition by their low CaO contents, variable K_2O/Na_2O contents, high Al_2O_3 and largely peraluminous compositions, indicated by the presence of peraluminous minerals (e.g. garnet, mica, topaz) (Cerny, 1982). Elements other than those found in common rock forming minerals rarely reach more that 2 or 3 weight percent in pegmatites (Cerny, 1982).

A basic classification of pegmatites based on their geological-petrogenetic criteria is proposed by Ginsburg et al. (1979). This classification system separates pegmatites based on their depth (pressure) of crystallization (Cerny, 1982). Most pegmatites are hosted by metamorphic rocks, but Ginsburg et al. (1979) emphasize that there is no direct genetic or temporal relationship between metamorphism and pegmatite origin (Cerny, 1982). Miarolitic pegmatites form at depths of 1.5 to 3.5 km (Cerny, 1982) and are the shallowest of the pegmatites. These shallow pegmatites usually occupy the upper parts of epizonal granites intruding rocks of lowest metamorphic grades (Cerny, 1982). Rare-earth element pegmatites

crystallize at intermediate depth (3.5 to 7 km depth) and contain minerals enriched in Li, Rb, Cs, Be, Ta, Sn, Nb (Cerny, 1982). Rare element pegmatites are interpreted to be fractionation products of differentiated granites (Cerny, 1982). Mica-bearing pegmatites crystallize at depths of 7 to 11 km and are hosted by amphibolite facies metamorphic rocks (Cerny, 1982). These mica-rich, rare-element poor magmas represent direct products of anatexis or are magmas separated from anatectic, autochthonous granites (Cerny, 1982). The Spruce Pine pegmatites are mica-bearing pegmatites hosted by biotite schists and amphibolites of the Ashe Metamorphic Suite. Pegmatites formed at the deepest levels (>11 km) are hosted by granulite facies metamorphic rocks and contain little to no economic mineralization, but are locally enriched in allanite, monazite, and corundum (Cerny, 1982). These deep pegmatites often grade into migmatites and have no obvious granitic parent (Cerny, 1982).

As depth of pegmatite formation increases, the relation between pegmatites and granites becomes less obvious, virtually disappearing in the deepest seated pegmatites (Cerny, 1982). It is important to note that not all pegmatites neatly fit into this classification. "Hybrid" pegmatites such as the rare-element rich miarolitic pegmatites of California, Brazil, and Afghanistan, and extensive beryl mineralization in mica pegmatites of India offer examples of "non-conforming" (Cerny, 1982).

A later classification scheme by Cerny (1991) divides pegmatites into two broad compositional families. The NYF (Nb-Y-F) family is associated with subalkaline to metaluminous A-type granites, although some peraluminous NYF pegmatites are known (London, 1996). NYF pegmatites are enriched in LREEs, between 100 and 300 times chondritic concentrations (Cerny, 1991; London, 1996). The LCT (Li-Cs-Ta) family may be derived from more varied sources, such as supracrustal metasedimentary sequences plus lower crystal

granulites (Cerny, 1991; London, 1996). LCT pegmatites are usually peraluminous and are enriched in elements thought to be liberated from rock-forming minerals at the onset of anatexis (London, 1996) and are mostly associated with S-type granites.

A separate classification system is described by Cerny (1982). This classification system breaks pegmatites down into three general types and further into many subtypes (Cerny, 1982). The first type of pegmatite is the mica-bearing and ceramic pegmatites, with the subtypes 1) oligoclase with muscovite and/or U, REE; and 2) oligoclase and microcline with muscovite and/or U, Th, REE, Nb, Ta (Cerny, 1982). The second type is the main rare-element pegmatite, with the subtypes 1) microcline with Be, Nb; 2) microcline and albite with Be, Ta or Be, Ta, Li, Cs; 3) albite with Be, Ta, Nb or Be, Ta, Nb, Li; and 4) albite and spodumene with Be, Nb, Sn (Cerny, 1982). The third group is the exotic rare-element pegmatite with the subtypes 1) amazonite and albite with Be, REE; 2) microcline and petalite; 3) muscovite and albite with Sn; and 4) lepidolite and albite with Ta, Cs, Be (Cerny, 1982).

Crystallization of Pegmatites

Raymond (2002) provides an overview of pegmatite petrogenesis based on the work of Jahns and Burnham (1969). According to the Jahns and Burnham (1969) model, pegmatite petrogenesis begins with emplacement of a hydrous silicate melt. Falling temperatures in the melt trigger crystallization. Aplites may form at the margin of shallow magma bodies, but are absent in intrusions at greater depth (Jahns and Burnham, 1969; Raymond, 2002). Anhydrous and hydrous mineral phases typical of granite crystallize in generally coarse grain size to produce a granite or pegmatitic granite. Grain size is largely controlled by degree of undercooling (Jahns and Burnham, 1969; Raymond, 2002). As crystallization proceeds, the melt becomes enriched in H_2O (Jahns and Burnham, 1969; Raymond, 2002).

Once crystallization has proceeded to the point that the residual melt becomes saturated with H_2O, a separate fluid phase will exsolve from the melt (Jahns and Burnham, 1969). Separation of the fluid phase, a process called resurgent boiling, may be delayed by crystallization of hydrous minerals, such as muscovite, because water will be removed from the melt and incorporated into the structures of such hydrous minerals. Separation of this water-rich phase from a felsic magma is virtually instantaneous (Burnham, 1967) and results in a system of fluid + melt + crystals. Composition of this fluid phase is dependent on temperature, pressure, bulk composition of the magma, and the nature of coexisting crystalline phases. The high water content of the fluid phase results in low viscosity and facilitates ion migration, resulting in rapid crystal growth. Rapid growth rate, together with low nucleation rate, results in local formation of very large crystals within the developing pegmatite body. Pressure from resurgent boiling may result in fracturing of crystallized material and infilling of these fractures with magma that quenches to form aplite (Jahns and Burnham, 1969; Raymond, 2002). Buoyant fluid phase has a tendency to rise, leading to asymmetric structures such as zones or cores in pegmatites (Jahns and Burnham, 1969; Raymond, 2002).

Once all melt is crystallized, the system consists of crystals and a fluid phase. After further cooling, shallow, epizonal pegmatites will contain pockets of fluid rich in uncommon ions, from which large crystals of tourmaline, beryl, spodumene, and other minerals crystallize (Jahns and Burnham, 1969; Raymond, 2002). Fluids under high pressures may fracture these pockets, resulting in the formation of aplites (Jahns and Burnham, 1969; Raymond, 2002). Fractures not immediately filled with aplite may later fill in with fluid to produce cross cutting veins (Jahns and Burnham, 1969; Raymond, 2002). Fluid may also interact with previously crystallized minerals, metasomatically altering them or replacing them with new

minerals stable at low temperature conditions (Jahns and Burnham, 1969; Raymond, 2002). Clay minerals and zeolites may develop in pockets and miarolitic cavities at this point (Jahns and Burnham, 1969; Raymond, 2002).

The Jahns-Burnham model does not explain how quartz cores and large crystals of feldspar form in pegmatites (Raymond, 2002). According to Burnham and Nekvasil (1986), quartz cores in pegmatites are not evidence of a magmatic equilibrium process. However, quartz cores are common in pegmatites and prevalent in pegmatites of the Spruce Pine area (Parker, 1952). Swanson (1977) has shown that feldspar and quartz crystals grow slower as melt reaches saturation. A different theory of pegmatite petrogenesis was proposed by London and coworkers based on fractional crystallization experiments on vapor-undersaturated Macusani glass (London et al., 1989). London et al. (1989) imply that nearly all phenomena observed in pegmatites can be produced through fractional crystallization of vapor-undersaturated magmas. While Jahns and Burnham (1969) and Burnham and Nekvasil (1986) attributed pegmatitic fabric and zonation to vapor saturation of a hydrous magma, London et al. (1989) state that these phenomena are caused by increasing concentrations of incompatible elements in crystallizing magmas. In particular, London et al. (1989) blame H, B, P, and F for "disrupting" the melt structure, thus causing differentiation of magma. The experiments of London et al. (1989) produce zoning sequences and textures that are characteristic of pegmatites. They also prove that quartz cores could be produced entirely by magmatic processes, dispelling Burnham and Nekvasil's (1986) claim that about 60 percent of the quartz in cores of pegmatites must be hydrothermal in origin. Simultaneous crystallization in two or more intermediate zones of pegmatites is also displayed in the experiments of London et al., (1989). The fractional crystallization experiments produced grain-size variations similar to those observed in natural pegmatites, with grain size increasing a

hundred-fold with increasing differentiation of the melt (London et al., 1989). Graphic feldspar-quartz intergrowths were also produced in these experiments (London et al., 1989).

Zoning in pegmatites can be compositional, textural, or both. Zones in a pegmatite reflect the shape or structure of the containing pegmatite body, although not all zones are continuous or complete across the entire pegmatite (Cameron et al., 1949). Cameron et al., (1949) divided the zones of pegmatites into four categories; the border zone, wall zone, intermediate zones, and core. Border zones form thin shells around the outer parts of pegmatites and are usually fine-grained or aplitic (Cameron et al., 1949). Contact between border zone and host rock can be sharp or gradational. The border zone coarsens towards the mineralogically similar wall zone (Cameron et al., 1949). Wall zones are thicker and coarser-grained than border zones and may be missing in the top portions of some pegmatites (Cameron et al., 1949). The intermediate zones of a pegmatite comprise all zones between the wall zone and the core and may be continuous or discontinuous (Cameron et al., 1949). Some pegmatites have several intermediate zones, while others have no intermediate zone and the wall zone directly contacts the core (Cameron et al., 1949). Cores of pegmatites are generally symmetrical with respect to the sides of a pegmatite body and usually reflect any irregularities in the shape of the pegmatite body (Cameron et al., 1949). Cores may be polymineralic, or, as is commonly the case for Spruce Pine pegmatites, monomineralic, usually smoky quartz (Cameron et al., 1949). Zoned pegmatites are believed by Jahns (1982) to crystallize from border zone, or margin, toward core. Correlation of primary mineral assemblages with falling temperatures in the outer zones of a pegmatite can be inferred from phase equilibrium relationships, but phase equilibrium relationships often fail to explain the mineral assemblages commonly observed in the cores of pegmatites (Jahns, 1982). An experiment by Burnham and Jahns in 1958 gave direct indication

that quartz cores may begin to develop relatively early during the crystallization of a zoned pegmatite body (Jahns, 1982). Thus, as complete solidification proceeds from the margin toward the core of the body, crystallization may be ongoing in two or more zones simultaneously. Eventually, after some portion of crystallization, the residual melt becomes saturated with respect to a fluid phase and resurgent boiling takes place (Jahns, 1982). Mineral assemblage of a pegmatite can change from border zone to core in response to crystallization of minerals of varying compositions, changing pressure, and volatile saturation. Cameron et al. (1949) derived a general compositional zoning sequence for Li-free granitic pegmatites in the southeastern United States from first formed to last formed as: 1) plagioclase-quartz-muscovite; 2) plagioclase-quartz; 3) quartz-perthite-plagioclase (±muscovite, ±biotite); 4) quartz-perthite; and lastly 5) quartz. This sequence most closely approximates the observed compositional zoning sequence of the Spruce Pine pegmatites.

One explanation of internal zonation in pegmatites was presented by London et al. (1989) based on experimentation. London et al., (1989) stated that mineral zoning patterns, sharp changes in grain size, the variety of mineral textures and oriented fabrics that typify pegmatites all resulted from the slow crystallization response of volatile-bearing granitic melts to cooling. The further the melt was cooled below its equilibrium liquidus before crystallization began, the greater the tendency for form pegmatitic instead of granitic fabrics (London, 1996). Pegmatitic fabric is formed when nucleation rates are slow, resulting in fewer crystals of larger size than in granitic fabric. Zoning is usually consistent in both structure and mineral assemblage within pegmatites in a given district (Cameron et al., 1949). The important concept of pegmatite crystallization is that magmas of near-eutectic composition were thought to have undergone non-

eutectic crystallization, which is crystallization of all phases at the eutectic in sequential order (London, 1996).

Several experimental studies used samples and compositions of pegmatitic material from Spruce Pine, North Carolina (Burnham, 1967; Burnham and Nekvasil, 1986; Fenn, 1986). Burnham and Nekvasil (1986) determined phase assemblage diagrams for a sample of the Spruce Pine pegmatite at 2 kbar and 5 kbar. The phase assembly diagram for Spruce Pine pegmatite at 5 kbar is shown in Figure 2. The expected crystallization history of Spruce Pine pegmatite at 2 kbar from the phase assemblage diagram is plagioclase, alkali feldspar, quartz, sillimanite, and vapor (Burnham and Nekvasil, 1986). Muscovite is formed from the reaction: muscovite + quartz = alkali feldspar + sillimanite + H_2O vapor. The expected crystallization history for the same Spruce Pine pegmatite at low water contents and 5 kbar pressure is plagioclase, quartz, alkali feldspar, and muscovite (Burnham and Nekvasil, 1986). At higher water contents, muscovite begins to crystallize before alkali feldspar and quartz (Burnham and Nekvasil, 1986). The presence of large crystals of plagioclase and muscovite near the margins of Spruce Pine pegmatites implies that the magma reached saturation with H_2O early in crystallization history (Jahns and Burnham, 1969; Burnham and Nekvasil, 1986). Burnham and Nekvasil (1986) also state that if the Spruce Pine pegmatite crystallized under closed system conditions at a confining pressure of 2.0 kbar (8 km), the pegmatite should contain 8 volume % void space and no primary muscovite.

Fenn (1986) used a sample of Spruce Pine pegmatite from a pegmatitic pod from Chalk Mountain, Mitchell County, North Carolina, in an experiment designed to replicate the intergrowth of quartz and feldspar known as graphic granite. Fenn (1986) provided a phase

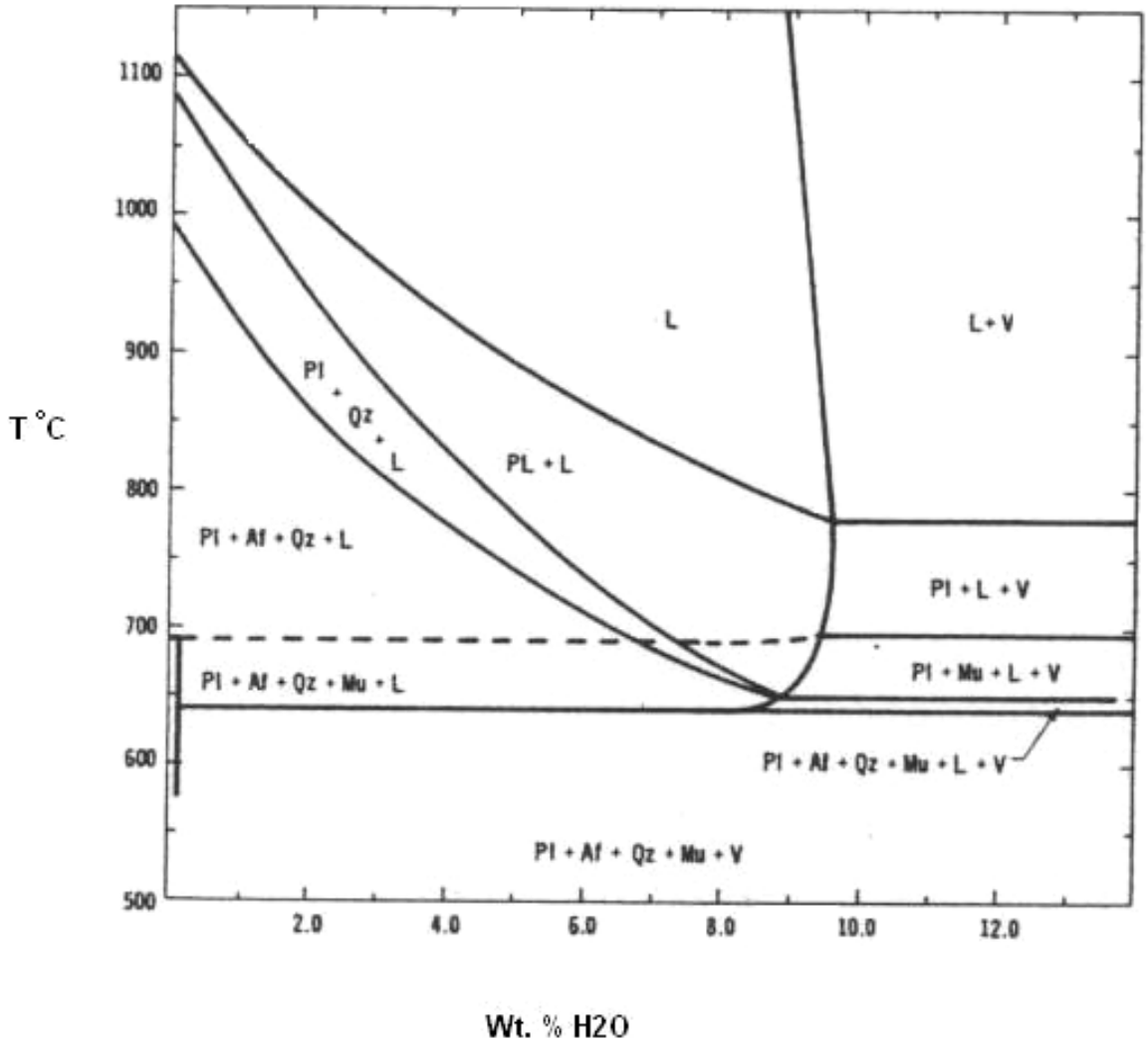

Figure 2 Phase assemblage diagram for Spruce Pine pegmatite at 5 kbar. L = liquid, V = vapor, Pl = plagioclase, Qz = quartz, Mu = muscovite, Af = alkali feldspar. Modified from Burnham and Nekvasil (1986).

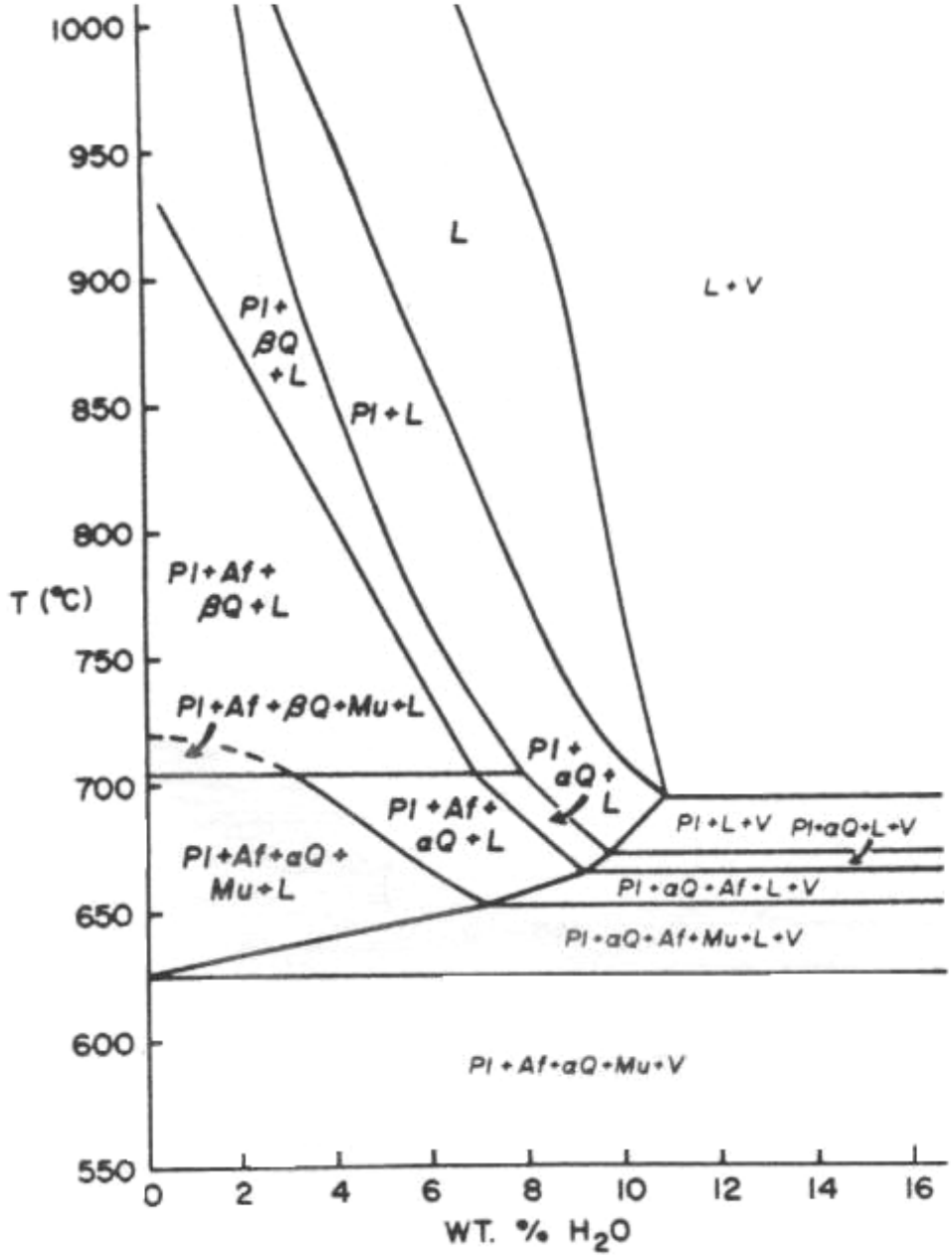

Figure 3 Phase equilibria for the Spruce Pine pegmatite composition modified from Fenn (1986). Q = quartz (α for alpha quartz, and β for beta quartz), Pl = plagioclase (oligoclase), Kf = alkali feldspar, Mu = muscovite, L = liquid, and V = vapor.

equilibria diagram (Figure 3) of the Spruce Pine pegmatite used in the experiment. The sequence of crystallization of Spruce Pine pegmatite at 5 kbar (15 km), based on Fenn's phase equilibria diagram, is plagioclase (oligoclase), β-quartz (<8 wt. % H_2O) or α-quartz (>8 wt. % H_2O), alkali feldspar, and muscovite. The solidus is ~625° C. Vapor is present throughout the crystallization history for a magma with more than 10 wt. % H_2O. As weight percent H_2O decreases, resurgent boiling is delayed in the cooling history. The experiment concluded that the origin of graphic intergrowth of quartz and alkali feldspar is the result of simultaneous growth of the two phases under conditions that favor the planar growth of the feldspar host (Fenn, 1986).

CHAPTER 3

GEOLOGIC BACKGROUND

Tectonic Setting

Spruce Pine granitoid rocks intrude the biotite schists and amphibolites of the Ashe Metamorphic Suite (Figure 4) (Butler, 1973). Xenoliths of metamorphic rock are common within the Spruce Pine granitoids. Xenoliths usually parallel the walls of plutons and range in size from a few centimeters to almost a kilometer in length (Parker, 1952). Contacts between the granitoid rocks and metamorphic wall rocks are sharp. The Ashe Metamorphic Suite lies in the uppermost of four thrust sheets in the Blue Ridge thrust complex, the Spruce Pine thrust sheet (Adams and Trupe, 1997). High pressure metamorphism is documented by the presence of eclogite at the base of the Spruce Pine thrust sheet (Adams and Trupe, 1997). The schists and amphibolites of the Ashe Metamorphic Suite record kyanite grade peak regional metamorphism (Adams and Trupe, 1997). Estimated peak metamorphic conditions are illustrated in Table 1. Evidence exists for multiple metamorphic events in the Ashe Metamorphic Suite in the Spruce Pine thrust sheet (Adams and Trupe, 1997). The Spruce Pine plutonic suite is discordant to the first deformation event in this region, dated at 430 Ma or older (Butler, 1973). No pegmatites have been observed that have been deformed by this Ordovician event (Adams and Trupe, 1997; Butler, 1973). The second deformational event occurred approximately 350 to 380 ma (Butler, 1973). Pegmatites in the Spruce Pine area show both concordant and discordant relationships relative to the main foliation (1st deformation) of the Ashe Metamorphic Suite (Adams and Trupe, 1997). Johnson (2001) concurs, stating that pegmatite dikes are commonly transposed

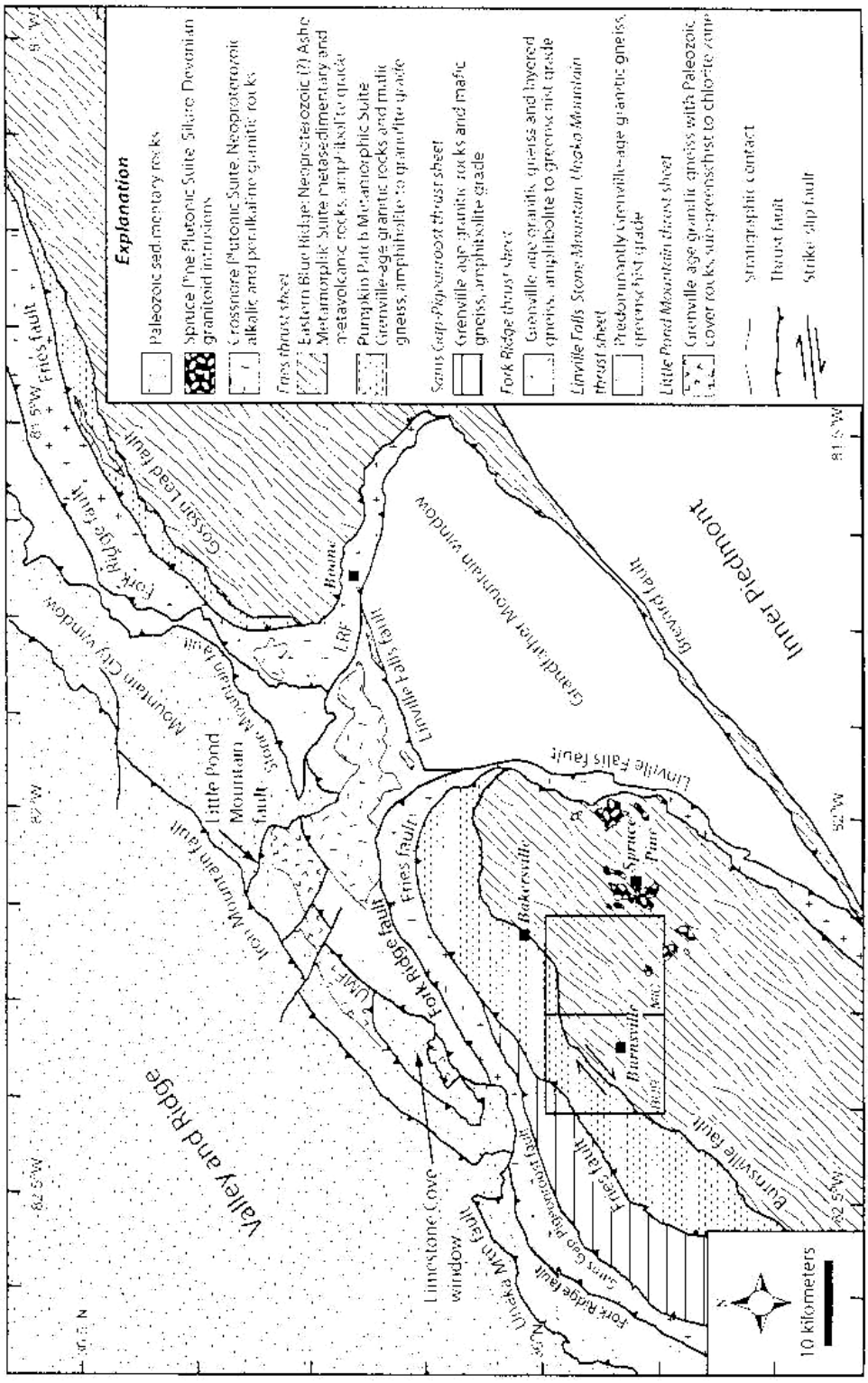

Figure 4 Tectonic map of western North Carolina with Spruce Pine District. From Trupe et al. (2003).

Table 1 Estimated metamorphic conditions in the Spruce Pine Thrust Sheet. Modified from Adams and Trupe, 1997.

Rock Type	Pressure (kbar)	Temperature (°C)
Pelitic Schist and Amphibolite	7-10	700
	7.5	600-650
	7-9 “peak”	640-700 “peak”
	4-6 “retrograde”	550-610 “retrograde”
	~7.5	650
	5-6.5 “retrograde”	550-610 “retrograde”
	8.5-11 “garnet amphibolite”	675-705 “garnet amphibolite”
Eclogite	13-17 “prograde”	625-790 “prograde”
	8.5-12 “retrograde”	650-730 “retrograde”
Garnet Inclusions in Eclogite	6-10	400-600
	8-12	450-680
	13-16	630-660
Eclogite Matrix	10-13	600-800
Pelitic schist adjacent to eclogite	6-8 “peak”	580-640 “peak”
	5.5-6.5 “retrograde”	565-610 “retrograde”

into the regional metamorphic foliation but are also found crosscutting the foliation. Butler (1973) states that the largest alaskite (granitoid) bodies occupy the cores of major folds of the second deformational event and that folding and plutonism are likely closely associated. Pegmatite ages are slightly younger than the ages of the second deformational episode, dated at approximately 380 ma (Butler, 1973). The pegmatites were likely emplaced in the late stages of folding associated with the Siluro-Devonian folding event (Butler, 1973). No middle- or high-grade metamorphism occurred after about 320 ma and most of the pegmatites in the Spruce Pine district crystallized before 350 ma (Butler, 1973).

Intrusion of Spruce Pine granitoid rocks occurred during amphibolite grade metamorphism, evidenced by the restriction of plutons to kyanite and higher metamorphic zones and the general absence of contact aureoles in the Ashe Metamorphic Suite (Adams and Trupe, 1997). Absence of recognizable aureoles and permeation of intrusive granitic material into metamorphic host rock is described by Butler (1973). This lack of contact metamorphism of host rocks leaves no indication of fluid interaction that may have accompanied pluton emplacement. Although contact metamorphism is rare in the Spruce Pine intrusions, two small (3 cm) metasomatic contact reaction zones (exocontacts) of biotite schist exist at the Crabtree pegmatite in Mitchell County (Tappen and Smith, 2003). Although care must be taken when using the presence of primary igneous muscovite as an indicator of pressure at crystallization, estimates for minimum pressure and depth of primary muscovite are 2 kbar, or 7.6 km depth (Miller et al., 1981). The occurrence of primary muscovite near the walls of the Spruce Pine pegmatite indicates a depth of crystallization where pressures were in excess of 3.0 kbar (Burnham and Nekvasil, 1986). Johnson (2001) describes moderate to strong foliation in the largest Spruce Pine plutons.

Ages of Spruce Pine Granitoid Rocks

Radiometric dating of muscovite, uraninite, samarskite, monazite, zircon, and whole rock pegmatites from the Spruce Pine plutonic suite yields a range of ages from 325 Ma to 580 Ma. Radiometric age dates are illustrated in Table 2. The Spruce Pine plutonic suite is widely accepted as Siluro-Devonian with general dates ranging from 450 to 380 Ma (Butler, 1973).

Geology of Spruce Pine Granites and Pegmatites

The intrusions are generally small but vary in shape, which may be partly controlled by the type of wall or host rock into which the pegmatites intrude (Cameron et al., 1949). The intrusive bodies range in size from a few cm to greater than 3 km (Butler, 1973). Shapes of intrusions range from equant plutons to long, narrow dikes, and lenses of pegmatite with tapered ends. Cameron et al. (1949) note elongate intrusions are particularly abundant in the northern and northeastern parts of the Spruce Pine district. Large plutons in the Spruce Pine area usually occupy topographic highs due to the greater resistance to weathering of felsic igneous plutons than the mafic metamorphic host rocks. This weathering difference, along with ease of mining, results in most of the mines and quarries in the Spruce Pine area being placed on high elevation knobs.

Pegmatite bodies are common in the Spruce Pine granitoid rocks and range from late stage cross-cutting dikes enclosed within granitic rocks to pods and lenses of pegmatitic rock with gradational contacts with host granites. Cameron et al., (1949) states that most mica-feldspar pegmatites in the southeastern United States appear to be derived from quartz diorite, granodiorite, and quartz monzonite magmas, and are similar in composition to nearby masses of

Table 2 Radiometric dates of selected Spruce Pine materials.

Technique	Material Dated	Age (Ma)	Reference
Rb-Sr	Muscovite	380	Butler, 1991
K-Ar	Muscovite	340	Butler, 1991
U-Pb	Uraninite	430 ± 20	Butler, 1991
Rb-Sr	Whole Rock Pegmatite	390 ± 27	Butler, 1991
Rb-Sr	Whole Rock Pegmatite	392 ± 15	Butler, 1991
Rb-Sr	Whole Rock Pegmatite	404 ± 14	Butler, 1991
Pb-U+Th	Uraninite	330	Jahns, 1955
Pb-U+Th	Uraninite	340	Jahns, 1955
Pb-U+Th	Uraninite	350	Jahns, 1955
Pb^{207}-Pb^{206}	Uraninite	355 ± 40	Jahns, 1955
Pb^{210}	Samarskite	325 ± 15	Jahns, 1955
Pb-U+Th	Monazite	580	Jahns, 1955
U-Pb	Zircon	377 ± 12	Trupe et al., 2003

intrusive rock. Metamorphic rock adjacent to the granitoid bodies has, in places, been selectively impregnated with lenses and streaks of pegmatite (Butler, 1973). Pods and lenses of pegmatite are also commonly hosted by schists and gneisses of the enclosing country rocks, forming sharp contacts between the two lithologies. A typical cross-section of a Spruce Pine pegmatite is shown in Figure 5.

In contrast to these sharp boundaries between igneous and metamorphic rocks, some pegmatites are enclosed entirely in granitoid rock with no distinct contact between the two. Jahns (1955) reported Spruce Pine pegmatite bodies that transect outer parts of a pluton and merge into the granitoid rock in the inner parts of the pluton. These pegmatites gradually coarsen from granites into pegmatites. Brobst (1962) reports that some pegmatitic masses change into finer-grained granitoid rock across narrow zones only 5 cm wide. Brobst (1962) also describes the margins of the pegmatite bodies as being generally finer grained than the interiors, with most of the grains in the margins being less than 6 mm across. Some pegmatites clearly intrude host granodiorites as dikes and sills and these intrusions have sharp contacts with the host granodiorite.

Spruce Pine pegmatites also vary internally in that some display compositional zoning, textural zoning, or both. Still others lack compositional and textural zonation. Nearly half of all pegmatites in the Spruce Pine district are homogeneous in mineral assemblage composition and texture (Parker, 1952). Those that are not homogeneous are zoned with concentric shells that roughly approximate the external shape of the pegmatite (Parker, 1952). Parker (1952) describes the simplest zoning as mineralogically homogeneous (plagioclase, quartz, and muscovite) thin, fine-grained border zone around a coarse-grained core. The more complexly zoned pegmatites display border zones of fine-grained plagioclase, quartz, and muscovite surrounding

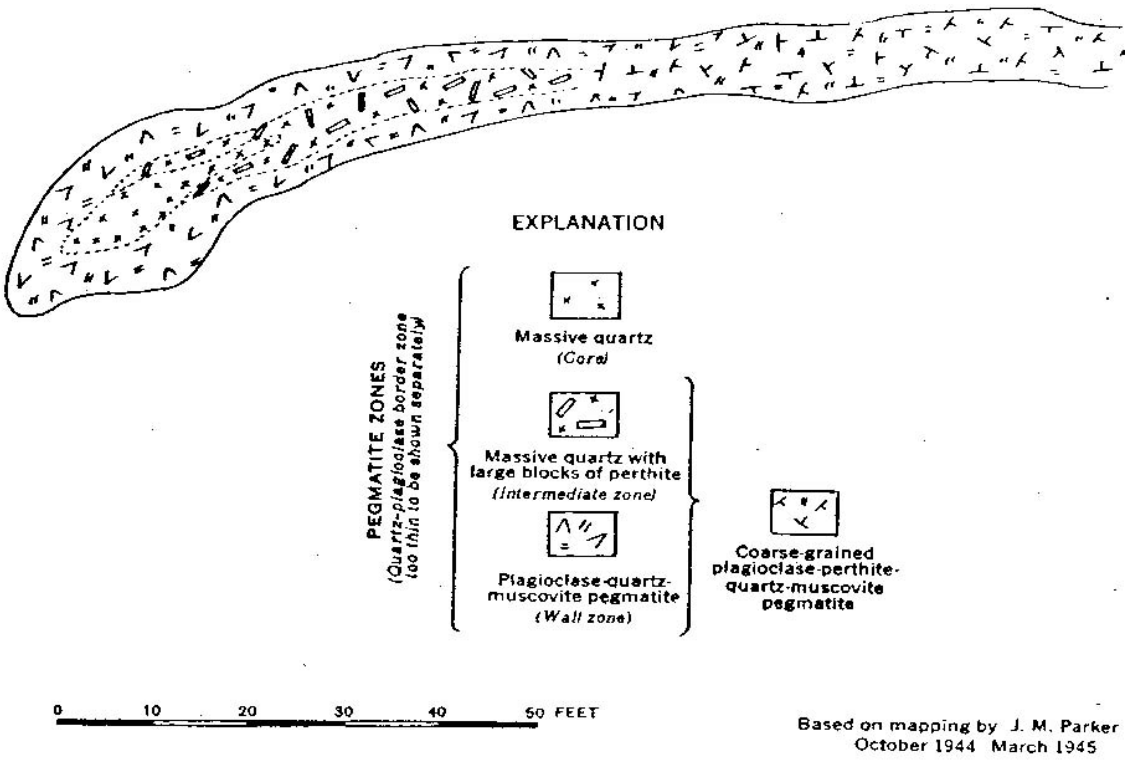

Figure 5 A typical zoned Spruce Pine pegmatite. The Little Hawk Ridge pegmatite in Mitchell County, North Carolina displays a typical cross section of a zoned Spruce Pine pegmatite. Telescopic zoning in this pegmatite include plagioclase-quartz-muscovite pegmatite wall zone, an intermediate zone composed of massive blocks of quartz and perthite, and a massive quartz core. Modified from Cameron et al., 1949.

coarser-grained wall rock of similar composition (Parker, 1952). The cores of these complexly zoned pegmatites are massive quartz or coarse perthite and quartz (Parker, 1952). Jahns (1955) reports tabular masses of quartz from centers of pegmatites from around the Spruce Pine area of western North Carolina.

Petrology of the Spruce Pine Intrusions

The Spruce Pine plutonic suite is described as closely related silicic igneous bodies, ranging from very large stocklike granitic masses through large and small pegmatitic sills, lenses, and dikes (Parker, 1952). The pegmatites consist mostly of alkali feldspar, plagioclase, quartz, muscovite, and small amounts of garnet. Minor beryl, uranium minerals, and columbium-tantalum minerals exists in a few of the pegmatites. Muscovite and coarse grain sizes attest to the hydrous nature of the Spruce Pine pegmatites, but these pegmatites are traditionally considered to be free of miarolitic cavities that, in other pegmatites, indicate magmas became saturated with volatiles after partial crystallization (Burnham and Nekvasil, 1986). Miarolitic cavities filled with pumpellyite, clinozoisite, chlorite, and albite are described from the McKinney mine in Mitchell County, North Carolina, adjacent to the Bon Ami mine (Wood and Abbott, 1996). The minerals in these cavities are attributed to late stage crystallization of a fluid phase at temperatures between 260°C and 370°C (Wood and Abbott, 1996).

Geochemistry of Granitoid Rocks and Pegmatites

Bulk Elemental Analysis

The bulk composition and normative mineralogy of several Spruce Pine granitoids is given in Table 3. These data indicate the peraluminous (A>CNK) nature of the Spruce Pine plutonic rocks. McSween et al. (1991) add that the rocks of the Spruce Pine Plutonic Suite are

depleted in incompatible trace elements. Classification of these rocks based on normative mineralogy is shown in Figure 6.

Mineralogy of Spruce Pine Granitoid Rocks

The Spruce Pine granodiorites and pegmatites are peraluminous. Molar aluminum content in these rocks is greater than the sum of the calcium, sodium, and potassium content. Peraluminous chemistry of these rocks is indicated by the presence of primary muscovite and garnet (Clarke, 1981). The Spruce Pine granodiorites and pegmatites also contain very minor amounts of biotite, zircon, epidote, and apatite.

Average modal mineralogy of the Spruce Pine pegmatites is given by Brobst (1962) as 40% oligoclase, 25% quartz, 20% perthitic microcline, and 15% muscovite. Parker (1952) estimates the average modal mineralogy of the pegmatites to be 45% plagioclase, 25% quartz, 20% microcline, and 10% muscovite. Butler (1973) concurs with others, listing major components as microcline, plagioclase, quartz, and muscovite, and notes the very low content of dark minerals. Maurice (1940) assigns plagioclase compositions of An_5 to An_{30} and adds minor biotite and garnet to the constituents. Many rarer phases seen in fractionated granitic pegmatites (tourmaline, beryl, spodumene) are very minor constituents, or are completely absent, in Spruce Pine pegmatites (Parker, 1952).

Parker (1952) notes the absence of perthitic microcline in many pegmatites and the nearly ubiquitous nature of the plagioclase and quartz. Maurice (1940) concurs, stating that although most of the pegmatites in the area are leucogranitic, some are completely absent of potash feldspar, some contain potash feldspar in equal proportions of plagioclase, and in some the potash feldspar dominates over plagioclase.

Table 3 Chemical compositions of Spruce Pine granitoid rocks and pegmatites.
[1.] Average from 500 tons alaskite (granodiorite) from Kesler and Olson, 1942.
[2.] Weighted average from 47,992 tons pegmatite from Kesler and Olson, 1942.
[3.] Composition of Spruce Pine pegmatite from Burnham, 1967.

Oxide	Granodiorite Wt % [1]	Pegmatite Wt % [2]	Pegmatite Wt % [3]
SiO_2	74.9	75.26	73.79
Al_2O_3	14.9	14.92	15.11
TiO_2	---	---	0.05
Fe_2O_3	0.33	0.28	0.26
FeO	---	---	0.16
MnO	---	---	0.05
MgO	---	---	0.07
Li_2O	---	---	0.01
CaO	1.0	1.10	0.97
K_2O	4.7	4.19	4.02
Na_2O	4.0	4.20	4.71
Rb_2O	---	---	0.005
H_2O^+	---	---	0.39
H_2O^-	---	---	0.07
CO_2	---	---	0.02
F	---	---	0.01
P_2O_5	---	---	0.01
Loss	0.2	0.28	---
Total	100.03	100.23	99.70
Normative Mineralogy			
Phase			
Quartz	31.50	32.44	31.71
Albite	33.85	35.54	40.01
Orthoclase	27.77	24.76	22.47
Anorthite	4.96	5.46	4.26
Hypersthene	---	---	0.29
Ilmenite	---	---	0.02
Calcite	---	---	0.15
Corundum	1.41	1.48	0.88
Magnetite	---	---	---
Hematite	0.33	0.28	---
Total	99.83	99.95	99.79

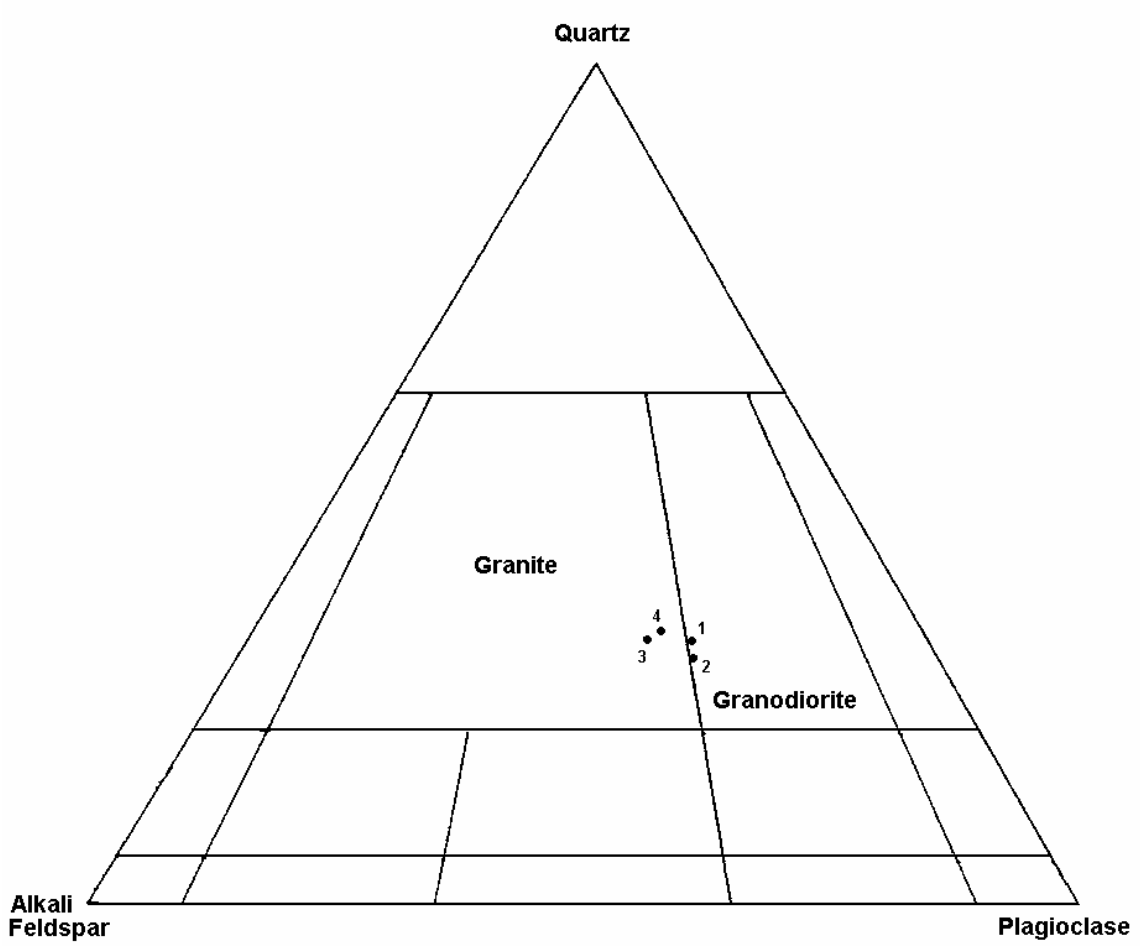

Figure 6 Classification of Spruce Pine granitoids based on normative mineralogy. Data points are as follows:

1. From Burnham, 1967.
2. From Burnham and Nekvasil, 1986.
3. Sample of Kesler and Olson, (1942).
4. Sample of Kesler and Olson, (1942).

The modal mineralogy of these granitoid rocks indicates that they are (according to the IUGS classification system) granodiorites. Spruce Pine granitoids are coarse-grained, resulting in some confusion in terminology. Parker (1952) and Maurice (1940) suggested calling the Spruce Pine granitoid rocks leucogranodioritic, fine-grained pegmatite instead of "alaskite," "granite," or "granodiorite." Part of this confusion comes from the gradational nature of the contact between the hypidiomorphic-granulated granitoids and pods or lenses with pegmatitic textures. In this study, the hypidiomorphic-granular granitoid rocks are termed granodiorites while the granitoid rocks with the pegmatitic texture are called pegmatites.

Garnets from peraluminous granites vary widely in composition, particularly with respect to Mn:Fe:Mg ratios (Clarke, 1981) (Figure 7). Almandine garnets with a large spessartine component are formed as late stage minerals in aplitic and pegmatitic rocks (Deer et al., 1992). Spessartine garnets are found mainly in pegmatitic/aplitic granites (Deer et al., 1992). Grossular garnet is been found with diopside or scapolite resulting from discharge of vapors associated with pegmatitic granites (Deer et al., 1992).

Garnets in the Spruce Pine plutons are usually small (less than 1 mm) but some as large as 15 mm in diameter are known. Garnets in host granodiorites are unaltered, red-brown euhedra and subhedra that reach up to 15 mm. Garnets in granodiorite are fairly evenly spaced and do not cluster into large groups of numerous crystals. Garnets in Spruce Pine pegmatites are unaltered, red-brown euhedra and subhedra that are typically smaller than garnets from granodiorite. Unlike garnets in the granodiorites, pegmatitic garnets often cluster into lenses and stringers with many tiny crystals concentrated in pegmatite zones. Garnet is found in all pegmatite zones except for quartz cores. Garnet is often closely associated with muscovite-rich areas in pegmatites.

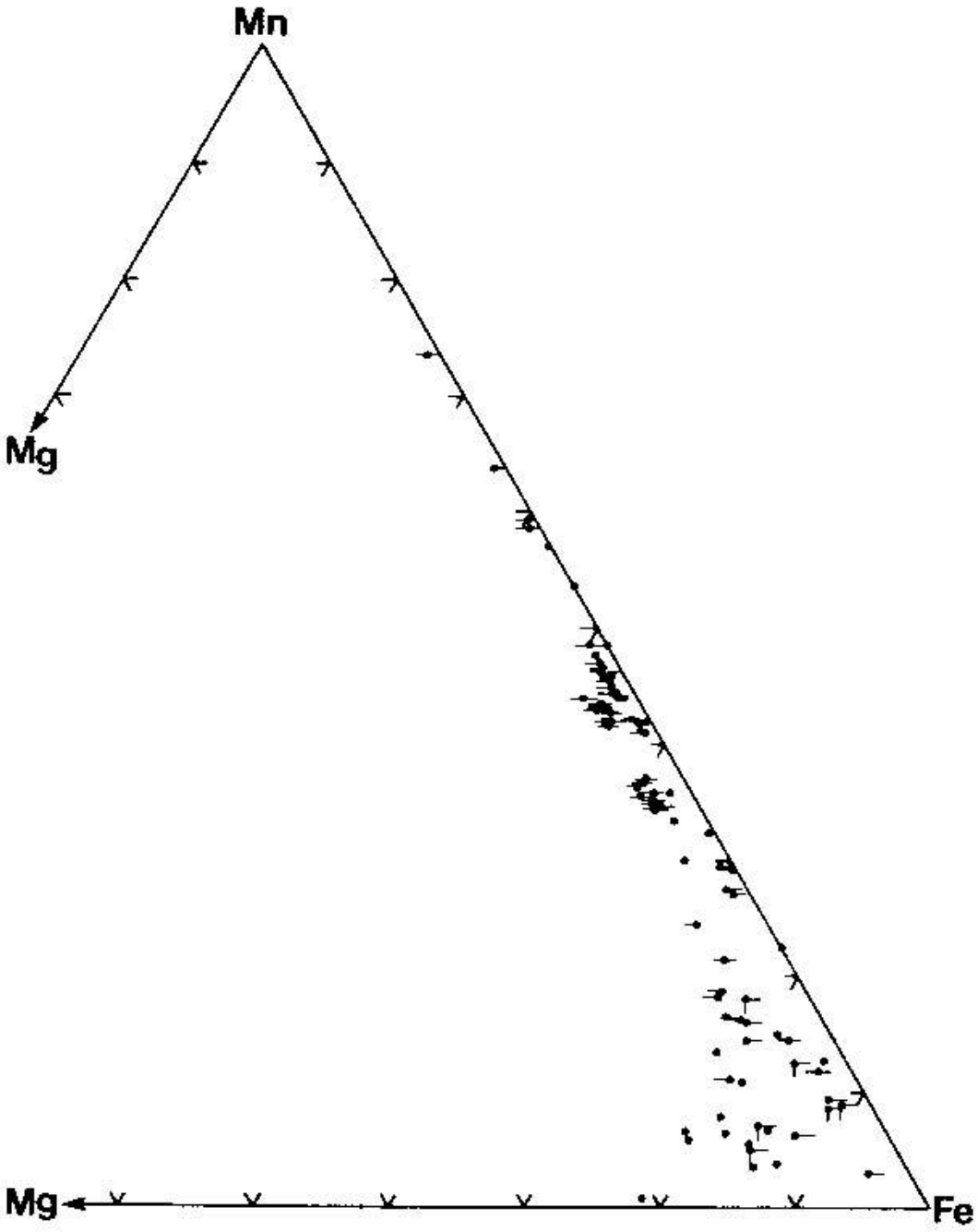

Figure 7 Variation in Mn:Fe:Mg ratios of garnets from peraluminous granitoid rocks. Largest variation is seen in Mn:Fe ratio, with most garnets richer in almandine than spessartine component. From Clarke, 1981.

Muscovite is a common indicator mineral for peraluminous granitic rocks, and may be present in granitic rocks as primary muscovite, that which crystallized from the magma, or secondary muscovite, that which forms from recrystallization or alteration of another aluminous mineral (Miller et al., 1981). Primary muscovite is usually coarse-grained, euhedral or subhedral, and is sharply terminated (Miller et al., 1981). Primary igneous muscovite may be richer in titanium, sodium, and aluminum, and poorer in magnesium and silicon than secondary muscovite (Figure 8) (Miller et al., 1981). Secondary muscovite is commonly finer-grained, subhedral or anhedral, and may enclose or be enclosed by another aluminous mineral (from which it formed) (Miller et al., 1981). Although muscovite is considered a white mica, tinting in several shades from trace elements is possible.

Muscovite in the Spruce Pine granitoids ranges in color from green to red to red-brown (Brobst, 1962; Parker, 1952). The mica in a single pegmatite is either of one color throughout or of two colors, each being limited to a distinct unit in the pegmatite (Parker, 1952). The green tint of some Spruce Pine muscovite is attributed to a few weight percent iron in the crystal structure. Muscovite grains range from small flakes (<1mm) to books as large as 4300 lbs (Parker, 1952). Inclusions of minerals between the sheets of muscovite are common and include quartz, plagioclase, garnet, biotite, apatite, epidote, tourmaline, and kyanite (Parker, 1952). Both plagioclase and alkali feldspar are usually present in peraluminous granites. Granitic plagioclase is more sodic than plagioclase crystallized from more basic rocks like basalt, as granitoids tend to have higher concentrations of sodium than more basic rocks (Deer et al., 1992).

Like other solid solution minerals, there is no fine line between plagioclase compositions that will or will not be found in granitoid rocks. However, plagioclase with more than around 40

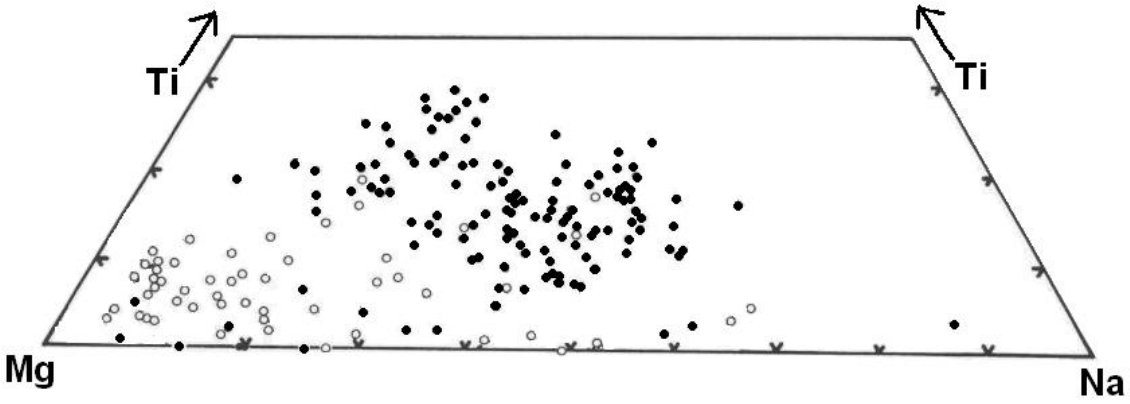

Figure 8 Compositional range of igneous muscovite. Primary (filled dot) and secondary (open circle) muscovite grains in granitoid plutons modified from Miller et al., (1981). Primary muscovite tends to be richer in Na and Ti than secondary muscovite.

to 50 percent anorthite component is uncharacteristic of granites and granitic pegmatites. Albite twinning is common in plagioclase. Alkali feldspar from granites generally ranges from ~20 to ~90 percent orthoclase component, but is reported to reach 97 percent orthoclase component in some plutons (Deer et al., 1992). Alkali feldspar is commonly twinned according to the Carlsbad and Pericline laws.

Feldspar, which makes up roughly 60 to 70 volume percent of the Spruce Pine granitoids, is perthitic microcline and plagioclase ranging in composition from Ab_{70} to Ab_{94} (Maurice, 1940; Parker, 1952; Brobst, 1962). Parker (1952) concurs that most of the plagioclase is oligoclase. Plagioclase is generally most abundant and microcline usually comprises the largest crystals (Brobst, 1962). Microcline-rich pegmatites commonly have cores of smoky quartz, with or without microcline crystals (Brobst, 1962). Graphic intergrowth of feldspar and quartz are common in pegmatites in the Spruce Pine area.

Accessory minerals in the Spruce Pine granodiorites and pegmatites include biotite, garnet, allanite, thulite, pyrite, pyrrhotite, epidote, beryl, tourmaline, columbite, tantalite, clinozoisite, pumpellyite, autunite, torbernite, apatite, uranium minerals, and samarskite (Parker, 1952; Brobst, 1962).

Crystallization History of Spruce Pine Pegmatites

The water-rich parent magma of the Spruce Pine Plutonic Suite formed deep in the crust and intruded metamorphic country rock above it. Contacts between host granodiorite and pegmatite units are gradational, indicating that the pegmatitic magma did not intrude the granodiorite from a different source, but formed from the same magma that formed the granodiorite surrounding the pegmatite. Intrusion of pegmatitic magma from a foreign source into granodiorite would have resulted in sharp boundaries between the granodiorite and the

pegmatite dike. Pegmatites in the Spruce Pine area not hosted by granodiorite owe their existence to parent magmas rising from a source deeper in the country rock. The hydrous magma began to cool after emplacement. Crystallization likely began at the contact between the metamorphic host rock and the magma. Plagioclase and muscovite crystals formed in this border zone. The presence of primary muscovite in hydrous melts of compositions similar to that of Spruce Pine implies that water pressures at time of crystallization were 4 kbar or higher, indicating a depth of crystallization of approximately 15 km or deeper (Burnham, 1967). Substitution of other components (e.g. Fe, Mg, Na) in muscovite my reduce this pressure estimate (Miller et al., 1981), but the presence of white mica still indicates at least 2 kbar pressure. Muscovite seems to be the only common primary mineral in felsic plutonic rocks in which the $(K_2O + Na_2O)/Al_2O_3$ ratio is significantly less than in alkali feldspars ($K_2O + Na_2O/Al_2O_3 = 1$) and whose early crystallization will result in residual melt richer in alkalis (Burnham, 1967). As the muscovite crystallized with the plagioclase in the border zone of the cooling magma, the crystallization front is enriched in alkalis and depleted in water. Without excess water, the formation of muscovite is a "self-arresting reaction" (Burnham, 1967). The muscovite stops forming in the crystallizing magma. The excess alkalis in the adjacent magma then begin to form zones rich in alkali feldspar and plagioclase, with little or no muscovite. The inward crystallization of these anhydrous minerals results in an increase in the water content of the adjacent magma. As the feldspars are crystallizing from the melt, quartz begins to crystallize in the core of the pegmatite. Jahns (1982) has shown that crystallization in a pegmatite melt need not be concentric from the margin inward, but can occur simultaneously in two or more zones. Quartz and alkali feldspar, which make up most of the pegmatite, crystallize over a temperature interval of only 10 or 15°C (Burnham and Nekvasil, 1986). Simultaneous

crystallization of alkali feldspar and quartz results in graphic intergrowths of the two minerals (Fenn, 1986) and may also explain the large euhedral perthite crystals that appear to "float" in the quartz cores of many pegmatites in the Spruce Pine area. Crystallization of anhydrous alkali feldspar, plagioclase, and quartz continues to pump water into the adjacent magma until the magma reaches saturation with respect to this fluid phase. As the magma becomes saturated with water, an aqueous phase is exsolved (Jahns, 1982). All sodium and potassium in excess of feldspar will be segregated into the exsolving fluid-rich phase (Burnham, 1967). The K/K + Na ratio is lower in the aqueous phase than in the coexisting condensed phases at all pressures and temperatures (Burnham, 1967). Figure 9 illustrates the normative composition of the aqueous phase in equilibrium with Spruce Pine pegmatite (Burnham, 1967). Exsolution of the fluid phase, referred to as resurgent boiling (Jahns, 1982), increases the pressure inside the crystallizing magma. The solid portion of the body may fracture when this internal pressure rises, allowing the exsolved phases to escape into surrounding areas of lower pressure, thus lowering the pressure of the rest of the crystallizing magma. As pressure decreases, dissolved solute in the aqueous phase decreases as well (Burnham, 1967). As pressure increases during resurgent boiling, more solute is dissolved into the exsolving aqueous phase. The sudden drop in pressure accompanying fracture of the solid portion of the body is likely to result in crystallization of the dissolved solute and the magma itself. Crystallization of fluids injected along the fractures in previously crystallized magma produces the dikes of pegmatite with sharp contacts that intrude the granodiorite. Decreasing pressure also makes the aqueous phase richer in normative quartz and poorer in normative albite or normative orthoclase (Burnham, 1967). Muscovite begins to form again using the water and potassium that has been concentrated in the

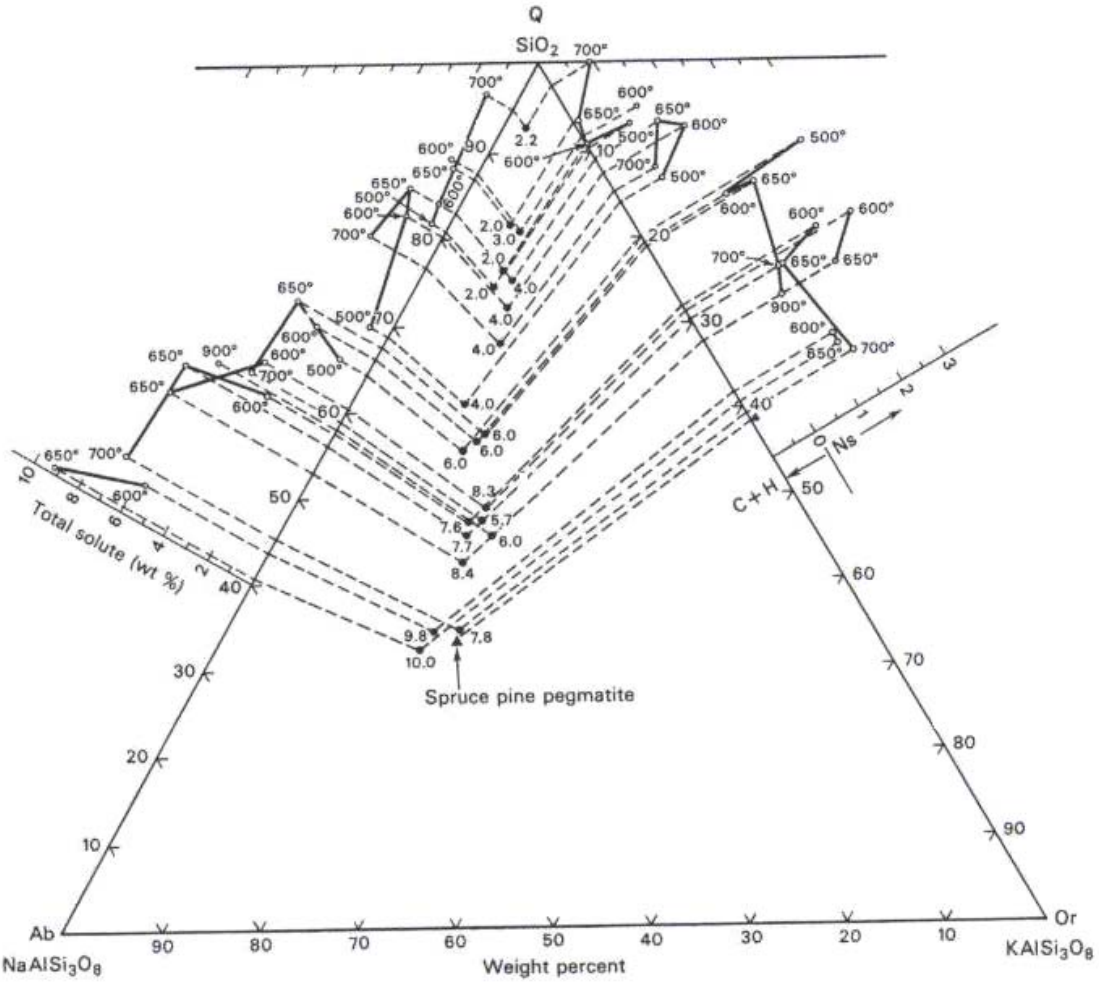

Figure 9 Normative composition of aqueous phase in equilibrium with Spruce Pine pegmatite. Spruce Pine pegmatite is indicated by triangle, field is projected from H_2O to the Ab-Or-Q plane (granitic plane). Aqueous phase is initially H_2O. Numbers next to data points are pressures in kilobars. Experimental temperatures are indicated on side diagrams. The total solute content of aqueous phase (in weight percent) as projected from Or corner is shown on left side of diagram. Normative sodium silicate (Ns) or corundum plus hematite (C + H) as projected from Ab corner is shown on right side of diagram. Diagram from Burhnam (1967).

aqueous phase. Large muscovite crystals commonly occupy the edges of quartz cores in Spruce Pine pegmatites (Parker, 1952;Brobst, 1962). These crystals of muscovite may take advantage of the water that migrated out toward the edge of the core as the quartz in the core crystallized. It is important to note that the miarolitic cavities (representing exsolved fluid phase) reported by Wood and Abbott (1996) and found during field work for this project are not in the quartz cores of pegmatites as would be expected if crystallization proceeded from the margin of the pegmatite through to the core. Instead, the magma reached saturation in water fairly early (Burnham and Nekvasil, 1986). The presence of muscovite zones in the pegmatite imply that the Spruce Pine magma was initially undersaturated with muscovite (Burnham and Nekvasil, 1986). When a closed system magma, such as Spruce Pine magma, cooled, the magma became saturated with respect to muscovite (Burnham and Nekvasil, 1986).

CHAPTER 4

METHODS

Field Mapping and Sampling

When selecting sites for study, the main criteria were access, quality of exposure of the host granodiorite and pegmatite, and ability to be sampled. Most land in the Spruce Pine area is privately owned by individuals or companies. Access to active mining sites is routinely denied due to liability issues. Many recent, fresh exposures were found at quarries and mines in various plutons, but access is difficult. The site to be studied needed a good exposure of granitic host rock and pegmatite. The site also must be conducive to sampling of appropriate zones of pegmatites.

Once a site within an area was chosen, meter tapes were stretched over the outcrop to form a grid. The grid was then transferred onto graph paper and the textural and compositional zones in the pegmatite were mapped to appropriate scale. Mineral assemblages in zones were noted using symbols similar to those of Cameron et al. (1949). Large (>3 cm diameter) single crystals, usually muscovite books and alkali feldspar crystals projecting or "floating" in the smoky quartz cores of the pegmatites, were mapped as individual grains.

The best locations for samples in the exposure were determined after the exposure was mapped. Samples were then retrieved, labeled, and their locations plotted on the map. Attempts were made to retrieve representative samples from each pegmatite zone and host material. Sampling of some zones was prevented due to difficulty of retrieving samples of appropriate size, friability of rock, and inaccessibility. Exposures on smooth mine walls proved especially

difficult to sample. Some pegmatite zones are extremely brittle, yielding small fragments of mineral grains and powder when attempts at sampling were made. Others zones are very tenacious and yield only powder when sampling was attempted. Still other zones, particularly in the Hootowl Mine, were not readily accessible due to location high on mine face. Sampling is limited to what could be retrieved in usable size and condition for thin sectioning.

Samples of appropriate size were slabbed and stained for feldspar determination. The staining procedures of Laniz et al. (1964) were used. Staining revealed the grain size of Spruce Pine granodiorites is highly variable (Figure10). Individual crystals in the stained slabs range from a few mms to cms in size. The basic premise of point counting in modal analysis is that the spacing between individual points is greater than the size of individual phases (Van der Plas and Tobi, 1965). Maximum grain size in the stained slabs is over 15 cm. Thus the point spacing for modal analysis of slabs should be greater than 15 cm, resulting in only a few points per slab and a poor estimate of modal abundance (Van der Plas and Tobi, 1965). Some of the slabs do not contain large (cm-scale) grains, but the presence of these grains in the outcrop still dictates the use of large point spacing. Hence, modal analysis was not performed on the stained slabs due to the large grain size.

Polished thin sections were made from the samples by Vancouver Petrographics. These thin sections were analyzed by petrographic microscope and electron microprobe. Mineral phases identified included quartz, plagioclase, alkali feldspar, muscovite, garnet, biotite, apatite, zircon, Fe-Ti oxides. Grain sizes in the samples range from < 0.1 mm to > 3 cm. Most samples were two-feldspar assemblages with plagioclase and alkali feldspar, present as perthite, antiperthite, or microcline.

Figure 10 Photograph of stained pegmatite and granodiorite slabs. Alkali feldspar is yellow and plagioclase shows up red. The coarsest grains in these slabs are over 15 cm wide.

Microprobe Procedures

Microprobe analysis of garnet, epidote, muscovite, and feldspar in polished thin sections were performed using the JEOL 8600 Superprobe electron microprobe at the University of Georgia. Minerals were used as standards. Routine machine conditions used an accelerating voltage of 15 keV and a 15 nA beam current. The beam was aligned and stabilized at the beginning of each microprobe session. Spot size was 5 microns for alkali feldspar and mica and 10 microns for plagioclase to prevent loss of alkalis. Details of microprobe analyses are given in Appendix A.

CHAPTER 5

BODIES STUDIED

Locations of bodies studied in the Spruce Pine area are illustrated in Figure 11. Locations range from abandoned mining sites to unmined outcrops.

Crabtree Creek Exposure

The Crabtree Creek Exposure (Figure 12) consists of an approximately 20 meter wide exposure of granodiorite and zoned pegmatite on Crabtree Creek Road in Mitchell County, North Carolina. The exposure mapped strikes N 45°W. This exposure is mainly granodiorite but grades into coarse-grained alkali feldspar-plagioclase-muscovite-garnet-quartz pegmatite (Figure 13). The rock at this location is fresh and unweathered. Grain size of the granodiorite ranges from less than 1 mm to 2 cm and contains areas of high concentrations of dendritic biotite locally called a crow's foot texture. Contact between granodiorite and pegmatite is gradational in the Crabtree Creek exposure. Granodiorite gradually coarsens to pegmatitic texture over about 10 cm. Grain sizes in the pegmatite range from less than 1 mm for garnets to greater than 16 cm for subhedral alkali feldspar crystals. This pegmatite contains a solid smoky gray quartz core with no distinct crystals visible. Large crystals of green muscovite, up to 8 cm in diameter and 4 cm thick, are concentrated along the margin of the quartz core. Occasionally, muscovite books of similar size appear to "float" in the quartz core. The pegmatite zone ranges from 30 cm to 60 cm wide and dips 65° NE. Ten samples were taken from different zones of this exposure. Representative samples were taken of granodiorite, granodiorite with crows-foot mica, quartz-plagioclase-perthite pegmatite, perthite pegmatite, graphic granite, quartz-plagioclase pegmatite,

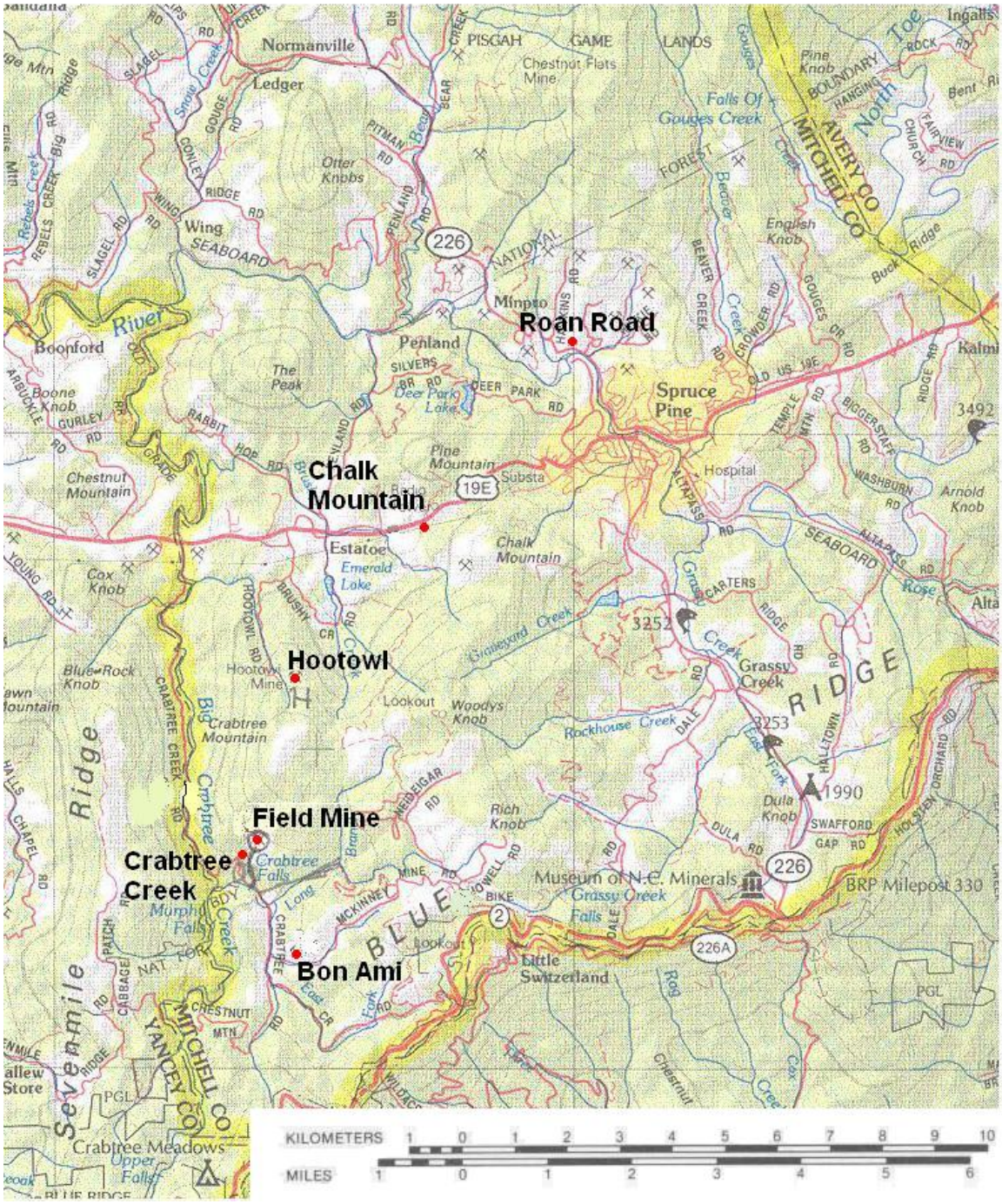

Figure 11 Map of Spruce Pine area with locations of bodies studied. North is toward top of map.

Figure 12 Photograph of Crabtree Creek exposure. Field of view of this pegmatite and granodiorite exposure on Crabtree Creek Road is 3 meters wide. Coarse-grained pegmatite zone left of vertical measuring tape dips to lower left.

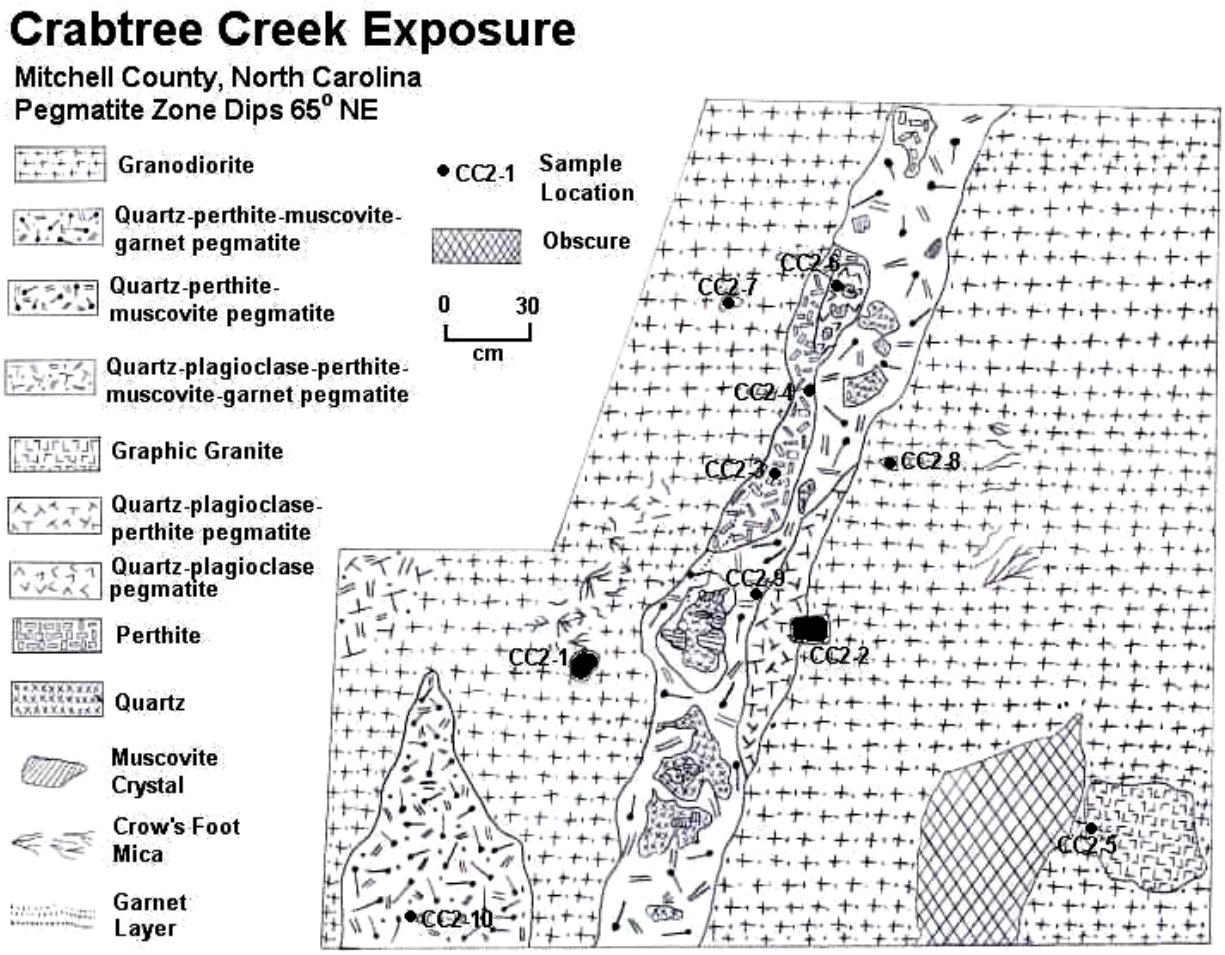

Figure 13 Geologic map of Crabtree Creek exposure. Sample locations are noted with the sample label in the appropriate area on the outcrop.

quartz-perthite-muscovite pegmatite, and quartz-perthite-muscovite-garnet pegmatite. These samples are labeled CC 2-1 through CC2-10. Sample locations are plotted on Figure 13. There was no visible metamorphic host material in the area.

Field Mine

The Field Mine is located approximately 50 meters directly upslope from the exposure along Crabtree Creek Road and is not visible from the road. The area directly in front of the outcrop is covered with saplings. The Field Mine displays a fairly fresh and unweathered rock surface near the base of the exposure. This unweathered rock displays a small zone of alkali feldspar-muscovite pegmatite with a thin, tenuous smoky gray quartz core (Figure 14). Pegmatite zone and quartz core dip ~ 40° S. Contact between the host granodiorite and pegmatite zone in this outcrop is sharp, with finer-grained granodiorite directly in contact with large, pegmatitic feldspar crystals. The host granodiorite contains patches of crow's foot textured biotite mica. Two samples (CC1-1, CC1-3) of this unweathered granodiorite (one with crows- foot mica texture) and one sample (CC1-2) of quartz-plagioclase-muscovite pegmatite were taken (Figure 15). Upslope from the unweathered rock, the granodiorite becomes highly weathered and saprolitic. Feldspars in this portion of the rock have altered to clays, leaving a white powder on tools and hands. Euhedral books of green muscovite ranging in size from less than 1 cm to about 3 cm are easily recovered from this frail weathered material. There was no visible metamorphic host material in the area.

Bon Ami Mine

The Bon Ami Mine is located on McKinney Mine Road in Mitchell County, North Carolina. A mining museum is open at this mine and, for a small fee, visitors can enter the mine

Figure 14 Photograph of Field Mine pegmatite and granodiorite. Field of view in this photo is about 1 meter. The coarse-grained pegmatite is easily discerned against the finer-grained granodiorite host. Gray areas are massive smoky quartz. Grain sizes in this pegmatite increase rapidly over a short distance, about 1 cm.

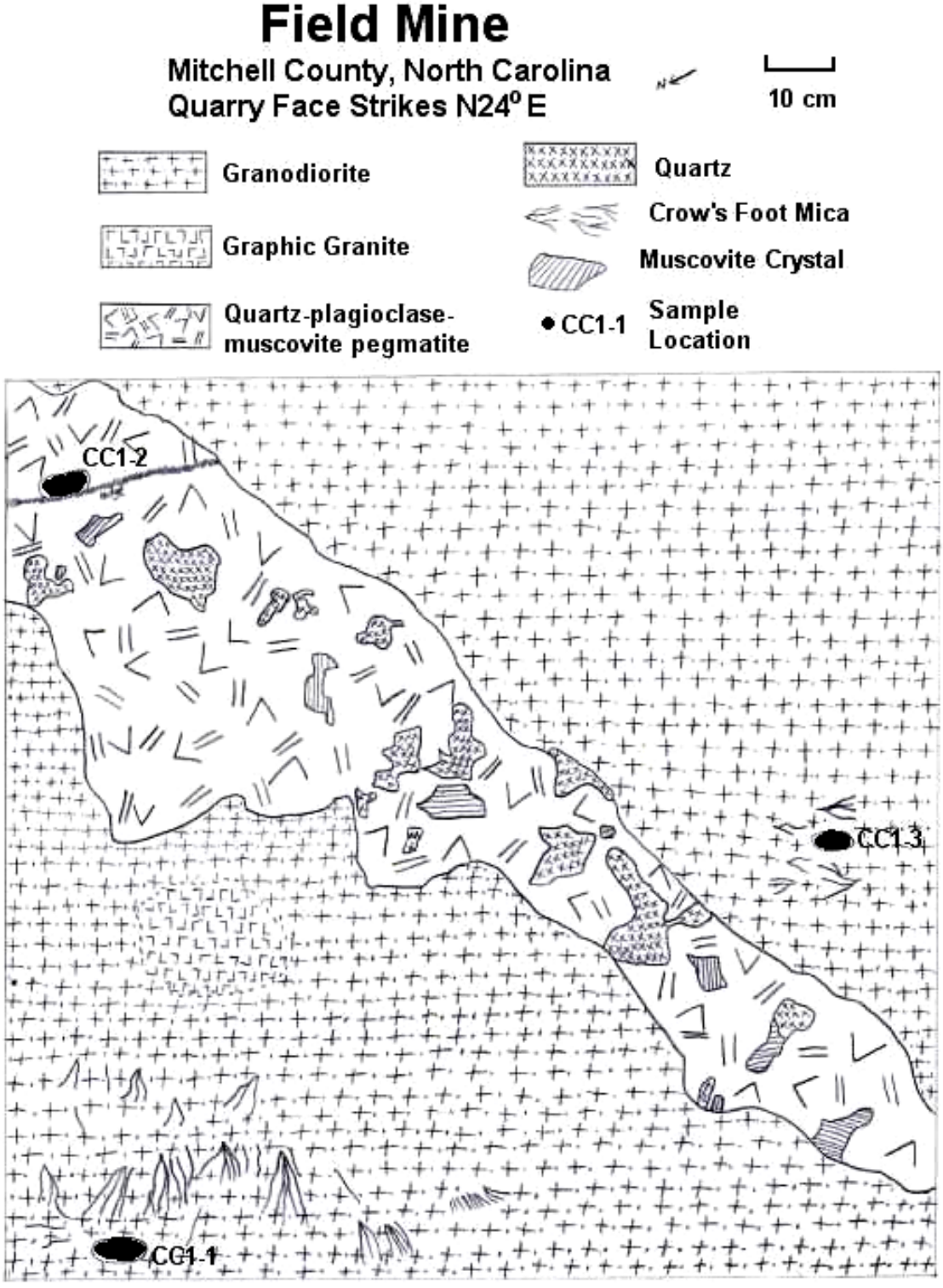

Figure 15 Geologic map of Field Mine pegmatite. Sample locations are noted with the sample label in the appropriate area on the outcrop.

and view the pegmatites. This mine, visible from McKinney Mine Road, is a small adit carved into the hillside. There are two openings to the adit, both facing the roadway, and the floor is flooded. The mine walls are almost completely pegmatitic, with various zones and multiple quartz cores. Large, wedge shaped books of muscovite are present in varying sizes, the largest being over 30 cm in diameter. Pegmatite was sampled and mapped at three areas in the Bon Ami mine. The three areas sampled and mapped are plotted on the map of Bon Ami mine (Figure 16). Bon Ami A, the first Bon Ami study area, is a zoned pegmatite on the back (underground) wall of the mine (Figure 17). The pegmatites on the back wall of the mine can be followed up to the roof. The roof displays several complexly zoned pegmatites with large gray quartz cores and quartz streamers. All zones in these pegmatites are subparallel and strike N 18°E. A representative sample of perthite pegmatite, quartz pegmatite (core), and quartz-plagioclase-perthite-muscovite-garnet pegmatite were taken. These samples are labeled MCK 1-1 through MCK 1-3. Sample locations are illustrated in Figure 18. Bon Ami B, the second Bon Ami study area, is on the outside of the column left during mining that separates the two openings (Figure 16). This rock face strikes N 85°E and consists of an alkali feldspar pegmatite zone with euhedral alkali feldspar crystals projecting into an anhedral, smoky gray quartz core (Figure 19). Two representative samples (MCK 2-1 through MCK 2-3) of quartz-plagioclase-perthite-muscovite-garnet pegmatite and one sample (MCK 2-2) of quartz pegmatite (core) were taken. Sample locations are illustrated in Figure 20. The pegmatite dips 80° SW. Slickensides are visible on the edges of this pegmatite and are roughly parallel to the rock face. Bon Ami C, the third Bon Ami study area, is located on the walkway down to the mine just outside of the

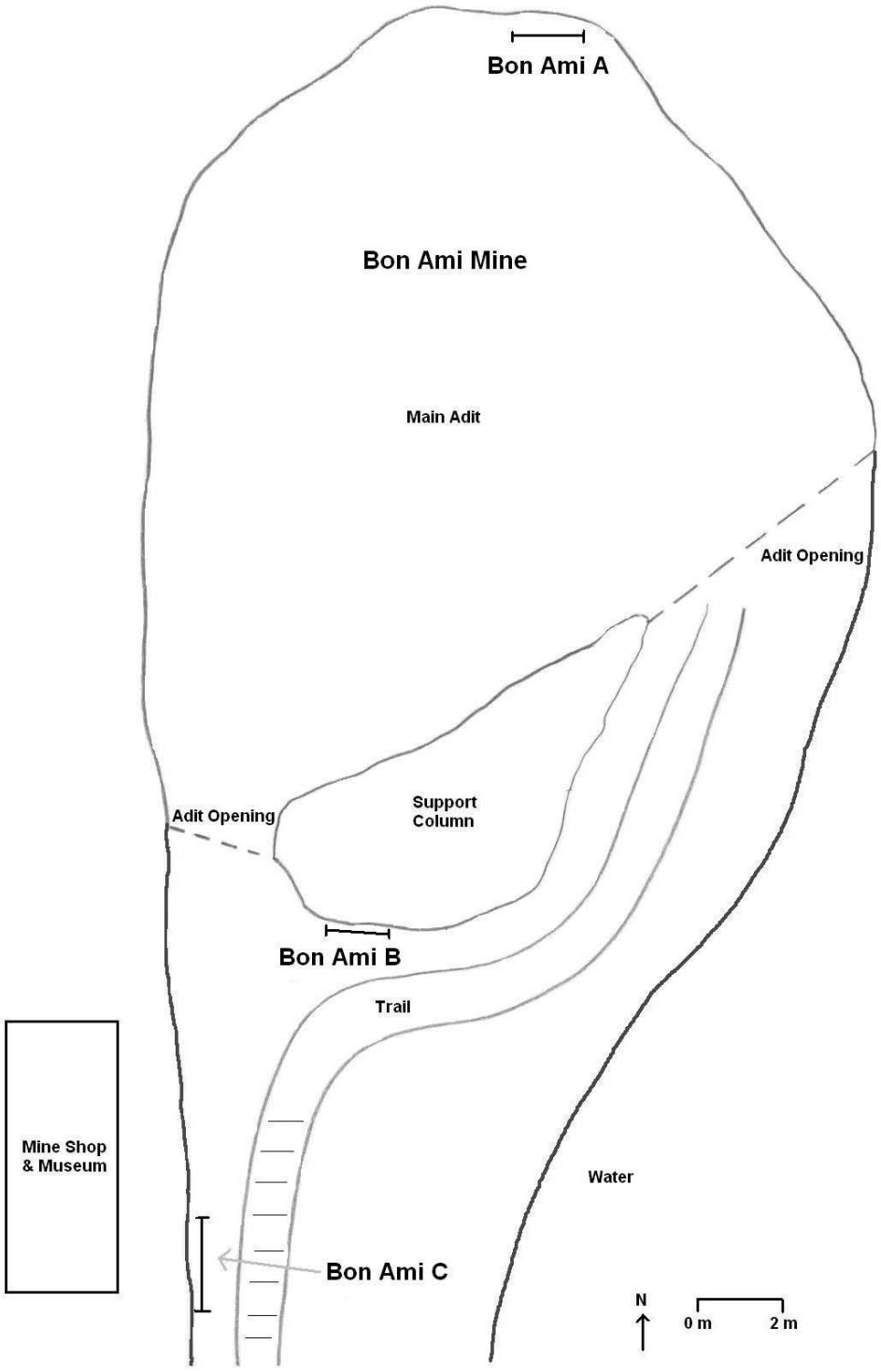

Figure 16 Locations of sampled pegmatite areas in Bon Ami mine. Bon Ami A is at back of underground adit, Bon Ami B is outside of support column, Bon Ami C is at back of Mine Shop and Museum near trail to adit.

Figure 17 Zoned pegmatite in Bon Ami A area. This area is located on the back wall of the adit (see Figure 13). Dark area at bottom of photo is staining left after water was drained from mine. Note parallel textural zoning on either side of smoky quartz core. Field of view in this photo is 4 meters wide.

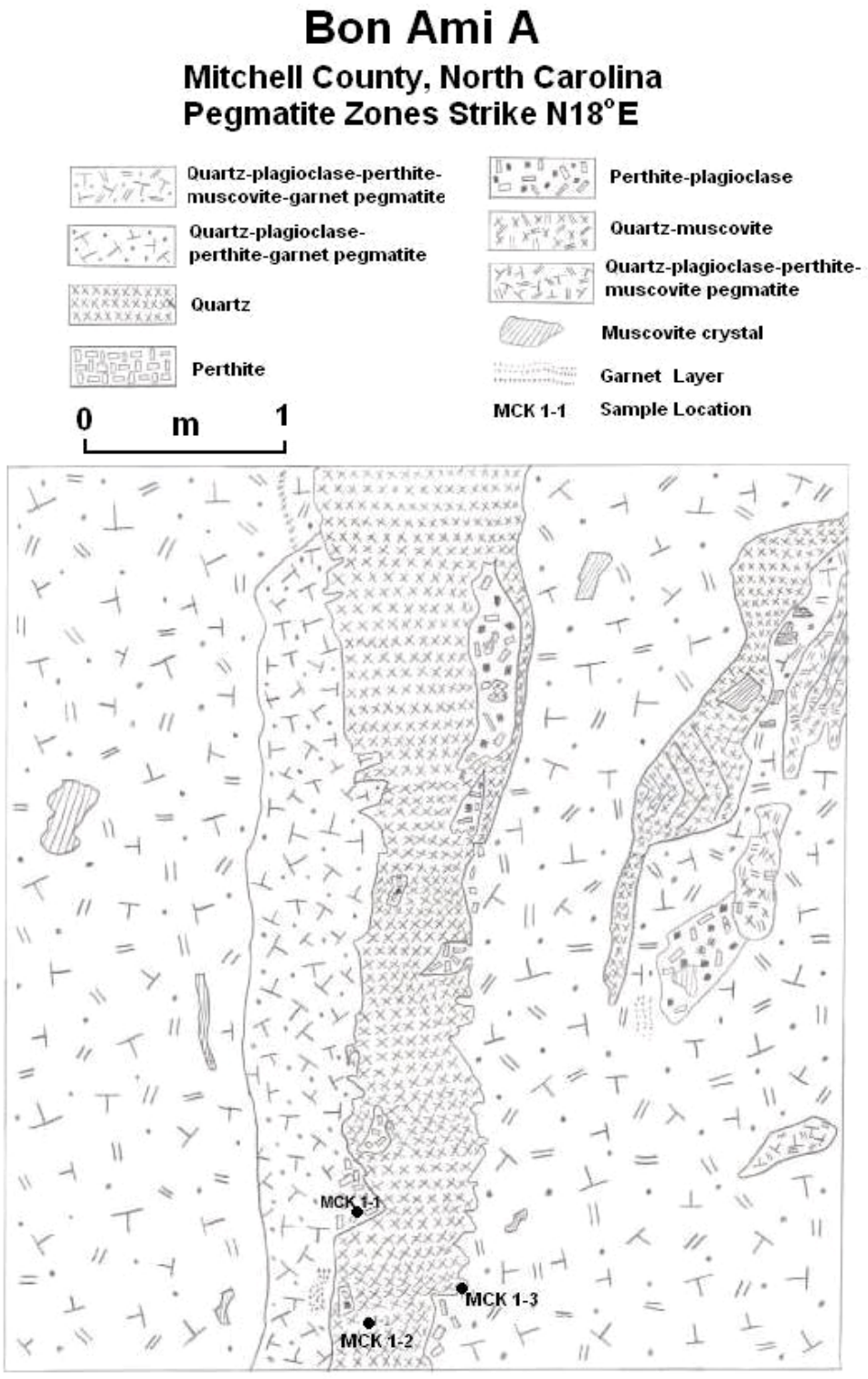

Figure 18 Geologic map of Bon Ami A area. Sample locations are noted with the sample label in the appropriate area on the outcrop.

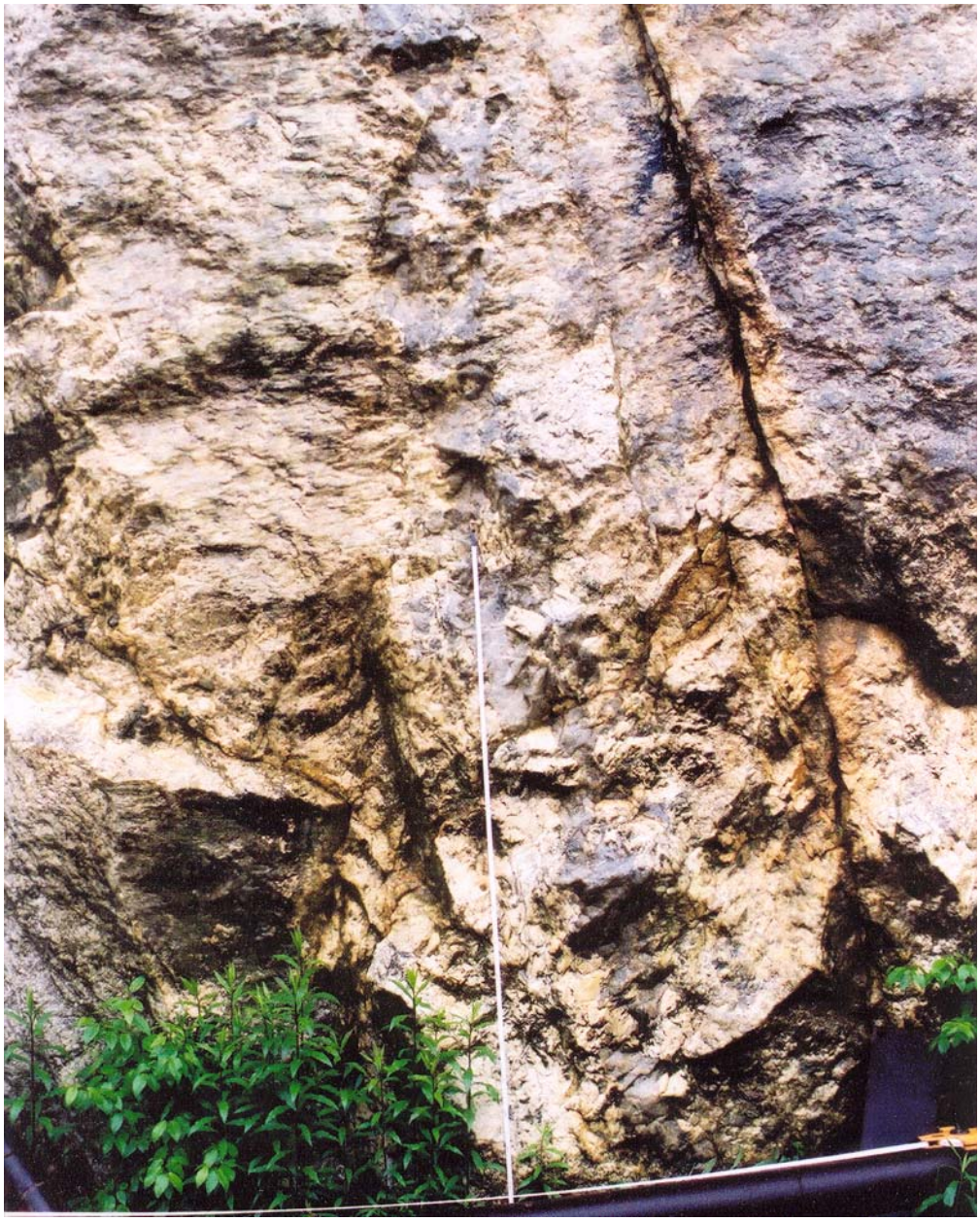

Figure 19 Pegmatite outcrop sampled at Bon Ami B. This pegmatite is located on the outside wall of the column that separates the two adit openings (see Figure 13). Tape lines are in place for mapping of pegmatite zones. Field of view is 2.5 meters wide.

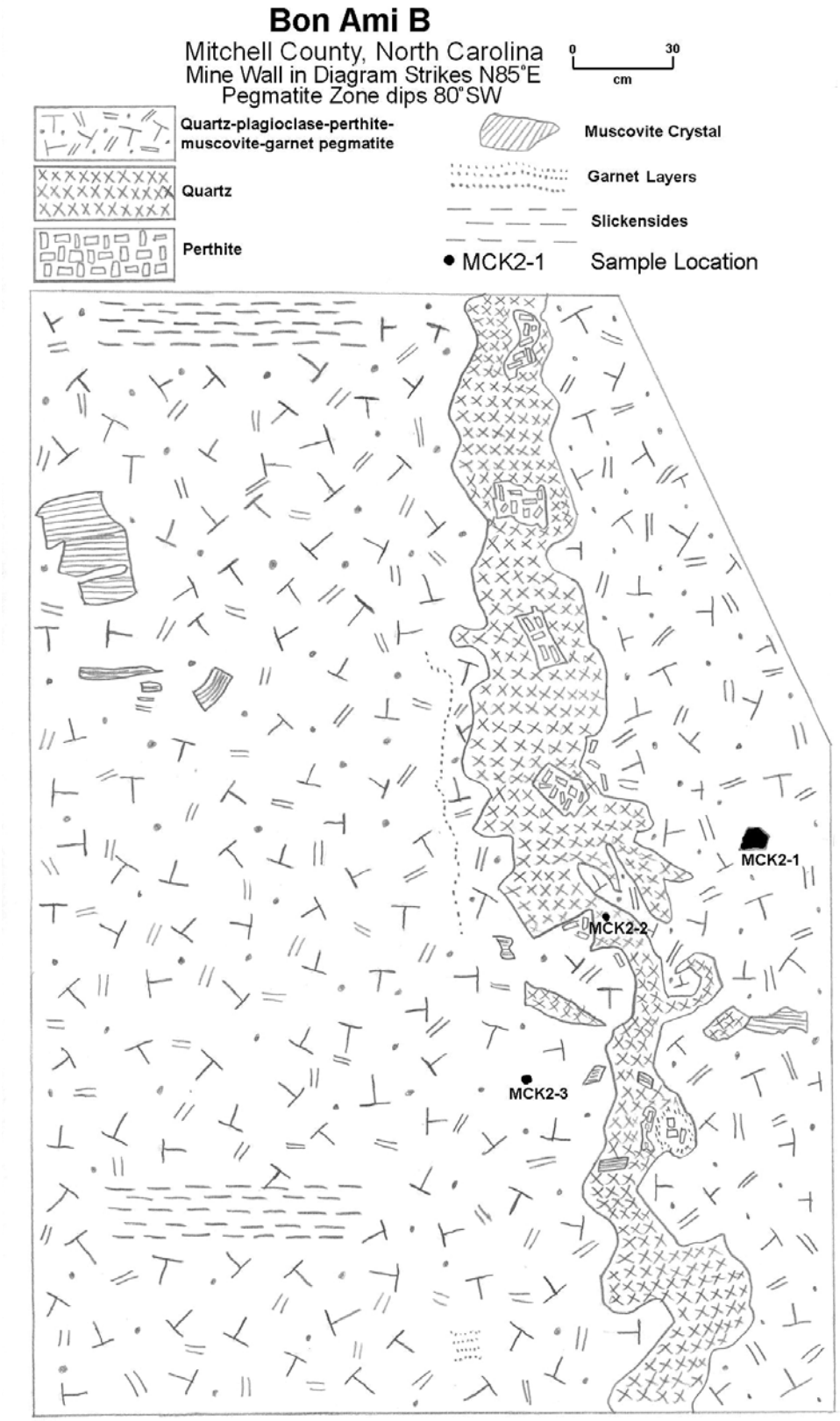

Figure 20 Geologic map of Bon Ami B area. This location is on the outside of the column separating the two openings.

tourist shop (Figure 16). The outcrop forms a wall that strikes roughly N 36°W. This area is more complex and consists of several pegmatite zones, including graphic granite, surrounding a curved smoky gray quartz core (Figure 21). Large green muscovite crystals were concentrated along the margin of the quartz core. Representative samples (MCK 3-1 through MCK 3-6) of host granodiorite, quartz pegmatite (core), and quartz-perthite-muscovite-garnet pegmatite were taken, and their locations plotted on Figure 22.

Hootowl Mine

Hootowl Mine is located at the end of Hootowl Road in Mitchell County, North Carolina (Figure 11). Hootowl mine is a large, cavernous hole in the mountain with two openings and a central support column. The support column is composed of coarse-grained alkali feldspar pegmatite. The roof exposes a small area of biotite schist host rock. Hootowl mine exposes fresh, unweathered coarse-grained granodiorite and several zones of pegmatite. Small miarolitic cavities were identified in samples retrieved from Hootowl. Hootowl was mapped and sampled in two areas, illustrated on Figure 23. The Northwest Hootowl study area is on the northwest wall of the mine just inside the entrance, striking N 45°E. This area displays several pegmatite zones, including alkali feldspar-plagioclase-muscovite-quartz, graphic granite, thin and thick gray quartz cores, burr mica (loosely consolidated small mica books), a biotite schist xenolith and biotite schist host rock (Figure 24). Burr mica is an old miner's term for small books of mica loosely held together with quartz or, as the case seems in Hootowl, smaller crystals of mica and cavities. The biotite schist xenolith is completely enclosed by a quartz-muscovite pegmatite zone. The biotite schist host material is disconnected from the xenolith, but is partially obscured by the floor of the mine, so it is difficult to determine if this is a biotite schist xenolith

Figure 21 Pegmatite outcrop sampled at Bon Ami C area. This pegmatite is located on the back side of the mining museum along the stairs descending to the adit (see Figure 13). Field of view is 3 meters wide.

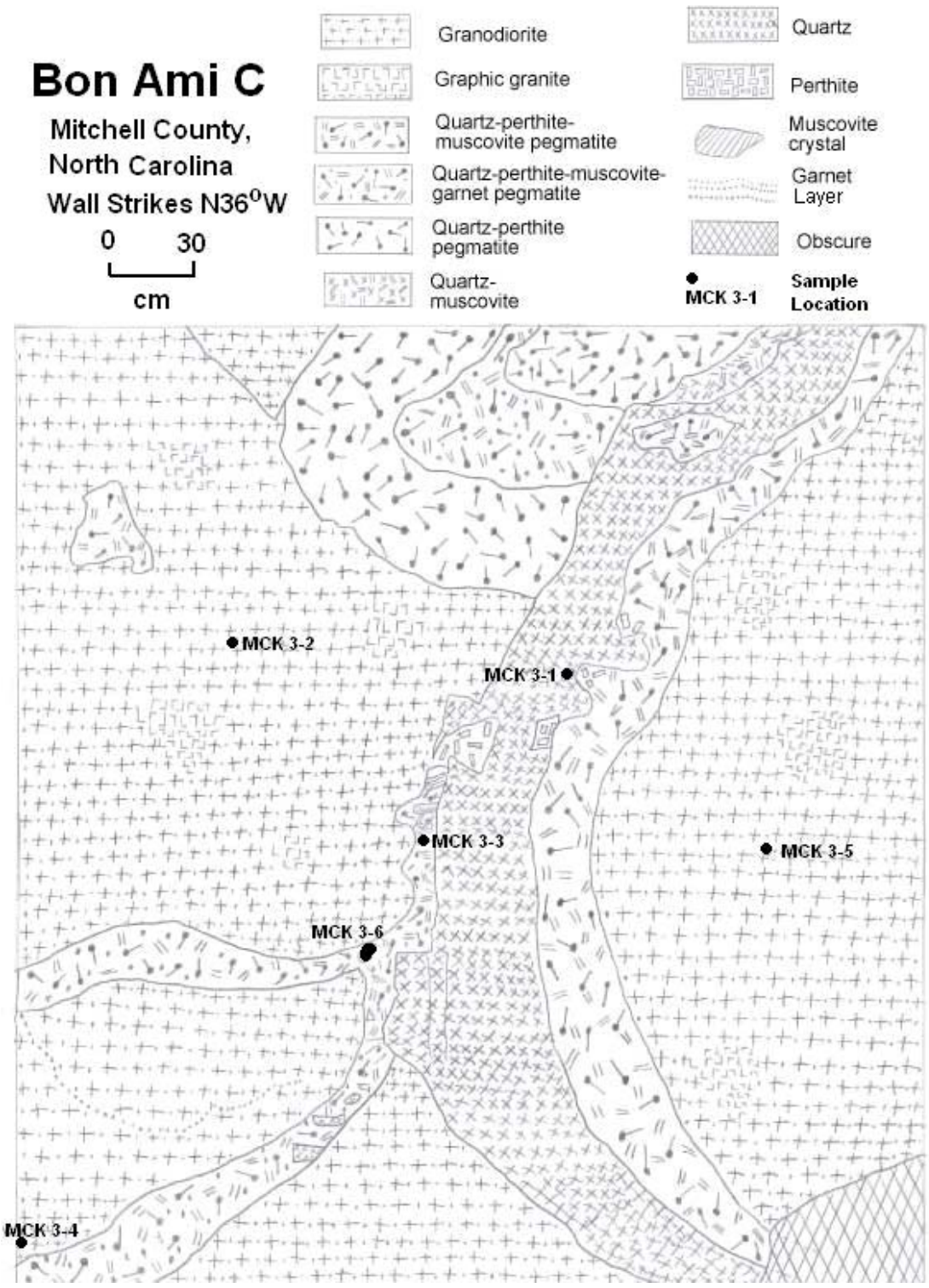

Figure 22 Geologic map of Bon Ami C area. This area is located just behind the mining museum along the stairs to the adit (see Figure 13). Note curvature of the smoky quartz core.

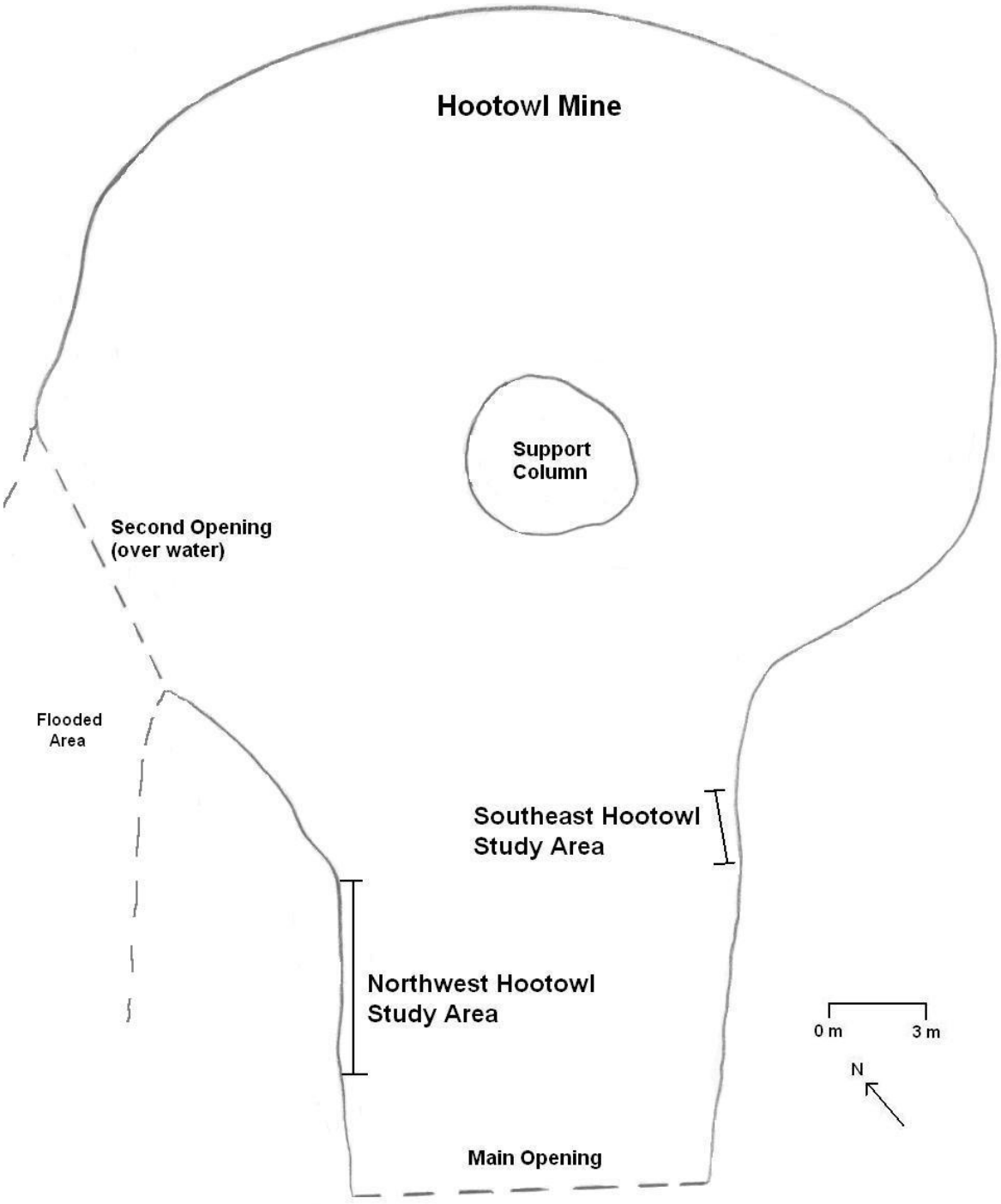

Figure 23 Map of Hootowl Mine with sampled pegmatite locations. Northwest Hootowl study area is located on the northwest wall of main opening. Southeast Hootowl study area is located on the southeast wall of the main opening.

Figure 24 Pegmatite exposure in Northwest Hootowl study area. Note the prominent quartz core dipping down from left. Black rock at bottom right is biotite schist host rock. Green coloration of rock in upper part of photo is due to moss. Leaf strewn floor of mine is seen at bottom. Field of view is about 18 meters wide.

completely surrounded by pegmatite or an upward projection of the metamorphic host rock. Representative samples of the biotite schist xenolith, quartz-muscovite pegmatite, biotite schist host rock, graphic granite, granodiorite/quartz-muscovite pegmatite contact, granodiorite, and a burr mica zone were taken. These samples (HO 1-1 through HO 1-7) are plotted on Figure 25. Miarolitic cavities were identified in sample HO 1-7 from this first mapped area. The Southeast Hootowl study area, is a coarse alkali feldspar-muscovite pegmatite with a gray quartz core hosted by granodiorite (Figure 26). This area is located opposite the first area on the southeast wall and strikes N 20°E. A sample each of granodiorite (HO 2-1) and quartz-plagioclase-muscovite-garnet pegmatite (HO 2-2) was taken and their locations plotted on Figure 27. Several grab samples were taken from material on the floor of the mine and could not be traced back to the area of occurrence. These samples were selected because they represented pegmatite zones present in the mine whose mineral assemblage was not identified in the two areas mapped and could not be located in a reachable area of the mine wall. These samples include quartz-plagioclase-muscovite pegmatite, quartz-plagioclase-muscovite-garnet pegmatite, graphic granite, a large single perthite crystal, and a biotite schist/muscovite-plagioclase-perthite-quartz pegmatite contact zone. Small (< 1cm) miarolitic cavities are visible in the biotite schist/pegmatite contact sample. These grab samples are labeled HOG 1 through HOG 7.

Exposure on Roan Road

A partially mined, exposed pluton of granodiorite is exposed on Roan Road in Mitchell County, North Carolina (Figure 11). This area is a bare rock outcrop with lichens, moss, and a few trees growing on its surface. Part of it has been mined and a block of material is gone, leaving several surfaces of the granodiorite exposed. The exposed material is very slightly weathered. The floor of the mined area is covered with

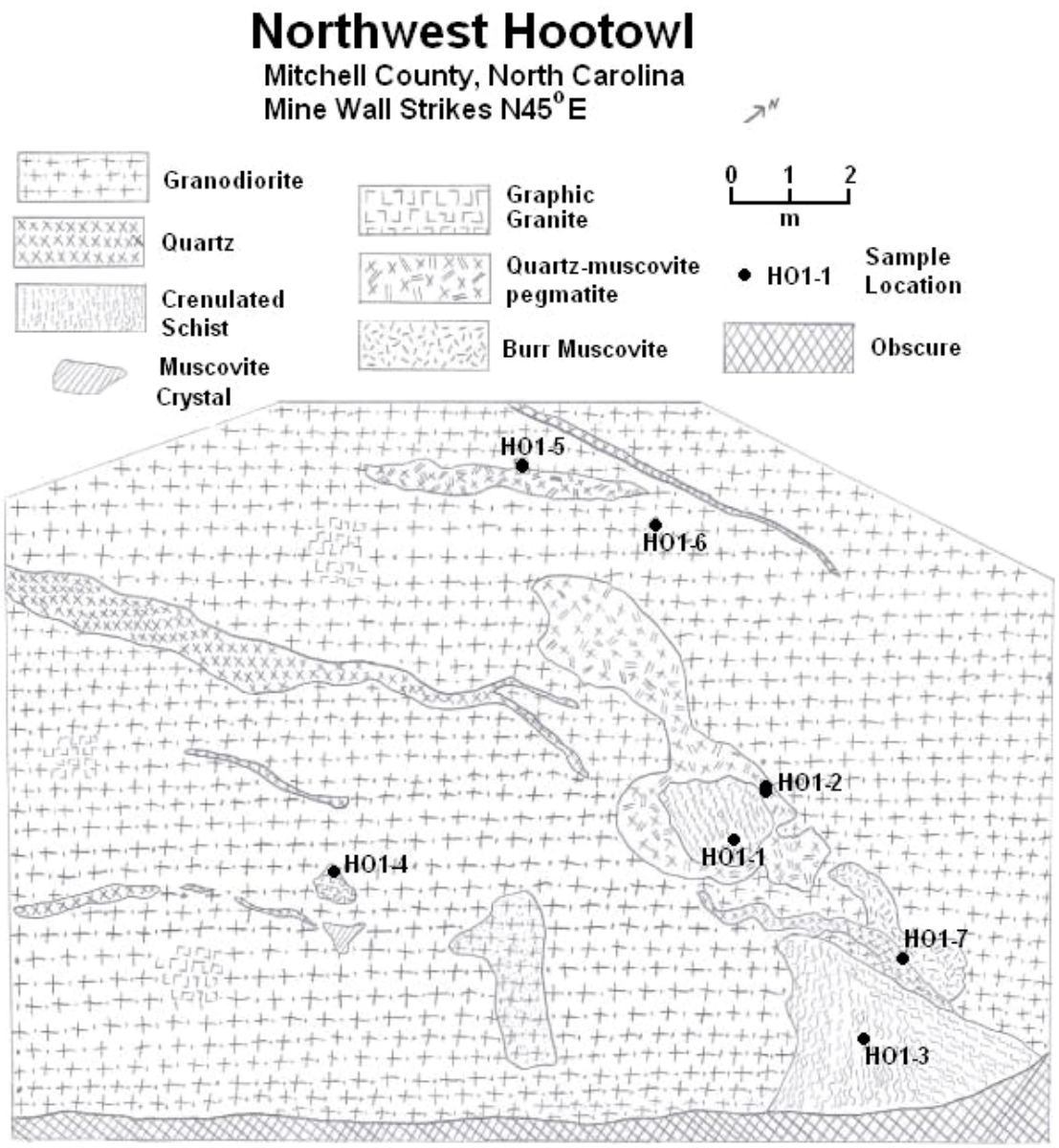

Figure 25 Geologic map of pegmatite exposure at Northwest Hootowl study area.

Figure 26 Pegmatite exposure at Southeast Hootowl study area. Dark crystals in coarse-grained pegmatite in center are muscovite cleavage surfaces. Field of view is 3.5 meters wide.

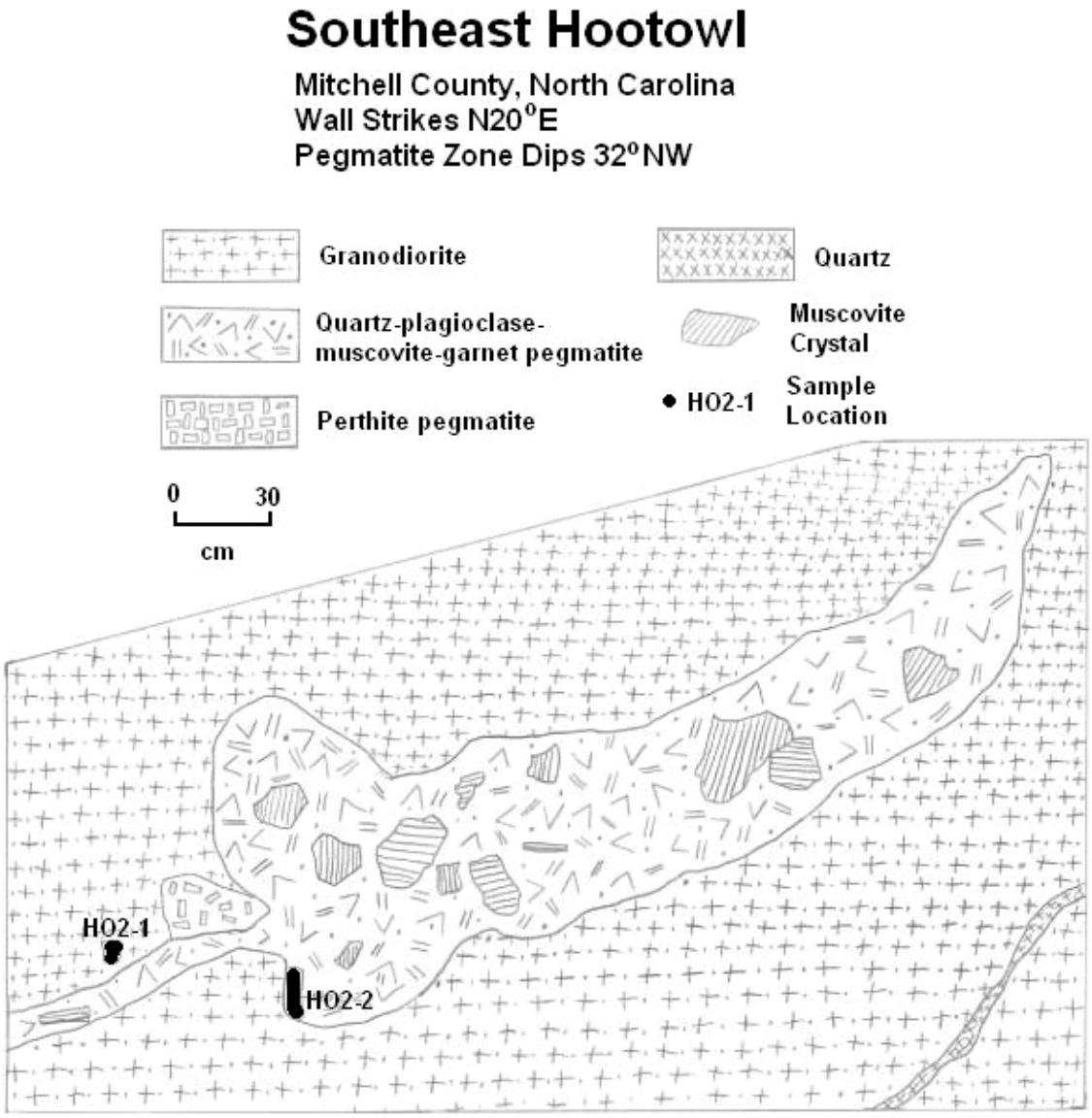

Figure 27 Geologic map of pegmatite exposed at Southeast Hootowl study area.

scrub bushes and trees. The granodiorite from this area is much richer in biotite than the other locations sampled. No zoned pegmatites were seen at this pluton, so no maps were drawn. A representative sample of this medium-grained granodiorite (labeled Roan Road) was taken. This area is visible from Roan Road and is shown in Figure 28.

Figure 28 Roan Road granodiorite outcrop. A small mining pit in this body is located to the right of this exfoliated granodiorite outcrop. Rock exposure in photo is about 10 meters wide.

CHAPTER 6

RESULTS

Mineralogy of the Pegmatites

Garnet

Garnet as red euhedra (<1 to ~15 mm) is a common accessory phase in the biotite schists and amphibolites of the Ashe Metamorphic Suite and in the both pegmatites and host granodiorites of the Spruce Pine Plutonic Suite. Garnet from the pegmatites and granodiorites is unaltered, but chlorite alteration is common in garnets from the Ashe Metamorphic Suite. The igneous garnet observed in this study lacks inclusions of any mineral and is often unfractured.

Garnet is found in all pegmatite zones except for the massive smoky quartz core. The garnet is red-brown and is often accompanied by muscovite. Flattened garnet is sometimes found between cleavage traces in muscovite crystals. Garnet is often euhedral and crystals are generally smaller (<1 – 2mm) in pegmatite zones than in host granodiorite. Small garnet euhedra often occur in patches or lenses with hundreds of tiny crystals clustered densely together. These lenses are common at the margins of pegmatite zones.

Compositions of garnet are given in Appendix C. The garnets are largely almandine-spessartine with less than 10 mole percent grossular and less than 3.3 mole percent pyrope. Rims of some garnet show enrichment in Ca, up to a maximum of 80 mole percent grossular component. Contacts between the Ca-rich rim and the Fe-Mn core of the garnets are abrupt, marked by a narrow zone of intermediate composition (Figure 29).

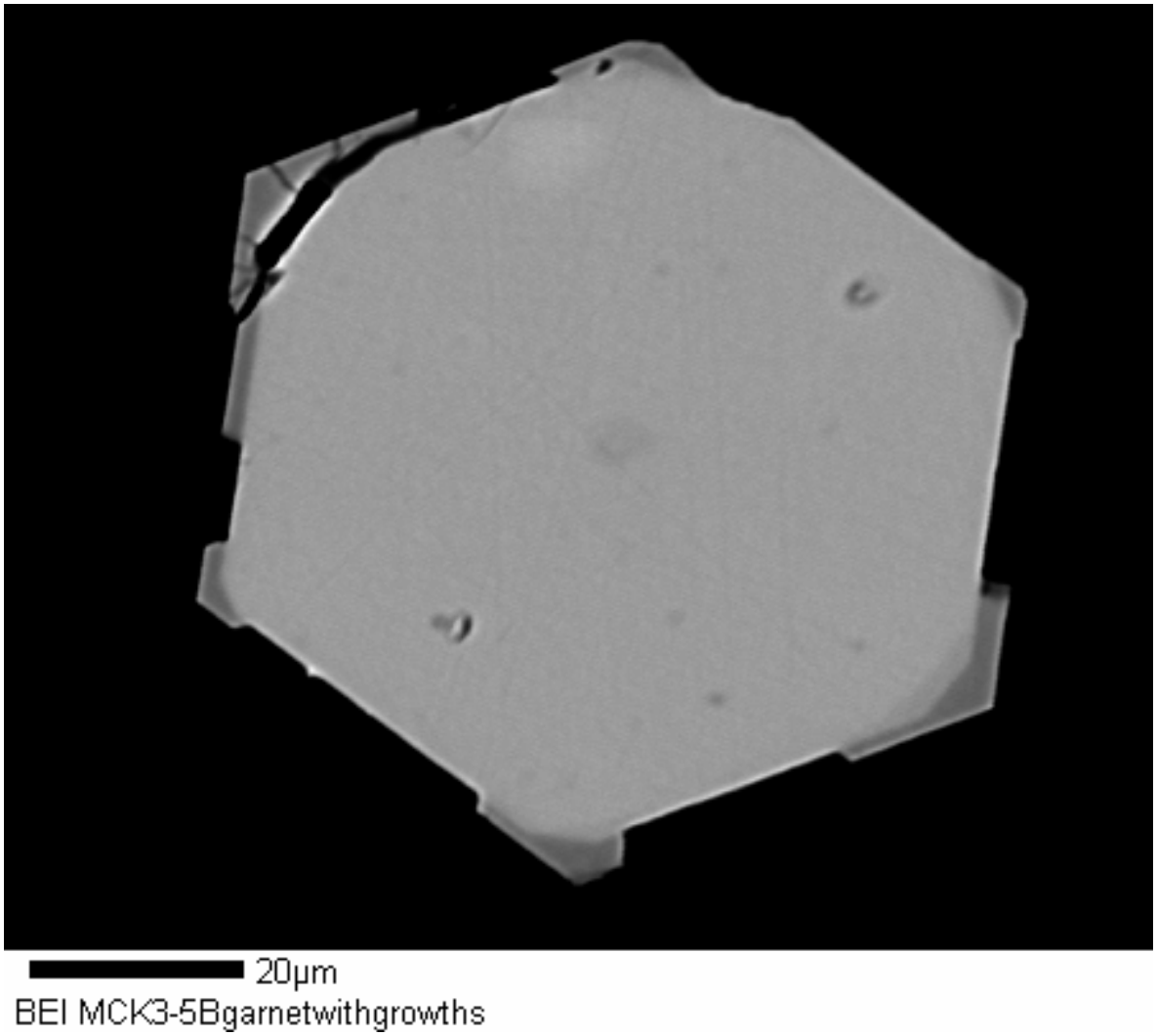

Figure 29 Backscatter electron image of grossular garnet growths on rim of almandine-spessartine garnet from granodiorite in Bon Ami C area (Figure 21). Grossular areas show up as darker gray shades in growths at corners of lighter shaded almandine-spessartine core. Note sharpness of contact between almandine-spessartine and grossular grossular garnet.

Garnet in the granodiorite often forms larger crystals (up to 15 mm) than garnet in the pegmatites, but color and shape remain similar. Garnet cores in the granodiorite are almandine-spessartine in composition and plot in the granitic garnet field compiled from Deer et al. (1992). Granodioritic garnets often display rims of increased grossular component. No garnet approaches end-member grossularite, but Ca-rich rims reach over 80 mole percent grossular component. Titanium is rarely present in detectable levels and chromium is never detected.

Garnet in the pegmatite zones forms small, red-brown crystals that commonly form streaks or lenses within pegmatites and at margins of pegmatite zones. Garnet is present as small, sparse euhedra in graphic granite and perthite pegmatite zones. The range in garnet composition (Fe:Mn ratios) is similar in all pegmatite zones. Grossular rims were observed on garnets from graphic granite, perthite-garnet pegmatite, quartz-plagioclase-muscovite-garnet pegmatite, quartz-plagioclase-perthite-muscovite-garnet pegmatite, and in grab samples from Hootowl Mine. Almandine-spessartine rims were observed on garnets from quartz-plagioclase pegmatite, quartz-plagioclase-muscovite pegmatite, and quartz-perthite-muscovite-garnet pegmatite. Rims were almandine-spessartine in garnets observed from quartz-perthite-muscovite pegmatite, and quartz-muscovite pegmatite.

Pegmatitic garnet compositions from the Field Mine are illustrated in Figure 30. Garnet from pegmatite in the Field Mine is almandine-spessartine and at least one garnet displays mid-Ca rim composition. No granodioritic garnet was analyzed from the Field Mine. Pegmatitic garnet compositions from Bon Ami B are illustrated in Figure 31. Pegmatitic garnet cores from Bon Ami B are low-Ca, almandine-spessartine in composition. Some pegmatitic garnets have mid-Ca rich rims. Garnet compositions in Bon Ami C are illustrated in Figure 32.

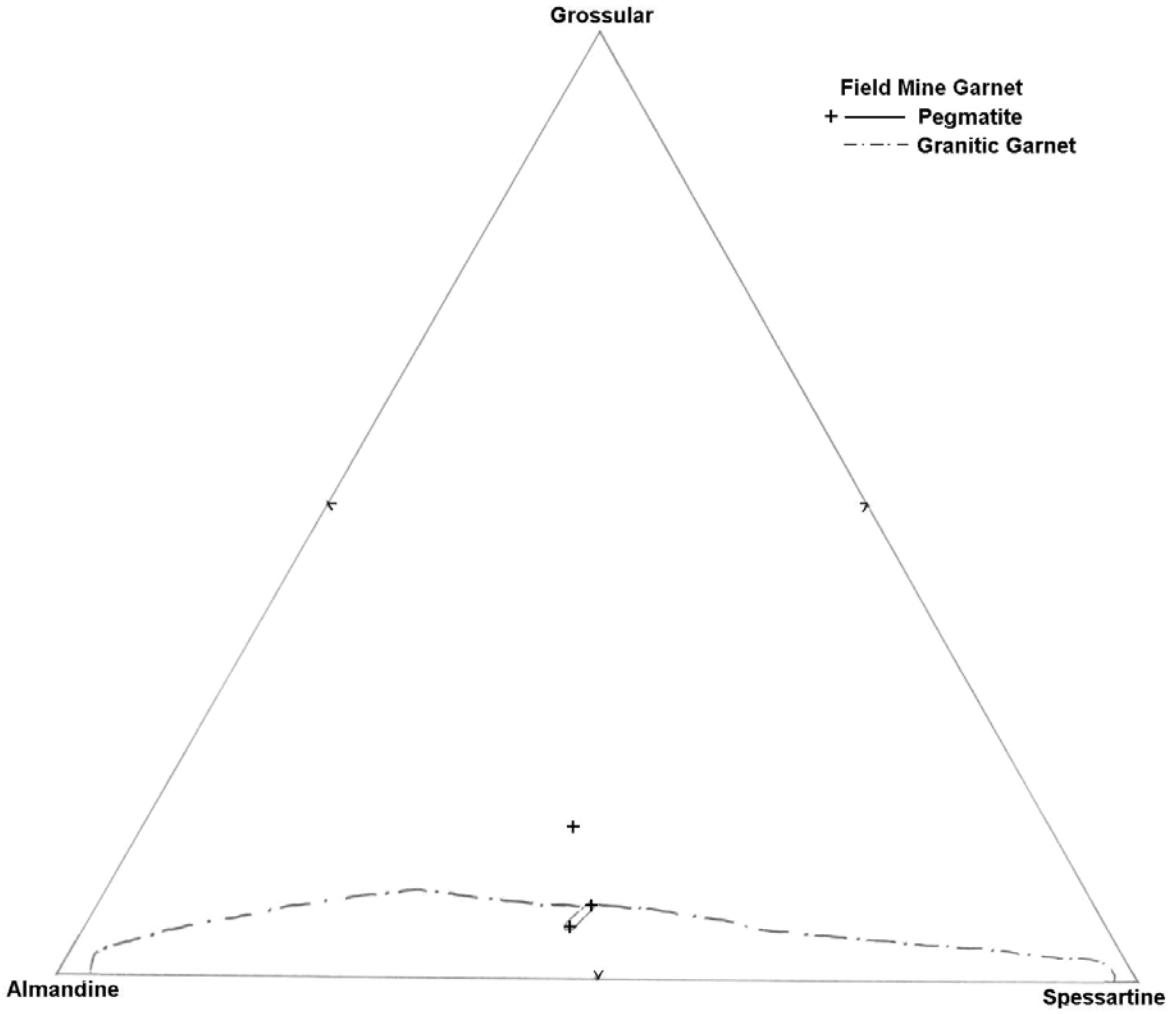

Figure 30 Pegmatitic garnet compositions from Field Mine. Almandine-spessartine cores plot in field for granitic garnet compiled from Deer et al. (1992). Note presence of mid-Ca garnet rim composition.

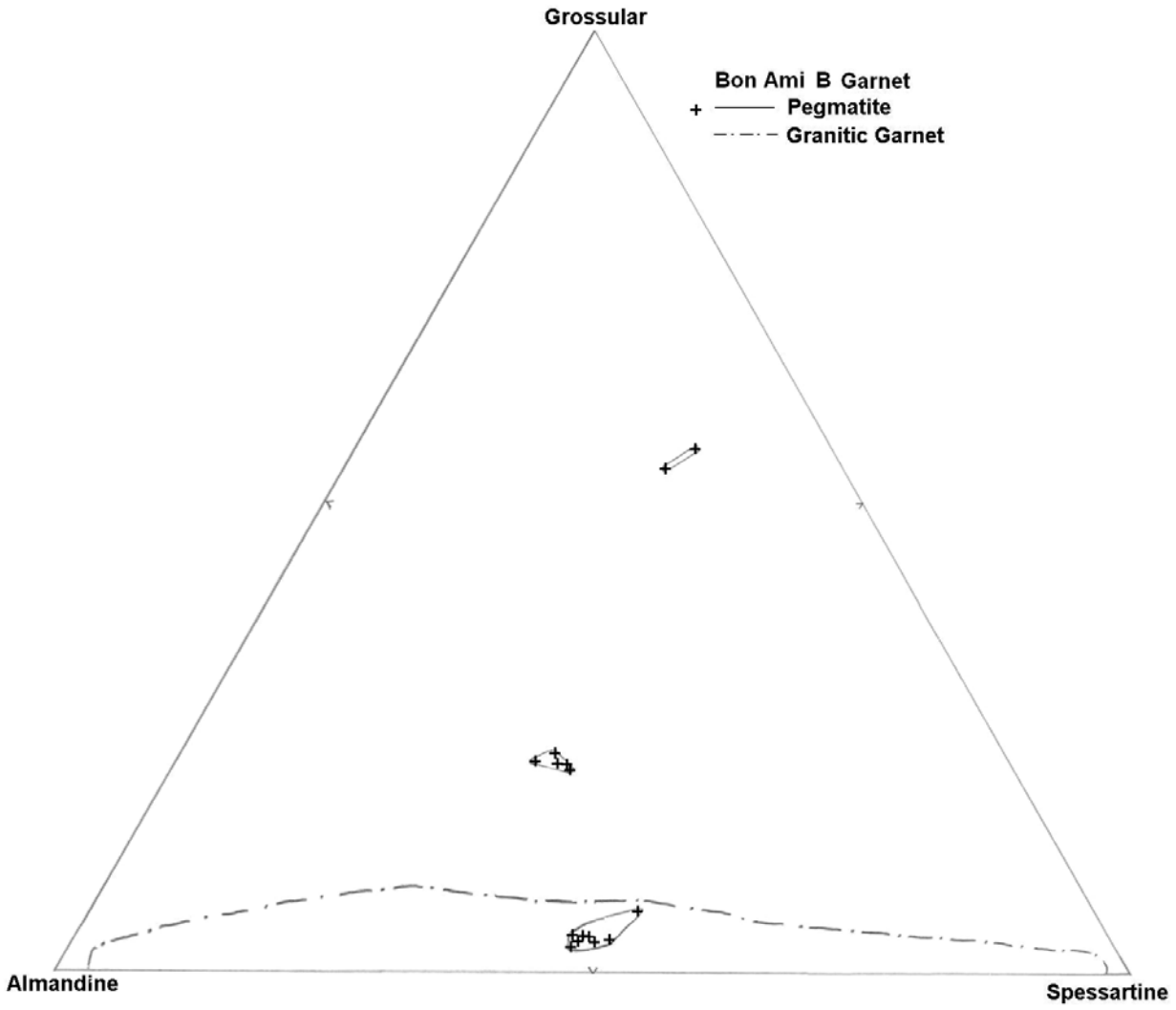

Figure 31 Pegmatitic garnets from Bon Ami B area. Garnet cores are almandine-spessartine and plot in the field for igneous garnet compiled from Deer et al. (1992). Mid-Ca and grossular rims are present in these garnets.

Almandine-spessartine garnet cores all plot within the field for granitic garnet compiled from Deer et al. (1992), while mid-Ca and grossular rims plot into two distinct fields (Figure 32). Mid-Ca and grossular rims are sometimes present on the same garnet (Figure 32). Garnet in the Crabtree Creek exposure is illustrated in Figure 33. Pegmatitic garnet cores from Crabtree Creek are low-Ca, almandine-spessartine in composition. Some pegmatitic garnets have mid-Ca rich rims. Garnet cores from Crabtree Creek granodiorite are almandine-spessartine, and some grains contain mid-Ca and grossular rims. The mid-Ca fields for pegmatitic and granodioritic garnets both contain similar amounts of Ca. Garnet compositions for pegmatitic and granodioritic garnets from Northwest Hootowl pegmatite are illustrated in Figure 34. Garnet cores from the granodiorite are almandine-spessartine and plot within the granitic garnet field compiled from Deer et al. (1992). Some granodioritic garnet grains contain rims of mid-Ca garnet. Garnet cores from the Northwest Hootowl pegmatite are almandine-spessartine and plot in the field for granodioritic garnet cores (Figure 34). A grossular rim was detected on a pegmatitic garnet from the graphic granite zone in Northwest Hootowl study area. Garnet compositions for pegmatitic garnet from the Southeast Hootowl pegmatite are illustrated in Figure 35. Garnet cores are almandine-spessartine and plot in the field for granitic garnet compiled from Deer et al. (1992). One garnet has a mid-Ca rich rim, but most garnet rims are grossular. No granodioritic garnet was analyzed from the Southeast Hootowl study area.

Figure 36 shows composition of garnets from all bodies studied. Almandine-spessartine garnet cores are found in granodiorite and pegmatite from all bodies studied. These cores plot within the granitic garnet compositional field compiled from Deer et al. (1992). Pegmatite and granodiorite garnet compositions from all bodies studied plot into separate distinct fields of almandine-spessartine cores, mid-Ca and grossular rims.

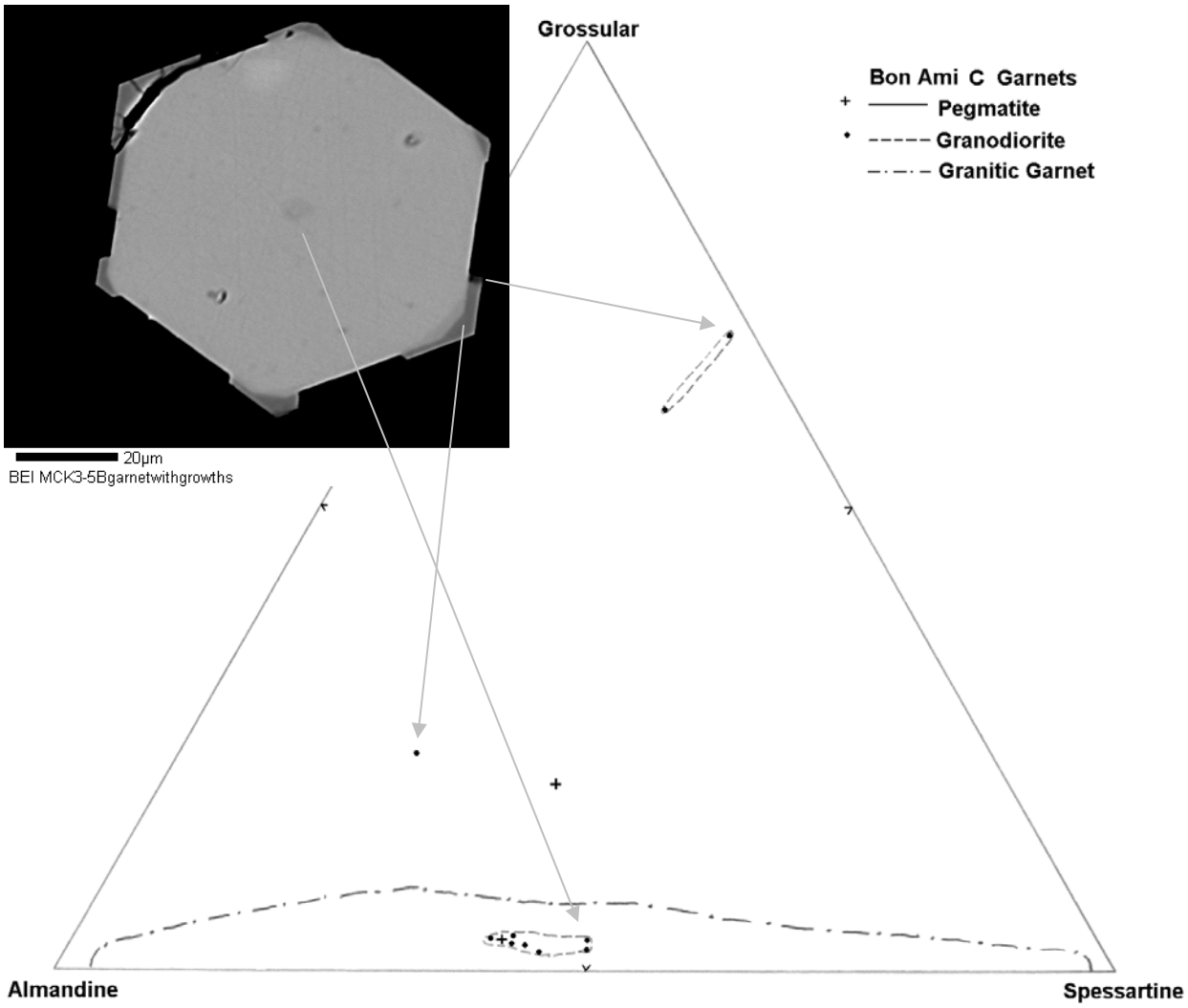

Figure 32 Composition of garnet from Bon Ami C area. Garnet cores are almandine-spessartine and plot in field for granitic garnet compiled from Deer et al. (1992). Note separation into three distinct fields differing in grossular component. Rim compositions of intermediate and grossular concentrations sometimes occur on the same garnet, as illustrated here.

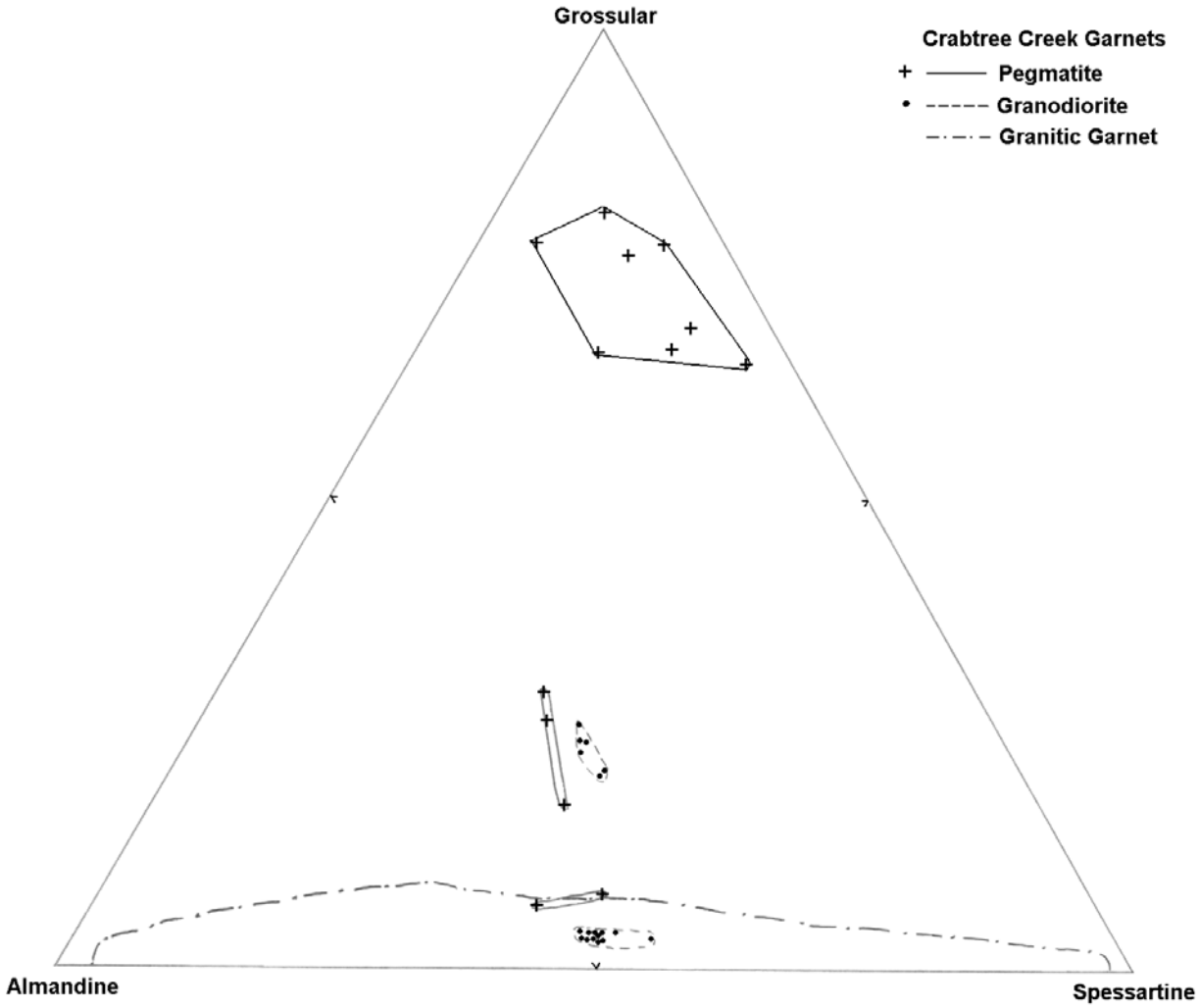

Figure 33 Composition of garnet from Crabtree Creek exposure. Garnet cores are almandine-spessartine and plot in field for granitic garnet compiled from Deer et al. (1992). Note separation into three distinct fields differing in grossular component.

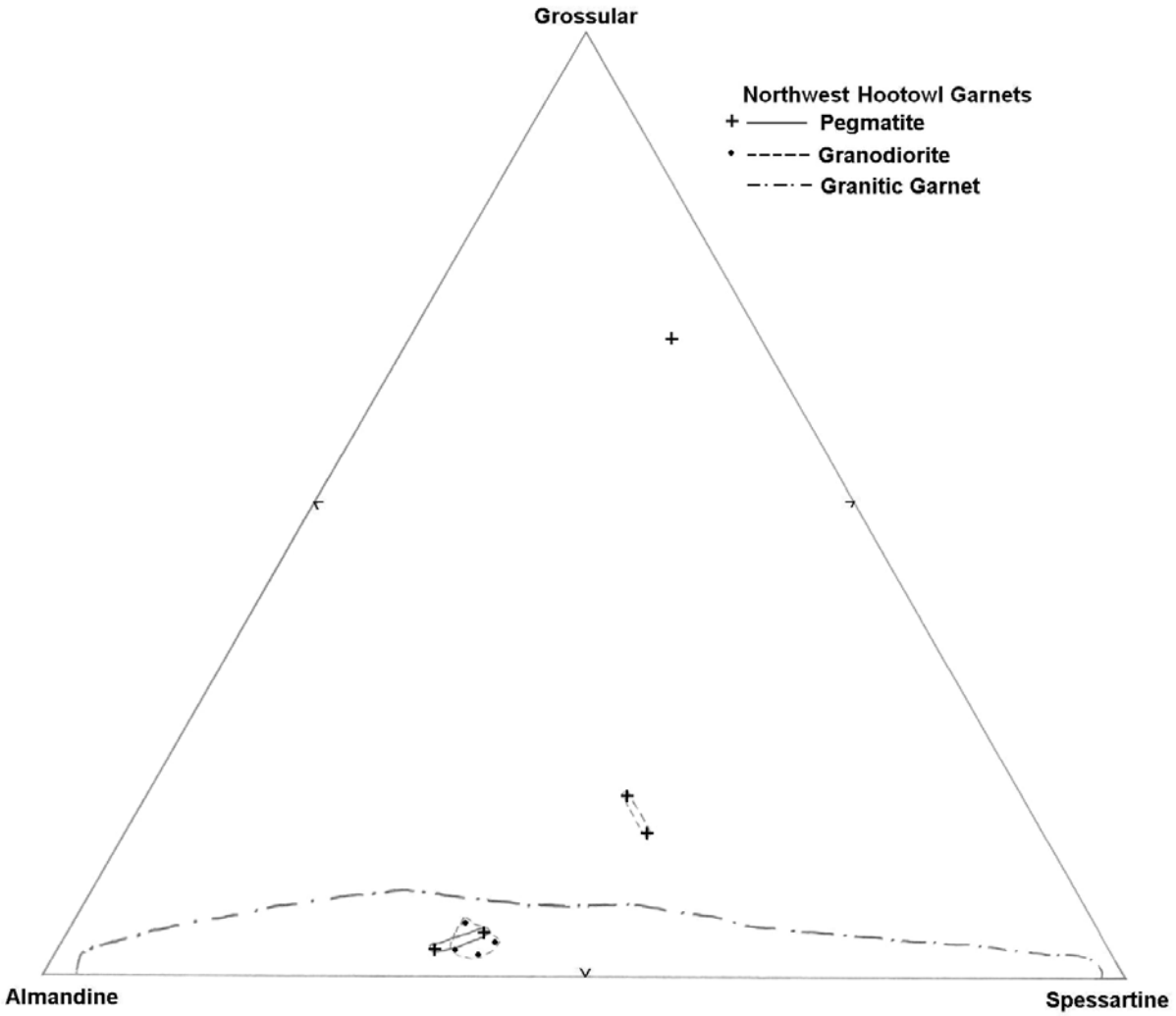

Figure 34 Garnet compositions from Northwest Hootowl study area. Granodioritic garnet cores are almandine-spessartine and plot within the granitic garnet field compiled from Deer et al. (1992). Some granodioritic garnet contains rims of mid-Ca garnet. Pegmatitic garnet cores are almandine-spessartine and plot with the granodioritic garnet cores in granitic garnet field. A grossular rim was detected on a pegmatitic garnet from this locality.

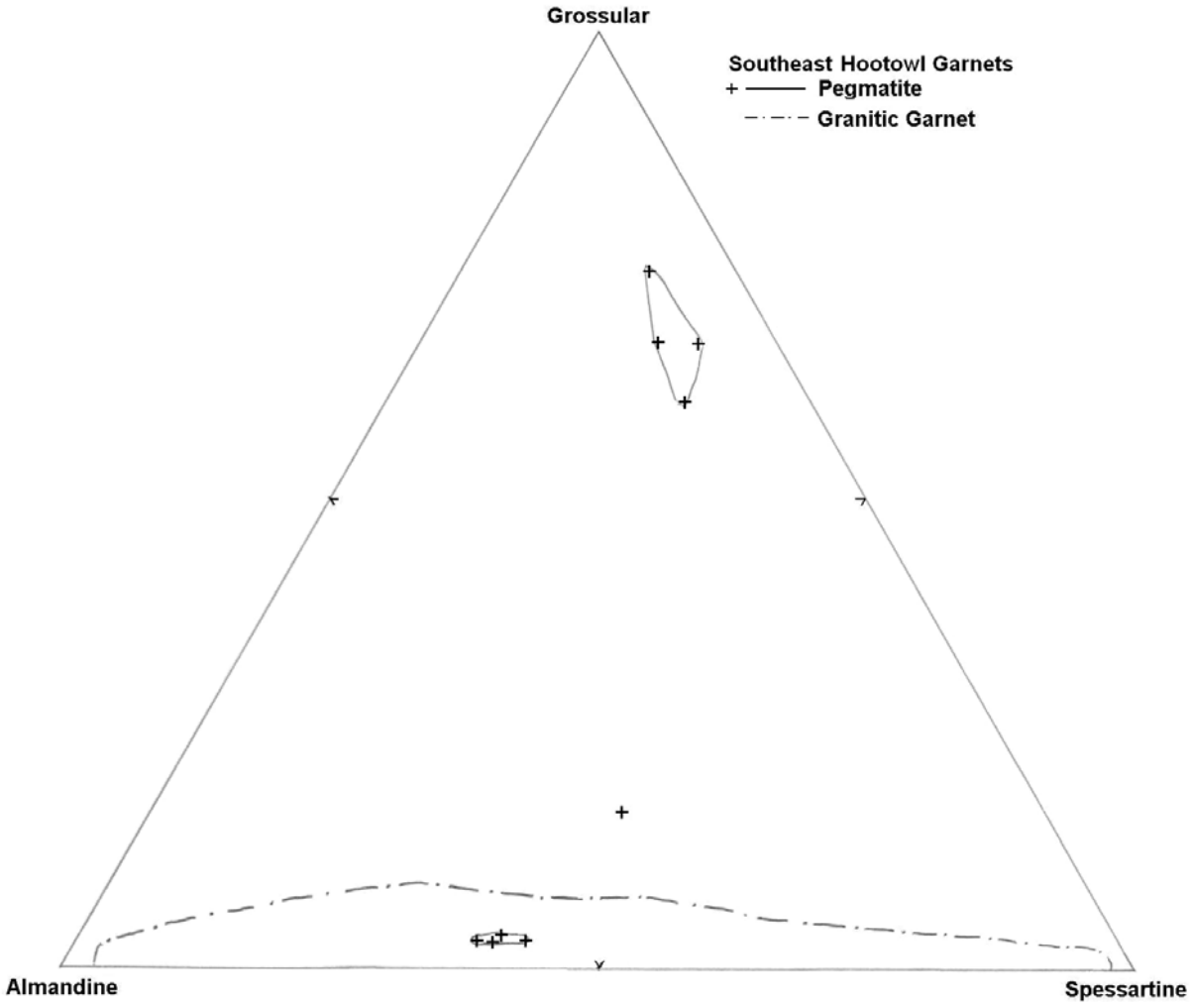

Figure 35 Pegmatitic garnet compositions from the Southeast Hootowl study area. Garnet cores are low-Ca almandine-spessartine and plot in the field for granitic garnet compiled from Deer et al. (1992). One garnet has a mid-Ca rich rim and most of the garnet rims are grossular.

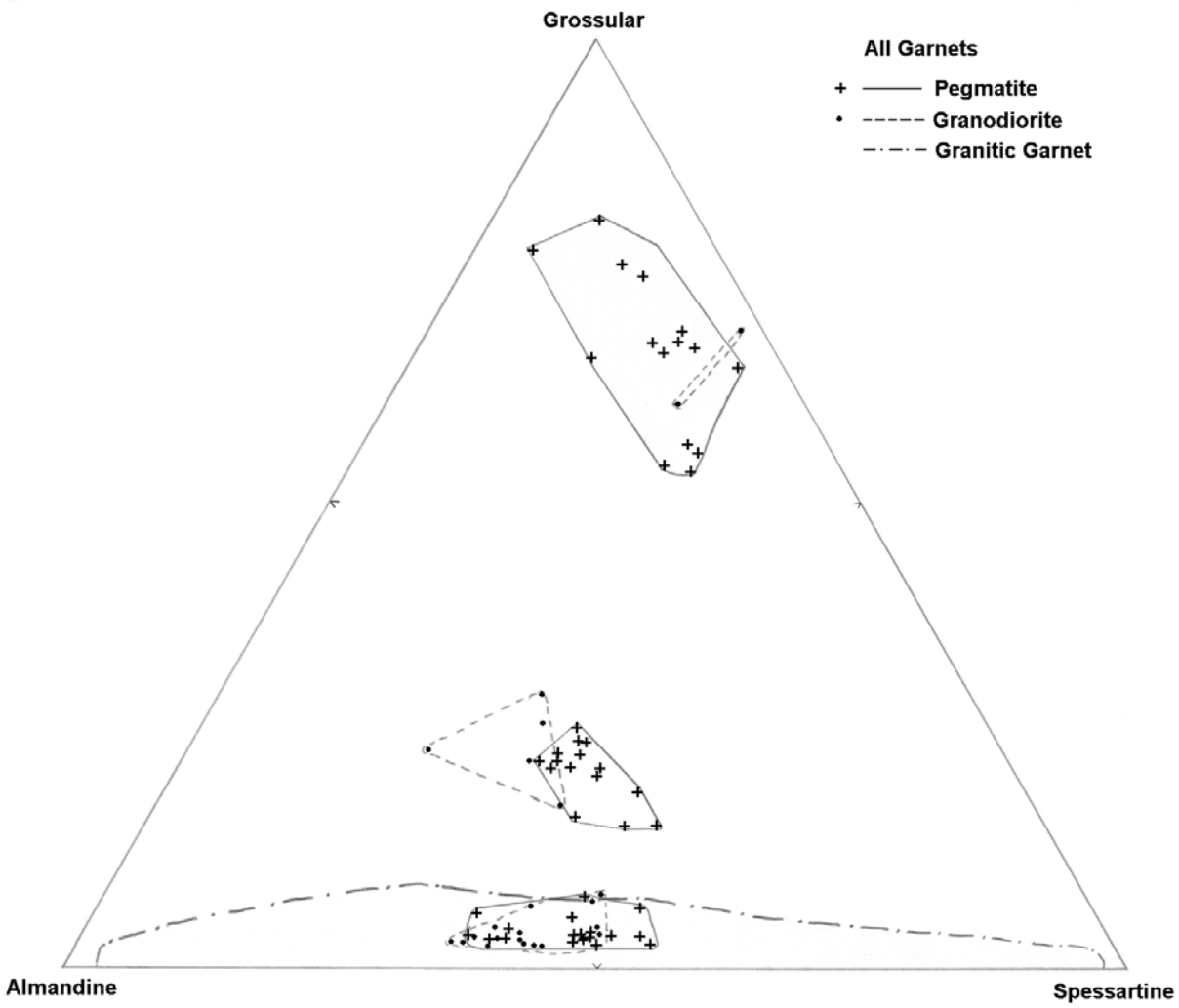

Figure 36 Summary of all garnet compositions. Garnet cores are almandine-spessartine and plot in field for granitic garnet compiled from Deer et al. (1992). Granitic and pegmatitic garnets have mid-Ca and grossular rims, resulting in separation into three distinct fields of different mole percent grossular component. There is prominent overlap in the granodiorite and pegmatite fields for almandine-spessartine cores, and some overlap in mid-Ca and grossular rim compositions.

Variation of Ca content in garnets is not limited to any certain pegmatite zone or any specific site studied, but is widespread over all garnet-bearing pegmatite zones and all bodies studied. Grossular garnet is also present as garnet 'cement' between almandine-spessartine garnets (Figure 37). No garnets were observed in Roan Road granodiorite.

Mica

Muscovite is the most common mica in the Spruce Pine plutonic suite. Biotite is found as an accessory phase in some granitoids, but is always less abundant than muscovite. Biotite is more abundant in rocks of the Ashe Metamorphic Suite than muscovite. Alteration of muscovite in granitoids is reflected by recrystallization to finer-grained white mica (Figure 38). Epidote is found partly included in muscovite and as crystals independent of muscovite in granodiorites of the Crabtree Creek exposure, the Northwest Hootowl study area, Bon Ami C, and the Roan Road granodiorite outcrop. Epidote also occurs in muscovite and as isolated grains in quartz-plagioclase-perthite pegmatite, perthite-garnet pegmatite, and quartz-plagioclase pegmatite of the Crabtree Creek exposure, and quartz-muscovite pegmatite of the Northwest Hootowl study area. Muscovite forms green to light brown (rum) grains that range in size from 1 to over 300 mm in diameter. Green and brown muscovite is colorless in thin section. The term "books" is often applied to larger muscovite grains. The euhedral shape and size of these muscovite crystals indicates that they are likely formed as primary muscovite from a crystallizing magma. Biotite grains in the Spruce Pine granitoids are generally smaller than coexisting muscovite. Dendritic biotite grains are found in some of the granitoids and this distinctive texture is termed "crow's foot" mica. "Crow's foot" mica is observed in the Crabtree Creek exposure, the Field Mine, and the Roan Road outcrop. The biotite is black in hand sample and is exhibits light to dark brown pleochroism in thin section.

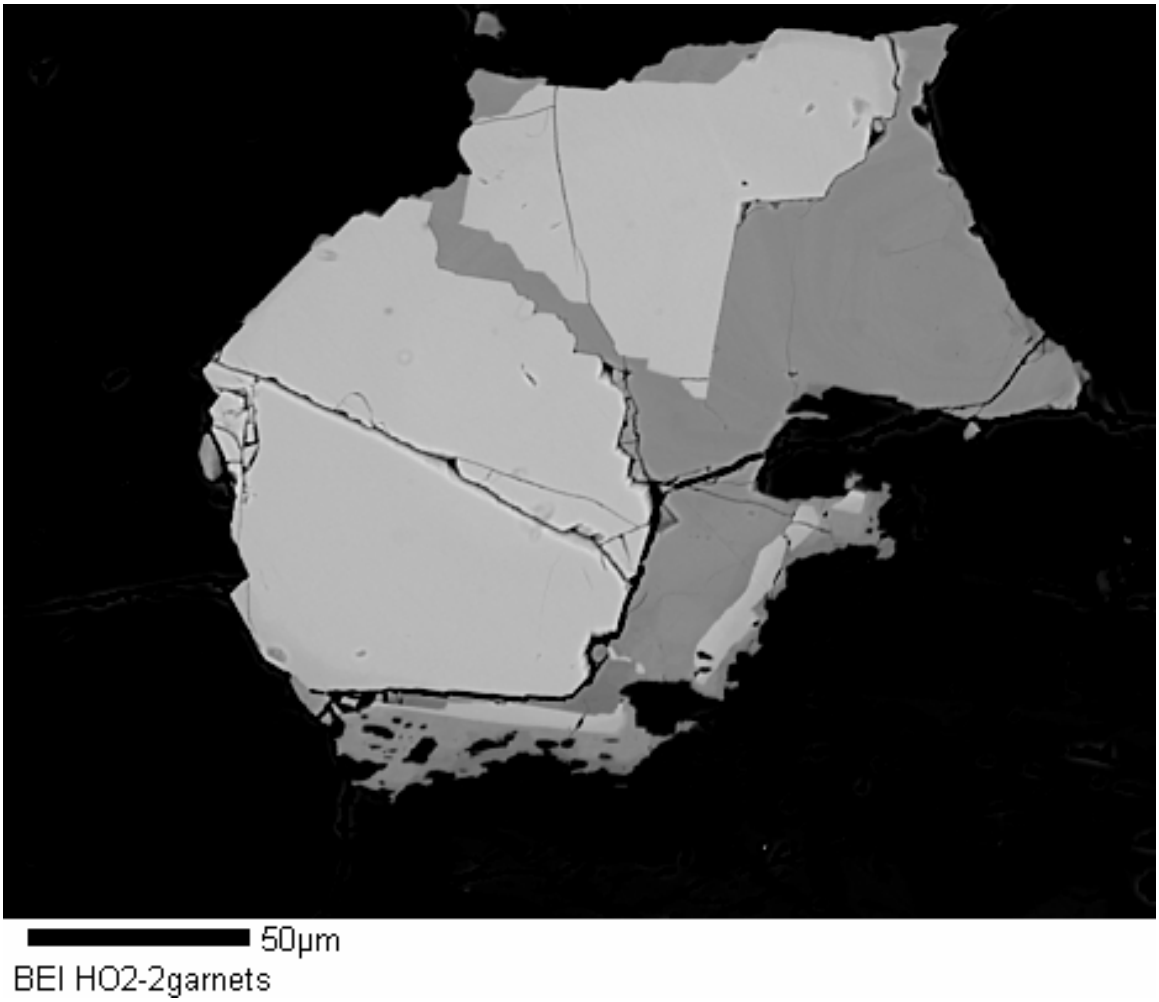

Figure 37 Backscatter electron image of grossular garnet between fragments of almandine-spessartine garnets from the Southeast Hootowl study area. Grossular garnet is shown in darker gray shading. The almandine-spessartine garnet was fractured before metasomatism. Grossular garnet then infilled the fracture. The thin almandine-spessartine fragment at lower right is likely an embayed remnant of previously crystallized garnet.

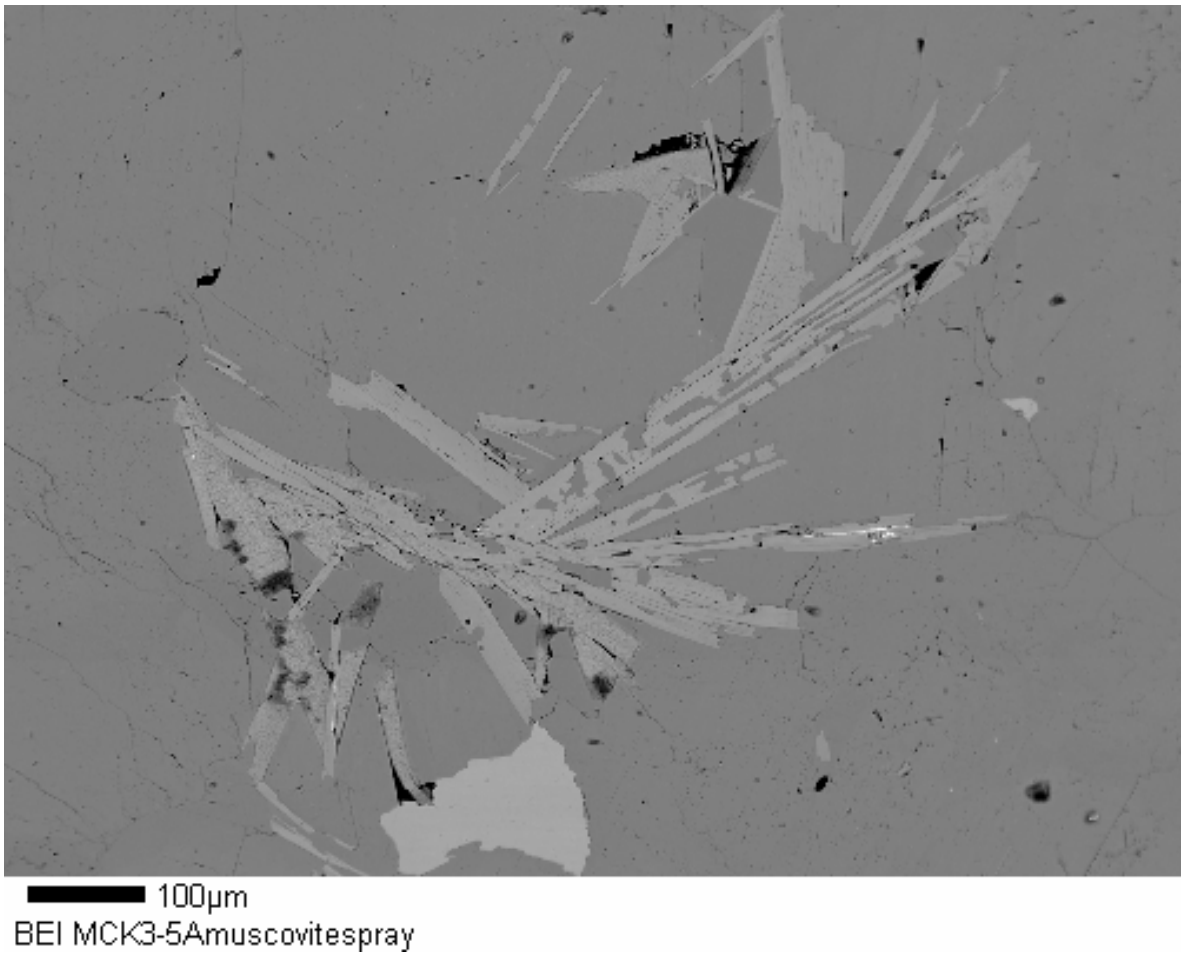

Figure 38 Backscatter electron image of small muscovite crystals in a spray pattern. The small size and pattern of crystallization possibly indicates recrystallization of the muscovite.

Muscovite is found in all pegmatite zones except for the quartz (± alkali feldspar) core. Largest muscovite crystals are observed in the following pegmatite zones: quartz-plagioclase-muscovite, quartz-plagioclase-muscovite-garnet, quartz-plagioclase-perthite-muscovite-garnet, quartz-perthite-muscovite-garnet. Muscovite in other pegmatite zones is small and sparse. Large books of muscovite tend to cluster around the border between feldspar rich pegmatite zones and massive smoky quartz crystals and cores. Large muscovite crystals cluster near the massive smoky quartz crystals in the quartz-perthite-muscovite zone of the Crabtree Creek exposure (Figure 13) and near massive smoky quartz crystals in the quartz, plagioclase-muscovite pegmatite zone of the Field Mine (Figure 15). Muscovite crystals are concentrated in the quartz-perthite-muscovite-garnet pegmatite zone near the quartz core of Bon Ami C (Figure 22). The largest crystals of muscovite observed in the Hootowl mine are located in the quartz-plagioclase-muscovite-garnet pegmatite of the Southeast Hootowl study area (Figure 27). Muscovite crystals in the granodiorite are smaller, but are of the same color as those in the pegmatite.

Compositions of mica are found in Appendix D. The white mica is not pure end-member muscovite, but has significant celadonitic (Fe-Mg) and lesser paragonitic (Na) components (Figures 39 through 56). Zoning in muscovite, if present, is minimal. A small muscovite grain (HO1-5musc1core-rim(w-ep); Appendix D) from Hootowl granodiorite displays minor zoning with a rim depleted in Fe. A muscovite grain (CC2-3musc2core-rim; Appendix D) from perthite-garnet pegmatite shows a similar Fe-poor rim. A muscovite grain (CC2-9musc2core-rim; Appendix D) from quartz-perthite-muscovite pegmatite also shows Fe depleted rim composition. Finer-grained, recrystallized muscovite does approach end-member muscovite in composition. Small muscovite grains (MCK3-1musc2core-rim(sm), MCK3-5Amuscspray;

Appendix D) have much less Fe and are closer to ideal muscovite.. Large muscovite books lack zoning.

Granodioritic muscovite contains significant celadonitic and paragonitic components consistent with an igneous origin (Miller, 1981; Zane and Rizzo, 1999). Chlorine is absent and fluorine is rarely present in significant quantities in granodioritic muscovite. According to Deer et al., (1992), white mica usually contains less than one weight percent fluorine and no chlorine is reported. Fluorine content may increase in micas of pegmatitic origin, such as lepidolite (Deer et al., 1992).

Muscovite analyses from the Field Mine (Figure 11) plot in the field for primary granitic muscovite (Figures 39 and 40) supporting the textural evidence that the muscovite is magmatic in origin. The pegmatitic and granodioritic muscovite fields overlap in both celadonite and paragonite substitution (Figures 39 and 40) indicating similar crystallization in both pegmatite and granodiorite. Muscovite from Field Mine granodiorite sample (CC1-3; Figure 15; Appendix D) contains measurable fluorine, but no significant chlorine is detected in any muscovite from Field Mine.

Muscovite from Bon Ami A (Figures 11 and 16) contains celadonitic and paragonitic components (Figures 41 and 42). Analyses plot in the field for primary granitic muscovite on Figures 41 and 42. Chlorine and fluorine is below detection levels in muscovite from Bon Ami A (Appendix D).

Muscovite from Bon Ami B (Figures 11 and 16) contains celadonitic and lesser paragonitic component (Figures 43 and 44). Several weight percent Fe + Mg and these

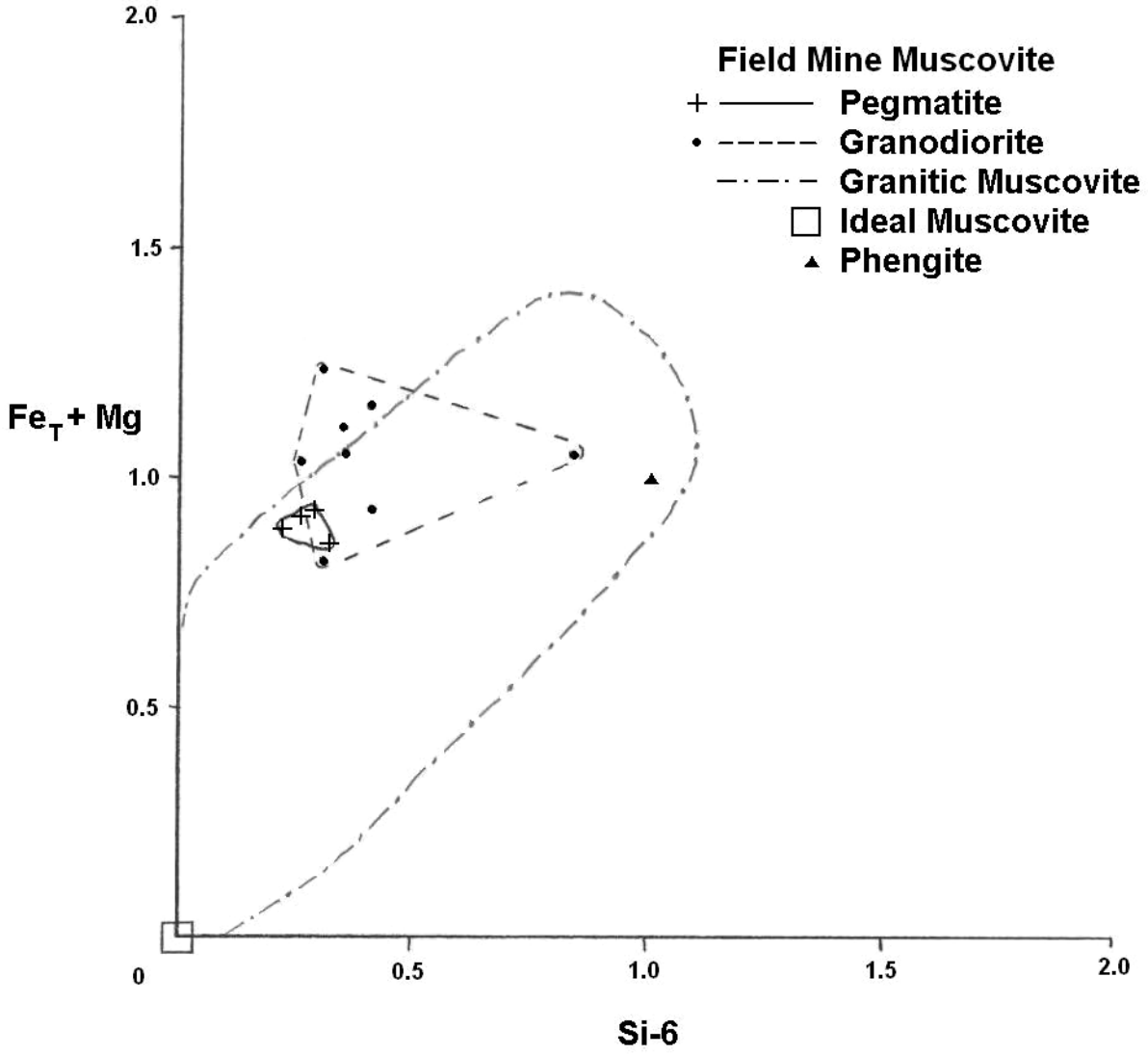

Figure 39 Celadonitic substitution in Field Mine muscovite. Most analyses plot in the range for granitic muscovite from Zane and Rizzo (1999). Substitutional space of phengite is illustrated by the triangle. Fe_T stands for total Fe.

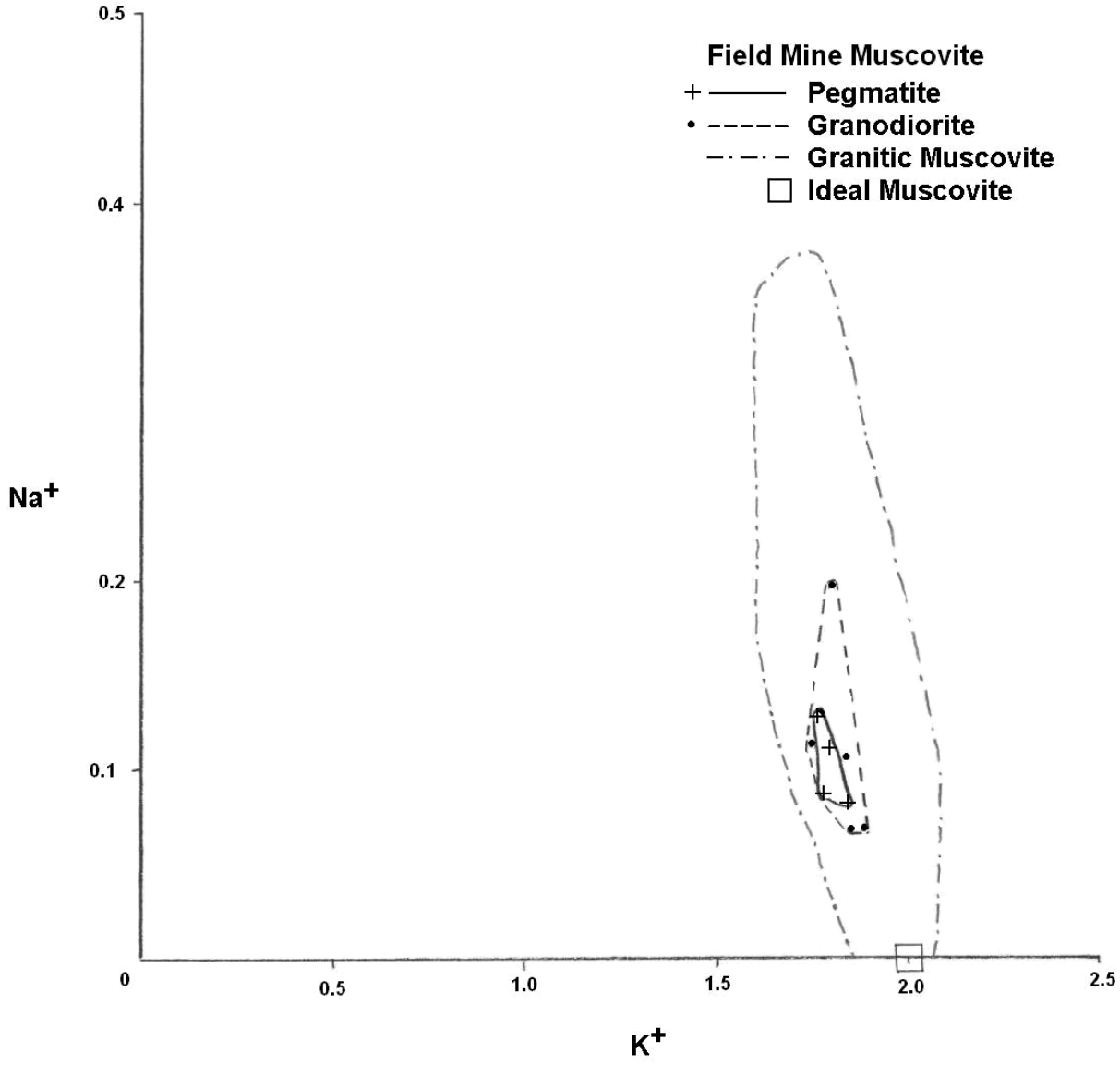

Figure 40 Paragonitic substitution in Field Mine muscovite. Significant overlap of granodiorite and pegmatite fields indicates similar paragonite substitution taking place in pegmatites and in host granodiorites. Granitic muscovite field from Zane and Rizzo (1999).

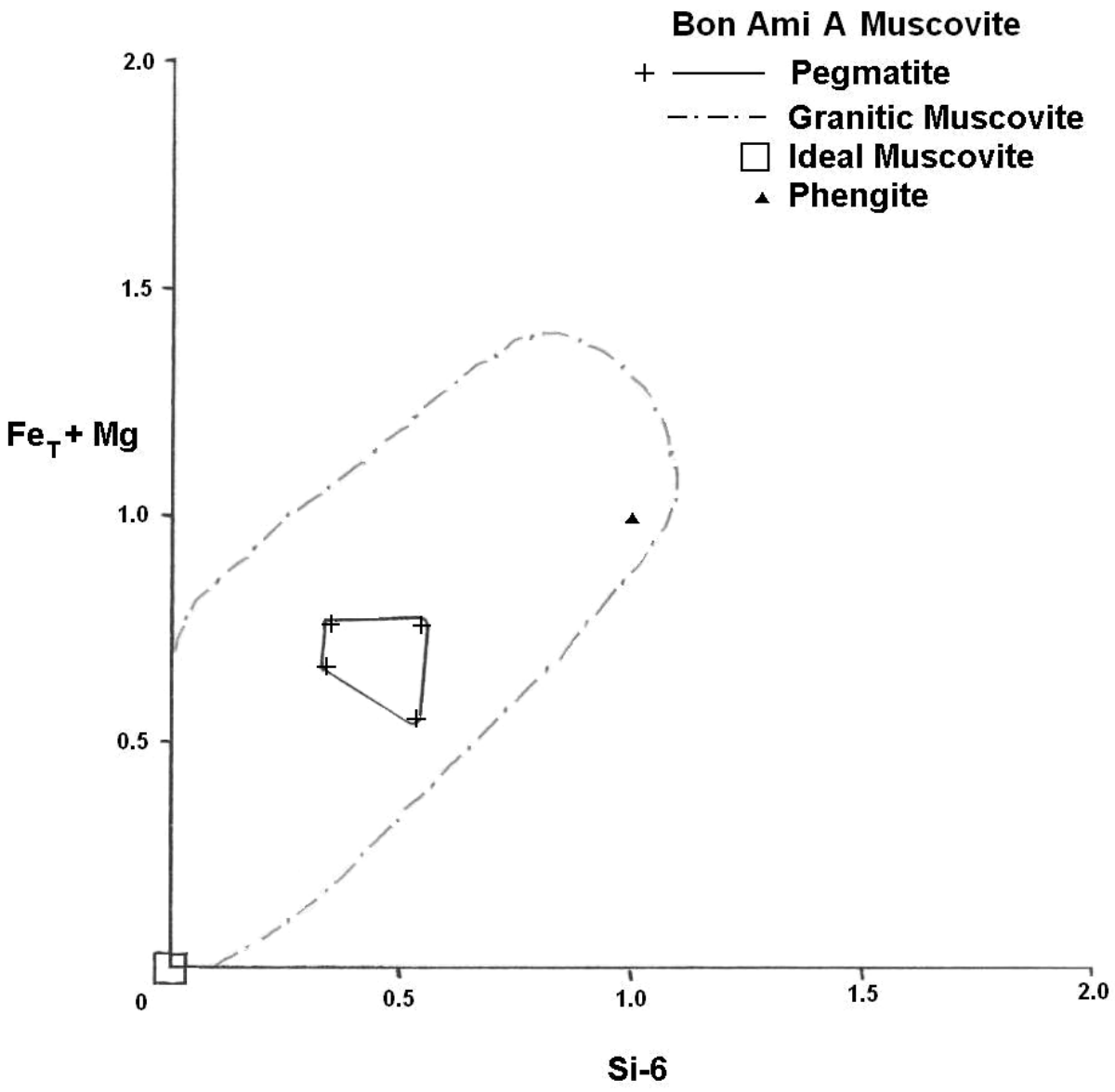

Figure 41 Celadonitic substitution in Bon Ami A muscovite. All analyses plot in the range for granitic muscovite from Zane and Rizzo (1999). Substitutional space of phengite is illustrated by the triangle. Fe_T stands for total Fe.

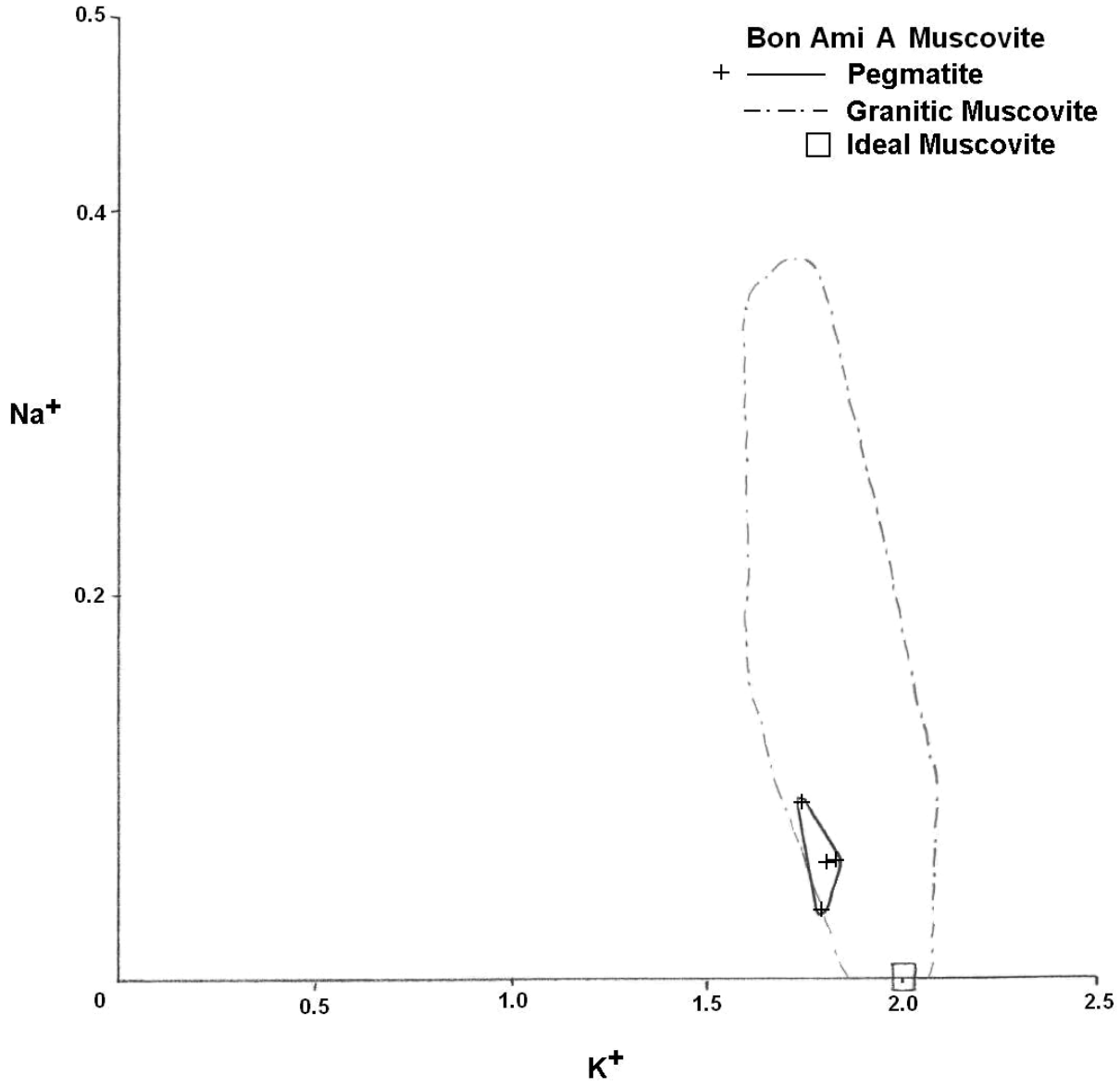

Figure 42 Paragonitic substitution in Bon Ami A muscovite. All analyses show Na/K substitution and none plot as ideal muscovite. Granitic muscovite field from Zane and Rizzo (1999).

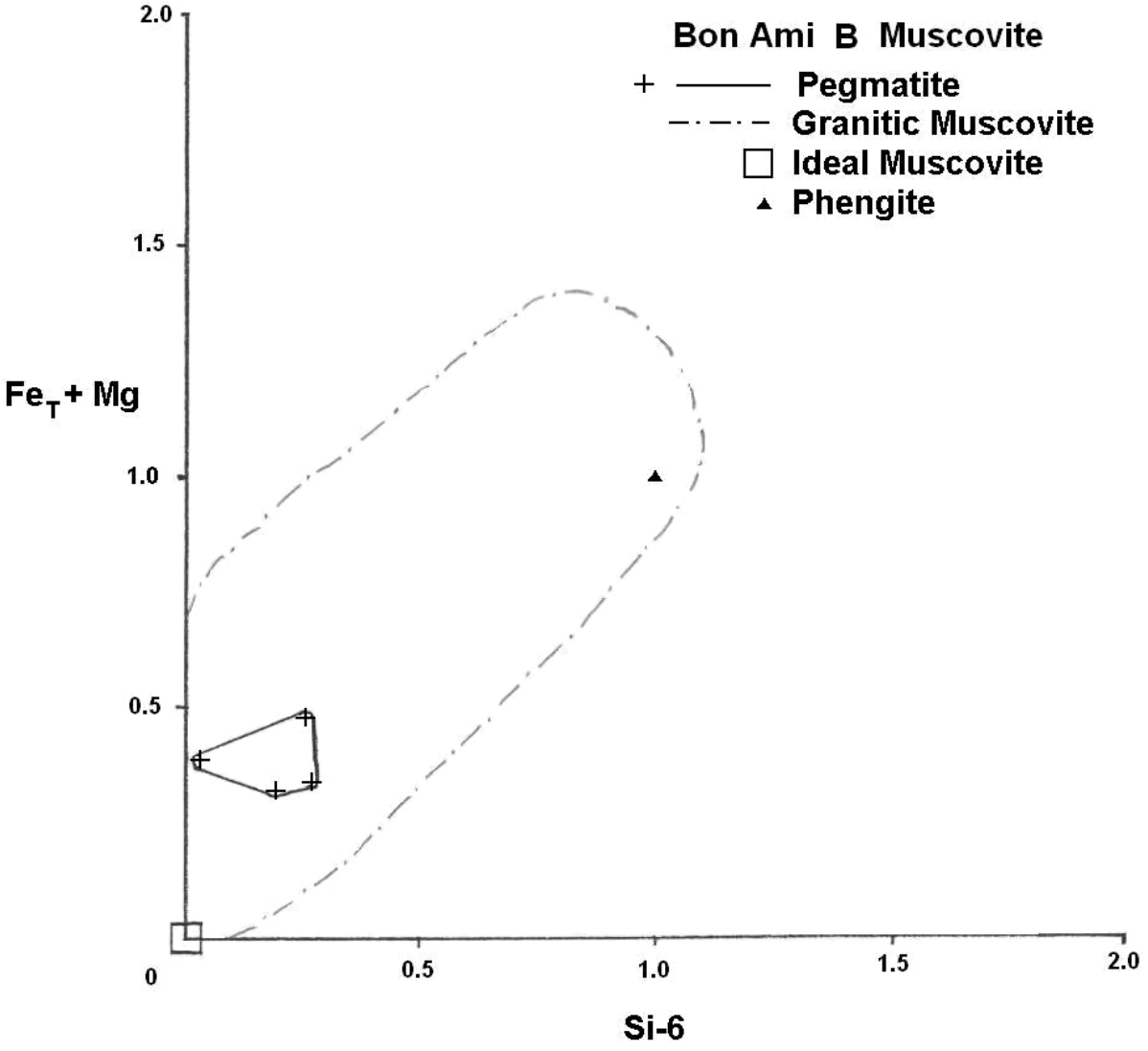

Figure 43 Celadonitic substitution in Bon Ami B muscovite. All analyses plot in the range for granitic muscovite from Zane and Rizzo (1999). Substitutional space of phengite is illustrated by the triangle. Fe_T stands for total Fe.

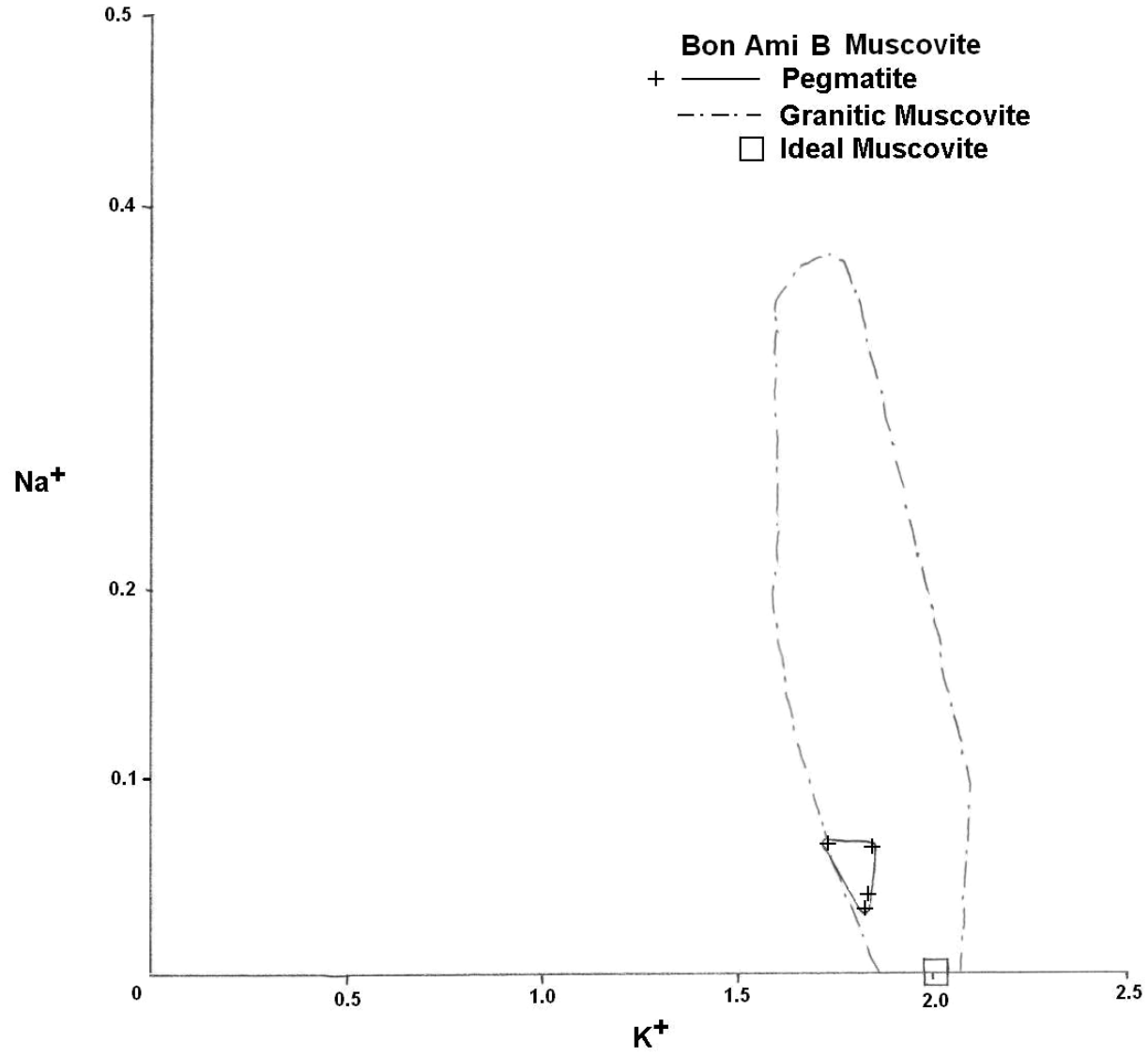

Figure 44 Paragonitic substitution in Bon Ami B muscovite. All analyses show Na/K substitution and none plot as ideal muscovite. Granitic muscovite field from Zane and Rizzo (1999).

components shift the mica composition away from end-member muscovite. Analyses plot in the field for primary granitic muscovite defined by Zane and Rizzo (1999), supporting the textural evidence that the muscovite is primary in origin. Fluorine and chlorine contents in pegmatitic muscovite from Bon Ami B are below detection levels (Appendix D).

Muscovite from Bon Ami C (Figures 11 and 16) plots in the field for primary granitic muscovite (Figures 45 and 46). The pegmatitic and granodioritic muscovite fields overlap in both celadonite and paragonite substitution (Figures 45 and 46). Chlorine is measured in granodiorite sample MCK3-2 (Figure 21; Appendix D), in quartz-perthite-muscovite-garnet pegmatite sample MCK3-6 (Figure 21; Appendix D), and in quartz pegmatite sample MCK3-1 (Figure 22; Appendix D). No significant fluorine is detected in muscovite from Bon Ami C (Appendix D).

Muscovite from Northwest Hootowl study area (Figures 11 and 23) contains variable amounts of Fe ranging from near end-member muscovite to a more celadonitic composition (Figures 47 and 48). All of the Northwest Hootowl muscovite analyses plot in the field for primary granitic muscovite taken from Zane and Rizzo (1999), supporting the textural evidence that most of the muscovite is primary. There is little overlap in the pegmatitic and granodioritic muscovite fields in celadonite substitution, but significant overlap in paragonite substitution (Figures 47 and 48). Significant chlorine is found in granodiorite sample HO1-5 (Figure 25; Appendix D). Fluorine is detected in muscovite in granodiorite sample HO1-5 (Figure 25; Appendix D), graphic granite sample HO1-4 (Figure 25; Appendix D), quartz-muscovite pegmatite sample HO1-2 (Figure 25; Appendix D), and in some grab samples from Hootowl Mine (Appendix D).

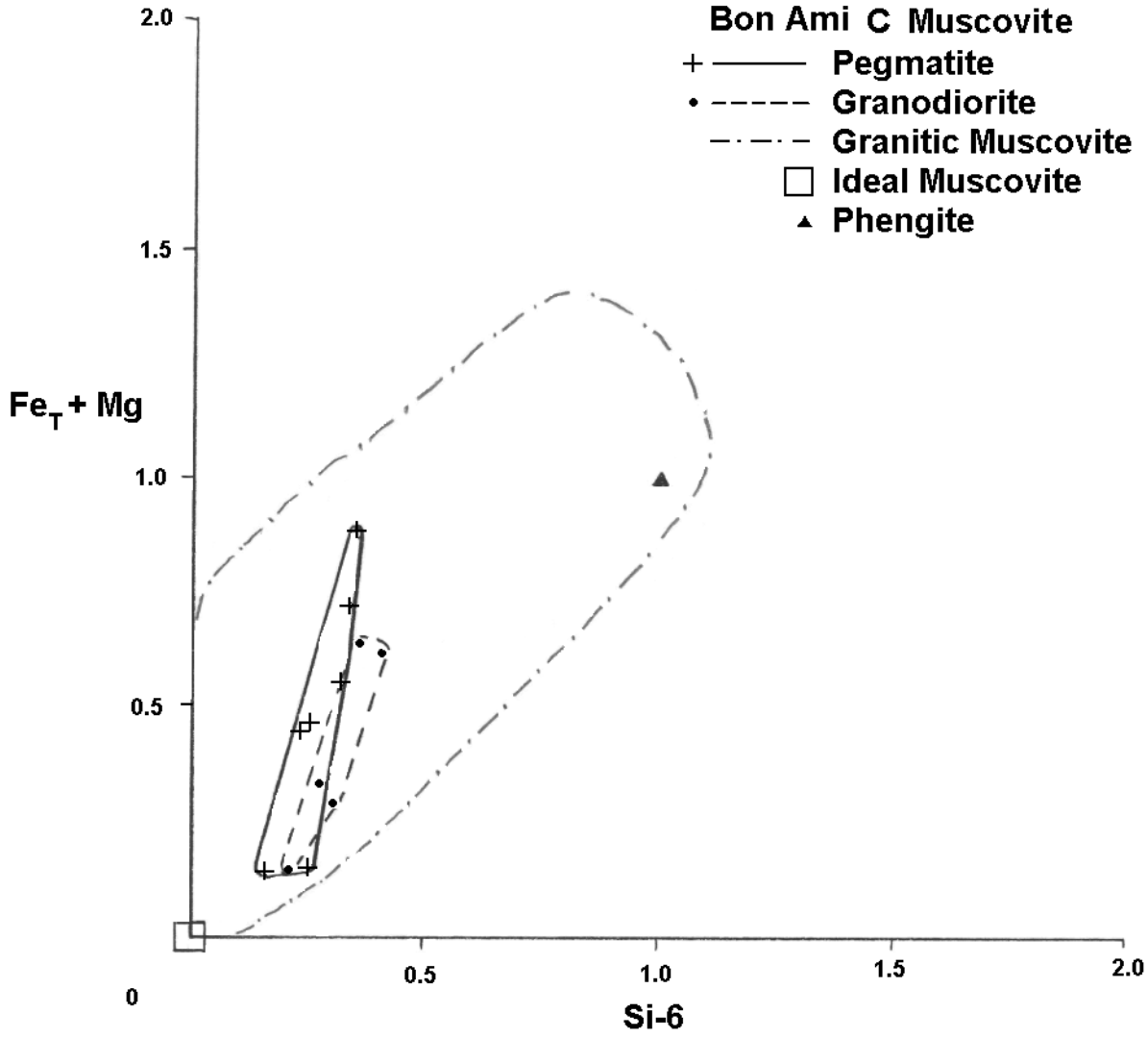

Figure 45 Celadonitic substitution in Bon Ami C muscovite. All analyses plot in the range for granitic muscovite from Zane and Rizzo (1999). Substitutional space of phengite is illustrated by the triangle. Fe_T stands for total Fe.

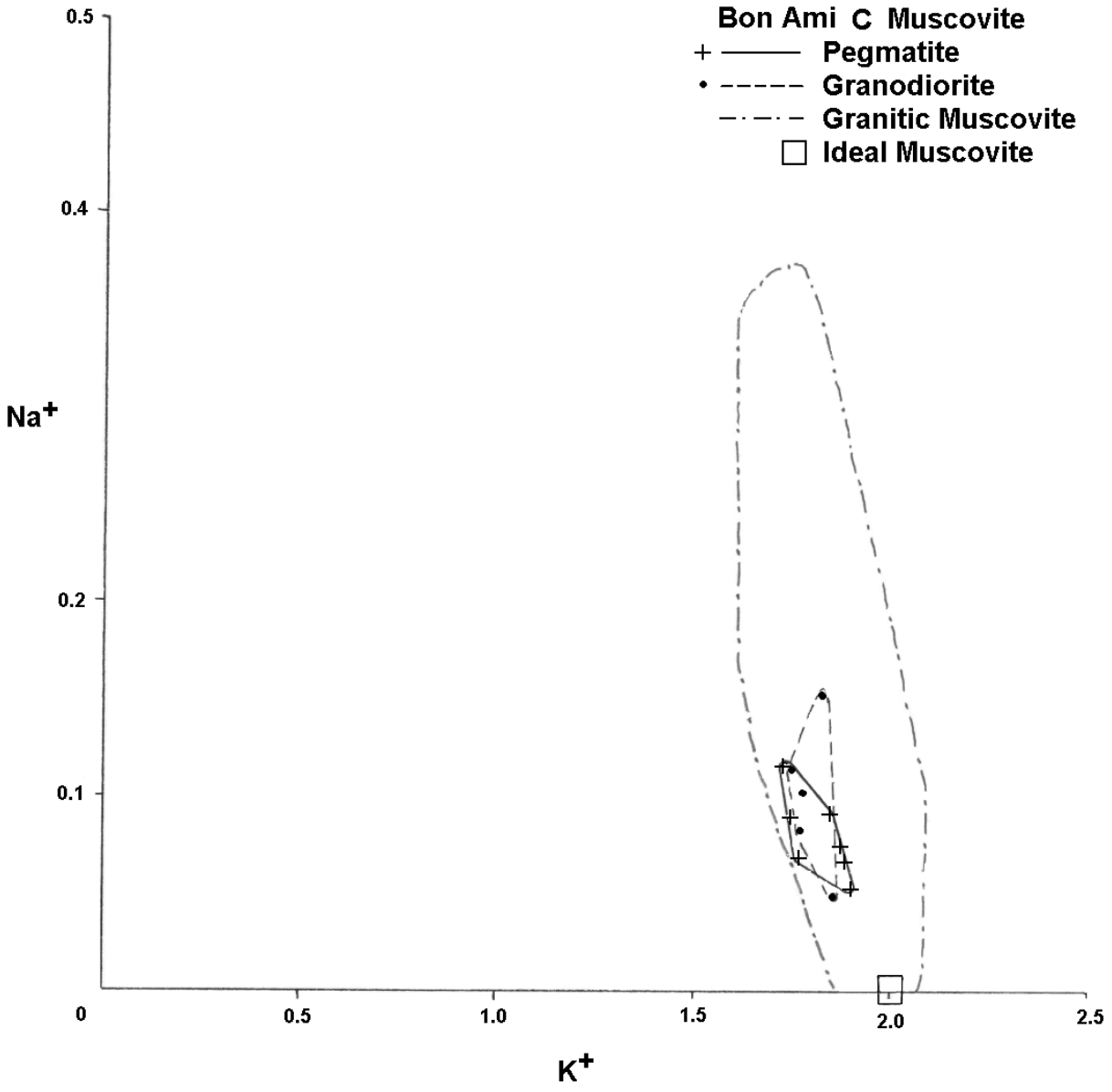

Figure 46 Paragonitic substitution in Bon Ami C muscovite. All analyses show Na/K substitution and none plot near ideal muscovite. Significant overlap of granodiorite and pegmatite fields indicates similar paragonite substitution taking place in pegmatites and in host granodiorites. Granitic muscovite field from Zane and Rizzo (1999).

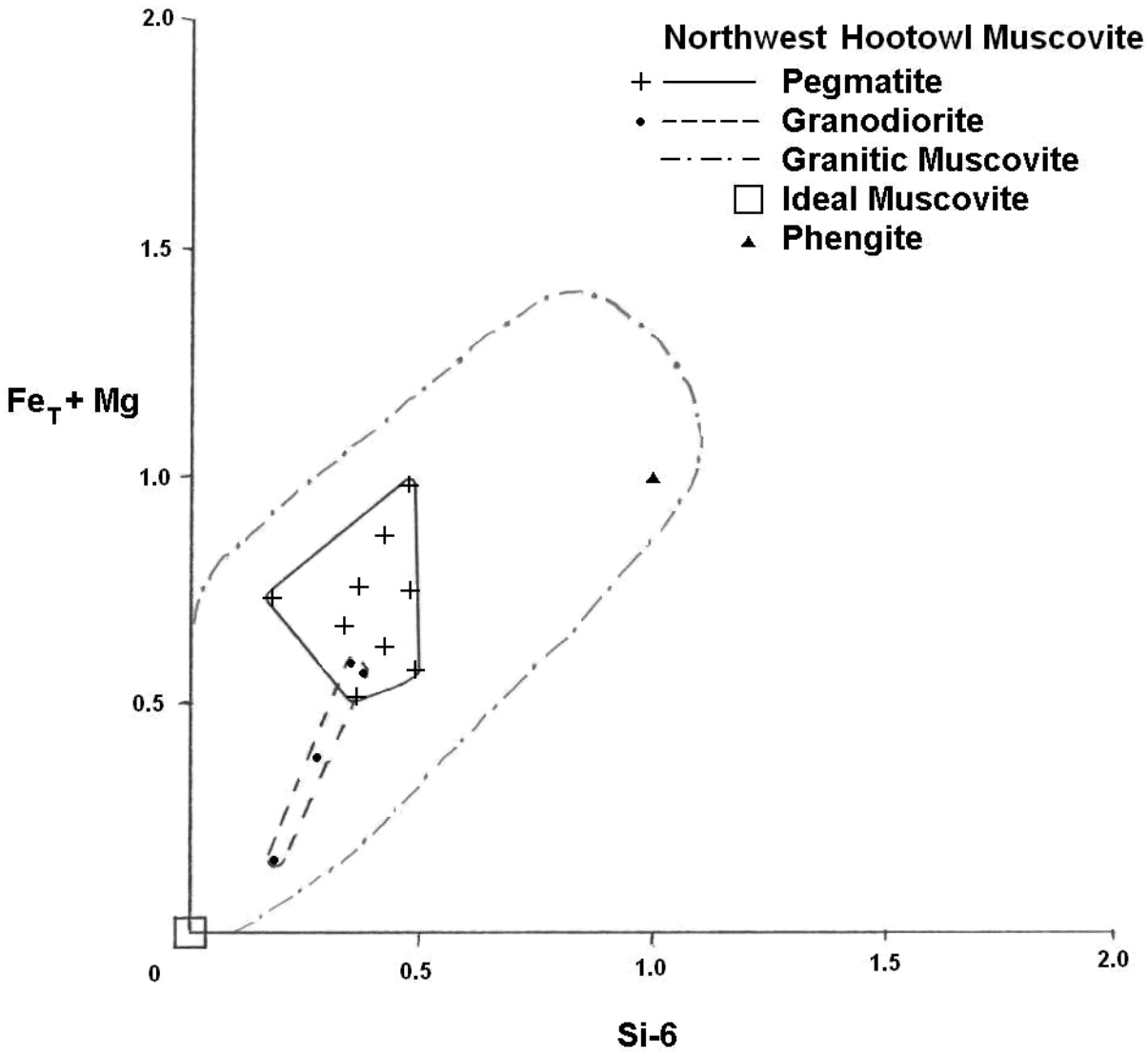

Figure 47 Celadonitic substitution in Northwest Hootowl muscovite. All analyses plot in the range for granitic muscovite from Zane and Rizzo (1999). Substitutional space of phengite is illustrated by the triangle. Fe_T stands for total Fe.

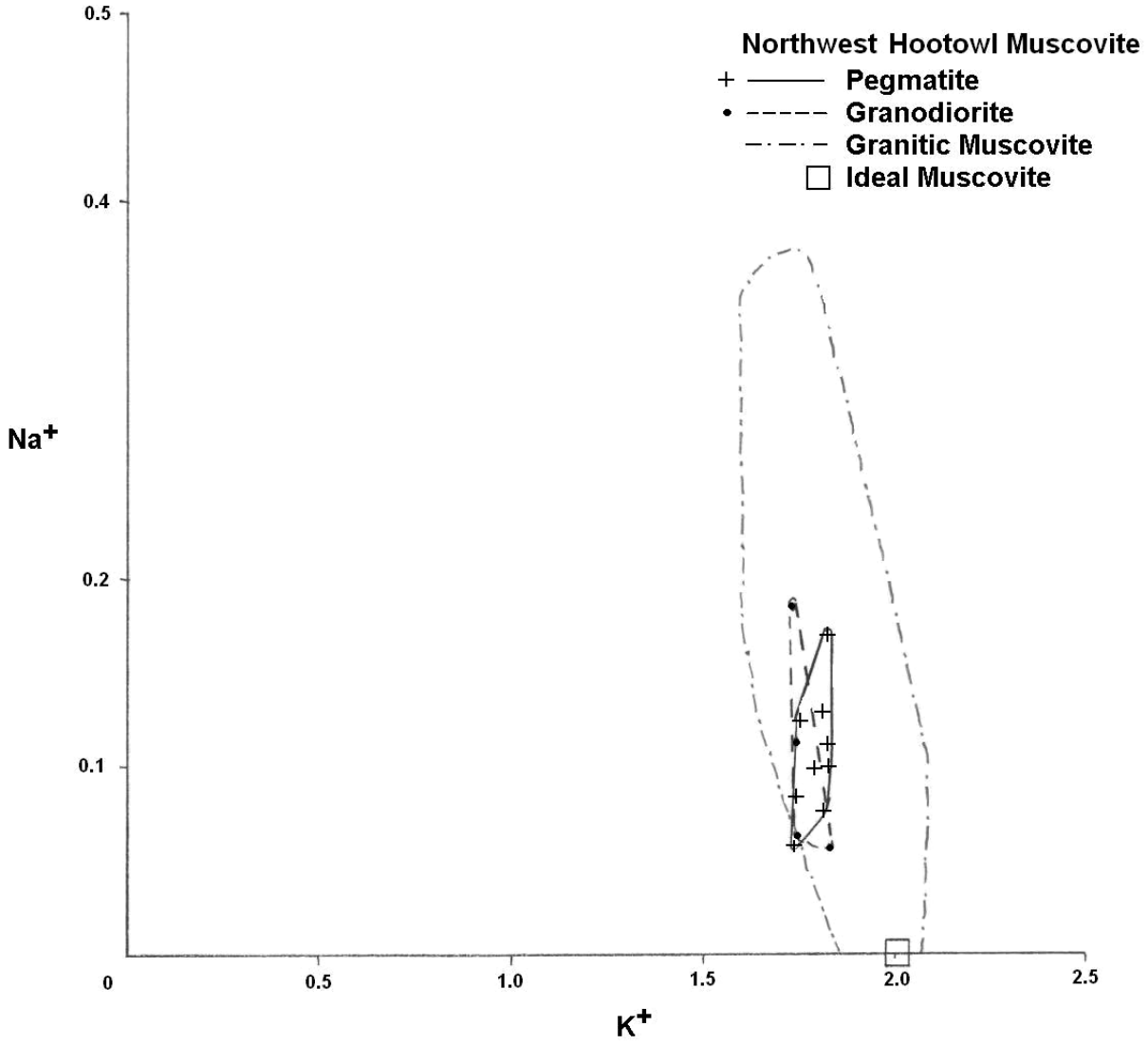

Figure 48 Paragonitic substitution in Northwest Hootowl muscovite. Significant overlap of granodiorite and pegmatite fields indicates similar paragonite substitution taking place in pegmatites and in host granodiorites. Granitic muscovite field from Zane and Rizzo (1999).

All muscovite from the Southeast Hootowl study area (Figures 11 and 23) contains celadonitic and paragonitic components (Figures 49 and 50). Muscovite analyses plot in the field for primary granitic muscovite from Zane and Rizzo (1999) in terms of celadonitic component (Figure 49), but the granodioritic muscovites plot outside the granitic muscovite field (Figure 50). Pegmatitic and granodioritic muscovite fields do not overlap in this pegmatite, possibly indicating different crystallization processes in granodiorite and pegmatite or possible recrystallization of muscovite in the granodiorite. No textural evidence of recrystallization is observed in muscovite from the Southeast Hootowl study area. Significant chlorine levels are not found in muscovite from the Southeast Hootowl study area. Fluorine is detected in muscovite in granodiorite sample HO2-1 (Figure 27; Appendix D) and in quartz-plagioclase-muscovite-garnet pegmatite sample HO2-2 (Figure 27; Appendix D).

Muscovite from the Crabtree Creek exposure (Figure 11) shows a wide range in Fe contents (0.36 to 6.40 wt. %), while the range of paragonitic component is more restricted (Figures 51 and 52). Most of the Crabtree Creek muscovite analyses plot in the field for primary granitic muscovite from Zane and Rizzo (1999), supporting the textural evidence that most of the muscovite is primary. A single analysis plots near end-member muscovite (Figure 51). This analysis is a rim composition at the edge of a crystal whose core is much richer in iron. The pegmatitic and granodioritic muscovite fields overlap in both celadonite and paragonite substitution (Figures 51 and 52), but the overlap in celadonitic components is far from complete. Muscovite in granodiorite sample CC2-1 (Figure 13; Appendix D), from perthite pegmatite sample CC2-3 (Figure 13; Appendix D), and from quartz-plagioclase sample CC2-6 (Figure 13; Appendix D) contain measurable chlorine. Fluorine above detection levels occurs in muscovite from granodiorite sample CC2-7 (Figure 13; Appendix D).

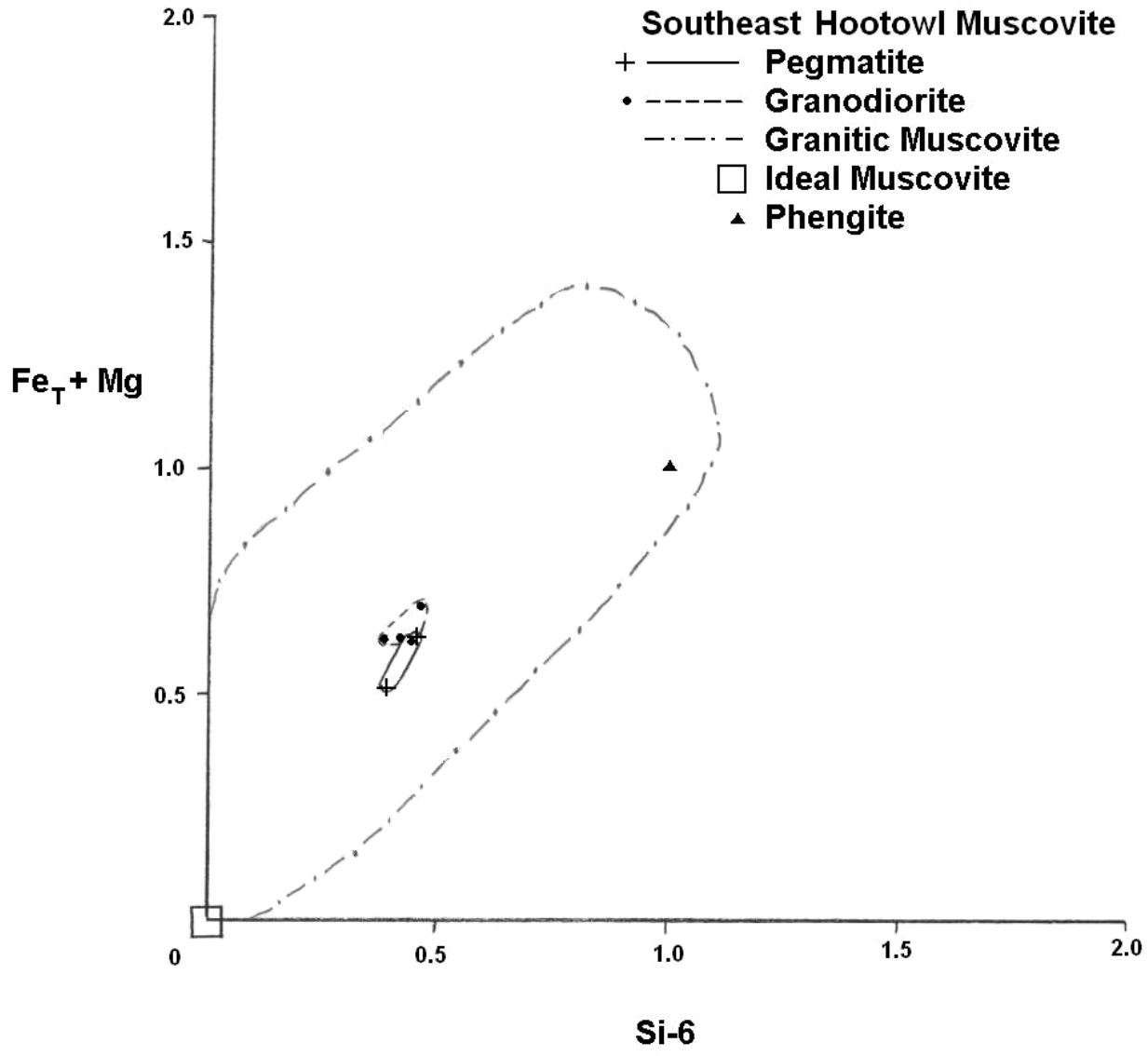

Figure 49 Celadonitic substitution in Southeast Hootowl muscovite. All analyses plot in the range for granitic muscovite from Zane and Rizzo (1999). Substitutional space of phengite is illustrated by the triangle. Fe_T stands for total Fe.

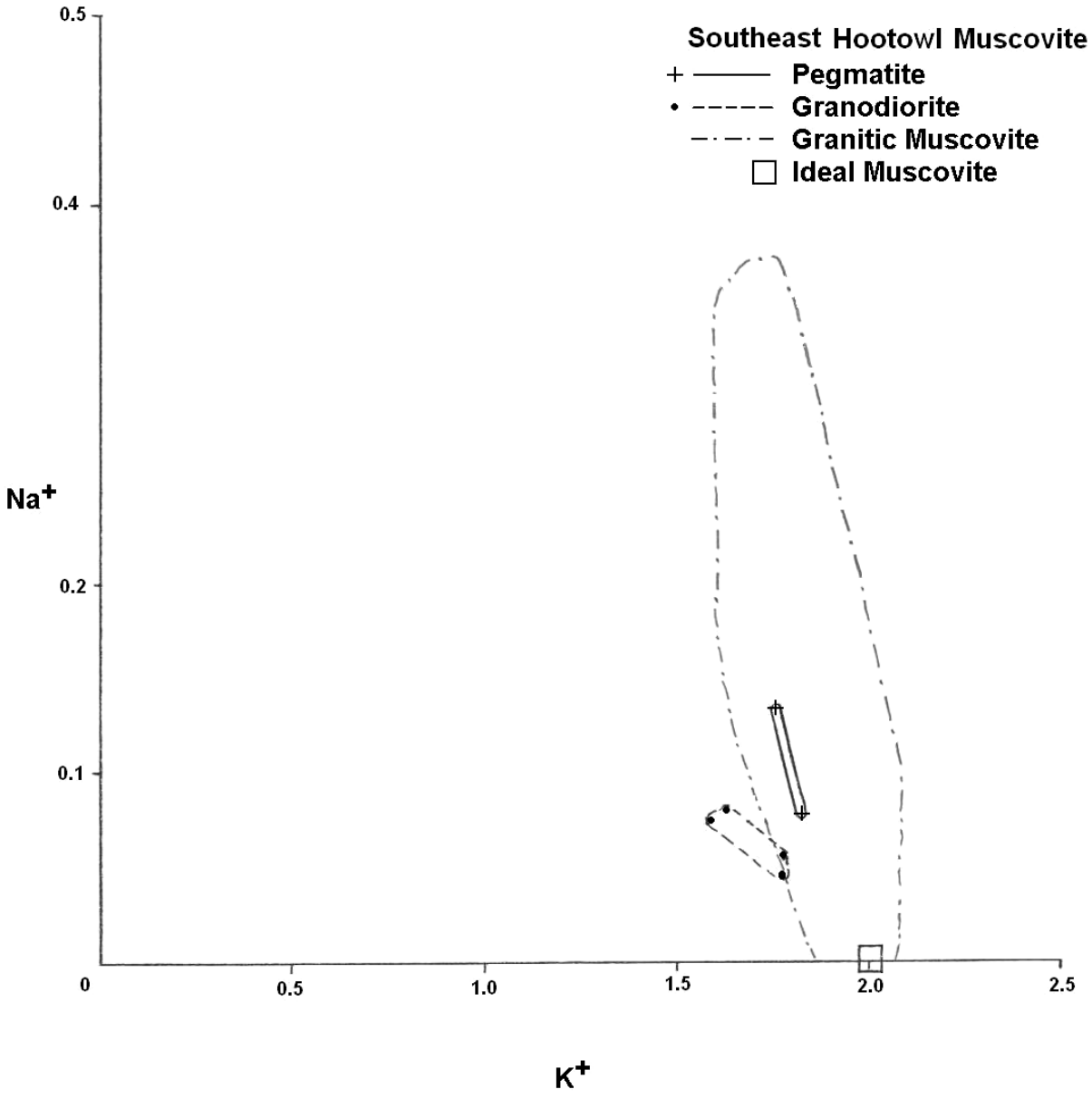

Figure 50 Paragonitic substitution in Southeast Hootowl muscovite. Lack of overlap in fields and granodioritic muscovite plotting outside of the granitic muscovite field may indicate some of this muscovite has been recrystallized. Granitic muscovite field from Zane and Rizzo (1999).

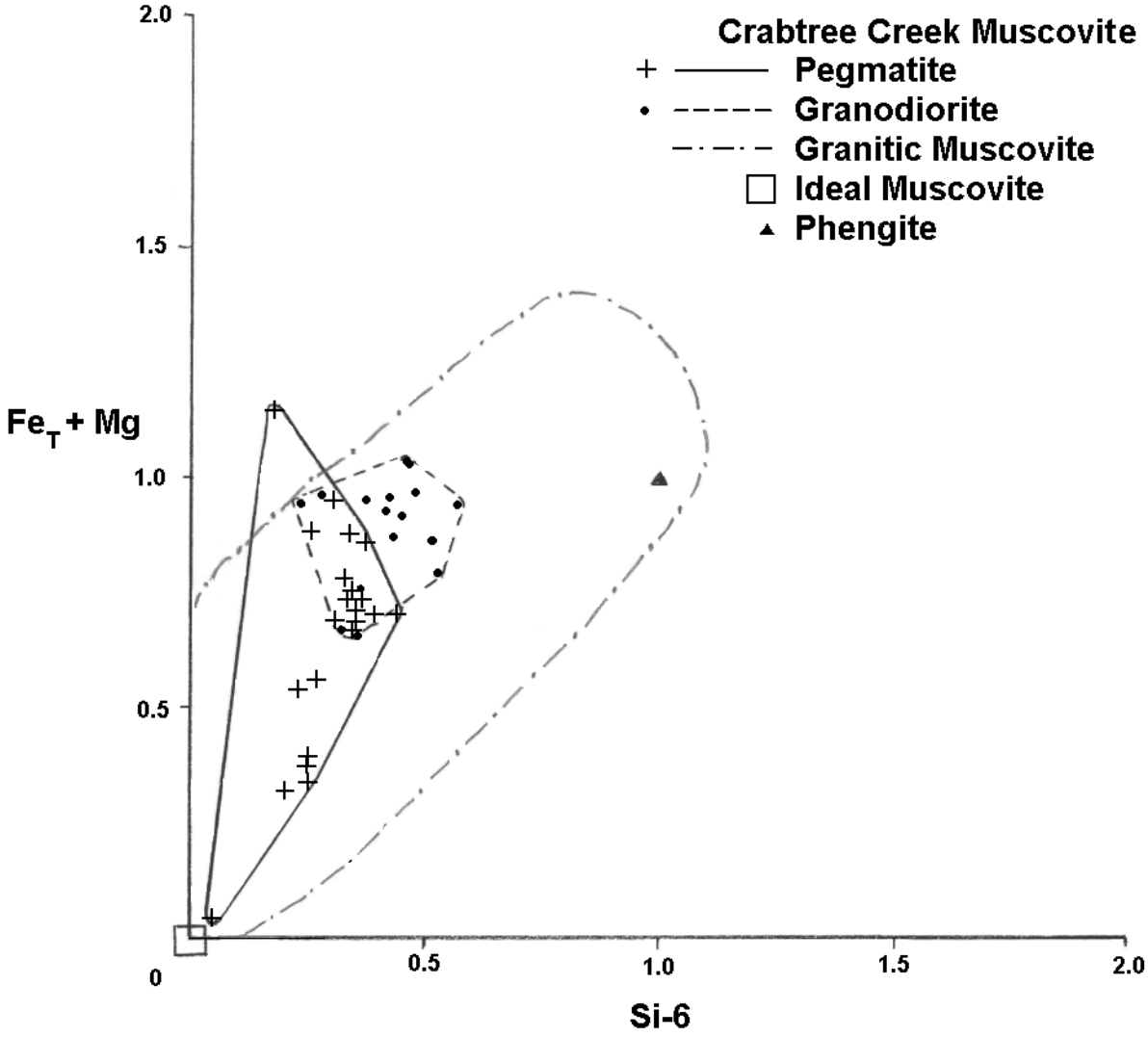

Figure 51 Celadonitic substitution in Crabtree Creek muscovite. Most analyses plot in the range for granitic muscovite from Zane and Rizzo (1999). Substitutional space of phengite is illustrated by the triangle. Fe_T stands for total Fe.

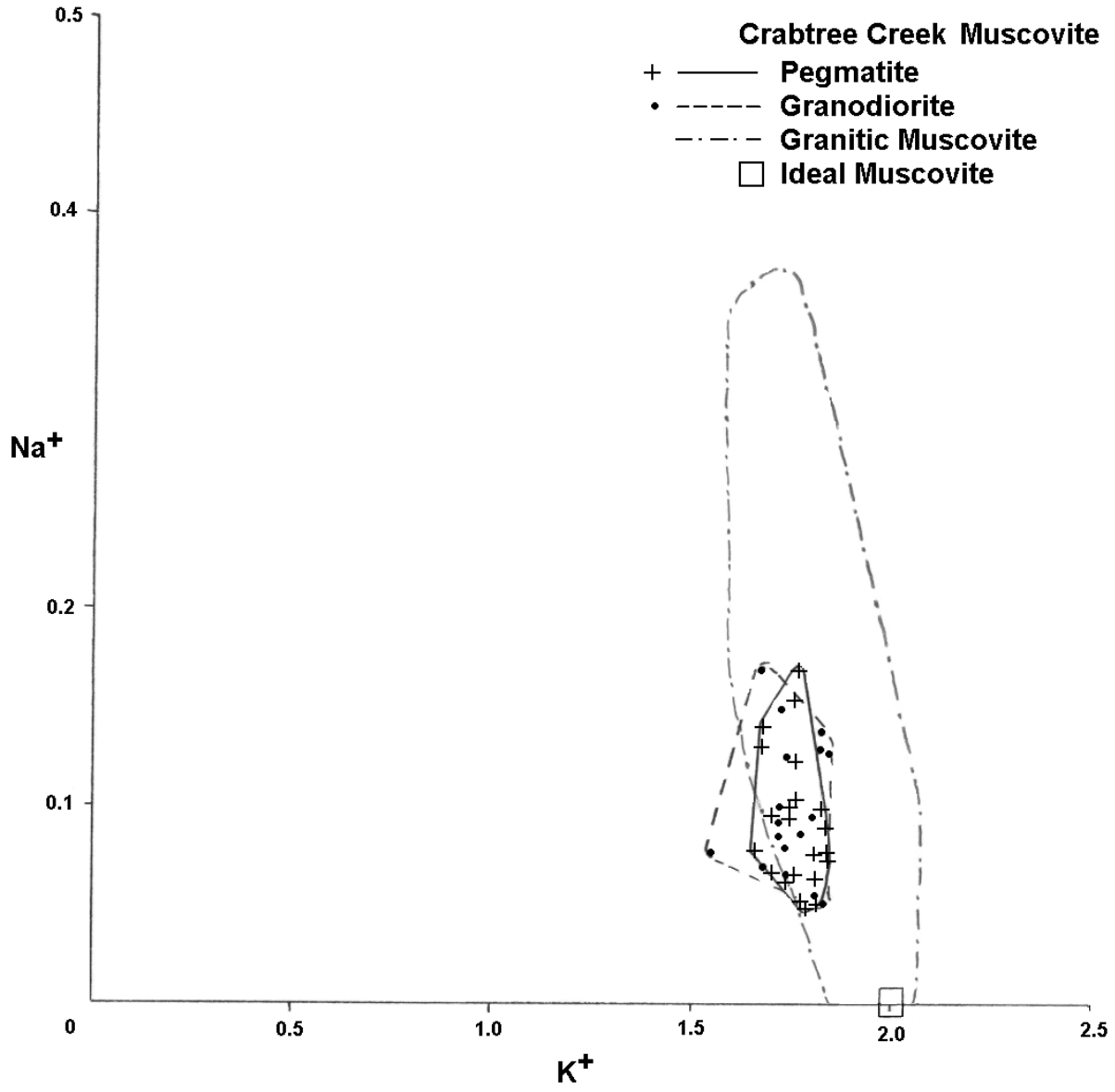

Figure 52 Paragonitic substitution in Crabtree Creek muscovite. Significant overlap of granodiorite and pegmatite fields indicates similar paragonite substitution taking place in pegmatites and in host granodiorites. Granitic muscovite field from Zane and Rizzo (1999).

A few analyses of muscovite from the Roan Road outcrop plot in the field for primary granitic muscovite (Figures 53 and 54) from Zane and Rizzo (1999), supporting the textural evidence that most of the muscovite is primary. Fluorine and chlorine contents in muscovite from the Roan Road granodiorite are below detection levels.

The biotite in host granodiorite contains slightly less potassium and less silica than the muscovite (Appendix D). Biotite also contains measurable manganese and titanium. Two analyses of granodioritic biotite detected fluorine. This biotite appears to be unzoned. One grain of biotite intergrown in granodioritic muscovite (CC1-1bioinmica2; Appendix D) is similar in composition to biotite independent of muscovite, with the exception of containing less potassium. Biotite was observed in a quartz-muscovite pegmatite unit of the Northwest Hootowl study area in minute amounts. This biotite was not analyzed because it is visible in hand sample but not in the prepared thin section.

Biotite from the biotite schist located at the base of the Northwest Hootowl study area (Figure 25) is much richer in Mg and Fe and poorer in Al than granodioritic biotite. Biotite from this schist contains significant fluorine. Biotite from the schist xenolith in the Northwest Hootowl study area contains slightly less Fe and Mg and slightly more Al than the biotite from the adjacent schist (Appendix D). One mica grain (HO1-1biotite1core-rim; Appendix D) from the xenolith contains much less Mg and Fe and much more Al than other biotite from the same unit. This grain appears to be an intermediate member of biotite-muscovite solid solution. All biotite from the schist and the xenolith contains measurable titanium.

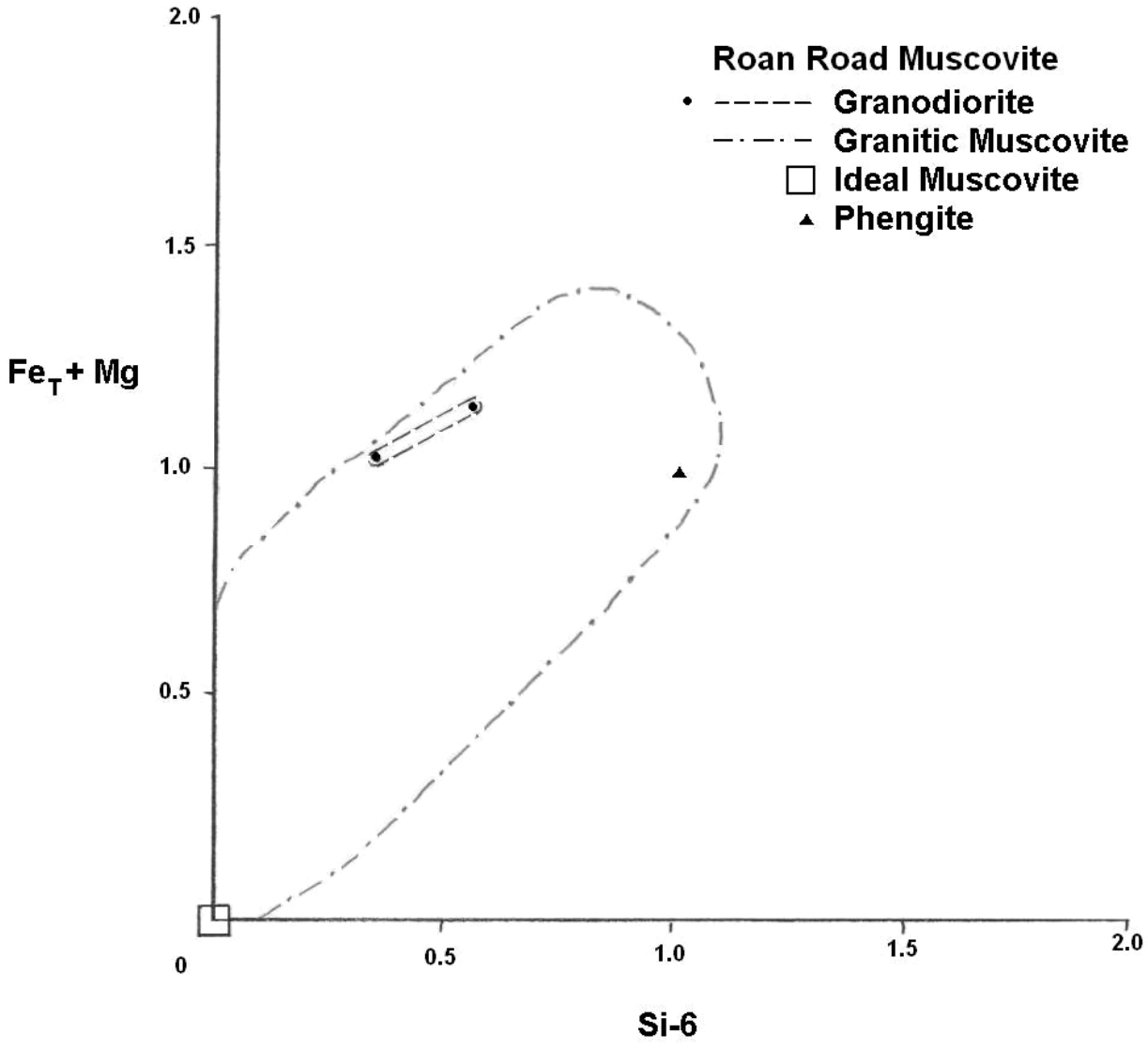

Figure 53 Celadonitic substitution in Roan Road muscovite. Both analyses plot in the range for granitic muscovite from Zane and Rizzo (1999). Substitutional space of phengite is illustrated by the triangle. Fe_T stands for total Fe.

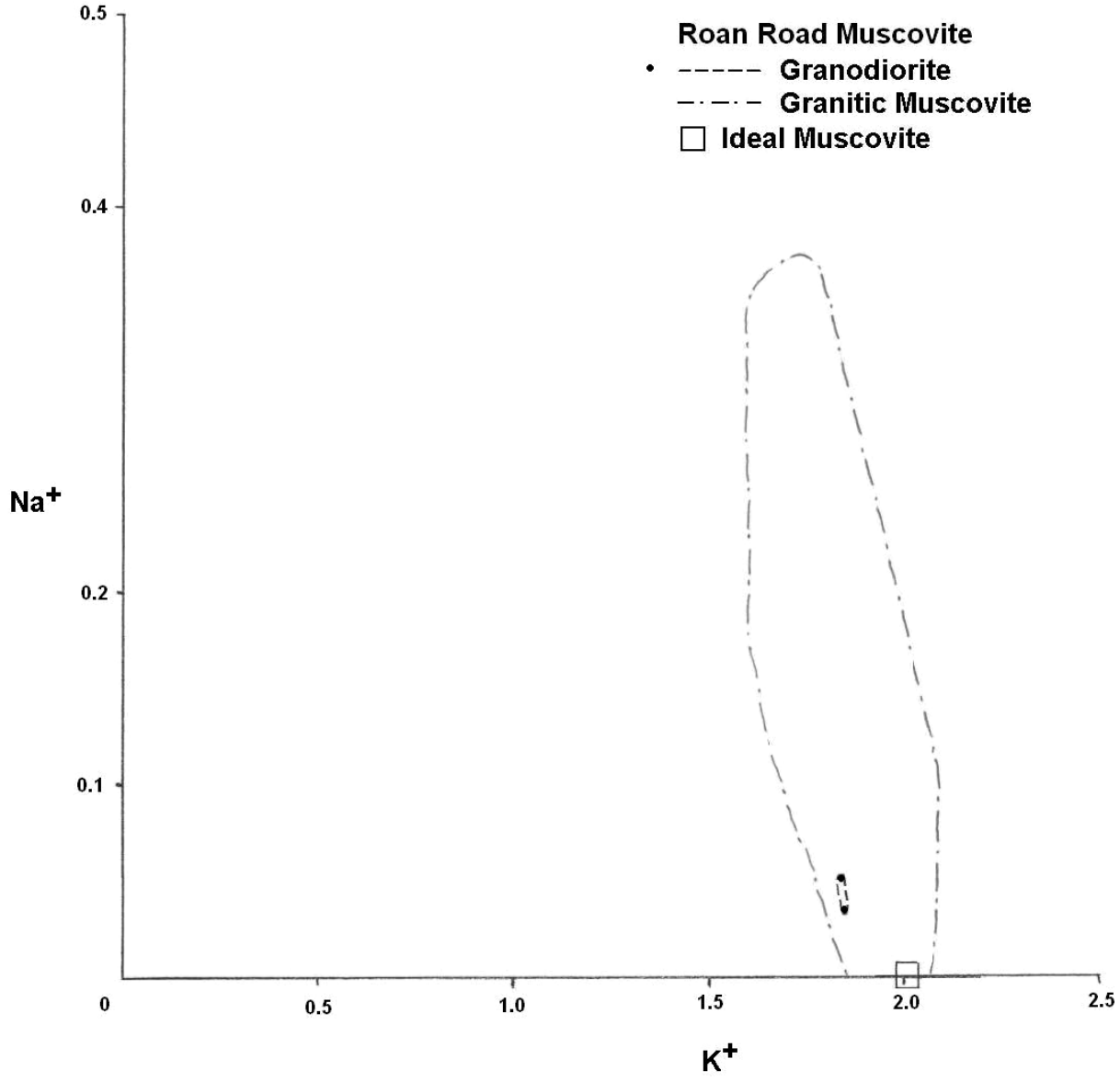

Figure 54 Paragonitic substitution in Roan Road muscovite. Both analyses show Na/K substitution and neither plot near ideal muscovite. Granitic muscovite field from Zane and Rizzo (1999).

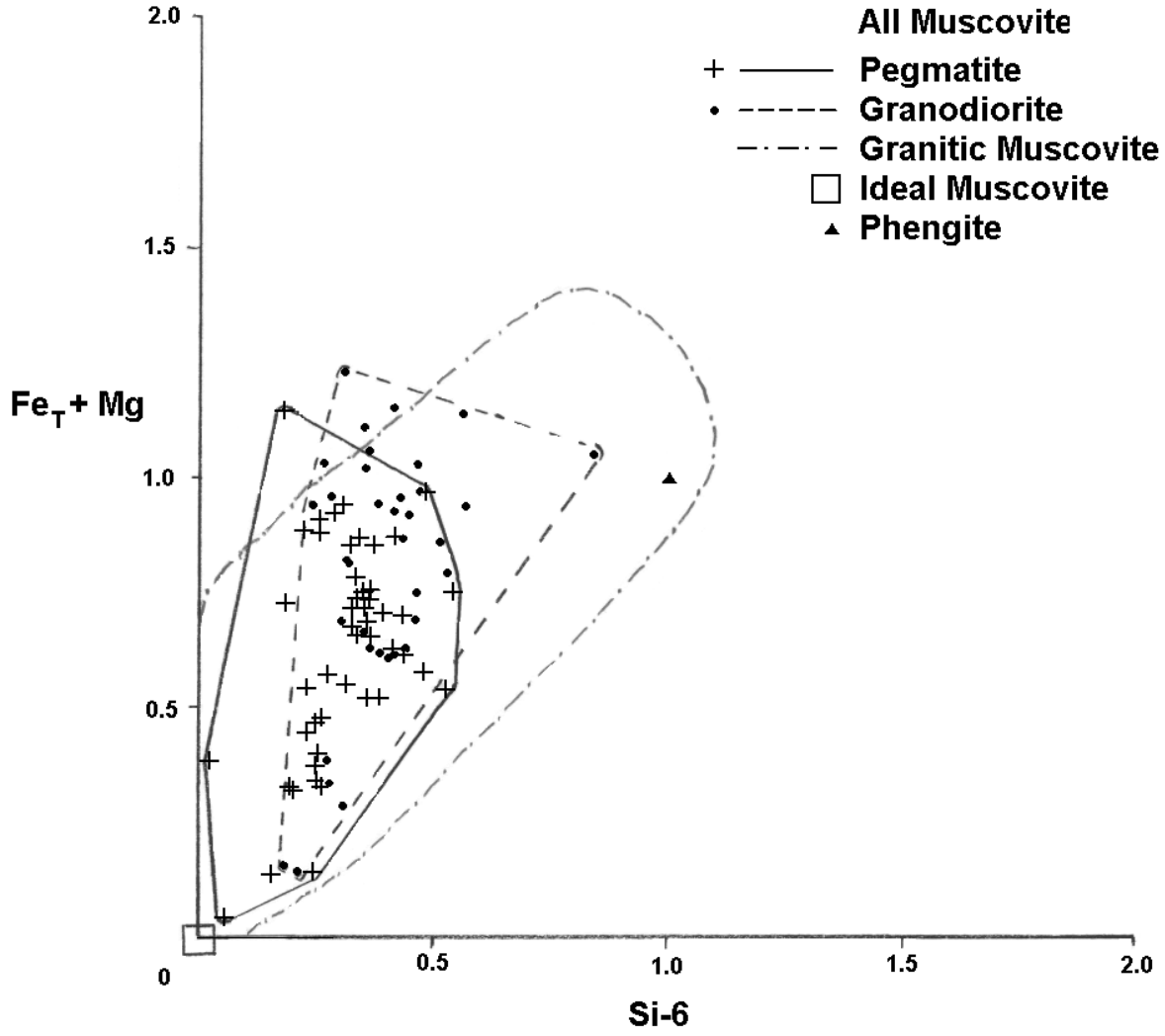

Figure 55 Summary of celadonitic substitution in all white mica analyses. Most analyses plot in the range for granitic muscovite from Zane and Rizzo (1999). Substitutional space of phengite is illustrated by the triangle. Fe_T stands for total Fe.

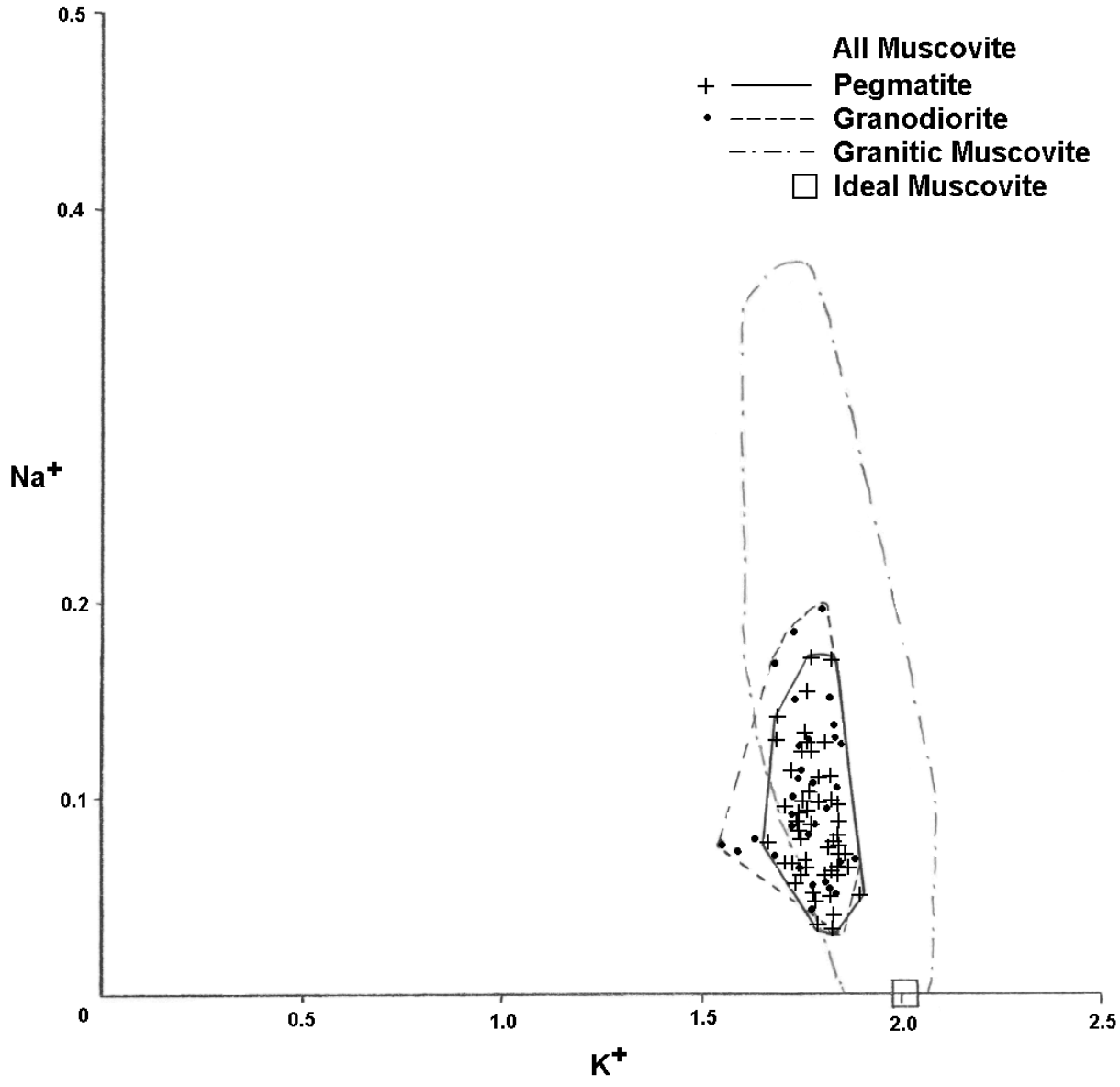

Figure 56 Summary of paragonitic substitution in all white mica analyses. Significant overlap of granodiorite and pegmatite fields indicates similar paragonite substitution taking place in pegmatites and in host granodiorites. Granitic muscovite field from Zane and Rizzo (1999).

Feldspar

Plagioclase is the most abundant feldspar in the Spruce Pine granodiorites, but various pegmatites and zones in pegmatites may be richer in alkali feldspar. Large crystals of feldspar occur in the granodiorite surrounded by a matrix of finer-grained feldspar, quartz, mica, and garnet. Plagioclase displays polysynthetic twinning in both hand sample and thin section. Plagioclase twins often show offset or bending due to accumulation of differential stress from tectonic or thermal factors. Alkali feldspar often displays Carlsbad twinning visible in thin section but rarely noticed in hand sample. Twinned alkali feldspar is often perthitic, with twinned albite exsolution lamella visible in thin section.

Plagioclase from the bodies studied is always white in color and sometimes has a chalky appearance on dry, fresh surfaces. Alkali feldspar from these bodies is nearly always white and often difficult to distinguish from plagioclase on all but very fresh surfaces. Alkali feldspar is rarely light pink in color, aiding in identification. Size of feldspar crystals ranges from a few dozen microns to upwards of 50 cm wide. The largest alkali feldspar crystals are usually perthitic. Large crystals of alkali feldspar or plagioclase graphically intergrown with quartz are common. Small crystals of muscovite and garnet are often found in this graphic granite. Many feldspars display myrmekitic texture in thin section.

Plagioclase is found in all pegmatite zones in some amount. Quartz-alkali feldspar (±muscovite, ±garnet) pegmatites have minor plagioclase as exsolution in perthite and as small, isolated grains that are not visible in outcrop or hand sample. Plagioclase grains in granodiorite range in size from microns up to 1.5 cm wide. The average size of plagioclase is noticeably smaller than the average pegmatitic feldspar crystal. Plagioclase crystals in pegmatite zones range in size from a few microns to over 30 cm wide. The largest plagioclase crystals occupy

the intermediate zones of pegmatites, as plagioclase crystals tend to get slightly smaller near quartz core. Margins of single plagioclase crystals are hard to trace in outcrop, but cleavage surfaces often offer good approximation of size of individual crystals and sometimes display striations that make it possible to distinguish the grains as plagioclase.

Alkali feldspar is found in all pegmatite zones in some amount. One pegmatite zone is nearly all perthitic alkali feldspar, while all other pegmatite zones contain some amount of alkali feldspar. Quartz cores of pegmatites sometimes have isolated crystals of alkali feldspar that appear to "float" in the quartz and are not attached to any feldspar pegmatite zone. Alkali feldspar grains in granodiorite range in size from microns up to 1.5 cm wide. Alkali feldspar crystals in pegmatite zones range in size from a few microns to over 50 cm wide, and are often larger than plagioclase crystals in similar pegmatite zones. The largest alkali feldspar crystals occupy the intermediate zones of pegmatites, as alkali feldspar crystals tend to get slightly smaller near quartz core. Margins of single alkali feldspar crystals are hard to trace in outcrop, but cleavage surfaces often offer good approximation of size of individual crystals. Perthitic texture is sometimes evident in outcrop.

Compositions of feldspar are given in Appendix E. Alkali feldspar in granodiorite and pegmatite is all near end-member potassium feldspar, with little Na substitution. Plagioclase in exsolution lamella in perthite is very near end-member albite, with little K or Ca substitution. Plagioclase crystals are oligoclase in composition, while exsolved plagioclase in perthite is albite with some Ca substitution. Most plagioclase crystals display very little zoning. The few zoned plagioclase crystals in granodiorite have rims richer in albite component. This Na enrichment in rims of granodioritic plagioclase is observed in all zoned plagioclases from all granodiorites. A plagioclase crystal (HO2-2plagcore-rimL; Appendix E) in quartz-plagioclase-muscovite-garnet

pegmatite provides the only analysis of a zoned plagioclase in which the rim is significantly richer in anorthite component than the core.

Plagioclase in the Field Mine is present as sodic oligoclase crystals and as albite exsolution in perthite (Figure 57). Granodioritic plagioclase from the Field Mine is calcic oligoclase. Sodic albite is observed as exsolution in perthite. Plagioclase crystals independent of perthite are calcic oligoclase. Pegmatitic plagioclase is oligoclase.

The only analysis of plagioclase in Bon Ami B is albite (Figure 58). This albite contains almost no potassium.

Exsolved plagioclase from granodioritic perthite from Bon Ami C is sodic albite (Figure 59). Pegmatitic plagioclase is oligoclase.

Granodioritic plagioclase from the Northwest Hootowl study area is present as oligoclase crystals and as sodic albite exsolution in alkali feldspar (Figure 60). Plagioclase crystals independent of perthite are calcic oligoclase. Pegmatitic plagioclase is oligoclase. Plagioclase exsolution in pegmatitic alkali feldspar is near end-member albite.

Pegmatitic plagioclase from the Southeast Hootowl study area is oligoclase (Figure 61). This pegmatitic oligoclase contains more orthoclase component than other pegmatitic plagioclase.

Crabtree Creek feldspar compositions are shown in Figure 62. Albite in the Crabtree Creek granodiorite is found as both exsolution in perthite and as single plagioclase crystals. Some plagioclase crystals are oligoclase in composition. Pegmatitic plagioclase is oligoclase. Alkali feldspar compositions show some sodium substitution and almost no anorthite component.

Feldspar composition from Roan Road granodiorite is shown in Figure 63. Plagioclase from Roan Road granodiorite is oligoclase with minor potassium.

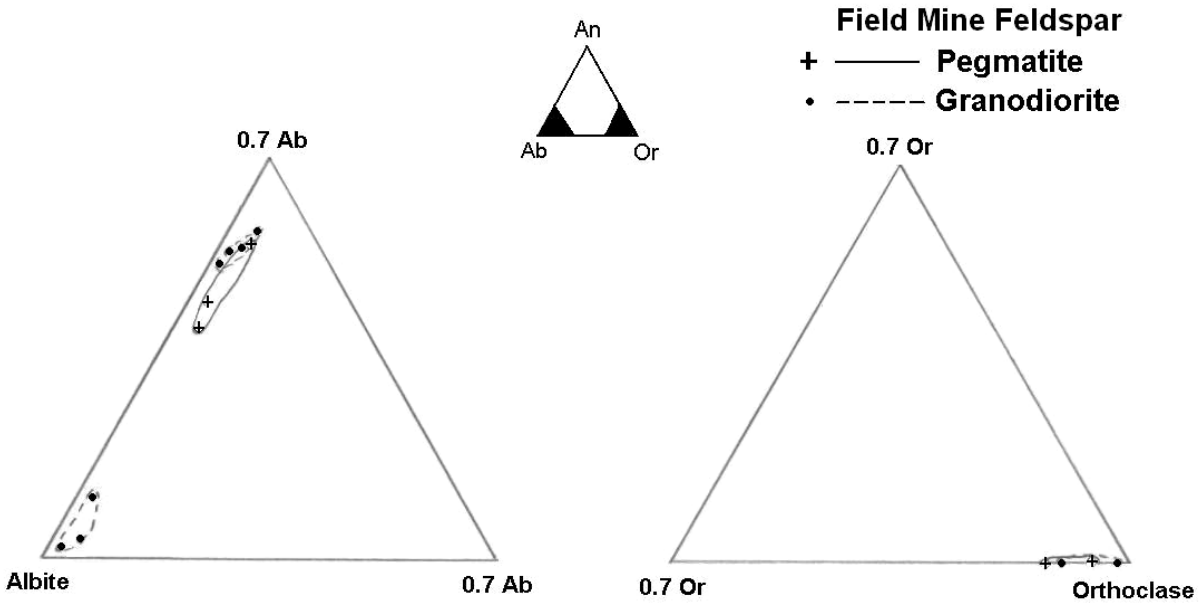

Figure 57 Field Mine feldspar compositions. Granodioritic plagioclase from the Field Mine is present as sodic albite exsolution in alkali feldspar and calcic oligoclase crystals. Plagioclase crystals independent of perthite are calcic oligoclase. Pegmatitic plagioclase is oligoclase. Granodioritic and pegmatitic alkali feldspar show sodium substitution, but very little calcium.

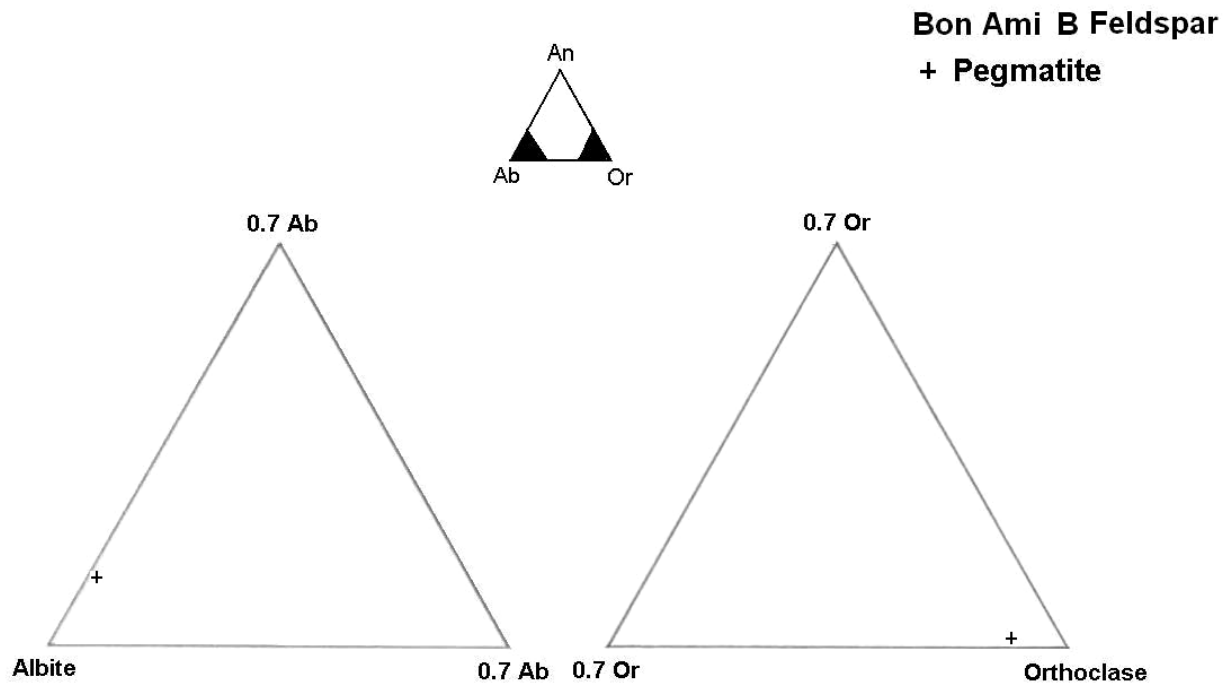

Figure 58 Bon Ami B feldspar composition. Pegmatitic plagioclase is albite. Pegmatitic alkali feldspar shows sodium substitution, but very little calcium.

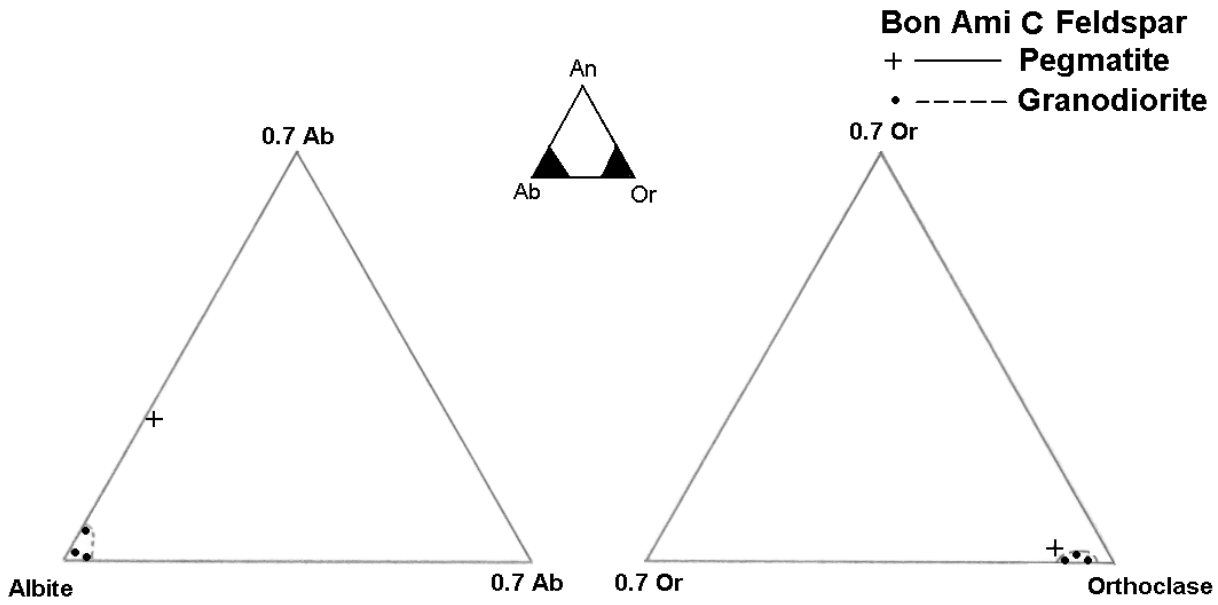

Figure 59 Bon Ami C feldspar compositions. Granodioritic plagioclase exsolution in alkali feldspar is sodic albite. Pegmatitic plagioclase is sodic oligoclase. Granodioritic and pegmatitic alkali feldspar show sodium substitution, but very little calcium.

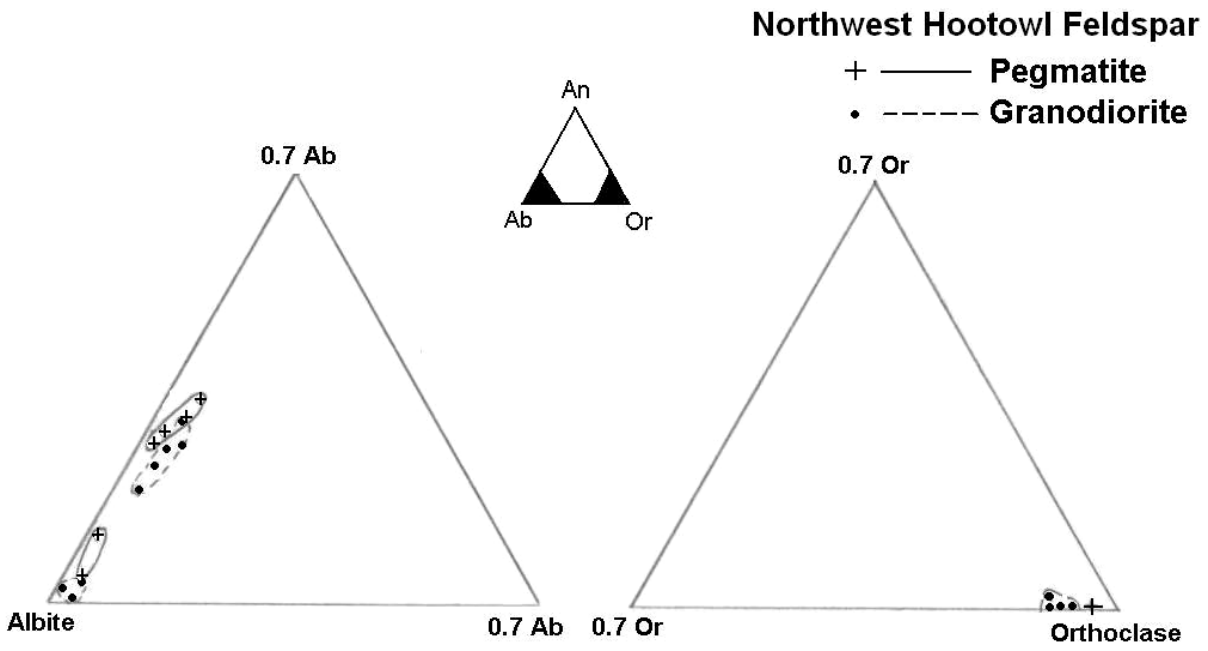

Figure 60 Northwest Hootowl feldspar compositions. Granodioritic plagioclase from the Northwest Hootowl study area is oligoclase. Sodic albite is seen as exsolution in granodioritic perthite. Plagioclase crystals independent of perthite are calcic oligoclase. Pegmatitic plagioclase is oligoclase. Plagioclase exsolution in pegmatitic alkali feldspar is albite. Granodioritic and pegmatitic alkali feldspar show sodium substitution, but very little calcium.

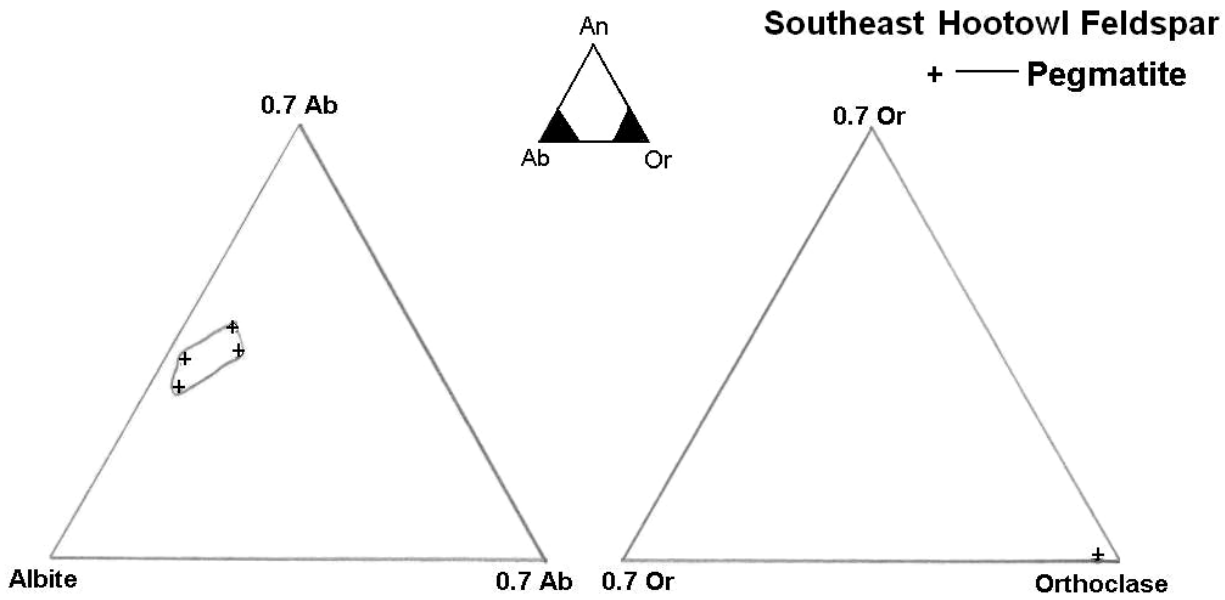

Figure 61 Southeast Hootowl feldspar compositions. Pegmatitic plagioclase is oligoclase. Pegmatitic alkali feldspar is near end-member orthoclase.

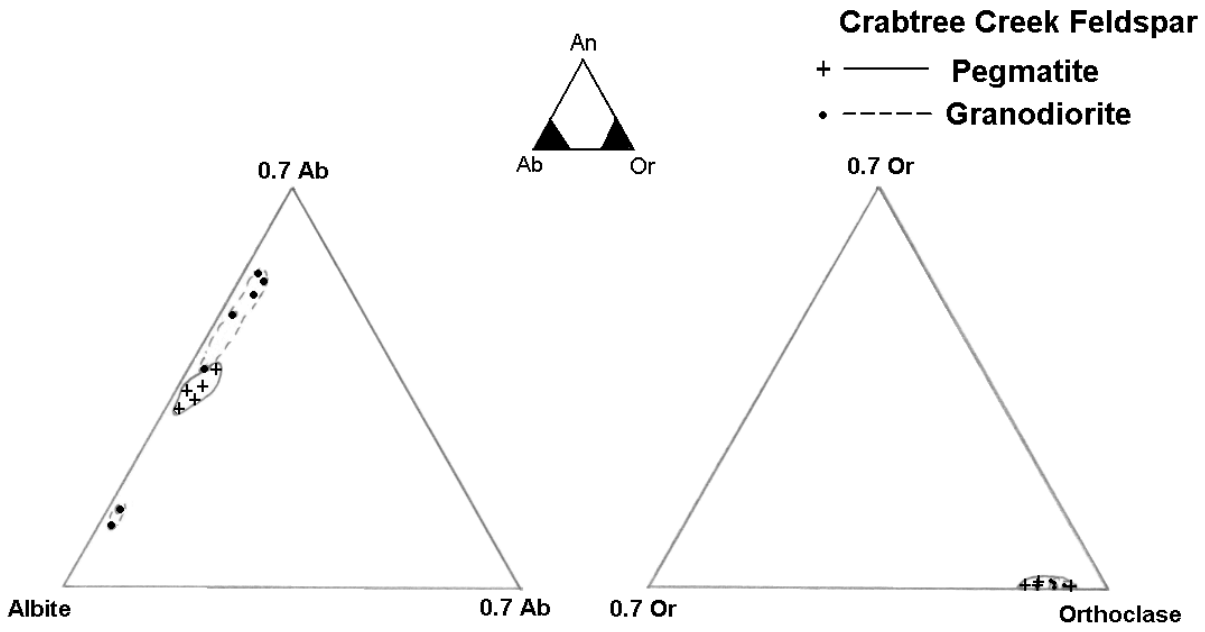

Figure 62 Crabtree Creek feldspar compositions. Granodioritic plagioclase is oligoclase. Plagioclase exsolution in granodioritic perthite is albite. Pegmatitic plagioclase is oligoclase. Alkali feldspar compositions show some sodium substitution and almost no anorthite component.

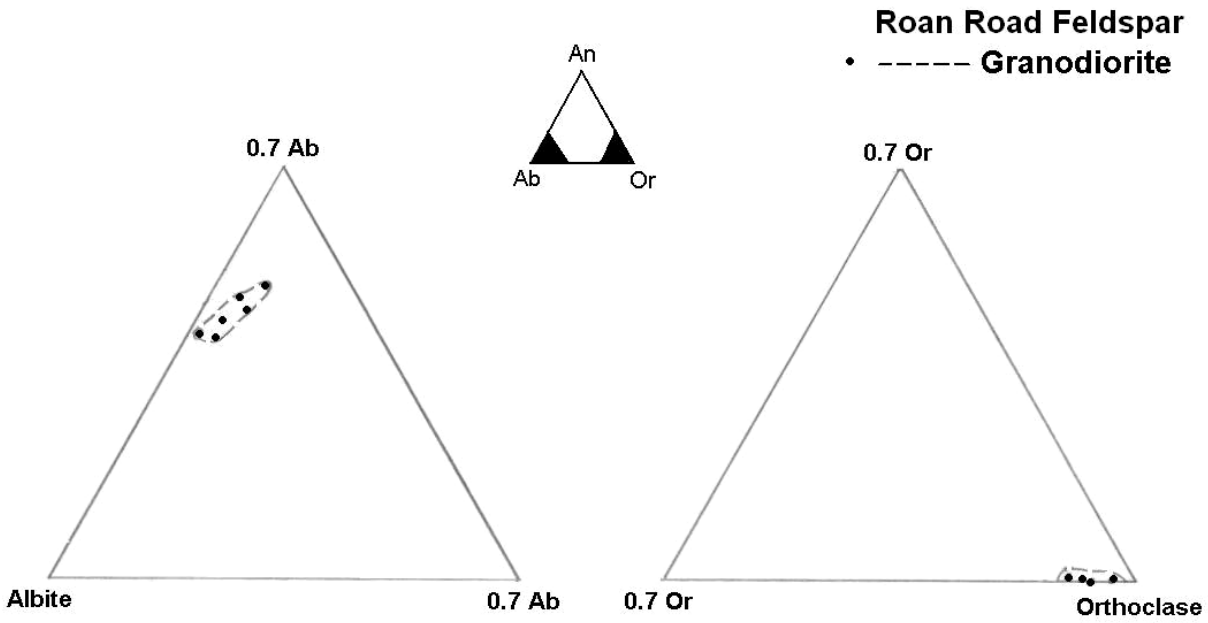

Figure 63 Roan Road feldspar compositions. Plagioclase is oligoclase with minor potassium and alkali feldspar shows slight sodium and almost no calcium.

Plagioclase from all bodies studied is similar in compositional range (Figure 64). Granodioritic plagioclase ranges from sodic to calcic oligoclase. Pegmatitic plagioclase is oligoclase. Exsolved plagioclase in alkali feldspar from granodiorite and pegmatite is albite. The pegmatite and granodiorite fields show extensive overlap, illustrating the similarity between feldspar compositions from pegmatites and granodiorites in single bodies as well as between all bodies studied. Plagioclase compositions from granodiorite and pegmatite nearly mimic each other.

Alkali feldspar in granodiorite is all near end-member orthoclase with less than 5 mole percent albite and anorthite components (Figures 57 through 64). Alkali feldspar in all pegmatite zones is near end-member orthoclase. Alkali feldspar in all pegmatite zones shows similar range in Na and very little Ca.

Epidote

Epidote occurs as an accessory mineral in both host granodiorites and some pegmatite zones. Epidote is usually observed as euhedral crystals partially enclosed by muscovite, sharing a crystal face parallel to cleavage trace of muscovite (Figure 65). Some epidote displays slight zoning when viewed by electron microprobe due to inhomogeneous distribution of trace amounts of rare earth elements. Compositions of epidote are given in Appendix F. The composition of epidote in Spruce Pine granodiorites and pegmatites approximates the composition of epidote from Deer et al., (1992). Epidote from the Spruce Pine granitoids contains variable iron (2.9 to 11.5 weight percent total iron; Appendix F).

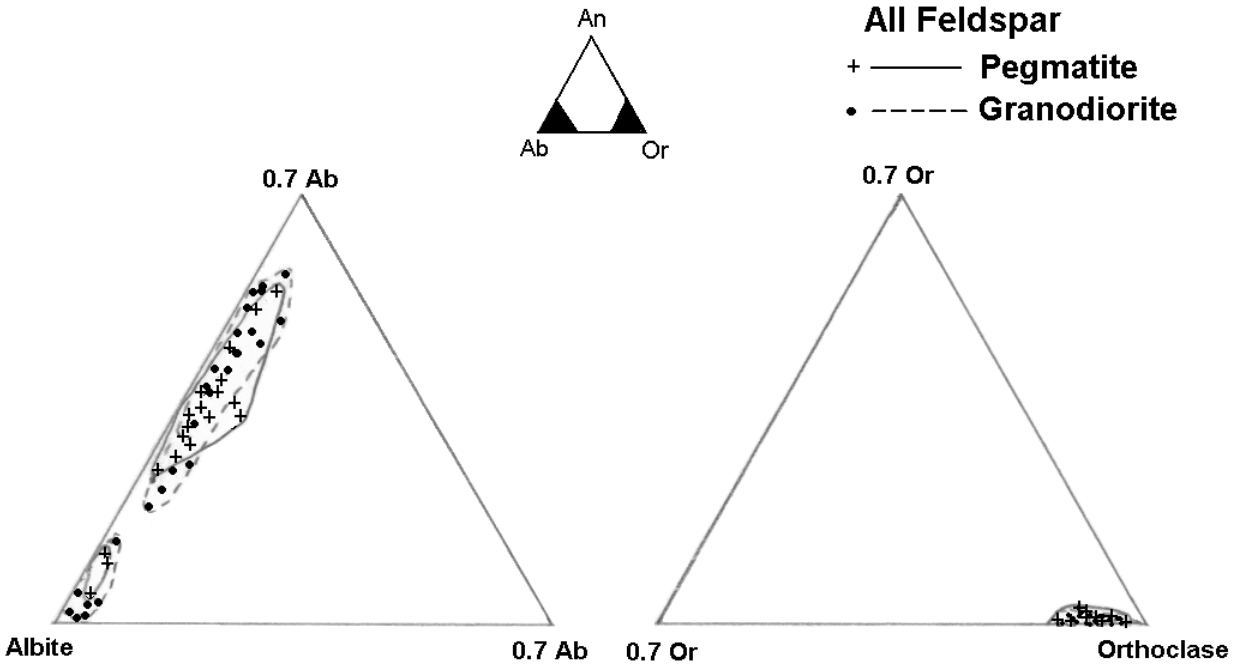

Figure 64 Summary of feldspar compositions from all bodies studied. Granodioritic plagioclase ranges from sodic to calcic oligoclase. Pegmatitic plagioclase ranges from sodic to calcic oligoclase. Exsolved plagioclase in alkali feldspar from granodiorite and pegmatite is albite. Few single crystals of plagioclase in granodiorite and pegmatite are albite. The pegmatite and granodiorite fields show extensive overlap, illustrating the similarity between feldspar compositions from pegmatites and granodiorites in single bodies as well as between all bodies studied. Plagioclase compositions from granodiorite and pegmatite nearly mimic each other.

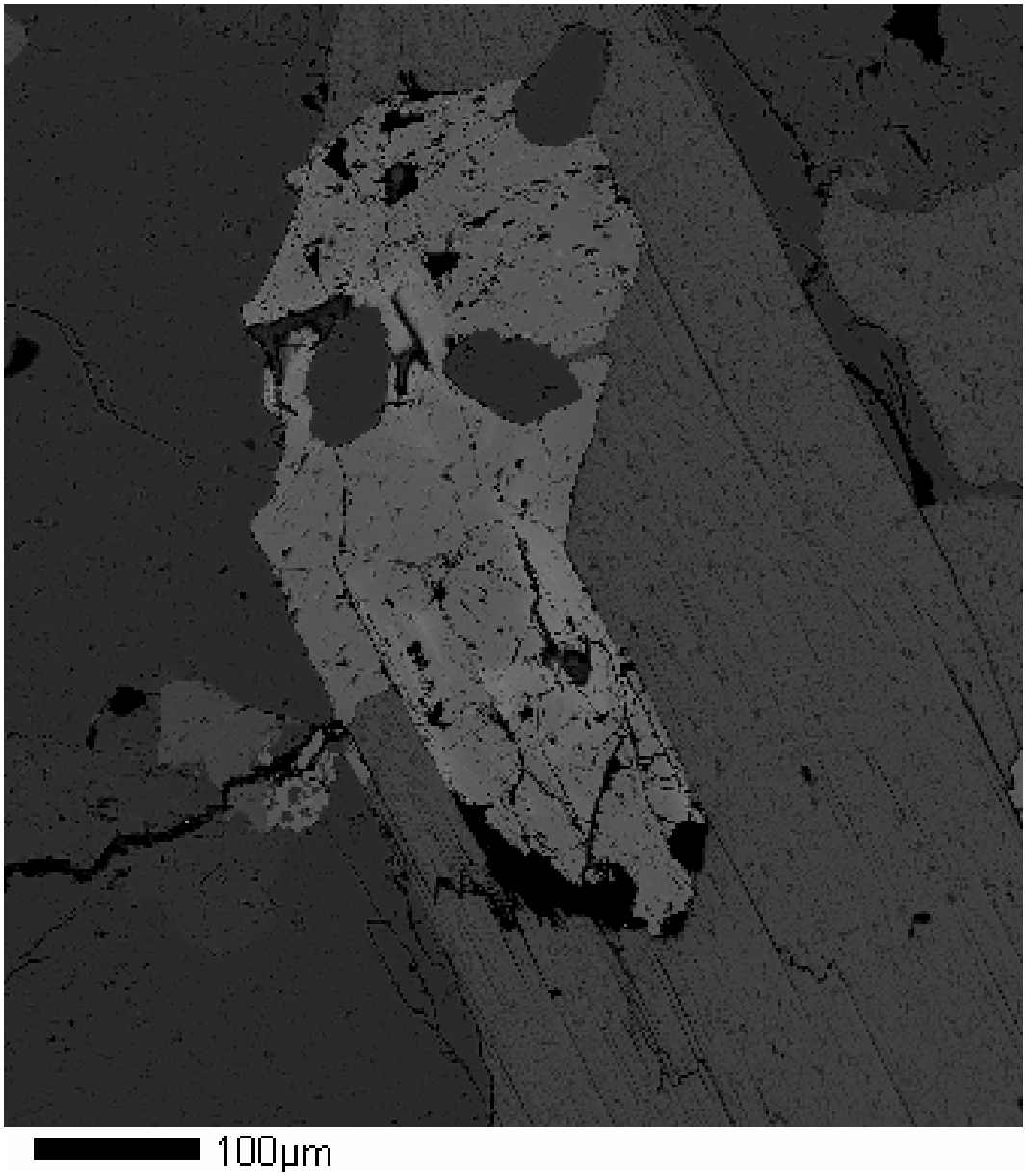

Figure 65 Backscatter electron image of epidote in muscovite. The epidote partially enclosed by muscovite crystal sharing cleavage face at right and crystal face at left. Other crystal faces of epidote cleanly truncate micaceous cleavage with no visible deformation. Slight zoning in this epidote is attributed to trace amounts of rare-earth elements.

CHAPTER 7

DISCUSSION

Pegmatite Zones

A comparison between pegmatite zones of Cameron et al. (1949) of the southeastern United States and those identified in this study is made in Table 4. Not all pegmatite zones were identified in each body and some pegmatites, such as Crabtree Creek and Bon Ami C, have multiple zones with distinct mineral assemblages.

Granodiorite Mineralogy

Garnet

Garnets in host granodiorite are almandine-spessartine with or without Ca-rich rims. The almandine-spessartine garnet cores plot in the field for granitic garnet (Figure 36), consistent with a magmatic origin of garnets. Inclusions are not observed in garnets from granodiorite, further suggesting that the garnets are not xenocrysts from the Ashe Metamorphic Suite. The presence of grossular-rich rims on some of these garnets hints at the introduction of extra calcium from a Ca-rich fluid at a late stage of crystallization or even post-crystallization. Late stage introduction of Ca through fluid interaction may be responsible for the growth of Ca-rich garnet rims.

Muscovite

Muscovite in the granodiorite shows significant celadonitic and paragonitic substitution (Figures 55 and 56). The iron contents of the muscovite is probably responsible for the green tint seen in all muscovite from the bodies studied. Most granodioritic muscovite plots in the field of

Table 4 Comparison of pegmatite zones. Zones of Cameron et al. (1949) approximate the pegmatite zones observed in this study.

Cameron et al. (1949) (minus garnet)	Location Observed in This Study
Quartz-muscovite	Bon Ami A, Bon Ami C, NW Hootowl
Plagioclase-quartz-muscovite	Field Mine, SE Hootowl
*Plagioclase-quartz	Crabtree Creek, Field Mine, Bon Ami C, NW Hootowl
Plagioclase	Not Observed
Quartz-perthite-plagioclase ±muscovite	Crabtree Creek, Bon Ami A, Bon Ami B,
Perthite-quartz-muscovite	Crabtree Creek, Bon Ami C
*Perthite-quartz	Crabtree Creek, Field Mine, Bon Ami C, NW Hootowl
Perthite	Crabtree Creek, Bon Ami A, Bon Ami B, Bon Ami C, SE Hootowl
Perthite euhedra-quartz	Bon Ami A,
Quartz	Crabtree Creek, Field Mine, Bon Ami A, Bon Ami B, Bon Ami C, NW Hootowl, SE Hootowl
*Perthite-quartz and plagioclase-quartz includes graphic granite.	
Zones identified but not listed in Cameron et al. (1949)	
Perthite-plagioclase	Bon Ami A
Burr muscovite	NW Hootowl

primary igneous muscovite defined by Zane and Rizzo (1999), lending credence to the claim that the muscovite is magmatic in origin.

Biotite

Biotite in the host granodiorite is nearly always present as "crow's foot" mica. This texture represents dendritic branching on individual biotite grains during crystallization. Such dendritic textures develop in response to a system which is super-saturated with respect to biotite.

Feldspar

Plagioclase compositions in granodiorite range from albite to oligoclase with very little zoning (Figure 64). Calcium enrichment in the rims of granodioritic plagioclase is absent. Thus, the late-stage, Ca-rich event recorded by the grossular rims on some garnet is not recorded by the plagioclase. Alkali feldspar in the granodiorite shows little Na and Ca (Figure 64). The addition of Ca to the system did not affect alkali feldspar.

Pegmatite Mineralogy

Garnet

Garnets from different pegmatite zones all appear similar. Nearly all are euhedral, red-brown crystals free of inclusions. Garnets in pegmatite zones are usually concentrated in lenses or stringers and the texture and compositions of those garnets are similar. Garnet core compositions are remarkably constant among all pegmatite zones and across all pegmatite bodies. Garnet cores are all almandine-spessartine (Fe:Mn = 1.5:1 to 1:1) and nearly all plot in the granitic garnet field compiled from Deer et al. (1992) (Figure 36) and are indistinguishable from garnets in the granodiorite. Ca-concentrations in pegmatitic garnet rims vary from zone to zone in the pegmatite. Not all zones have garnets with grossular-rich rims. Some garnets from

the quartz-plagioclase pegmatite, quartz-plagioclase-muscovite pegmatite, and quartz-perthite-muscovite-garnet pegmatite have only mid-Ca rims. No garnet analyzed from these zones had a grossular-rich rim composition. Garnets from quartz-perthite-muscovite pegmatite and quartz-muscovite pegmatite lack Ca-enriched rims. Pegmatite zones with grossular-rich and mid-Ca garnet rims have been affected by Ca-rich metasomatism. Pegmatite zones whose garnets lack high- or mid-Ca components probably did not experienced the same Ca-enrichment event.

Permeability of pegmatite and granodiorite did not control the degree of Ca-enrichment in garnet rims, as Ca enrichment levels vary between pegmatite and granodiorite at different localities. Permeability of the rock did not influence the path of the Ca-rich fluid. In the Crabtree Creek exposure, Ca enrichment in garnet rims from granodiorite is more extensive than Ca enrichment in pegmatitic garnet rims. In Bon Ami C area and Northwest Hootowl study area, pegmatitic garnet rims are more Ca-rich than garnet rims from adjacent granodiorite. Thus, the Ca-enrichment event does not show a preference for either pegmatite or granodiorite. Pegmatitic garnet from the Field Mine, Bon Ami B area, and the Southeast Hootowl study area display Ca-rich rims. Sampling of granodiorite adjacent to these pegmatites could provide data to compare Ca enrichment of garnet rims from the granodiorite and the pegmatite. Aside from these observations from a limited sample set, more extensive sampling and analysis of these pegmatites and granodiorites is needed to test the hypothesis that grossular rims are found in all pegmatites and granodiorites.

Grossular garnet often occurs in rocks that have undergone calcium metasomatism (Deer et al. 1982) and can form from hydrothermal solutions (Jamtveit, 1991). The garnets from Spruce Pine may have a hydrogrossular component, as shown by a slight decrease in microprobe totals with increased grossular component (Figure 66). This decrease in oxide totals, no more

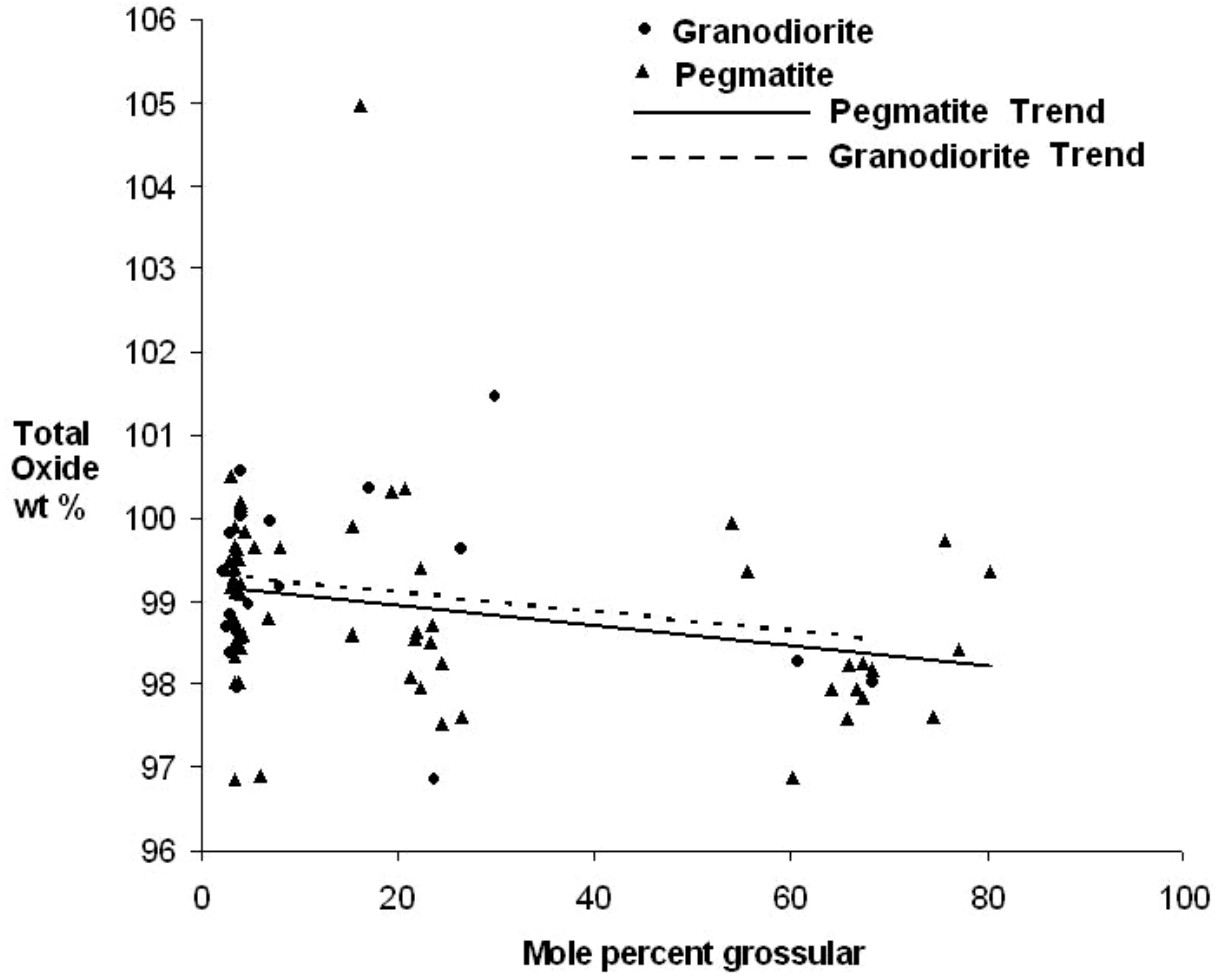

Figure 66 Chart of decreasing microprobe totals with increasing grossular component in garnet. The drop in oxide totals with increasing grossular component may be the result of water in the garnet structure. The dotted trendline displays decrease in oxide totals with increasing grossular component for granodioritic garnets. The undotted trendline shows decrease in oxide totals with increasing grossular component for pegmatitic garnets. The two trendlines have very similar slopes, indicating amounts of volatile in the garnet increases similarly in pegmatites and granodiorites. The trendlines are functions of least squares regression and are generated by Excel plots.

than a few percent below 100, may be due to presence of unanalyzed water in the garnet structure, hinting at a water rich fluid as agent of Ca-enrichment.

Most pegmatitic garnets are solid solutions of spessartine and almandine with almost no other significant garnet component (Deer et al. 1982). To my knowledge, garnet with a high grossular component has not been reported from other pegmatites.

Muscovite

Muscovite compositions are similar in all pegmatite zones. Muscovite contains significant celadonitic (mainly Fe) and paragonitic components. Small differences in volatile chemistry are observed between pegmatite zones.

There is no relation between the concentration of fluorine and chlorine in muscovite and the concentration of Ca in garnet rims (Figure 67). Muscovite from the Field Mine and Bon Ami B pegmatites lacks measurable fluorine and chlorine, but pegmatitic garnets from Field Mine have mid-Ca rims and Bon Ami B pegmatite contains garnets with grossular rims. These two study areas show Ca enrichment in the absence of fluorine and chlorine.

Muscovite from Bon Ami C area and granodiorite contains chlorine but lacks fluorine. Garnets from Bon Ami C area boast grossular rims while granodioritic garnet rims are mid-Ca. Chlorine contents in the pegmatite and granodiorite are similar, but Ca-enrichment in garnet rims differs slightly.

Pegmatitic muscovite from Crabtree Creek contains chlorine but lacks fluorine, while garnets from the pegmatite have mid-Ca rims. Muscovite from Crabtree Creek granodiorite contains measurable amounts of fluorine and chlorine. Garnets from Crabtree Creek granodiorite have grossular-rich rims. Chlorine is present in muscovite from pegmatite and granodiorite, but Ca enrichment in garnets differs.

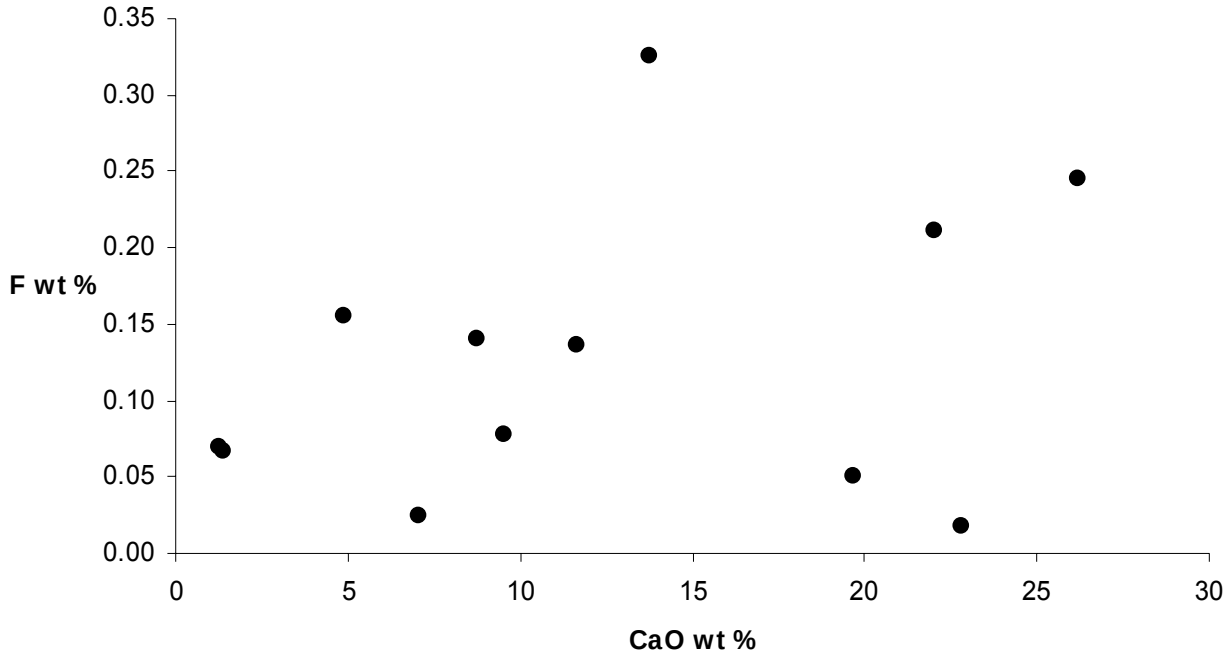

Figure 67 Chart of weight percent fluorine in muscovite versus weight percent calcium in garnet rims. There is no apparent relation between fluorine in muscovite and degree of Ca-enrichment in rims of garnets.

Muscovite from Northwest Hootowl pegmatite contains fluorine but lacks chlorine, and granodioritic muscovite contains fluorine and chlorine. Pegmatitic garnets in this body have Grossular-rich rim compositions, while granodioritic garnet rims are low-Ca. Pegmatitic muscovite from Southeast Hootowl study area contains fluorine but lacks chlorine. Garnet from this pegmatite boasts grossular rims.

The presence of chlorine and fluorine in muscovites from the granodiorites and adjacent pegmatites varies from body to body and is independent of Ca enrichment in garnet rims. Fluorine and chlorine contents of muscovites are similar in affinity for pegmatite and granodiorite bodies.

Biotite

Biotite was observed in only one sample of quartz-muscovite pegmatite zone of Northwest Hootowl study area in minute amounts. This biotite was not analyzed. In thin section, this light-brown, pleochroic grain looks similar to biotite from the granodiorite.

Plagioclase

Plagioclase is found in nearly all pegmatitic zones. Pegmatitic plagioclase ranges from sodic albite as exsolution lamella in perthite, to single crystals of calcic oligoclase. Plagioclase in graphic granite ranges from albite to oligoclase. Plagioclase in quartz-plagioclase-muscovite-garnet pegmatite ranges from sodic oligoclase to calcic oligoclase. Plagioclase in quartz-plagioclase-perthite-muscovite-garnet pegmatite is albite exsolution lamella in perthite and crystals of sodic oligoclase. Plagioclase from quartz-plagioclase pegmatite is oligoclase. Some plagioclase in this zone is antiperthitic, with exsolution of near-end member orthoclase. Plagioclase in quartz-plagioclase-muscovite pegmatite is oligoclase. Plagioclase composition in two-feldspar pegmatite zones is similar to that in one-feldspar pegmatite zones. Most

plagioclase crystals from other pegmatites display very little zoning (Martin, 1982). The plagioclase likely equilibrated with the melt during crystallization. Water in the melt facilitates ion migration, aiding in equilibration of feldspar with melt. One zoned plagioclase (Ab_{81} to Ab_{69}; HO2-2plagcore-rimL; Appendix E) in quartz-plagioclase-muscovite-garnet pegmatite was observed to have a rim richer in Ca than the core. This crystal provides the only example of a zoned pegmatitic plagioclase in which the rim is significantly richer in anorthite component than the core. The zoning in this crystal may reflect that the quartz-plagioclase-muscovite-garnet pegmatite experienced the same Ca-rich metasomatic event that caused calcium enrichment in garnet rims. Unzoned plagioclase is typical of pegmatites, but zoning of Rb and Sr was found by Martin (1982). Thus, the lack of zoning in plagioclase from Spruce Pine pegmatites is typical of pegmatites.

Alkali Feldspar

Alkali feldspar is found in all pegmatite zones. One pegmatite zone is nearly all perthitic alkali feldspar. Quartz cores of pegmatites sometimes have isolated crystals of alkali feldspar that appear to "float" in the quartz and are not attached to any feldspar pegmatite zone. Alkali feldspar from all pegmatite zones displays the same limited Na substitution and minor anorthite component (Figure 64). Alkali feldspar is unzoned and does not appear to be affected by the Ca-rich metasomatic event. Zoning of incompatible trace elements, such as B and Rb, in pegmatitic alkali feldspar is reported by Martin (1982) and Jahns (1955). However, major element zoning of pegmatitic alkali feldspar with respect to alkalis is not reported in the literature (e.g., unzoned feldspars from Peggy's Cove, Nova Scotia, Kontak, 2002) and thus, the lack of zoning in alkali feldspar from Spruce Pine pegmatites is not remarkable.

Epidote

Epidote is observed in the following pegmatite zones: quartz-plagioclase-muscovite, quartz-plagioclase-perthite, perthite-garnet, quartz-plagioclase, quartz-muscovite, graphic granite, quartz-plagioclase-muscovite-garnet, and quartz-plagioclase-perthite-garnet. Epidote is usually partially enclosed in muscovite crystals, in which it shares a crystal face with a cleavage plane of the muscovite. The epidote crystal sharply truncates other cleavage planes in the muscovite. Muscovite crystals that host epidote have iron contents very similar to muscovites without epidote, so leaching of iron from whole crystals of muscovite to nurture epidote growth is not likely. Garnets in all zones that contain epidote hosted by muscovite have some Ca-enrichment of rims. Occasionally, the epidote forms subhedral to anhedral crystals in feldspar, independent of muscovite. Garnet from samples in which epidote, independent of muscovite, occurs (CC2-1, CC2-3, CC2-6, HO1-4, MCK3-5A; Appendix F) all have rims that have been enriched in calcium. Epidote as a primary igneous phase in peraluminous rocks is reported by Whitney et al. (1976), but epidote may also form from Ca-rich fluids during metasomatism. London et al. (1989) state that the last residual fluid phase in pegmatites is enriched in calcium. Calcium-rich metasomatic fluids may have triggered the growth of epidote at the expense of muscovite, formed the grossular rims on garnet, and may be related to the occurrence of pumpellyite and clinozoisite at McKinney Mine (Wood and Abbott, 1996). Ca-rich metasomatism may have triggered the crystallization of epidote at the expense of muscovite in granodiorite and pegmatite. Muscovite crystals from Crabtree Creek granodiorite sample CC2-7 (Appendix D) contain inclusions of epidote and detectable fluorine. Garnets from this granodiorite sample display mid-Ca rims. Muscovite from quartz-plagioclase pegmatite sample CC2-6 (Appendix D) also contains a crystal of epidote and measurable chlorine. Garnet rims in

this pegmatite zone are mid-Ca. Samples HO1-2 and HO1-5 (Appendix D) both contain epidote and detectable fluorine. Garnets in zones with epidote included in muscovite have rims that display some Ca-enrichment. All muscovite crystals with epidote inclusions have iron contents very similar to those of muscovites that lack epidote. If epidote crystallized at the expense of muscovite, the iron content of the muscovite was not altered. Some iron was provided by the recrystallized portion of the muscovite crystal, and any other iron needed for recrystallization of muscovite to epidote was introduced from somewhere other than the muscovite. The Ca-rich fluid added calcium to the rims of garnets and provided the calcium needed for the crystallization of epidote.

Post-Magmatic Recrystallization

Some post-magmatic recrystallization is expected in granitic rocks. The slow-cooling from magmatic conditions allows time for minerals to readjust to lower temperatures. The exsolution of albite from alkali feldspar to form perthite or the mottled extinction of quartz are common examples of cooling-related recrystallization in granitic rocks. Textures within Spruce Pine granitoids indicate a more extensive recrystallization. Straining of feldspar twins, bending of muscovite cleavage, recrystallization of muscovite, presence of grossular rims on garnet, and presence of epidote all indicate post-magmatic recrystallization. Fractures offsetting polysynthetic twinning in plagioclase are observed in granodiorite and in many zones in pegmatite. Such fractures may be due to directed stress associated with cooling of the deep-seated pluton or from external tectonic forces. The Spruce Pine pegmatites formed at the same time or slightly after the Acadian orogeny and were also subjected to the stresses of the later Alleghenian orogeny. Offsets of twinning are sometimes associated with sutured grain

boundaries in quartz grains adjacent the plagioclase crystal. Feldspar straining is not evident in all feldspars from all zones in each body.

Fine-grained muscovite splaying off from larger muscovite crystals is seen in some pegmatites. This fine-grained muscovite has lower iron content than larger muscovite in the same zone. Recrystallization of igneous muscovite to finer-grained metamorphic muscovite may have excluded iron in the process.

Grossular-rich rims of garnet crystals may indicate percolation of a late-stage Ca-rich fluid that added calcium to rims of preexisting garnets. The addition of calcium to the system at such a late stage of crystallization may have triggered a second growth period of garnets using the now abundant calcium. The Ca-rich fluid may not be related to Spruce Pine magmatism, but may be related to later metamorphic events.

The introduction of a Ca-rich fluid may have resulted in the recrystallization of muscovite into epidote, using Ca and OH^- from the fluid and Fe, Al, and Si from the muscovite. Further evidence for a Ca-rich fluid event is the discovery of zoisite and pumpellyite in a cavity at the McKinney Mine, Mitchell County, North Carolina (Wood and Abbott, 1996). The McKinney Mine is adjacent to the Bon Ami Mine, which may also have been subjected to the same Ca-rich fluid event. Epidote is not found in all bodies studied, but all garnet bearing bodies have garnets with Ca-rich rims resulting from the presence of Ca-rich fluid. Every body sampled displays either epidote or grossular-rich garnet, or both, indicating the presence of a Ca-rich fluid.

Formation of Spruce Pine Pegmatites

Pegmatites hosted by granodiorite crystallized from alkali-rich fluids formed early in the crystallization of the host granodiorite. The mineralogical similarity of the pegmatites and host

granodiorites indicates that the pegmatites did not form from a late stage residual melt enriched in rare-elements. The deep-seated magmas were able to dissolve more water than shallower magmas because of the high pressure. This water-rich magma probably fractionated an alkali and silica rich fluid phase (Figure 9) shortly after crystallization commenced. Coarse-grained pegmatite crystallized from this segregated fluid phase. The pegmatite dikes hosted by rocks of the Ashe Metamorphic Suite and not associated with nearby granodiorite crystallized from an alkali and silica rich fluid phase that migrated away from its parent magma. Lack of enrichment in incompatible elements and the absence of exotic mineralization that often characterizes rocks formed from late-stage residual melts are both largely absent in the Spruce Pine plutonic suite. The absence of exotic minerals in the pegmatites indicates either fractionation of the fluid phase occurred early in the cooling history, before incompatible elements were concentrated enough to crystallize exotic minerals, or that elements that normally comprise exotic pegmatite minerals were present in low abundances in the parent magma. High water content of the magma resulted in the exsolution of an alkali and silica rich fluid phase fairly early during crystallization. Any incompatible or exotic elements diluted in the magma were not taken up by feldspars, muscovite, or quartz and would be concentrated in this fluid phase. Any incompatible elements would have remained in the fluid until crystallization concentrated them enough to crystallize minerals such as tourmaline, spodumene, or any other exotic minerals often associated with very fractionated pegmatites. Since crystallization ultimately concentrates incompatible elements enough to form exotic minerals, the lack of such minerals rich in incompatible elements indicates that these elements were absent from the parent magma of the Spruce Pine pegmatites or the magmatic system was not closed and some fluid escaped.

Spruce Pine pegmatites fit into the mica-bearing pegmatite class of Cerny (1982), along with many other mica-bearing pegmatites of the southern Appalachians. Most pegmatites in this group lack rare-element mineralization and may have had crystallization histories similar to Spruce Pine pegmatites. Most mica-bearing pegmatites crystallize between 7 and 11 km depth from peraluminous magma generated by anatectic melting of continental crust, usually metapelite or other rock of similar composition. It is important to note that reports of Ca-enriched garnet rims are absent from the literature on mica-bearing pegmatites.

The similarity in mineral composition and assemblage in all bodies studied implies that the bodies are all related somehow. Although these bodies are separated in space and do not appear to be connected anywhere at the surface, they may represent fingers of magma that ascended from a larger magma body underlying the Spruce Pine district. Wood (1996) summarized this idea, stating that the Spruce Pine plutons may represent the top of a larger magmatic body still buried. The connectivity of these plutons and pegmatites deeper in the crust provides a possible reason for their mineralogical similarity.

CHAPTER 8

CONCLUSIONS

The peraluminous rocks of the Spruce Pine plutonic suite represent melts that crystallized at high pressures deep in the crust. Granodiorite crystallized directly from parent magma. Pegmatite hosted by granodiorite crystallized from a fluid phase rich in alkalis, aluminum, and silica. Miarolitic cavities are absent in these mica-bearing pegmatites because the high pressure prevented their formation. The lack of minerals associated with highly fractionated pegmatites (beryl, spodumene, tourmaline) is due to the absence of the appropriate elements in the parent magma.

A Ca-rich fluid event occurred in all bodies at some point late during or after crystallization. This Ca-rich fluid affected host granodiorite and pegmatite zones, triggering grossular rich overgrowth in garnet rims and facilitating the growth of epidote at the expense of muscovite.

The similar compositions of garnet, muscovite, and feldspar in pegmatite and host granodiorite of several different igneous bodies proves that the composition of these minerals cannot be used to distinguish a pegmatite from its host granodiorite or other pegmatites. Thus, mineral compositions cannot be used as a tool for the identification of potentially economically valuable pegmatites. However, the similarity of minerals in pegmatites and granodiorites shows that pegmatite mineralogy can be used to model processes in the whole magmatic system.

Recommendations for Future Work

Characterizing the mineralogy of the pegmatites from quarries which industrial grade silica is mined may provide a tool with which future deposits may be compared. Samples should be taken and analyzed in a similar manner as the samples in this project. Differences in the mineralogy of silica-producing and non-productive quarries may be a useful prospecting tool. Distribution of grossular rims and epidote should be explored more thoroughly to determine if a stronger link between the two exist. A strong link between the presence of epidote and grossular rims on garnets will reinforce the secondary nature of the epidote. The transition of almandine-spessartine to grossular garnets should be explored further. A microprobe transect across a garnet with grossular rim should be done to determine sharpness and gradation of the transition.

REFERENCES CITED

Adams, M. G., and Trupe, C. H., 1997, Conditions and timing of metamorphism in the blue ridge thrust complex, northwestern North Carolina and eastern Tennessee, in Paleozoic structure, metamorphism, and tectonics of the Blue Ridge of western North Carolina: 1997 Field trip guidebook for Carolina Geological Society, p. 33-47.

Brobst, D. A., 1962, Geology of the Spruce Pine district: Avery, Mitchell, and Yancey Counties, North Carolina: Contributions to economic geology, Geological Survey Bulletin 1122-A, 26 p.

Burnham, C. W., 1967, Hydrothermal fluids at the magmatic stage. In H. L. Barnes, Ed., Geochemistry of Hydrothermal Ore Deposits, 1st ed, Holt, Rinehart and Wilson, New York, p. 34-76.

Burnham, C. W., and Nekvasil, H., 1986, Equilibrium properties of granitic pegmatite magmas: American Mineralogist, v. 71, p. 239-263.

Butler, J. R., 1973, Paleozoic deformation and metamorphism in part of the Blue Ridge Thrust Sheet, North Carolina: American Journal of Science, Cooper v. 273A, p. 72-88.

Butler, J. R., 1991, Metamorphism: Geology of the Carolinas, University of Tennessee Press, p. 127-141.

Cameron, E. N., Jahns, R. H., McNair, A. H., and Page, L. R., 1949, Internal structure of granitic pegmatites: Economic Geology Monograph 2, 115 p.

Cerny, P., 1982, Anatomy and classification of granitic pegmatites: MAC Short Course Handbook 8, p. 1-39.

Cerny, P. 1991, Fertile granites of precambrian rare-element pegmatite fields: Is geochemistry controlled by tectonic setting or source lithologies?: Precambrian Research, v. 51, p. 429-468.

Clarke, D. B., 1981, The mineralogy of peraluminous granites: A review: Canadian Mineralogist, v. 19, p. 3-17.

Deer, W. A., Howie, R. A., and Zussman, J., 1992, An introduction to the rock forming minerals, 2nd ed. Prentice Hall, New York, p. 696.

Deer, W. A., Howie, R. A., and Zussman, J., 1982, An introduction to the rock forming minerals, v. 1A Orthosilicates. Prentice Hall, New York, p. 468-657.

Fenn, P. M., 1986, On the origin of graphic granite: American Mineralogist, v. 71, p. 325-330.

Jahns, R. H., 1955, The study of pegmatites: Economic Geology, 50th anniversary volume, p. 1025-1130.

Jahns, R. H., 1982, Internal evolution of pegmatite bodies: In Cerny, P. (ed.) Granitic pegmatites in science and industry: Mineral Association of Canada Short Course Handbook 8, p. 293-327.

Jahns, R. H., and Burnham, C. W., 1969, Experimental studies of pegmatite genesis. I. A model for the derivation and crystallization of granitic pegmatite:. Economic Geology, v. 64, p. 843-864.

Jamtveit, B., 1991, Oscillatory zonation patterns in hydrothermal grossular-andradite garnet: Nonlinear dynamics in regions of immiscibility: American Mineralogist, v. 76, p. 1319-1327.

Johnson, B. J., Miller, B. V., and Stewart, K. G., 2001, The nature and timing of Acadian deformation in the Southern Appalachian Blue Ridge constrained by the Spruce Pine Plutonic Suite, western North Carolina, Abstract, GSA Abstracts with Programs, v. 30, no. 2, p. 30.

Kesler, T. L., and Olson, J. C., 1942, Muscovite in the Spruce Pine District, North Carolina: United States Geological Survey, Bulletin 936-A, p. 1-38.

Kontak, D. J., Dostal, J., Kyser, T. K., and Archibald, D. A., 2002, A petrological, geochemical, isotopic, and fluid-inclusion study of 370 Ma pegmatite-aplite sheets, Peggys Cove, Nova Scotia, Canada: Canadian Mineralogist, v. 40, p. 1249-1286.

Laniz, R. V., Stevens, R. E., and Norman, M. B., 1964, Staining of plagioclase feldspar and other minerals: U.S. Geological Survey Professional Paper 501B, p. B152-B153.

London, D., 1996, Granitic pegmatites: Transactions of the Royal Society of Edinburgh: Earth Sciences, v. 87, p. 305-319.

London, D., Morgan. G. B. VI, and Hervig, R. L., 1989, Vapor-undersaturated experiments in the system macusanite-H_2O, at 200MPa, and the internal differentiation of granitic pegmatites: Contributions to Mineralogy and Petrology, v. 102, p. 1-17.

Martin, R. F., 1982, Quartz and the feldspars: In Cerny, P. (ed.) Granitic pegmatites in science and industry: Mineral Association of Canada Short Course Handbook 8, p. 41-62.

Maurice, C. S., 1940, The pegmatites of the Spruce Pine District, North Carolina: Economic Geology, v. 35, p. 49-78; 158-187.

Miller, C. F., Stoddard, E. F., Bradfish, L. J., and Dollase, W. A., 1981, Composition of plutonic muscovite: Genetic implications: Canadian Mineralogist, v. 19, p. 25-34.

McSween, H. Y., Jr., Speer, J. A., and Fullagar, P. D., 1991, Plutonic rocks, in Horton, J. W., Jr., and Zullo, V. A., eds. The geology of the Carolinas: Carolina Geological Society 50th anniversary volume: University of Tennessee Press, Knoxville, p. 109-126.

Parker, J. M., 1952, Geology and structure of part of the Spruce Pine District, North Carolina, A progress report: North Carolina Department of Conservation and Development, Division of Mineral Resources, Bulletin Number 65, p. 26.

Raymond, L. A., 2002, Petrology: The study of igneous, sedimentary, and metamorphic Rocks. 2nd ed. McGraw Hill: Boston, p. 222-226.

Reed, S. J. B., 1996, Electron microprobe analysis and scanning electron microscopy in geology: Cambridge University Press, Cambridge, England, p. 201.

Sterrett, D. B., 1923, Mica deposits of the United States: United States Geological Survey Bulletin 740, p. 342.

Swanson, S. E., 1977, Relation of nucleation and crystal-growth rate to the development of granitic textures: American Mineralogist, v. 62, p. 966-978.

Tappen, C. M., and Smith, M. S., 2003, The Crabtree Pegmatite, Spruce Pine District, North Carolina: Mineralization and host rock relations: Southeastern Geology, v. 41, no. 4, p. 201-223.

Trupe, C. H., Stewart, K. G., Adams, M. G., Waters, C. L., Miller, B. V., and Hewitt, L. K., 2003, The Burnsville fault: Evidence for the timing and kinematics of southern Appalachian Acadian dextral transform tectonics: Geological Society of America Bulletin, v. 115, no. 11, p. 1365-1376.

Van Der Plas, L., and Tobi, A. C., 1965, A chart for judging the reliability of point counting results: American Journal of Science, v. 263, p. 87-90.

Whitney, J. A., Jones, L. M., and Walker, R. L., 1976, Age and origin of the Stone Mountain Granite, Lithonia District, Georgia: Geological Society of America Bulletin, v. 87, p. 1067-1077.

Wood, K. Y., and Abbott, R. N., Jr., 1996, Pumpellyite and clinozoisite from the McKinney Mine, Spruce Pine District, North Carolina: The Mineralogical Record, v. 27, p. 289-290.

Wood, P. A., 1996, Petrogenesis of the Spruce Pine pegmatites, North Carolina [M.S. thesis]: Blacksburg, Virginia Polytechnic Institute and State University, p. 99.

Zane, A., and Rizzo, G. 1999, The compositional space of muscovite in granitic rocks: Canadian Mineralogist, v. 32, p. 1229-1238.

APPENDIX A

ELECTRON MICROPROBE ANALYSIS ROUTINES FOR GARNET, MUSCOVITE, AND FELDSPAR.

Garnet was analyzed for iron, manganese, magnesium, calcium, titanium, chromium, aluminum, and silicon. The elements, standards, and crystals used are as follows: iron, fayalite, LIF; manganese, SPES (spessartine), LIF; magnesium, olivine1, TAP; calcium, sphene, PET; titanium TiO_2, PET; chromium, chromite5, LIF; aluminum, SPIN (spinel), TAP; silicon, almandine, TAP. Counting time on standard peaks was 10 seconds. Peak positions ($K_{\alpha 1}$) for elements are as follows: iron, 134.828; manganese, 146.337; magnesium, 107.685; calcium, 107.516; titanium, 87.991; chromium, 159.416; aluminum, 90.745; and silicon, 77.427. Minimum detection levels (in oxide wt %) for these elements are as follows: iron, 0.17; manganese, 0.14; magnesium, 0.06; calcium, 0.04; titanium, 0.08; chromium, 0.14; aluminum, 0.05; and silicon, 0.05. Background was assumed to be linear and was measured on both sides of the peak position of each element. A 10 second counting time on peak and a 1 micron beam diameter was used for garnet analysis. Precision of analysis is ensured through analysis of the cmt pyrope standard and the Barton 36 CG garnet standard. The known composition of the garnet standards were reproduced to $\leq 5\%$ error for major oxide components. This analytical routine worked well as evidenced by good, reproducible totals. All chromium reported is below detection levels. All other oxides are significant components of the garnets being analyzed.

Muscovite analyses used an accelerating voltage of 15 keV and a 5 nA beam current. The beam was aligned and stabilized at the beginning of each microprobe session. Muscovite

was analyzed for iron, manganese, magnesium, calcium, titanium, potassium, sodium, chlorine, fluorine, aluminum, and silicon. Muscovite is hydrous and is subject to the loss of the volatile alkali elements K and Na (Reed, 1996). Therefore, these elements were measured first in each analysis before the beam volatilized them. The elements, standards, and crystals used are as follows: iron, fayalite, LIF; manganese, SPES (spessartine), LIF; magnesium, olivine1, TAP; calcium, sphene, PET; titanium, TiO_2, PET; aluminum, SPIN (spinel), TAP; silicon, diopside5A, TAP; potassium, orthoclase 10, PET; sodium, ABOX (Amelia albite, calibrated with 10 micron beam diameter), TAP; chlorine, scapolite, PET; and fluorine, FPHL (glass standard), LDE1. Counting time was 10 seconds on standard peaks. Peak positions ($K_{\alpha 1}$) for elements are as follows: iron, 134.893; manganese, 146.378; magnesium, 107.675; calcium, 107.526; titanium, 88.011; potassium, 119.773; sodium, 129.560; chlorine, 151.335; fluorine, 85.299; aluminum, 90.740; and silicon, 77.427. Minimum detection levels (in oxide weight %) for these elements are as follows: iron, 0.27; manganese, 0.34; magnesium, 0.09; calcium, 0.07; titanium, 0.13; aluminum, 0.08; silicon, 0.09; potassium, 0.05; sodium, 0.09; chlorine, 0.04; and fluorine, 0.27. Background was assumed to be linear and was measured on both sides of the peak position of each element. A 10 second counting time on peak position and a 5 micron beam diameter is used for muscovite analysis. Precision of analysis is ensured through analysis of the Lemhi biotite standard. The known composition of the Lemhi biotite standard was reproduced to $\leq 5\%$ error for the major oxide components.

Plagioclase and alkali feldspar analyses were done using an accelerating voltage of 15 keV and a 5 nA beam current. The beam was aligned and stabilized at the beginning of each microprobe session. Plagioclase and alkali feldspar were analyzed for iron, manganese, magnesium, calcium, titanium, potassium, sodium, barium, aluminum, and silicon. Plagioclase

and alkali feldspar are subject to the loss of the volatile elements K and Na under the electron beam (Reed, 1996). Therefore, these elements were measured first in each analysis. The elements, standards, and crystals used are as follows: iron, fayalite, LIF; manganese, SPES (spessartine), LIF; magnesium, olivine1, TAP; calcium, anorthite, PET; titanium, TiO_2, PET; potassium, Or 10 (orthoclase), PET; sodium, ABOX (Amelia albite), TAP; barium, benitoite, PET; aluminum, anorthite, TAP; and silicon, ABOX (Amelia albite), TAP. Counting time was 10 seconds on peak position. Peak positions ($K_{\alpha 1}$) for elements are as follows: iron, 134.848; manganese, 146.362; magnesium, 107.680; calcium, 107.548; titanium, 88.041; potassium, 119.793; sodium, 129.575; barium, 88.785; aluminum, 90.690; and silicon, 77.429. Minimum detection limits (oxide wt. %) for these elements are as follows: iron, 0.23; manganese, 0.23; magnesium, 0.07; calcium, 0.05; titanium, 0.10; potassium, 0.03, sodium, 0.13; barium, 0.18; aluminum, 0.06; and silicon, 0.07. Background was assumed to be linear and was measured on both sides of the peak position of each element. A 10 second counting time on peak and a 10 micron beam diameter is used for plagioclase and alkali feldspar analyses. Precision of analyses is ensured through analysis of the DSC BxA-A-Au, labradorite, Amelia Albite, and the microcline standards. The known compositions for these standards were reproduced to $\leq 5\%$ error for major component oxides. TiO_2, MgO, FeO, and MnO concentrations were all measured at below minimum detection levels for this instrument.

APPENDIX B

MINERAL ASSEMBLAGES IN GRANODIORITE AND PEGMATITE SAMPLES FROM SPRUCE PINE, NORTH CAROLINA.

Zone Key:

GRD ---------- Host Granodiorite
GG ---------- Graphic Granite
Q-PL-M - Quartz-Plagioclase-Muscovite Pegmatite
Q-PL-PE - Quartz-Plagioclase-Perthite Pegmatite
PE-G ---------- Perthite-Garnet Pegmatite
Q-PL ---------- Quartz-Plagioclase Pegmatite
Q-PE-M - Quartz-Perthite-Muscovite Pegmatite
Q-PE-M-G - Quartz-Perthite-Muscovite-Garnet Pegmatite
Q-M ---------- Quartz-Muscovite Pegmatite
Q-PL-M-G - Quartz-Plagioclase-Muscovite-Garnet Pegmatite
PE ---------- Perthite Pegmatite
Q-PL-PE-G - Quartz-Plagioclase-Perthite-Garnet Pegmatite
Q-PL-PE-M-G Quartz-Plagioclase-Perthite-Muscovite-Garnet Pegmatite
Q --------- Quartz

Sample	Zone	Phases in Thin Section	Phases in Hand Sample	Notes
CC 1-1	GRD	Quartz Plagioclase Microcline Muscovite Biotite Epidote	Quartz Plagioclase Garnet Biotite Muscovite	Some myrmekite
CC 1-2	Q-PL-M	Quartz Plagioclase Microcline Muscovite Garnet Epidote	Quartz Plagioclase Perthite Muscovite Garnet	

CC 1-3	GRD	Quartz Plagioclase Microcline Muscovite Biotite Epidote	Quartz Perthite Plagioclase Biotite Muscovite Garnet	Some myrmekite
CC 2-1	GRD	Quartz Microcline Plagioclase Muscovite Garnet Fe-Ti Oxides Epidote	Quartz Perthite Plagioclase Muscovite Garnet	Lots of myrmekite
CC 2-2A	GRD	Quartz Plagioclase Microcline Muscovite Epidote	Quartz Muscovite Plagioclase Garnet	Graphic Texture
CC 2-2B	Q-PL-PE	Quartz Plagioclase Perthite Muscovite Epidote	Quartz Plagioclase Muscovite Biotite Garnet	
CC 2-3	PE-G	Quartz Microcline Plagioclase Muscovite Garnet	Quartz Microcline Plagioclase Garnet	Little myrmekite Graphic texture
CC 2-4	PE-G	Quartz Perthite Plagioclase Muscovite Epidote	Perthite	Some myrmekite
CC 2-5	GG	Quartz Perthite Muscovite Plagioclase Garnet Zircon	Quartz Perthite Muscovite	Graphic texture
CC 2-6	Q-PL	Quartz Plagioclase Muscovite Microcline Garnet Epidote Apatite	Quartz Plagioclase	

CC 2-7	GRD	Quartz Plagioclase Microcline Garnet Muscovite Epidote	Quartz Plagioclase Muscovite Garnet	Minor myrmekite
CC 2-8	GRD	Quartz Microcline Plagioclase Muscovite Epidote Biotite	Quartz Perthite Plagioclase Muscovite Garnet	Quartz-perthite-muscovite intergrowths
CC 2-9	Q-PE-M	Quartz Perthite Plagioclase Microcline Muscovite Garnet	Quartz Perthite Muscovite Garnet	
CC 2-10	Q-PE-M-G	Quartz Perthite Muscovite	Perthite Quartz	Quartz euhedra
HO 1-1	Biotite Schist Xenolith	Quartz Muscovite Biotite Epidote Garnet Zircon	Biotite Quartz	Radiohaloes around zircon in biotite
HO 1-2	Q-M	Quartz Plagioclase Muscovite Epidote Biotite Zircon Fe-Ti oxides	Quartz Muscovite Plagioclase Biotite	
HO 1-3	Biotite Schist	Quartz Zircon Amphibole Biotite Sphene Zircon	Biotite	
HO 1-4	GG	Quartz Microcline Plagioclase Muscovite Garnet Epidote	Quartz Plagioclase Garnet Muscovite	Some myrmekite

HO 1-5	GRD	Quartz Plagioclase Microcline Muscovite Garnet	Quartz Muscovite Garnet Plagioclase	Some myrmekite
HO 1-6	GRD	Quartz Microcline Plagioclase Garnet	Quartz Perthite Plagioclase Muscovite Garnet	Garnet with quartz core Some myrmekite
HO 1-7	Q-M	Plagioclase Muscovite	Quartz Plagioclase Muscovite Thulite? Apatite	Small miaroles
HO 2-1	GRD	Quartz Plagioclase Muscovite	Quartz Plagioclase Muscovite	Sericite alteration
HO 2-2	Q-PL-M-G	Quartz Plagioclase Muscovite Epidote	Quartz Plagioclase Muscovite Garnet Fe-Ti Oxides	
HOG 1	Grab sample	Quartz Microcline Plagioclase Muscovite	Quartz Perthite Muscovite	
HOG 2	Grab sample	Quartz Microcline Plagioclase Muscovite	Quartz Perthite Muscovite	
HOG 3	Grab sample	Quartz Microcline Plagioclase Muscovite Garnet Oxides	Quartz Plagioclase Muscovite Garnet	
HOG 4	Grab sample	Quartz Plagioclase Microcline Muscovite	Quartz Perthite Muscovite	Some myrmekite

HOG 6	Grab sample	Quartz Perthite Muscovite	Quartz Perthite	
HOG 7A	Grab sample	Quartz Microcline Muscovite Garnet Biotite Oxides	Quartz Perthite Muscovite Garnet	Graphic texture
HOG 7B	Grab sample	Quartz Plagioclase Microcline Garnet Muscovite	Quartz Perthite Muscovite Garnet	Some myrmekite
HOG CON	Pegmatite-Biotite Schist Contact	No thin section	Quartz Muscovite Perthite	Small miaroles
MCK 1-1	PE	Quartz Perthite Plagioclase Muscovite	Perthite	
MCK 1-2	Q	No thin section	Quartz	
MCK 1-3	Q-PL-PE-G	Quartz Muscovite Microcline Plagioclase Oxides Epidote Carbonate?	Quartz Plagioclase Muscovite	
MCK 2-1	Q-PL-PE-M-G	Quartz Plagioclase Garnet Muscovite Zircon Carbonate vein fill	Quartz Plagioclase Garnet	
MCK 2-3	Q-PL-PE-M-G	Quartz Plagioclase Muscovite Garnet	Quartz Plagioclase Garnet	
MCK 3-1	Q	Quartz Perthite Microcline Plagioclase Muscovite	Quartz Perthite	

MCK 3-2	GRD	Quartz Microcline Plagioclase Muscovite Garnet	Quartz Perthite Garnet	Graphic texture
MCK 3-3	Q-PE-M-G	Quartz Microcline Plagioclase Muscovite Garnet	Quartz Plagioclase Garnet Muscovite	Muscovite with oxides and radiohaloes
MCK 3-4	GRD	No thin section	Quartz Plagioclase Garnet Muscovite	
MCK 3-5A	GRD	Quartz Plagioclase Microcline Muscovite Garnet Epidote	Quartz Plagioclase Garnet	Some muscovite sprays Graphic texture
MCK 3-5B	GRD	Quartz Plagioclase Microcline Muscovite Garnet	Quartz Plagioclase Garnet	Microcline is interstitial Graphic texture
MCK 3-6	Q-PE-M-G	Quartz Microcline Plagioclase Garnet Muscovite	Quartz Plagioclase Muscovite Garnet	Some myrmekite Small miaroles
Roan Road	GRD	Quartz Plagioclase Microcline Epidote Biotite Muscovite Garnet	Quartz Plagioclase Perthite Muscovite Garnet	

APPENDIX C

ELECTRON MICROPROBE ANALYSES OF GARNETS FROM SPRUCE PINE GRANODIORITES AND PEGMATITES.

Zone Key:

GRD ----------	Host Granodiorite
GG ----------	Graphic Granite
Q-PL-M -	Quartz-Plagioclase-Muscovite Pegmatite
Q-PL-PE -	Quartz-Plagioclase-Perthite Pegmatite
PE-G ----------	Perthite-Garnet Pegmatite
Q-PL ----------	Quartz-Plagioclase Pegmatite
Q-PE-M -	Quartz-Perthite-Muscovite Pegmatite
Q-PE-M-G -	Quartz-Perthite-Muscovite-Garnet Pegmatite
Q-M ----------	Quartz-Muscovite Pegmatite
Q-PL-M-G -	Quartz-Plagioclase-Muscovite-Garnet Pegmatite
PE ----------	Perthite Pegmatite
Q-PL-PE-G -	Quartz-Plagioclase-Perthite-Garnet Pegmatite
Q-PL-PE-M-G	Quartz-Plagioclase-Perthite-Muscovite-Garnet Pegmatite
Q ---------	Quartz

Peg Zone		GRD	GRD	GRD	GRD	GRD
Oxide	MDL Ox wt%	CC2-1g1	CC2-1g1rim	CC2-1g	CC2-1grim	CC2-7g1
SiO_2	0.052	36.670	37.380	37.160	37.760	37.550
TiO_2	0.078	0.073	0.000	0.001	0.048	0.037
Al_2O_3	0.047	20.230	21.090	20.610	21.090	21.070
MgO	0.055	0.889	0.582	1.285	0.552	0.815
FeO	0.172	18.870	17.030	21.430	16.760	18.250
CaO	0.038	3.280	12.640	2.830	10.610	7.020
MnO	0.142	19.150	12.720	16.660	12.800	15.530
Cr_2O_3	0.144	0.000	0.011	0.000	0.011	0.089
Total		99.16	101.45	99.98	99.63	100.36
Numbers of ions on the basis of 12O						
Si		3.013	2.961	3.018	3.022	3.011
Al^{IV}			0.039			
Al^{VI}		1.959	1.930	1.973	1.989	1.992
Ti		0.005		0.000	0.003	0.002
Mg		0.109	0.069	0.156	0.066	0.097
Fe2+		1.297	1.128	1.456	1.122	1.224
Mn		1.333	0.853	1.146	0.868	1.055
Ca		0.288	1.073	0.247	0.910	0.603
Total		8.00	8.05	8.00	7.98	7.98
Mn#		0.49	0.42	0.42	0.42	0.44
Pyrope = 0 - 3.3%						
Alman		45.7	40.2	52.4	41.7	44.7
Spess		46.4	30.0	40.7	31.9	38.1
Gross		7.9	29.8	6.9	26.4	17.2

Zone	GRD	GRD	GRD	GRD	GRD	GRD
Oxide	HO1-6g1	HO1-6g2	MCK3-2g1core	MCK3-2g1rim	MCK3-2g2core	MCK3-2g2rim
SiO_2	36.450	36.210	36.120	36.290	36.000	35.520
TiO_2	0.016	0.055	0.007	0.036	0.009	0.000
Al_2O_3	20.740	20.670	21.140	21.090	20.880	21.090
MgO	0.419	0.489	0.252	0.204	0.226	0.236
FeO	26.350	23.680	23.680	22.040	24.450	23.160
CaO	1.264	2.014	1.720	1.192	1.673	1.286
MnO	14.540	15.850	17.630	17.520	16.680	17.490
Cr_2O_3	0.034	0.000	0.000	0.000	0.110	0.066
Total	99.81	98.97	100.55	98.37	100.03	98.85
Numbers of ions on the basis of 12O						
Si	2.997	2.993	2.957	3.008	2.964	2.954
Al^{IV}	0.003	0.007	0.043		0.036	0.046
Al^{VI}	2.007	2.007	1.996	2.060	1.990	2.021
Ti	0.001	0.003	0.000	0.002	0.001	0.000
Mg	0.051	0.060	0.031	0.025	0.028	0.029
Fe2+	1.812	1.637	1.621	1.528	1.683	1.611
Mn	1.013	1.110	1.222	1.230	1.163	1.232
Ca	0.111	0.178	0.151	0.106	0.148	0.115
Total	8.00	8.00	8.02	7.96	8.01	8.01
Mn#	0.35	0.40	0.43	0.44	0.40	0.43
Pyrope = 0 - 3.3%						
Alman	62.5	57.0	55.0	54.1	57.1	55.2
Spess	34.5	38.2	41.0	43.0	39.0	41.7
Gross	3.0	4.8	4.0	2.9	3.9	3.1

Zone	GRD	GRD	GRD	GRD	GRD
Oxide	MCK3-5Bg1core	MCK3-5Bg1rim	MCK3-5Bg2core	MCK3-5Bg2rimnotch	MCK3-5Bg3core
SiO_2	36.180	37.980	35.820	38.180	35.650
TiO_2	0.084	0.049	0.042	0.053	0.077
Al_2O_3	20.300	22.130	20.230	21.160	20.470
MgO	0.361	0.000	0.678	0.000	0.536
FeO	20.010	0.851	19.800	4.770	20.400
CaO	1.484	25.880	1.500	23.600	1.094
MnO	20.180	11.150	19.880	10.510	20.470
Cr_2O_3	0.022	0.000	0.000	0.000	0.000
Total	98.62	98.04	97.95	98.27	98.70
Numbers of ions on the basis of 12O					
Si	3.008	2.978	2.996	3.014	2.972
Al^{IV}		0.022	0.004		0.028
Al^{VI}	1.989	2.023	1.990	1.969	1.982
Ti	0.005	0.003	0.003	0.003	0.005
Mg	0.045	0.000	0.085	0.000	0.067
Fe2+	1.391	0.056	1.385	0.315	1.422
Mn	1.421	0.741	1.408	0.703	1.445
Ca	0.132	2.174	0.134	1.996	0.098
Total	7.99	8.00	8.01	8.00	8.02
Mn#	0.50	0.93	0.49	0.69	0.49
Pyrope = 0 - 3.3%					
Alman	48.0	2.2	48.1	12.3	48.6
Spess	48.4	29.4	48.3	27.0	48.8
Gross	3.6	68.3	3.6	60.7	2.6

Zone	GRD	GRD	GG	GG	GG	GG
Oxide	MCK3-5Bg4core	MCK3-5Bg4rim	HO1-4g1core	HO1-4g1rim	HO1-4g2core	HO1-4g2core2
SiO_2	35.800	36.390	36.670	37.350	36.460	36.020
TiO_2	0.011	0.036	0.028	0.000	0.027	0.006
Al_2O_3	20.100	20.510	20.600	21.340	20.510	20.840
MgO	0.835	0.132	0.426	0.273	0.326	0.357
FeO	22.770	21.540	24.550	14.960	25.670	23.590
CaO	0.964	9.460	1.153	8.030	1.415	1.633
MnO	18.810	8.800	16.050	18.360	15.270	16.720
Cr_2O_3	0.066	0.000	0.000	0.000	0.000	0.034
Total	99.36	96.87	99.48	100.31	99.68	99.20
Numbers of ions on basis of 12O						
Si	2.973	3.014	3.010	2.998	3.004	2.979
Al^{IV}	0.027			0.002		0.021
Al^{VI}	1.940	2.002	1.993	2.017	1.992	2.010
Ti	0.001	0.002	0.002		0.002	0.000
Mg	0.103	0.016	0.052	0.033	0.040	0.044
Fe2+	1.582	1.492	1.685	1.004	1.769	1.632
Mn	1.323	0.617	1.116	1.248	1.066	1.171
Ca	0.086	0.840	0.134	0.691	0.125	0.145
Total	8.04	7.98	7.99	7.99	8.00	8.00
Mn#	0.44	0.29	0.39	0.55	0.37	0.41
Pyrope = 0 - 3.3%						
Alman	53.5	54.1	58.8	36.2	60.6	56.2
Spess	44.2	22.1	38.4	44.4	36.1	39.9
Gross	2.3	23.8	2.8	19.4	3.3	3.9

Zone	GG	GG	GG	PE-G	PE-G	PE-G
Oxide	HO1-4g2rim	HO1-4g3core	HO1-4g3dark	CC2-3g1	CC2-3g1rim	CC2-3g2core
SiO_2	37.170	36.340	37.400	35.880	37.130	35.110
TiO_2	0.000	0.047	0.043	0.074	0.021	0.033
Al_2O_3	21.390	20.390	20.660	20.460	20.510	20.340
MgO	0.311	0.414	0.000	0.893	0.000	0.731
FeO	14.940	23.290	3.340	20.140	4.240	19.360
CaO	6.260	2.333	27.040	1.375	26.730	1.382
MnO	19.750	13.990	9.770	20.550	9.550	19.840
Cr_2O_3	0.071	0.091	0.000	0.000	0.059	0.054
Total	99.89	96.90	98.25	99.37	98.24	96.85
Numbers of ions on the basis of 12O						
Si	3.001	3.042	2.964	2.968	2.953	2.970
Al^{IV}			0.036	0.032	0.047	0.030
Al^{VI}	2.035	2.012	1.894	1.962	1.876	1.998
Ti		0.003	0.003	0.005	0.001	0.002
Mg	0.037	0.052		0.110		0.092
Fe2+	1.009	1.631	0.222	1.393	0.282	1.369
Mn	1.351	0.992	0.656	1.440	0.643	1.422
Ca	0.542	0.209	2.295	0.122	2.277	0.125
Total	7.98	7.94	8.07	8.03	8.08	8.01
Mn#	0.56	0.37	0.75	0.49	0.70	0.49
Pyrope = 0 - 3.3%						
Alman	36.5	58.8	8.3	47.9	10.5	47.7
Spess	48.2	35.3	24.3	48.9	23.6	48.9
Gross	15.3	5.9	67.3	3.3	66.0	3.4

Zone	PE-G	PE-G	PE-G	PE-G	PE-G	PE-G
Oxide	CC2-3g2rim	CC2-3g3	CC2-3g3rim	CC2-3g4core	CC2-3g4rim	CC2-3g4core
SiO_2	38.210	35.590	35.730	35.750	36.590	36.650
TiO_2	0.025	0.073	0.023	0.079	0.000	0.011
Al_2O_3	20.260	20.320	20.750	20.250	20.810	20.190
MgO	0.000	0.846	0.304	0.561	0.312	0.828
FeO	4.090	20.690	15.940	19.990	15.700	20.150
CaO	31.190	1.426	10.010	1.659	9.940	1.727
MnO	5.950	20.530	14.760	20.160	14.850	20.520
Cr_2O_3	0.000	0.032	0.011	0.000	0.045	0.033
Total	99.73	99.51	97.53	98.45	98.25	100.11
Numbers of ions on the basis of 12O						
Si	2.975	2.951	2.953	2.983	2.990	3.005
Al ^{IV}	0.025	0.049	0.047	0.017	0.010	
Al ^{VI}	1.834	1.937	1.974	1.974	1.994	1.951
Ti	0.001	0.005	0.001	0.005		0.001
Mg		0.105	0.037	0.070	0.038	0.101
Fe2+	0.266	1.435	1.102	1.395	1.073	1.381
Mn	0.392	1.442	1.033	1.425	1.028	1.425
Ca	2.601	0.127	0.887	0.148	0.870	0.152
Total	8.09	8.05	8.03	8.02	8.00	8.02
Mn#	0.60	0.48	0.48	0.49	0.48	0.49
Pyrope = 0 - 3.3%						
Alman	9.9	48.5	39.2	47.8	38.8	47.5
Spess	14.4	48.1	36.3	48.2	36.7	48.4
Gross	75.6	3.3	24.6	4.0	24.5	4.1

Zone	PE-G	PE-G	PE-G	PE-G	PE-G	PE-G
Oxide	CC2-3g4rim	CC2-3g5core	CC2-3g5rim	CC2-3g6int	CC2-3g6rim	CC2-3g7core
SiO_2	37.760	35.570	39.880	37.350	37.730	36.540
TiO_2	0.005	0.009	0.044	0.014	0.000	0.061
Al_2O_3	21.110	20.560	18.150	20.550	20.320	20.150
MgO	0.000	0.906	0.063	0.420	0.000	0.935
FeO	2.880	20.400	6.890	16.520	4.100	20.570
CaO	26.890	1.440	25.920	8.720	33.120	1.512
MnO	9.540	19.830	6.640	16.780	4.040	19.850
Cr_2O_3	0.000	0.065	0.000	0.000	0.059	0.000
Total	98.19	98.78	97.59	100.35	99.37	99.62
Numbers of ions on the basis of 12O						
Si	2.978	2.958	3.166	3.007	2.944	3.007
Al^{IV}	0.022	0.042			0.056	
Al^{VI}	1.940	1.972	1.698	1.950	1.812	1.954
Ti	0.000	0.001	0.003	0.001		0.004
Mg		0.112	0.007	0.050		0.115
Fe2+	0.190	1.419	0.457	1.112	0.268	1.416
Mn	0.637	1.396	0.447	1.144	0.267	1.383
Ca	2.273	0.128	2.205	0.753	2.769	0.133
Total	8.04	8.03	7.98	8.02	8.12	8.01
Mn#	0.77	0.48	0.49	0.50	0.50	0.47
Pyrope = 0 - 3.3%						
Alman	7.3	49.0	17.5	39.3	9.9	49.1
Spess	24.3	47.6	16.8	39.9	9.8	47.3
Gross	68.4	3.5	65.7	20.8	80.3	3.6

Zone	PE-G	PE-G	PE-G	PE-G	Q-PL	Q-PL
Oxide	CC2-3g7rim	CC2-3g8core	CC2-3g8rim	CC2-3g9	CC2-6g1	CC2-6g1rim
SiO_2	37.210	36.190	37.750	35.820	36.700	36.800
TiO_2	0.056	0.059	0.012	0.000	0.035	0.020
Al_2O_3	21.300	20.540	21.690	20.650	20.630	20.180
MgO	0.000	0.864	0.000	0.712	1.005	0.613
FeO	2.124	20.030	1.846	19.720	20.210	15.670
CaO	30.730	1.445	24.670	1.367	1.600	8.610
MnO	7.010	20.760	11.960	20.230	18.910	16.200
Cr_2O_3	0.000	0.000	0.000	0.000	0.000	0.000
Total	98.43	99.89	97.93	98.50	99.09	98.09
Numbers of ions on the basis of 12O						
Si	2.922	2.975	2.981	2.979	3.015	3.019
Al ^{IV}	0.078	0.025	0.019	0.021		
Al ^{VI}	1.894	1.965	1.999	2.003	1.997	1.951
Ti	0.003	0.004	0.001		0.002	0.001
Mg		0.106		0.088	0.123	0.075
Fe2+	0.139	1.377	0.122	1.371	1.389	1.075
Mn	0.467	1.446	0.800	1.425	1.316	1.126
Ca	2.586	0.127	2.087	0.122	0.141	0.757
Total	8.09	8.02	8.01	8.01	7.98	8.00
Mn#	0.77	0.49	0.87	0.49	0.47	0.49
Pyrope = 0 - 3.3%						
Alman	5.3	47.4	4.8	47.7	49.6	38.7
Spess	17.6	49.2	31.1	49.0	46.4	40.0
Gross	77.1	3.4	64.1	3.3	3.9	21.3

Zone	Q-PL	Q-PL	Q-PL	Q-PL	Q-PE-M	Q-PE-M	Q-PE-M
Oxide	CC2-6g2core	CC2-6g2rim	CC2-6g5	CC2-6g5rim	CC2-9g1	CC2-9g1rim	CC2-9g2
SiO_2	35.960	37.140	36.290	36.770	36.110	36.040	36.020
TiO_2	0.037	0.013	0.045	0.016	0.057	0.029	0.135
Al_2O_3	20.580	20.680	20.800	21.010	20.280	20.430	19.770
MgO	0.931	0.362	0.807	0.419	0.876	0.757	0.782
FeO	19.640	15.330	19.840	16.170	20.820	19.250	19.320
CaO	1.714	10.470	1.525	9.510	1.289	1.400	1.624
MnO	19.740	13.620	19.260	14.830	19.720	20.090	20.930
Cr_2O_3	0.000	0.000	0.000	0.000	0.000	0.034	0.023
Total	98.60	97.61	98.57	98.73	99.15	98.03	98.60
Numbers of ions on the basis of 12O							
Si	2.981	3.032	3.000	2.989	2.989	3.003	3.001
Al^{IV}	0.002			0.011	0.011		
Al^{VI}	2.009	1.990	2.026	2.002	1.967	2.006	1.942
Ti	0.002	0.001	0.003	0.001	0.004	0.002	0.008
Mg	0.115	0.044	0.099	0.051	0.108	0.094	0.097
Fe2+	1.362	1.047	1.372	1.100	1.441	1.341	1.346
Mn	1.386	0.942	1.348	1.021	1.383	1.418	1.477
Ca	0.152	0.916	0.135	0.828	0.114	0.125	0.145
Total	8.01	7.97	7.98	8.00	8.02	7.99	8.02
Mn#	0.48	0.46	0.48	0.47	0.47	0.50	0.51
Pyrope = 0 - 3.3%							
Alman	47.8	38.9	48.8	39.9	49.8	47.3	46.1
Spess	48.0	34.6	47.4	36.6	47.1	49.3	50.0
Gross	4.2	26.6	3.8	23.5	3.1	3.4	3.9

Zone	Q-PE-M	Q-PE-M	GRD	Q-PL-M	Q-PL-M	Q-PL-M
Oxide	CC2-9g2rstnd	CC2-9g3	HO1-5gcore	CC1-2g1core	CC1-2g1rimzone	CC1-2g1rim
SiO_2	36.020	35.850	36.630	37.000	36.590	43.090
TiO_2	0.045	0.080	0.000	0.057	0.022	0.024
Al_2O_3	20.260	20.580	21.010	20.470	20.610	20.780
MgO	0.609	0.611	0.308	1.388	1.295	0.654
FeO	17.950	17.770	24.890	20.200	19.240	17.860
CaO	1.569	1.417	1.793	2.156	3.240	6.480
MnO	21.520	22.000	15.170	18.300	18.650	16.040
Cr_2O_3	0.069	0.023	0.046	0.087	0.000	0.033
Total	98.04	98.33	99.85	99.66	99.65	104.96
Numbers of ions on the basis of 12O						
Si	3.005	2.984	3.000	3.017	2.988	3.243
Al^{IV}		0.016			0.012	
Al^{VI}	1.992	2.003	2.029	1.967	1.971	1.843
Ti	0.003	0.005		0.004	0.001	0.001
Mg	0.076	0.076	0.038	0.169	0.158	0.073
Fe2+	1.252	1.237	1.705	1.378	1.314	1.124
Mn	1.521	1.551	1.052	1.264	1.290	1.023
Ca	0.140	0.126	0.157	0.188	0.284	0.523
Total	7.99	8.00	7.98	7.99	8.02	7.83
Mn#	0.53	0.54	0.38	0.45	0.47	0.46
Pyrope = 0 - 3.3%						
Alman	43.7	43.1	59.5	49.7	46.8	44.2
Spess	52.4	53.4	36.2	45.0	45.3	39.7
Gross	3.8	3.4	4.3	5.3	7.9	16.0

Zone	Q-PE-M-G	Q-PE-M-G	Q-PL-M-G	Q-PL-M-G	Q-PL-M-G	Q-PL-M-G
Oxide	MC3-3g1core	MCK3-3g1rim	HO2-2g1core	HO2-2g1rim	HO2-2g2core	HO2-2g2rimzone
SiO_2	35.490	36.890	35.930	37.600	36.570	37.360
TiO_2	0.080	0.000	0.000	0.016	0.000	0.021
Al_2O_3	20.770	21.010	21.250	21.570	21.050	21.660
MgO	0.374	0.297	0.340	0.000	0.341	0.000
FeO	23.950	17.480	24.930	3.200	23.640	3.000
CaO	1.419	8.740	1.319	28.610	1.435	25.890
MnO	17.010	14.120	15.390	6.630	16.350	9.940
Cr_2O_3	0.011	0.000	0.077	0.000	0.033	0.073
Total	99.10	98.54	99.24	97.63	99.42	97.94
Numbers of ions on the basis of 12O						
Si	2.950	3.005	2.967	2.962	3.004	2.953
Al ^{IV}	0.050		0.033	0.038		0.047
Al ^{VI}	1.985	2.017	2.035	1.965	2.039	1.971
Ti	0.005	0.000	0.000	0.001	0.000	0.001
Mg	0.046	0.036	0.042	0.000	0.042	0.000
Fe2+	1.665	1.191	1.721	0.211	1.624	0.199
Mn	1.198	0.974	1.076	0.443	1.138	0.666
Ca	0.126	0.763	0.117	2.415	0.126	2.193
Total	8.03	7.99	7.99	8.04	7.97	8.03
Mn#	0.41	0.44	0.38	0.68	0.41	0.77
Pyrope = 0 - 3.3%						
Alman	56.5	43.3	59.9	8.3	57.1	7.7
Spess	40.1	35.0	37.0	17.2	39.5	25.6
Gross	3.3	21.7	3.2	74.4	3.5	66.7

Zone	Q-PL-M-G	Q-PL-M-G	Q-PL-M-G	Q-PL-M-G	Q-PL-M-G
Oxide	HO2-2g3core	HO2-2g3intergran	HO2-2g3core2	HO2-2g3smallergrain	HO2-2g3dark
SiO_2	36.000	37.200	36.250	36.620	37.640
TiO_2	0.000	0.009	0.050	0.014	0.000
Al_2O_3	21.130	20.620	21.080	21.380	20.560
MgO	0.369	0.000	0.465	0.236	0.000
FeO	24.360	4.400	23.480	15.770	4.660
CaO	1.311	26.900	1.269	6.150	23.290
MnO	16.110	8.670	17.860	18.360	10.730
Cr_2O_3	0.000	0.036	0.044	0.057	0.000
Total	99.28	97.84	100.50	98.59	96.88
Numbers of ions on the basis of 12O					
Si	2.973	2.961	2.965	2.993	3.020
Al ^{IV}	0.027	0.039	0.035	0.007	
Al ^{VI}	2.029	1.896	1.997	2.053	1.944
Ti	0.000	0.001	0.003	0.001	0.000
Mg	0.045	0.000	0.057	0.029	0.000
Fe2+	1.682	0.293	1.606	1.078	0.313
Mn	1.127	0.584	1.237	1.271	0.729
Ca	0.116	2.294	0.111	0.539	2.002
Total	8.00	8.07	8.01	7.97	8.01
Mn#	0.39	0.67	0.43	0.53	0.70
Pyrope = 0 - 3.3%					
Alman	58.3	11.0	55.1	39.2	12.0
Spess	38.6	21.7	41.9	45.6	27.7
Gross	3.1	67.3	3.0	15.3	60.2

Zone	Q-PL-PE-M-G	Q-PL-PE-M-G	Q-PL-PE-M-G	Q-PL-PE-M-G
Oxide	MCK2-1ginqtz(core)	MCK2-1ginqtz(rim)	MCK2-1ginqtz(rimdk)	MCK2-1g2core
SiO_2	36.110	35.950	36.730	36.120
TiO_2	0.019	0.000	0.040	0.005
Al_2O_3	20.870	21.100	21.010	20.850
MgO	0.390	0.559	0.246	0.621
FeO	21.380	20.860	17.420	20.670
CaO	1.710	1.219	9.220	1.708
MnO	19.710	19.110	14.750	20.060
Cr_2O_3	0.011	0.000	0.000	0.100
Total	100.20	98.80	99.42	100.13
Numbers of ions on the basis of 12O				
Si	2.965	2.976	2.979	2.964
Al^{IV}	0.035	0.024	0.021	0.036
Al^{VI}	1.985	2.035	1.987	1.980
Ti	0.001	0.000	0.002	0.000
Mg	0.048	0.069	0.030	0.076
Fe2+	1.468	1.444	1.181	1.418
Mn	1.371	1.340	1.013	1.394
Ca	0.150	0.108	0.801	0.150
Total	8.02	8.00	8.01	8.02
Mn#	0.47	0.47	0.46	0.48
Pyrope = 0 - 3.3%				
Alman	50.0	50.6	42.1	48.7
Spess	46.1	46.4	35.6	47.3
Gross	4.0	3.0	22.3	4.0

Zone	Q-PL-PE-M-G	Q-PL-PE-M-G	Q-PL-PE-M-G	Q-PL-PE-M-G	Q-PL-PE-M-G
Oxide	MCK2-1g3core	MCK2-1g3rim	MCK2-1g4core	MCK2-1g4rim	MCK2-3g1core
SiO_2	35.470	36.360	36.120	36.870	35.470
TiO_2	0.021	0.092	0.042	0.014	0.059
Al_2O_3	20.540	20.730	20.850	20.830	20.570
MgO	0.615	0.443	0.714	0.306	0.438
FeO	20.580	17.090	20.640	17.700	19.490
CaO	1.316	8.990	1.586	8.900	1.629
MnO	20.680	14.900	19.560	13.340	20.920
Cr_2O_3	0.033	0.011	0.000	0.011	0.000
Total	99.26	98.62	99.51	97.97	98.58
Numbers of ions on the basis of 12O					
Si	2.948	2.974	2.974	3.016	2.959
Al^{IV}	0.052	0.026	0.026		0.041
Al^{VI}	1.960	1.972	1.997	2.008	1.982
Ti	0.001	0.006	0.003	0.001	0.004
Mg	0.076	0.054	0.088	0.037	0.054
Fe2+	1.431	1.169	1.421	1.211	1.360
Mn	1.456	1.032	1.364	0.924	1.479
Ca	0.117	0.788	0.140	0.780	0.146
Total	8.04	8.02	8.01	7.98	8.03
Mn#	0.49	0.46	0.47	0.43	0.51
Pyrope = 0 - 3.3%					
Alman	48.3	41.7	49.4	44.3	46.4
Spess	48.6	36.4	46.8	33.4	49.8
Gross	3.1	21.9	3.8	22.3	3.9

	Hootowl Grab Samples		
Oxide	HOG3core	HOG3dark(rim)	HOG3dark(rim)
SiO_2	36.370	37.180	37.120
TiO_2	0.019	0.054	0.055
Al_2O_3	20.870	19.890	19.780
MgO	0.331	0.000	0.000
FeO	26.520	5.500	5.710
CaO	1.318	22.260	21.860
MnO	15.700	11.940	13.260
Cr_2O_3	0.022	0.036	0.000
Total	101.15	96.86	97.79
Numbers of ions on the basis of 12O			
Si	2.968	3.010	2.996
Al^{IV}	0.032		0.004
Al^{VI}	1.975	1.898	1.877
Ti	0.001	0.003	0.003
Mg	0.040	0.000	0.000
Fe2+	1.810	0.373	0.385
Mn	1.085	0.819	0.906
Ca	0.115	1.931	1.890
Total	8.03	8.03	8.06
Mn#	0.37	0.69	0.70
Pyrope = 0 - 3.3%			
Alman	60.9	13.9	14.0
Spess	36.1	30.1	32.5
Gross	3.0	56.1	53.5

APPENDIX D

ELECTRON MICROPROBE ANALYSES OF MUSCOVITE AND BIOTITE FROM SPRUCE PINE GRANODIORITES AND PEGMATITES.

Zone Key:

GRD ----------	Host Granodiorite
GG ----------	Graphic Granite
Q-PL-M -	Quartz-Plagioclase-Muscovite Pegmatite
Q-PL-PE -	Quartz-Plagioclase-Perthite Pegmatite
PE-G ----------	Perthite-Garnet Pegmatite
Q-PL ----------	Quartz-Plagioclase Pegmatite
Q-PE-M -	Quartz-Perthite-Muscovite Pegmatite
Q-PE-M-G -	Quartz-Perthite-Muscovite-Garnet Pegmatite
Q-M ----------	Quartz-Muscovite Pegmatite
Q-PL-M-G -	Quartz-Plagioclase-Muscovite-Garnet Pegmatite
PE ----------	Perthite Pegmatite
Q-PL-PE-G -	Quartz-Plagioclase-Perthite-Garnet Pegmatite
Q-PL-PE-M-G	Quartz-Plagioclase-Perthite-Muscovite-Garnet Pegmatite
Q ---------	Quartz

Zone		GRD	GRD	GRD	GRD
Oxide	Ox Wt% MDL	CC1-1musccore	CC1-1muscrim	CC1-1musc2core	CC1-1musc2biot
SiO_2	0.0905	45.020	45.360	45.260	35.680
TiO_2	0.1336	0.170	0.225	0.154	1.033
Al_2O_3	0.0801	29.070	30.730	28.990	16.330
MgO	0.0921	1.421	1.273	1.773	8.410
FeO	0.272	5.320	4.720	5.950	22.450
CaO	0.0747	0.000	0.000	0.003	0.012
MnO	0.3382	0.000	0.000	0.000	0.829
K_2O	0.0544	9.910	10.500	10.560	9.310
Na_2O	0.091	0.299	0.184	0.192	0.000
Cl	0.0353	0.000	0.000	0.012	0.038
F	0.269	0.027	0.124	0.035	0.460
Total		91.24	93.12	92.93	94.55
Number of ions on the basis of 22O, ignoring H_2O^+					
Si		6.406	6.310	6.366	5.586
Al^{IV}		1.594	1.690	1.634	2.414
Al^{VI}		3.280	3.350	3.172	0.600
Ti		0.018	0.024	0.016	0.122
Fe		0.634	0.550	0.700	2.940
Mn		0.000	0.000	0.000	0.110
Mg		0.301	0.264	0.372	1.962
Ca		0.000	0.000	0.000	0.002
Na		0.111	0.067	0.070	0.000
K		1.798	1.864	1.896	1.860
F		0.012	0.055	0.016	0.228
Cl		0.000	0.000	0.003	0.010
Total		14.15	14.17	14.25	15.83
Mg/(Fe+Mg)		0.32	0.32	0.35	0.40
K+Na		1.91	1.93	1.97	1.86

Zone	GRD	GRD	GRD	GRD	GRD
Oxide	CC1-1musc2rim	CC1-1mica2biotite	CC1-1bioinmica2	CC1-3musc1	CC1-3musc2
SiO_2	46.300	35.710	36.280	44.490	45.280
TiO_2	0.091	1.231	1.297	0.212	0.166
Al_2O_3	28.600	16.720	16.640	28.460	29.050
MgO	2.056	7.950	7.810	1.847	1.742
FeO	6.330	21.920	21.670	7.110	6.310
CaO	0.000	0.021	0.051	0.019	0.000
MnO	0.328	0.963	0.669	0.218	0.000
K_2O	10.490	9.320	8.800	9.900	9.970
Na_2O	0.297	0.044	0.094	0.233	0.351
Cl	0.008	0.000	0.011	0.000	0.000
F	0.167	0.296	0.208	0.314	0.306
Total	94.67	94.18	93.53	92.80	93.18
Number of ions on the basis of 22O, ignoring H_2O^+					
Si	6.410	5.600	5.690	6.302	6.350
Al^{IV}	1.590	2.400	2.310	1.698	1.650
Al^{VI}	3.076	0.692	0.766	3.052	3.150
Ti	0.009	0.145	0.153	0.023	0.017
Fe	0.734	2.876	2.842	0.842	0.740
Mn	0.038	0.128	0.089	0.026	0.000
Mg	0.424	1.858	1.824	0.390	0.364
Ca	0.000	0.004	0.009	0.003	0.000
Na	0.107	0.018	0.387	0.086	0.129
K	1.852	1.864	1.762	1.788	1.784
F	0.073	1.468	0.103	0.141	0.136
Cl	0.002	0.000	0.003	0.000	0.000
Total	14.32	17.05	15.94	14.35	14.32
Mg/(Fe+Mg)	0.37	0.39	0.39	0.32	0.33
K+Na	1.96	1.88	2.15	1.87	1.91

Zone	GRD	GRD	GRD	GRD
Oxide	CC1-3musc2	CC1-3musc2rim	CC2-1musc1core	CC2-1musc1rimneargnt
SiO_2	45.180	45.580	44.850	46.680
TiO_2	0.237	0.071	0.170	0.162
Al_2O_3	30.460	23.560	30.100	28.960
MgO	1.497	1.405	1.501	1.716
FeO	6.250	6.010	5.530	5.290
CaO	0.000	0.165	0.000	0.047
MnO	0.000	0.000	0.192	0.055
K_2O	9.930	9.400	10.230	9.550
Na_2O	0.318	0.502	0.355	0.196
Cl	0.012	0.035	0.000	0.089
F	0.062	0.220	0.124	0.115
Total	93.94	86.95	93.05	92.86

Number of ions on the basis of 22O, ignoring H_2O^+

Si	6.272	6.842	6.288	6.490
Al^{IV}	1.728	1.158	1.712	1.510
Al^{VI}	3.256	3.008	3.262	3.236
Ti	0.025	0.008	0.018	0.017
Fe	0.726	0.754	0.648	0.616
Mn	0.000	0.000	0.023	0.006
Mg	0.310	0.314	0.314	0.356
Ca	0.000	0.026	0.000	0.007
Na	0.115	0.197	0.130	0.071
K	1.758	1.800	1.828	1.694
F	0.027	0.104	0.055	0.051
Cl	0.003	0.009	0.000	0.021
Total	14.22	14.22	14.28	14.07
Mg/(Fe+Mg)	0.30	0.29	0.33	0.37
K+Na	1.87	2.00	1.96	1.77

Zone	GRD	GRD	GRD	GRD
Oxide	CC2-1musc2core	CC2-1musc2rim	CC2-1musc3core	CC2-1musc3rim
SiO_2	44.050	46.160	45.860	45.270
TiO_2	0.087	0.241	0.206	0.123
Al_2O_3	30.260	29.160	29.770	29.140
MgO	1.453	1.678	1.636	1.471
FeO	5.510	5.310	5.250	5.290
CaO	0.019	0.047	0.000	0.003
MnO	0.000	0.164	0.027	0.082
K_2O	10.160	10.200	9.880	10.100
Na_2O	0.343	0.158	0.174	0.376
Cl	0.012	0.000	0.008	0.016
F	0.237	0.177	0.168	0.000
Total	92.13	93.30	92.98	91.87

Number of ions on the basis of 22O, ignoring H_2O^+

Si	6.236	6.422	6.382	6.410
Al^{IV}	1.764	1.578	1.618	1.590
Al^{VI}	3.286	3.202	3.264	3.274
Ti	0.009	0.025	0.022	0.013
Fe	0.652	0.618	0.610	0.626
Mn	0.000	0.019	0.003	0.010
Mg	0.307	0.348	0.339	0.311
Ca	0.003	0.007	0.000	0.000
Na	0.127	0.058	0.063	0.139
K	1.836	1.810	1.754	1.824
F	0.106	0.078	0.074	0.000
Cl	0.003	0.000	0.002	0.004
Total	14.33	14.17	14.13	14.20
Mg/(Fe+Mg)	0.32	0.36	0.36	0.33
K+Na	1.96	1.87	1.82	1.96

Zone	GRD	GRD	GRD
Oxide	CC2-2Amusc1core(w-ep)	CC2-2Amusc1rim(w-ep)	CC2-7musc1core(w-ep)
SiO_2	46.330	46.160	47.030
TiO_2	0.139	0.119	0.176
Al_2O_3	32.010	31.980	30.030
MgO	0.735	0.906	1.520
FeO	4.600	4.370	5.030
CaO	0.016	0.065	0.035
MnO	0.000	0.027	0.160
K_2O	9.680	9.940	9.950
Na_2O	0.469	0.415	0.279
Cl	0.000	0.012	0.026
F	0.000	0.133	0.181
Total	93.98	94.13	94.42
Number of ions on the basis of 22O, ignoring H_2O^+			
Si	6.346	6.320	6.438
Al^{IV}	1.654	1.680	1.562
Al^{VI}	3.514	3.480	3.284
Ti	0.014	0.012	0.018
Fe	0.526	0.500	0.576
Mn	0.000	0.003	0.019
Mg	0.150	0.185	0.310
Ca	0.002	0.010	0.005
Na	0.168	0.148	0.100
K	1.692	1.736	1.736
F	0.000	0.058	0.079
Cl	0.000	0.003	0.006
Total	14.07	14.13	14.13
Mg/(Fe+Mg)	0.22	0.27	0.35
K+Na	1.86	1.88	1.84

Zone	GRD	GRD	GRD
Oxide	CC2-7musc1rim(w-ep)	CC2-7musc2core(w-ep,ap)	CC2-7musc2rim(w-ep,ap)
SiO_2	49.380	47.180	48.180
TiO_2	0.318	0.147	0.141
Al_2O_3	29.180	31.670	29.960
MgO	2.125	1.399	1.353
FeO	4.700	4.300	4.660
CaO	0.043	0.076	0.110
MnO	0.120	0.000	0.147
K_2O	10.180	10.420	10.120
Na_2O	0.239	0.238	0.351
Cl	0.016	0.014	0.000
F	0.479	0.253	0.213
Total	96.78	95.70	95.24
Number of ions on the basis of 22O, ignoring H_2O^+			
Si	6.572	6.352	6.522
Al^{IV}	1.428	1.648	1.478
Al^{VI}	3.148	3.378	3.304
Ti	0.032	0.015	0.014
Fe	0.522	0.484	0.528
Mn	0.014	0.000	0.017
Mg	0.422	0.281	0.273
Ca	0.006	0.011	0.016
Na	0.083	0.084	0.124
K	1.728	1.790	1.748
F	0.199	0.108	0.091
Cl	0.004	0.003	0.000
Total	14.16	14.15	14.12
Mg/(Fe+Mg)	0.45	0.37	0.34
K+Na	1.81	1.87	1.87

Zone	GRD	GRD	GRD	GRD
Oxide	CC2-8musc1core(w-ep)	CC2-8musc1rim(w-ep)	CC2-8musc2core	CC2-8musc2rim
SiO_2	48.160	48.460	47.360	46.510
TiO_2	0.164	0.156	0.237	0.247
Al_2O_3	29.760	29.970	30.540	29.720
MgO	1.767	1.622	1.558	1.409
FeO	5.940	4.920	5.240	5.600
CaO	0.025	0.000	0.000	0.016
MnO	0.173	0.040	0.067	0.240
K_2O	10.550	10.760	8.940	9.810
Na_2O	0.270	0.151	0.220	0.251
Cl	0.000	0.012	0.032	0.000
F	0.176	0.230	0.141	0.154
Total	96.99	96.32	94.33	93.96
Number of ions on the basis of 22O, ignoring H_2O^+				
Si	6.462	6.504	6.440	6.418
Al^{IV}	1.538	1.496	1.560	1.582
Al^{VI}	3.168	3.244	3.336	3.252
Ti	0.017	0.016	0.024	0.026
Fe	0.666	0.552	0.596	0.646
Mn	0.020	0.005	0.008	0.028
Mg	0.353	0.324	0.316	0.290
Ca	0.004	0.000	0.000	0.002
Na	0.095	0.053	0.078	0.090
K	1.806	1.842	1.552	1.728
F	0.075	0.098	0.061	0.067
Cl	0.000	0.003	0.007	0.000
Total	14.20	14.14	13.98	14.13
Mg/(Fe+Mg)	0.35	0.37	0.35	0.31
K+Na	1.90	1.90	1.63	1.82

Zone	GRD	GRD	GRD	GRD
Oxide	HO1-5musc1core(w-ep)	HO1-5musc1rim(w-ep)	HO1-5musc2core	HO1-5musc2rim
SiO_2	48.300	47.590	47.100	47.510
TiO_2	0.137	0.002	0.117	0.004
Al_2O_3	32.900	36.940	32.520	34.670
MgO	0.756	0.191	0.860	0.194
FeO	3.860	1.210	3.680	3.220
CaO	0.013	0.000	0.010	0.000
MnO	0.187	0.027	0.000	0.147
K_2O	10.380	11.010	10.080	10.590
Na_2O	0.328	0.165	0.520	0.173
Cl	0.004	0.012	0.016	0.197
F	0.293	0.230	0.133	0.116
Total	97.16	97.38	95.04	96.82
Number of ions on the basis of 22O, ignoring H_2O^+				
Si	6.378	6.188	6.360	6.276
Al^{IV}	1.622	1.812	1.640	1.724
Al^{VI}	3.498	3.848	3.538	3.674
Ti	0.014	0.000	0.012	0.000
Fe	0.426	0.132	0.416	0.356
Mn	0.021	0.003	0.000	0.016
Mg	0.149	0.037	0.173	0.038
Ca	0.002	0.000	0.001	0.000
Na	0.113	0.056	0.183	0.060
K	1.750	1.826	1.738	1.784
F	0.123	0.095	0.057	0.049
Cl	0.001	0.003	0.004	0.044
Total	14.10	14.00	14.12	14.02
Mg/(Fe+Mg)	0.26	0.22	0.29	0.10
K+Na	1.86	1.88	1.92	1.84

Zone	GRD	GRD	GRD	GRD
Oxide	HO2-1musc1core(sm)	HO2-1musc1rim(sm)	HO2-1musc2core	HO2-1musc2rim
SiO_2	47.690	48.340	48.440	46.190
TiO_2	0.204	0.127	0.222	0.109
Al_2O_3	31.530	32.300	31.740	31.110
MgO	1.026	0.955	1.221	0.882
FeO	3.850	3.940	4.120	3.810
CaO	0.006	0.019	0.024	0.043
MnO	0.067	0.107	0.040	0.080
K_2O	9.510	10.590	9.400	10.160
Na_2O	0.227	0.165	0.218	0.116
Cl	0.000	0.034	0.030	0.024
F	0.293	0.143	0.191	0.227
Total	94.40	96.72	95.65	92.75
Number of ions on the basis of 22O, ignoring H_2O^+				
Si	6.446	6.414	6.460	6.390
Al^{IV}	1.554	1.586	1.540	1.610
Al^{VI}	3.470	3.464	3.448	3.462
Ti	0.021	0.013	0.022	0.011
Fe	0.436	0.438	0.460	0.440
Mn	0.008	0.012	0.005	0.009
Mg	0.207	0.189	0.243	0.182
Ca	0.001	0.003	0.003	0.006
Na	0.080	0.057	0.076	0.042
K	1.638	1.794	1.598	1.792
F	0.125	0.060	0.080	0.099
Cl	0.000	0.008	0.007	0.006
Total	13.99	14.04	13.94	14.05
Mg/(Fe+Mg)	0.32	0.30	0.35	0.29
K+Na	1.72	1.85	1.67	1.83

Zone	GRD	GRD	GRD	GRD
Oxide	MCK3-2musc1core	MCK3-2musc1rim	MCK3-2musc2core	MCK3-2musc2rim
SiO_2	47.440	47.790	46.310	47.680
TiO_2	0.042	0.002	0.069	0.115
Al_2O_3	35.050	35.120	31.650	32.270
MgO	0.054	0.111	0.446	0.520
FeO	2.900	2.443	4.740	4.580
CaO	0.025	0.019	0.000	0.000
MnO	0.000	0.067	0.040	0.134
K_2O	10.470	10.620	10.410	10.200
Na_2O	0.235	0.296	0.424	0.326
Cl	0.000	0.030	0.020	0.040
F	0.067	0.063	0.102	0.045
Total	96.28	96.56	94.21	95.91
Number of ions on the basis of 22O, ignoring H_2O^+				
Si	6.278	6.300	6.362	6.400
Al^{IV}	1.722	1.700	1.638	1.600
Al^{VI}	3.746	3.758	3.486	3.504
Ti	0.004	0.000	0.007	0.012
Fe	0.320	0.269	0.544	0.514
Mn	0.000	0.007	0.005	0.015
Mg	0.011	0.022	0.091	0.104
Ca	0.004	0.003	0.000	0.000
Na	0.081	0.102	0.152	0.114
K	1.768	1.786	1.824	1.746
F	0.028	0.026	0.044	0.019
Cl	0.000	0.007	0.005	0.009
Total	13.96	13.98	14.16	14.04
Mg/(Fe+Mg)	0.03	0.07	0.14	0.17
K+Na	1.85	1.89	1.98	1.86

Zone	GRD	GRD	GRD	GG	GG
Oxide	RoanRdmusc1	RoanRdmusc2	MCK3-5Amuscspray	CC2-5musc1	HO1-4muscingt
SiO_2	46.090	47.350	46.560	45.650	49.070
TiO_2	0.131	0.012	0.008	0.016	0.216
Al_2O_3	29.900	27.500	36.060	32.490	31.720
MgO	1.362	2.005	0.013	0.638	1.179
FeO	6.450	6.290	1.312	3.950	3.190
CaO	0.000	0.049	0.043	0.000	0.049
MnO	0.133	0.120	0.000	0.192	0.241
K_2O	10.460	10.420	10.940	10.390	10.260
Na_2O	0.144	0.099	0.142	0.210	0.164
Cl	0.026	0.010	0.000	0.004	0.000
F	0.207	0.229	0.050	0.098	0.358
Total	94.90	94.08	95.13	93.64	96.45
Number of ions on the basis of 22O, ignoring H_2O^+					
Si	6.346	6.562	6.204	6.278	6.490
Al^{IV}	1.654	1.438	1.796	1.722	1.510
Al^{VI}	3.198	3.054	3.868	3.546	3.434
Ti	0.014	0.001	0.001	0.002	0.022
Fe	0.744	0.730	0.146	0.454	0.352
Mn	0.016	0.014	0.000	0.022	0.027
Mg	0.280	0.414	0.003	0.131	0.232
Ca	0.000	0.007	0.006	0.000	0.007
Na	0.052	0.036	0.049	0.075	0.057
K	1.836	1.842	1.860	1.822	1.732
F	0.090	0.100	0.021	0.043	0.150
Cl	0.006	0.002	0.000	0.001	0.000
Total	14.23	14.20	13.95	14.10	14.01
Mg/(Fe+Mg)	0.27	0.36	0.02	0.22	0.40
K+Na	1.89	1.88	1.91	1.90	1.79

Zone	GG	GG	PE	PE	PE
Oxide	HO1-4musc2core	HO1-4musc2rim	CC2-3musc1	CC2-3musc2core	CC2-3musc2rim
SiO_2	47.610	48.290	45.550	45.500	45.540
TiO_2	0.173	0.103	0.024	0.079	0.148
Al_2O_3	32.810	32.230	34.050	31.690	38.150
MgO	0.860	0.966	0.331	0.931	0.045
FeO	3.100	3.880	2.800	4.350	0.362
CaO	0.000	0.013	0.044	0.000	0.000
MnO	0.080	0.107	0.110	0.000	0.000
K_2O	10.230	10.690	9.740	9.980	10.350
Na_2O	0.350	0.218	0.186	0.178	0.228
Cl	0.000	0.002	0.016	0.043	0.027
F	0.347	0.271	0.000	0.071	0.000
Total	95.56	96.77	92.85	92.82	94.85
Number of ions on the basis of 22O, ignoring H_2O^+					
Si	6.366	6.410	6.242	6.308	6.044
Al^{IV}	1.634	1.590	1.758	1.692	1.956
Al^{VI}	3.538	3.452	3.742	3.486	4.012
Ti	0.017	0.010	0.002	0.008	0.015
Fe	0.346	0.432	0.320	0.504	0.040
Mn	0.009	0.012	0.013	0.000	0.000
Mg	0.171	0.191	0.068	0.192	0.009
Ca	0.000	0.018	0.006	0.000	0.000
Na	0.122	0.075	0.067	0.064	0.079
K	1.746	1.810	1.702	1.766	1.752
F	0.147	0.114	0.000	0.031	0.000
Cl	0.000	0.000	0.004	0.010	0.006
Total	14.10	14.12	13.92	14.06	13.91
Mg/(Fe+Mg)	0.33	0.31	0.17	0.28	0.18
K+Na	1.87	1.89	1.77	1.83	1.83

Zone	PE	PE	PE	PE	Q-PL
Oxide	CC2-3musc3	CC2-4musc1core	CC2-4musc1rim	CC2-4musc2	CC2-6musc1
SiO_2	44.730	45.850	44.720	44.660	47.080
TiO_2	0.000	0.012	0.071	0.000	0.167
Al_2O_3	34.130	31.100	30.380	33.130	32.010
MgO	0.150	0.257	0.406	0.320	0.908
FeO	2.484	6.400	5.710	4.240	4.910
CaO	0.038	0.019	0.065	0.000	0.000
MnO	0.000	0.082	0.219	0.137	0.000
K_2O	10.270	10.390	9.770	10.100	9.880
Na_2O	0.169	0.269	0.252	0.468	0.273
Cl	0.016	0.027	0.008	0.008	0.018
F	0.000	0.000	0.000	0.195	0.000
Total	91.99	94.41	91.60	93.26	95.25
Number of ions on the basis of 22O, ignoring H_2O^+					
Si	6.200	6.338	6.342	6.188	6.364
Al^{IV}	1.800	1.662	1.658	1.812	1.636
Al^{VI}	3.776	3.404	3.420	3.598	3.462
Ti	0.000	0.001	0.008	0.000	0.017
Fe	0.288	0.740	0.678	0.490	0.554
Mn	0.000	0.010	0.026	0.016	0.000
Mg	0.031	0.053	0.086	0.661	0.183
Ca	0.006	0.003	0.010	0.000	0.000
Na	0.061	0.097	0.093	0.170	0.096
K	1.816	1.832	1.768	1.786	1.704
F	0.000	0.000	0.000	0.086	0.000
Cl	0.004	0.006	0.002	0.002	0.004
Total	13.98	14.15	14.09	14.81	14.02
Mg/(Fe+Mg)	0.10	0.07	0.11	0.57	0.25
K+Na	1.88	1.93	1.86	1.96	1.80

Zone	Q-PL	Q-PL	Q-PL	Q-PL
Oxide	CC2-6musc1(std)rim	CC2-6musc2core	CC2-6musc2rim	CC2-6musc3core(w-ep)
SiO_2	47.190	47.510	47.610	47.400
TiO_2	0.094	0.135	0.167	0.176
Al_2O_3	34.990	32.210	32.680	32.260
MgO	0.354	0.821	0.812	0.803
FeO	2.980	4.920	4.510	4.830
CaO	0.000	0.022	0.049	0.003
MnO	0.013	0.027	0.187	0.054
K_2O	10.290	10.310	9.780	9.910
Na_2O	0.177	0.278	0.224	0.370
Cl	0.044	0.016	0.020	0.032
F	0.000	0.098	0.058	0.097
Total	96.13	96.35	96.10	95.93
Number of ions on the basis of 22O, ignoring H_2O^+				
Si	6.254	6.362	6.356	6.362
Al^{IV}	1.746	1.638	1.644	1.638
Al^{VI}	3.718	3.446	3.498	3.466
Ti	0.009	0.014	0.017	0.018
Fe	0.330	0.550	0.504	0.542
Mn	0.002	0.003	0.021	0.006
Mg	0.070	0.164	0.162	0.161
Ca	0.000	0.003	0.007	0.000
Na	0.061	0.097	0.078	0.130
K	1.740	1.760	1.666	1.696
F	0.000	0.041	0.024	0.041
Cl	0.010	0.004	0.005	0.007
Total	13.94	14.08	13.98	14.07
Mg/(Fe+Mg)	0.18	0.23	0.24	0.23
K+Na	1.80	1.86	1.74	1.83

Zone	Q-PL	Q-M	Q-M	Q-M
Oxide	CC2-6musc3rim(w-ep)	HO1-2musc1core	HO1-2musc1rim	HO1-2musc2core(w-ep)
SiO_2	48.080	47.800	48.620	46.690
TiO_2	0.093	0.836	0.766	0.060
Al_2O_3	32.060	29.800	29.530	31.900
MgO	0.983	2.492	2.456	1.360
FeO	4.570	3.450	4.400	3.560
CaO	0.021	0.033	0.005	0.043
MnO	0.040	0.147	0.120	0.040
K_2O	10.400	10.490	10.290	10.500
Na_2O	0.297	0.260	0.233	0.481
Cl	0.038	0.000	0.000	0.002
F	0.213	0.552	0.320	0.350
Total	96.79	95.86	96.74	94.98
Number of ions on the basis of 22O, ignoring H_2O^+				
Si	6.398	6.418	6.478	6.334
Al^{IV}	1.602	1.582	1.522	1.666
Al^{VI}	3.426	3.134	3.116	3.432
Ti	0.009	0.084	0.077	0.006
Fe	0.508	0.386	0.490	0.404
Mn	0.005	0.017	0.014	0.005
Mg	0.195	0.499	0.488	0.275
Ca	0.003	0.005	0.001	0.006
Na	0.103	0.091	0.081	0.170
K	1.764	1.796	1.748	1.818
F	0.090	0.234	0.135	0.150
Cl	0.009	0.000	0.000	0.000
Total	14.11	14.25	14.15	14.27
Mg/(Fe+Mg)	0.28	0.56	0.50	0.40
K+Na	1.87	1.89	1.83	1.99

Zone	Q-M	Q-M	Q-M	Q-PL-M
Oxide	HO1-2musc2rim(w-ep)	HO1-7musccore	HO1-7muscrim	CC1-2largemuscrim
SiO_2	47.960	44.570	46.980	45.200
TiO_2	0.294	0.156	0.168	0.269
Al_2O_3	30.080	32.120	31.530	30.230
MgO	1.674	0.898	0.938	1.651
FeO	3.660	4.650	5.050	4.370
CaO	0.126	0.000	0.000	0.090
MnO	0.000	0.173	0.000	0.000
K_2O	10.590	10.280	10.460	10.290
Na_2O	0.280	0.307	0.361	0.221
Cl	0.000	0.024	0.024	0.000
F	0.413	0.080	0.097	0.222
Total	95.08	93.26	95.61	92.54

Number of ions on the basis of 22O, ignoring H_2O^+

Si	6.488	6.196	6.364	6.318
Al^{IV}	1.512	1.804	1.636	1.682
Al^{VI}	3.282	3.460	3.398	3.300
Ti	0.030	0.016	0.017	0.028
Fe	0.414	0.540	0.572	0.510
Mn	0.000	0.020	0.000	0.000
Mg	0.338	0.186	0.189	0.344
Ca	0.018	0.000	0.000	0.014
Na	0.099	0.111	0.128	0.081
K	1.828	1.824	1.808	1.834
F	0.177	0.035	0.042	0.098
Cl	0.000	0.006	0.005	0.000
Total	14.19	14.20	14.16	14.21
Mg/(Fe+Mg)	0.45	0.26	0.25	0.40
K+Na	1.93	1.94	1.94	1.91

Zone	Q-PL-M	Q-PL-M	Q-PL-M	Q-PL-PE
Oxide	CC1-2largemusccore	CC1-2musc2rim	CC1-2musc2core	CC2-2Bmusc1core
SiO_2	45.520	44.220	45.110	45.500
TiO_2	0.241	0.296	0.229	0.178
Al_2O_3	30.850	29.940	31.670	30.440
MgO	1.530	1.411	1.188	1.351
FeO	5.220	5.080	5.640	5.200
CaO	0.000	0.034	0.000	0.031
MnO	0.137	0.246	0.000	0.000
K_2O	10.110	9.780	10.240	9.900
Na_2O	0.239	0.343	0.311	0.429
Cl	0.000	0.008	0.000	0.000
F	0.009	0.221	0.167	0.000
Total	93.86	91.58	94.55	93.03
Number of ions on the basis of 22O, ignoring H_2O^+				
Si	6.292	6.276	6.210	6.344
Al^{IV}	1.708	1.724	1.790	1.656
Al^{VI}	3.318	3.284	3.348	3.346
Ti	0.025	0.032	0.024	0.019
Fe	0.604	0.604	0.650	0.606
Mn	0.016	0.030	0.000	0.000
Mg	0.315	0.299	0.244	0.281
Ca	0.000	0.005	0.000	0.005
Na	0.086	0.127	0.112	0.156
K	1.782	1.772	1.798	1.760
F	0.004	0.099	0.728	0.000
Cl	0.000	0.002	0.000	0.000
Total	14.15	14.25	14.90	14.17
Mg/(Fe+Mg)	0.34	0.33	0.27	0.32
K+Na	1.87	1.90	1.91	1.92

Zone	Q-PL-PE	Q-PL-PE	Q-PL-PE	Q-PE-M
Oxide	CC2-2Bmusc1rim	CC2-2Bmusc2core(w-ep)	CC2-2Bmusc2rim(w-ep)	CC2-9musc1core
SiO_2	45.700	45.510	46.730	47.110
TiO_2	0.245	0.253	0.012	0.283
Al_2O_3	29.860	30.440	30.850	31.870
MgO	1.409	1.653	1.423	0.920
FeO	5.000	5.310	3.590	4.640
CaO	0.000	0.000	0.003	0.014
MnO	0.164	0.000	0.165	0.200
K_2O	10.320	10.450	10.230	10.320
Na_2O	0.196	0.245	0.134	0.345
Cl	0.008	0.000	0.004	0.008
F	0.222	0.097	0.000	0.000
Total	93.12	93.96	93.14	95.71
Number of ions on the basis of 22O, ignoring H_2O^+				
Si	6.366	6.300	6.434	6.358
Al^{IV}	1.634	1.700	1.566	1.642
Al^{VI}	3.270	3.266	3.438	3.428
Ti	0.026	0.026	0.001	0.029
Fe	0.582	0.614	0.412	0.524
Mn	0.019	0.000	0.019	0.023
Mg	0.292	0.341	0.292	0.185
Ca	0.000	0.000	0.000	0.002
Na	0.071	0.089	0.048	0.122
K	1.834	1.846	1.796	1.776
F	0.098	0.043	0.000	0.000
Cl	0.002	0.000	0.001	0.002
Total	14.19	14.22	14.01	14.09
Mg/(Fe+Mg)	0.33	0.36	0.41	0.26
K+Na	1.91	1.93	1.84	1.90

Zone	Q-PE-M	Q-PE-M	Q-PE-M	Q-PE-M-G
Oxide	CC2-9musc1rim	CC2-9musc2core	CC2-9musc2rim	CC2-10musc1core(sm)
SiO_2	46.730	47.190	47.220	46.880
TiO_2	0.326	0.213	0.064	0.036
Al_2O_3	31.820	31.940	34.990	34.760
MgO	0.953	0.810	0.305	0.388
FeO	4.850	4.680	2.620	2.487
CaO	0.091	0.000	0.000	0.140
MnO	0.040	0.146	0.107	0.294
K_2O	9.790	10.650	10.750	10.520
Na_2O	0.398	0.214	0.219	0.143
Cl	0.024	0.000	0.000	0.000
F	0.000	0.146	0.121	0.000
Total	95.02	95.99	96.39	95.65

Number of ions on the basis of 22O, ignoring H_2O^+

Si	6.344	6.352	6.252	6.250
Al^{IV}	1.656	1.648	1.748	1.750
Al^{VI}	3.434	3.420	3.712	3.712
Ti	0.033	0.022	0.006	0.004
Fe	0.550	0.528	0.290	0.277
Mn	0.005	0.017	0.012	0.033
Mg	0.193	0.163	0.601	0.077
Ca	0.013	0.000	0.000	0.020
Na	0.141	0.075	0.076	0.050
K	1.696	1.830	1.816	1.790
F	0.000	0.062	0.051	0.000
Cl	0.005	0.000	0.000	0.000
Total	14.07	14.12	14.56	13.96
Mg/(Fe+Mg)	0.26	0.24	0.67	0.22
K+Na	1.84	1.91	1.89	1.84

Zone	Q-PE-M-G	Q-PE-M-G	Q-PE-M-G	Q-PE-M-G
Oxide	CC2-10musc1rim(sm)	MCK3-3musc1	MCK3-6musc1core	MCK3-6musc2
SiO_2	45.070	45.860	45.880	46.480
TiO_2	0.000	0.249	0.143	0.036
Al_2O_3	32.550	30.280	31.590	32.830
MgO	0.190	0.501	0.845	0.290
FeO	5.280	6.810	4.730	4.380
CaO	0.121	0.020	0.047	0.003
MnO	0.000	0.040	0.000	0.000
K_2O	10.320	10.350	9.740	10.790
Na_2O	0.147	0.249	0.321	0.180
Cl	0.000	0.006	0.040	0.004
F	0.040	0.140	0.044	0.062
Total	93.72	94.51	93.38	95.06
Number of ions on the basis of 22O, ignoring H_2O^+				
Si	6.230	6.346	6.332	6.306
Al^{IV}	1.770	1.654	1.668	1.694
Al^{VI}	3.532	3.286	3.470	3.556
Ti	0.000	0.026	0.015	0.004
Fe	0.610	0.788	0.546	0.496
Mn	0.000	0.005	0.000	0.000
Mg	0.039	0.103	0.174	0.059
Ca	0.018	0.003	0.007	0.000
Na	0.053	0.090	0.116	0.064
K	1.820	1.826	1.714	1.868
F	0.017	0.061	0.019	0.027
Cl	0.000	0.001	0.009	0.001
Total	14.09	14.19	14.07	14.07
Mg/(Fe+Mg)	0.06	0.12	0.24	0.11
K+Na	1.87	1.92	1.83	1.93

Zone	Q-PL-M-G	Q-PL-M-G	Q-PL-PE-G	Q-PL-PE-G
Oxide	HO2-2musccore	HO2-2muscrim	MCK1-3musc2core	MCK1-3musc2rim
SiO_2	48.050	48.070	47.930	49.230
TiO_2	0.121	0.266	0.127	0.040
Al_2O_3	32.940	31.450	29.800	31.630
MgO	0.634	1.033	1.244	1.075
FeO	3.530	3.670	4.390	3.110
CaO	0.032	0.043	0.047	0.084
MnO	0.067	0.080	0.013	0.107
K_2O	10.350	10.620	10.540	10.600
Na_2O	0.390	0.213	0.170	0.106
Cl	0.016	0.000	0.000	0.000
F	0.147	0.344	0.080	0.144
Total	96.28	95.79	94.34	96.13
Number of ions on the basis of 22O, ignoring H_2O^+				
Si	6.394	6.442	6.542	6.532
Al^{IV}	1.606	1.558	1.458	1.468
Al^{VI}	3.560	3.408	3.336	3.478
Ti	0.012	0.027	0.013	0.004
Fe	0.392	0.412	0.500	0.344
Mn	0.008	0.009	0.001	0.012
Mg	0.126	0.206	0.253	0.213
Ca	0.005	0.006	0.007	0.012
Na	0.136	0.075	0.061	0.037
K	1.758	1.816	1.836	1.794
F	0.062	0.146	0.035	0.060
Cl	0.004	0.000	0.000	0.000
Total	14.06	14.10	14.04	13.95
Mg/(Fe+Mg)	0.24	0.33	0.34	0.38
K+Na	1.89	1.89	1.90	1.83

Zone	Q-PL-PE-G	Q-PL-PE-G	Q-PL-PE-M-G	Q-PL-PE-M-G
Oxide	MCK1-3musc3core	MCK1-3musc3rim	MCK2-1musc2core	MCK2-1musc2rim
SiO_2	46.630	46.390	46.140	47.490
TiO_2	0.252	0.173	0.000	0.002
Al_2O_3	31.560	31.550	33.460	35.150
MgO	1.256	1.151	0.128	0.033
FeO	4.470	3.870	4.070	2.870
CaO	0.000	0.028	0.014	0.011
MnO	0.000	0.080	0.080	0.134
K_2O	10.000	10.330	10.610	10.860
Na_2O	0.258	0.170	0.184	0.120
Cl	0.008	0.012	0.012	0.012
F	0.080	0.178	0.067	0.005
Total	94.51	93.93	94.77	96.69
Number of ions on the basis of 22O, ignoring H_2O^+				
Si	6.350	6.348	6.266	6.270
Al^{IV}	1.650	1.652	1.734	1.730
Al^{VI}	3.414	3.438	3.622	3.738
Ti	0.026	0.018	0.000	0.000
Fe	0.510	0.442	0.462	0.318
Mn	0.000	0.009	0.009	0.015
Mg	0.255	0.235	0.026	0.006
Ca	0.000	0.004	0.002	0.002
Na	0.092	0.061	0.065	0.041
K	1.738	1.804	1.838	1.828
F	0.034	0.077	0.029	0.002
Cl	0.002	0.003	0.003	0.003
Total	14.07	14.09	14.06	13.95
Mg/(Fe+Mg)	0.33	0.35	0.05	0.02
K+Na	1.83	1.86	1.90	1.87

Zone	Q-PL-PE-M-G	Q-PL-PE-M-G	Q	Q
Oxide	MCK2-1musc3core	MCK2-1musc3rim	MCK3-1musc1core	MCK3-1musc1rim
SiO_2	45.920	40.650	46.020	45.930
TiO_2	0.044	0.042	0.030	0.091
Al_2O_3	35.140	32.870	33.150	33.730
MgO	0.086	0.069	0.266	0.241
FeO	2.710	3.050	3.670	3.670
CaO	0.030	0.000	0.000	0.000
MnO	0.161	0.027	0.334	0.161
K_2O	9.990	9.700	10.890	10.730
Na_2O	0.191	0.087	0.145	0.208
Cl	0.000	0.026	0.008	0.000
F	0.027	0.000	0.090	0.018
Total	94.30	86.52	94.60	94.78
Number of ions on the basis of 22O, ignoring H_2O^+				
Si	6.198	6.028	6.268	6.236
Al^{IV}	1.802	1.972	1.732	1.764
Al^{VI}	3.788	3.772	3.590	3.632
Ti	0.004	0.005	0.003	0.009
Fe	0.306	0.378	0.418	0.416
Mn	0.018	0.003	0.039	0.018
Mg	0.017	0.015	0.054	0.049
Ca	0.004	0.000	0.000	0.000
Na	0.067	0.034	0.052	0.074
K	1.720	1.836	1.892	1.858
F	0.012	0.000	0.039	0.008
Cl	0.000	0.007	0.002	0.000
Total	13.94	14.05	14.09	14.06
Mg/(Fe+Mg)	0.05	0.04	0.11	0.10
K+Na	1.79	1.87	1.94	1.93

Zone	Q	Q	BSX	BSX
Oxide	MCK3-1musc2core(sm)	MCK3-1musc2rim(sm)	HO1-1biotite1core	HO1-1biotite1rim
SiO_2	46.770	45.790	49.530	49.850
TiO_2	0.012	0.000	0.421	0.365
Al_2O_3	35.680	36.230	27.980	28.190
MgO	0.070	0.059	3.450	3.060
FeO	1.223	1.278	3.130	3.470
CaO	0.014	0.041	0.032	0.017
MnO	0.000	0.000	0.013	0.000
K_2O	10.310	10.190	10.330	10.560
Na_2O	0.198	0.254	0.249	0.125
Cl	0.146	0.044	0.012	0.014
F	0.000	0.054	0.427	0.744
Total	94.42	93.94	95.57	96.40
Number of ions on the basis of 22O, ignoring H_2O^+				
Si	6.256	6.164	6.634	6.626
Al^{IV}	1.744	1.836	1.366	1.374
Al^{VI}	3.880	3.910	3.052	3.042
Ti	0.001	0.000	0.042	0.036
Fe	0.137	0.144	0.350	0.386
Mn	0.000	0.000	0.002	0.000
Mg	0.014	0.012	0.688	0.606
Ca	0.002	0.006	0.005	0.002
Na	0.069	0.089	0.087	0.044
K	1.758	1.748	1.766	1.792
F	0.000	0.023	0.181	0.313
Cl	0.033	0.010	0.003	0.003
Total	13.89	13.94	14.18	14.22
Mg/(Fe+Mg)	0.09	0.08	0.66	0.61
K+Na	1.83	1.84	1.85	1.84

Zone	BSX	BSX	BS	BS	
Oxide	HO1-1biotite2core	HO1-1biotite2rim	HO1-3biotite1	HO1-3biotite2	HOG1musc1core
SiO_2	39.980	40.380	38.640	39.590	47.250
TiO_2	1.005	1.024	1.137	1.152	0.169
Al_2O_3	16.080	16.490	15.960	15.710	32.050
MgO	15.220	14.890	16.510	16.480	1.131
FeO	11.430	11.880	12.770	12.400	3.040
CaO	0.022	0.053	0.011	0.012	0.134
MnO	0.343	0.422	0.198	0.093	0.000
K_2O	9.830	9.950	9.500	9.510	9.590
Na_2O	0.077	0.047	0.119	0.067	0.245
Cl	0.014	0.000	0.000	0.018	0.004
F	1.836	1.745	0.956	1.334	0.343
Total	95.84	96.88	95.80	96.37	93.96
Number of ions on the basis of 22O, ignoring H_2O^+					
Si	5.800	5.802	5.658	5.734	6.398
Al^{IV}	2.200	2.198	2.342	2.266	1.602
Al^{VI}	0.550	0.596	0.412	0.416	3.514
Ti	0.110	0.111	0.125	0.125	0.017
Fe	1.388	1.428	1.564	1.502	0.344
Mn	0.042	0.051	0.025	0.011	0.000
Mg	3.292	3.188	3.602	3.558	0.228
Ca	0.003	0.008	0.002	0.002	0.019
Na	0.029	0.017	0.046	0.025	0.087
K	1.820	1.824	1.774	1.756	1.656
F	0.842	0.793	0.443	0.611	0.147
Cl	0.003	0.000	0.000	0.004	0.001
Total	16.08	16.02	15.99	16.01	14.01
Mg/(Fe+Mg)	0.70	0.69	0.70	0.70	0.40
K+Na	1.85	1.84	1.82	1.78	1.74

	Hootowl Grab Samples			
Oxide	HOG1musc1rim	HOG2musc1core(sm)	HOG2musc1rim(sm)	HOG3musccore
SiO_2	48.020	47.690	48.000	47.350
TiO_2	0.137	0.175	0.318	0.111
Al_2O_3	32.830	32.490	31.530	32.280
MgO	1.154	0.996	1.325	0.942
FeO	3.520	3.150	3.310	3.680
CaO	0.114	0.000	0.000	0.022
MnO	0.134	0.054	0.121	0.187
K_2O	10.120	10.150	10.610	10.390
Na_2O	0.217	0.307	0.217	0.290
Cl	0.012	0.006	0.000	0.034
F	0.538	0.237	0.362	0.223
Total	96.80	95.25	95.79	95.51
Number of ions on the basis of 22O, ignoring H_2O^+				
Si	6.344	6.394	6.422	6.368
Al^{IV}	1.656	1.606	1.578	1.632
Al^{VI}	3.456	3.528	3.394	3.484
Ti	0.014	0.018	0.032	0.011
Fe	0.390	0.354	0.370	0.414
Mn	0.015	0.006	0.014	0.021
Mg	0.227	0.199	0.264	0.189
Ca	0.016	0.000	0.000	0.003
Na	0.075	0.108	0.076	0.102
K	1.706	1.736	1.810	1.782
F	0.225	0.100	0.153	0.095
Cl	0.003	0.001	0.000	0.008
Total	14.13	14.05	14.11	14.11
Mg/(Fe+Mg)	0.37	0.36	0.42	0.31
K+Na	1.78	1.84	1.89	1.88

	Hootowl Grab Samples			
Oxide	HOG3muscrim	HOG4musc1core	HOG4musc1rim	HOG6musc1core
SiO_2	47.510	46.890	46.680	46.950
TiO_2	0.068	0.012	0.159	0.030
Al_2O_3	31.960	33.570	32.240	33.260
MgO	0.821	0.614	0.856	0.334
FeO	3.790	3.070	3.390	3.700
CaO	0.022	0.000	0.013	0.000
MnO	0.094	0.000	0.000	0.040
K_2O	10.420	10.170	10.410	10.290
Na_2O	0.338	0.311	0.226	0.396
Cl	0.000	0.008	0.000	0.000
F	0.200	0.329	0.343	0.191
Total	95.22	94.97	94.32	95.19
Number of ions on the basis of 22O, ignoring H_2O^+				
Si	6.408	6.304	6.342	6.328
Al^{IV}	1.592	1.696	1.658	1.672
Al^{VI}	3.490	3.624	3.506	3.610
Ti	0.007	0.001	0.016	0.003
Fe	0.428	0.346	0.386	0.418
Mn	0.011	0.000	0.000	0.005
Mg	0.165	0.123	0.173	0.067
Ca	0.003	0.000	0.002	0.000
Na	0.119	0.109	0.080	0.139
K	1.794	1.744	1.804	1.770
F	0.086	0.140	0.147	0.082
Cl	0.000	0.002	0.000	0.000
Total	14.10	14.09	14.12	14.09
Mg/(Fe+Mg)	0.28	0.26	0.31	0.14
K+Na	1.91	1.85	1.88	1.91

	Hootowl Grab Samples		
Oxide	HOG6musc1rim(sm)	HOG7Amusccore	HOG7Amuscrim
SiO_2	46.880	47.840	47.650
TiO_2	0.058	0.131	0.165
Al_2O_3	37.620	33.600	32.440
MgO	0.030	0.728	0.824
FeO	0.278	3.490	3.190
CaO	0.000	0.006	0.000
MnO	0.013	0.080	0.000
K_2O	10.810	10.350	10.380
Na_2O	0.205	0.361	0.202
Cl	0.018	0.000	0.010
F	0.073	0.241	0.282
Total	95.99	96.83	95.14
Number of ions on the basis of 22O, ignoring H_2O^+			
Si	6.152	6.328	6.398
Al^{IV}	1.848	1.672	1.602
Al^{VI}	3.970	3.566	3.530
Ti	0.006	0.013	0.017
Fe	0.031	0.386	0.358
Mn	0.002	0.009	0.000
Mg	0.006	0.144	0.165
Ca	0.000	0.001	0.000
Na	0.070	0.125	0.071
K	1.810	1.746	1.778
F	0.030	0.101	0.120
Cl	0.004	0.000	0.002
Total	13.93	14.09	14.04
Mg/(Fe+Mg)	0.16	0.27	0.32
K+Na	1.88	1.87	1.85

APPENDIX E

ELECTRON MICROPROBE ANALYSES OF PLAGIOCLASE AND ALKALI FELDSPAR

FROM SPRUCE PINE GRANODIORITES AND PEGMATITES.

Zone Key:

GRD ----------	Host Granodiorite
GG ----------	Graphic Granite
Q-PL-M -	Quartz-Plagioclase-Muscovite Pegmatite
Q-PL-PE -	Quartz-Plagioclase-Perthite Pegmatite
PE-G ----------	Perthite-Garnet Pegmatite
Q-PL ----------	Quartz-Plagioclase Pegmatite
Q-PE-M -	Quartz-Perthite-Muscovite Pegmatite
Q-PE-M-G -	Quartz-Perthite-Muscovite-Garnet Pegmatite
Q-M ----------	Quartz-Muscovite Pegmatite
Q-PL-M-G -	Quartz-Plagioclase-Muscovite-Garnet Pegmatite
PE ----------	Perthite Pegmatite
Q-PL-PE-G -	Quartz-Plagioclase-Perthite-Garnet Pegmatite
Q-PL-PE-M-G	Quartz-Plagioclase-Perthite-Muscovite-Garnet Pegmatite
Q ---------	Quartz

Zone		GG	GG	GG	GG
Oxide	MDL wt%	HO1-4kspar1L	HO1-4plagexinksparL	HO1-4ksparinqtzS	HO1-4plagL
SiO_2	0.0713	65.520	68.700	66.140	67.940
TiO_2	0.0989	0.000	0.000	0.044	0.014
Al_2O_3	0.0603	18.420	19.090	18.140	20.640
MgO	0.0651	0.000	0.010	0.015	0.022
FeO	0.2284	0.000	0.022	0.000	0.133
MnO	0.2308	0.000	0.000	0.013	0.027
CaO	0.0493	0.060	0.199	0.006	1.568
K_2O	0.0332	15.710	0.123	16.000	0.096
Na_2O	0.1341	0.690	11.970	0.526	11.180
BaO	0.1758	0.000	0.049	0.066	0.025
Total		100.40	100.16	100.95	101.64
Number of ions on the basis of 8O					
Si		3.006	3.002	3.020	2.936
Al		0.996	0.983	0.976	1.051
Fe		0.000	0.001	0.000	0.005
Ti		0.000	0.000	0.002	0.000
Mg		0.000	0.001	0.001	0.001
Mn		0.000	0.000	0.001	0.001
Na		0.061	1.014	0.047	0.937
Ca		0.003	0.009	0.000	0.073
K		0.920	0.007	0.932	0.005
Ba		0.000	0.001	0.001	0.000
Total		4.99	5.02	4.98	5.01
Mole percentages					
Albite		4.2	97.4	3.2	87.0
Anorthite		0.4	1.6	0.0	12.2
Orthoclase		95.4	1.0	96.8	0.7

Zone	GG	GG	GG	GG	GG	GRD
Oxide	HO1-4plagL	HO1-4ksparS	HO1-4plagL	HO1-4ksparS	HO1-4plagL	HO1-6plagcoreM
SiO_2	67.990	64.860	66.900	65.560	67.920	68.610
TiO_2	0.000	0.000	0.000	0.024	0.000	0.048
Al_2O_3	20.520	17.890	20.400	18.110	20.200	20.200
MgO	0.000	0.000	0.004	0.000	0.038	0.022
FeO	0.033	0.000	0.011	0.000	0.122	0.033
MnO	0.000	0.107	0.067	0.027	0.000	0.080
CaO	1.491	0.025	1.930	0.000	1.185	1.037
K_2O	0.058	15.870	0.226	15.830	0.057	0.176
Na_2O	11.780	0.668	11.250	0.613	11.910	11.720
BaO	0.000	0.021	0.000	0.000	0.000	0.021
Total	101.87	99.44	100.79	100.16	101.43	101.95
Number of ions on the basis of 8O						
Si	2.935	3.012	2.924	3.016	2.944	2.955
Al	1.044	0.979	1.051	0.982	1.032	1.026
Fe	0.001	0.000	0.000	0.000	0.004	0.001
Ti	0.000	0.000	0.000	0.001	0.000	0.002
Mg	0.000	0.000	0.000	0.000	0.002	0.001
Mn	0.000	0.004	0.002	0.001	0.000	0.003
Na	0.986	0.060	0.953	0.055	1.001	0.979
Ca	0.069	0.001	0.090	0.000	0.055	0.048
K	0.003	0.940	0.126	0.929	0.003	0.010
Ba	0.000	0.000	0.000	0.000	0.000	0.000
Total	5.04	5.00	5.15	4.98	5.04	5.02
Mole percentages						
Albite	88.4	4.0	83.9	3.7	90.6	90.6
Anorthite	11.2	0.2	14.4	0.0	9.0	8.0
Orthoclase	0.4	95.8	1.7	96.3	0.4	1.4

Zone	GRD	GRD	GRD	GRD
Oxide	HO1-6plagrimM	HO1-6plagcore2M	HO1-6plagrim2M	HO1-6plagcore3S
SiO_2	68.840	68.570	68.720	68.190
TiO_2	0.000	0.000	0.000	0.012
Al_2O_3	19.330	20.680	19.620	20.980
MgO	0.012	0.000	0.002	0.000
FeO	0.000	0.000	0.000	0.000
MnO	0.000	0.067	0.027	0.000
CaO	0.040	1.268	0.144	1.575
K_2O	0.164	0.212	0.192	0.328
Na_2O	12.300	11.940	12.380	11.980
BaO	0.000	0.049	0.000	0.000
Total	100.69	102.79	101.08	103.06
Number of ions on the basis of 8O				
Si	2.994	2.936	2.981	2.917
Al	0.991	1.044	1.003	1.058
Fe	0.000	0.000	0.000	0.000
Ti	0.000	0.000	0.000	0.000
Mg	0.001	0.000	0.000	0.000
Mn	0.000	0.002	0.001	0.000
Na	1.037	0.991	1.014	0.994
Ca	0.002	0.058	0.007	0.072
K	0.009	0.012	0.011	0.018
Ba	0.000	0.001	0.000	0.000
Total	5.03	5.04	5.02	5.06
Mole percentages				
Albite	98.4	89.0	97.4	86.3
Anorthite	0.3	9.5	1.1	11.3
Orthoclase	1.3	1.6	1.5	2.4

Zone	GRD	GRD	GRD	GRD	GRD
Oxide	HO1-6plagrim3S	HO1-6plagcore	HO1-6ksparmassL	HO1-6plagcoreM	HO1-6plagrimM
SiO_2	68.210	66.960	65.370	67.950	67.950
TiO_2	0.014	0.000	0.000	0.004	0.000
Al_2O_3	20.750	21.080	18.710	20.340	19.770
MgO	0.000	0.008	0.015	0.000	0.012
FeO	0.044	0.133	0.022	0.000	0.089
MnO	0.013	0.000	0.000	0.054	0.161
CaO	1.427	1.608	0.003	0.573	0.254
K_2O	0.249	0.211	15.880	0.057	0.085
Na_2O	11.490	10.390	0.320	10.940	10.890
BaO	0.119	0.000	0.000	0.041	0.074
Total	102.32	100.39	100.32	99.96	99.28
Number of ions on the basis of 8O					
Si	2.933	2.923	3.000	2.968	2.987
Al	1.051	1.085	1.012	1.047	1.024
Fe	0.002	0.005	0.001	0.000	0.003
Ti	0.000	0.000	0.000	0.000	0.000
Mg	0.000	0.001	0.001	0.000	0.001
Mn	0.000	0.000	0.000	0.002	0.006
Na	0.958	0.880	0.028	0.926	0.929
Ca	0.066	0.075	0.000	0.027	0.012
K	0.014	0.012	0.930	0.003	0.005
Ba	0.002	0.000	0.000	0.001	0.001
Total	5.03	4.98	4.97	4.97	4.97
Mole percentages					
Albite	87.3	85.1	2.0	94.6	97.0
Anorthite	10.8	13.2	0.0	5.0	2.3
Orthoclase	1.9	1.7	98.0	0.5	0.8

Zone	GRD	GRD	GRD	Q-PL-M-G	Q-PL-M-G
Oxide	HO1-6plagcoreS	HO1-6plagrimS	HO1-6kspar	HO2-2plagcoreL	HO2-2plagrimL
SiO_2	68.110	67.810	65.140	66.580	63.390
TiO_2	0.000	0.012	0.000	0.028	0.012
Al_2O_3	19.500	20.100	18.990	20.280	19.130
MgO	0.000	0.016	0.000	0.104	0.443
FeO	0.000	0.000	0.177	0.000	0.000
MnO	0.000	0.161	0.000	0.080	0.000
CaO	0.109	0.090	0.000	1.825	3.260
K_2O	0.113	0.066	15.620	0.443	0.457
Na_2O	11.190	11.560	0.620	9.820	8.440
BaO	0.000	0.033	0.000	0.000	0.124
Total	99.02	99.85	100.55	99.16	95.26
Number of ions on the basis of 8O					
Si	2.998	2.969	2.985	2.942	2.926
Al	1.012	1.037	1.026	1.056	1.041
Fe	0.000	0.000	0.007	0.000	0.000
Ti	0.000	0.000	0.000	0.001	0.000
Mg	0.000	0.001	0.000	0.007	0.031
Mn	0.000	0.006	0.000	0.003	0.000
Na	0.955	0.982	0.055	0.841	0.755
Ca	0.005	0.004	0.000	0.864	0.161
K	0.006	0.004	0.913	0.025	0.027
Ba	0.000	0.001	0.000	0.000	0.002
Total	4.98	5.00	4.99	5.74	4.94
Mole percentages					
Albite	98.1	98.7	3.8	81.2	69.4
Anorthite	1.0	0.8	0.0	15.1	26.8
Orthoclase	1.0	0.6	96.2	3.7	3.8

Zone	Q-PL-M-G	Q-PL-M-G	Q-PL-M-G	Q-PL-M-G	GRD
Oxide	HO2-2plagrimL	HO2-2ksparS	HO2-2plagcoreL	HO2-2plagrimL	MCK3-2ksparL
SiO_2	67.080	65.310	69.860	69.810	66.120
TiO_2	0.000	0.000	0.000	0.000	0.000
Al_2O_3	20.440	18.890	21.470	21.530	18.800
MgO	0.096	0.031	0.000	0.044	0.004
FeO	0.000	0.067	0.000	0.089	0.155
MnO	0.054	0.080	0.000	0.134	0.054
CaO	1.786	0.019	1.520	1.439	0.063
K_2O	0.446	16.540	0.132	0.195	15.310
Na_2O	10.080	0.314	9.670	10.160	0.608
BaO	0.000	0.050	0.000	0.157	0.000
Total	99.98	101.30	102.65	103.56	101.11
Number of ions on the basis of 8O					
Si	2.941	2.984	2.961	2.947	3.004
Al	1.056	1.017	1.072	1.071	1.007
Fe	0.000	0.003	0.000	0.003	0.006
Ti	0.000	0.000	0.000	0.000	0.000
Mg	0.006	0.002	0.000	0.003	0.000
Mn	0.002	0.003	0.000	0.005	0.002
Na	0.857	0.028	0.795	0.831	0.054
Ca	0.084	0.001	0.069	0.065	0.003
K	0.025	0.964	0.007	0.011	0.887
Ba	0.000	0.001	0.000	0.003	0.000
Total	4.97	5.00	4.90	4.94	4.96
Mole percentages					
Albite	81.9	1.9	85.4	86.1	3.8
Anorthite	14.5	0.1	13.4	12.2	0.4
Orthoclase	3.6	98.0	1.2	1.7	95.8

Zone	GRD	GRD	GRD	GRD
Oxide	MCK3-2plagcoreTINY	MCK3-2plagrimTINY	MCK3-2plagcoreL	MCK3-2plagcoreL
SiO_2	70.780	69.250	71.280	68.050
TiO_2	0.000	0.000	0.012	0.000
Al_2O_3	19.760	19.810	20.450	20.030
MgO	0.024	0.020	0.052	0.000
FeO	0.000	0.000	0.000	0.045
MnO	0.000	0.054	0.000	0.000
CaO	0.065	0.062	0.093	0.323
K_2O	0.130	0.107	0.098	0.044
Na_2O	10.910	11.530	11.050	11.090
BaO	0.000	0.033	0.000	0.000
Total	101.67	100.87	103.04	99.58
Number of ions on the basis of 8O				
Si	3.024	2.996	3.006	2.980
Al	0.995	1.010	1.017	1.034
Fe	0.000	0.000	0.000	0.002
Ti	0.000	0.000	0.000	0.000
Mg	0.002	0.001	0.003	0.000
Mn	0.000	0.002	0.000	0.000
Na	0.904	0.967	0.904	0.942
Ca	0.003	0.003	0.004	0.015
K	0.007	0.006	0.005	0.002
Ba	0.000	0.001	0.000	0.000
Total	4.93	4.99	4.94	4.98
Mole percentages				
Albite	98.2	98.6	98.3	96.8
Anorthite	0.6	0.5	0.8	2.8
Orthoclase	1.2	0.9	0.9	0.4

Zone	GRD	Q-PE-M-G	Q-PE-M-G	Q-PE-M-G
Oxide	MCK3-2plagrimL	MCK3-3kspar	MCK3-3plagex	MCK3-3kspar(perth)
SiO_2	68.260	63.600	68.290	65.140
TiO_2	0.000	0.024	0.000	0.033
Al_2O_3	20.140	18.850	19.980	18.460
MgO	0.000	0.042	0.012	0.027
FeO	0.000	0.022	0.000	0.000
MnO	0.108	0.000	0.000	0.134
CaO	0.081	0.000	0.090	0.000
K_2O	0.066	16.120	0.114	15.760
Na_2O	11.440	0.322	11.430	0.548
BaO	0.000	0.033	0.058	0.000
Total	100.09	99.01	99.97	100.10
Number of ions on the basis of 8O				
Si	2.977	2.971	2.982	3.000
Al	1.035	1.038	1.028	1.002
Fe	0.000	0.001	0.000	0.000
Ti	0.000	0.001	0.000	0.001
Mg	0.000	0.003	0.001	0.002
Mn	0.004	0.000	0.000	0.005
Na	0.967	0.029	0.968	0.049
Ca	0.004	0.000	0.004	0.000
K	0.004	0.961	0.006	0.926
Ba	0.000	0.001	0.001	0.000
Total	4.99	5.00	4.99	4.99
Mole percentages				
Albite	98.7	2.0	98.2	3.4
Anorthite	0.7	0.0	0.8	0.0
Orthoclase	0.6	98.0	1.0	96.6

Zone	Q-PL-PE-M-G	Q-PL-PE-M-G	Q-PL-PE-M-G	Q-PL-PE-M-G	GRD
Oxide	MCK2-1ksparinplag	MCK2-1plag	MCK2-1kspar	MCK2-1plag	CC1-1ksparcoreL
SiO_2	64.580	65.590	63.840	67.200	65.080
TiO_2	0.000	0.000	0.000	0.012	0.012
Al_2O_3	18.680	20.540	18.620	20.760	18.950
MgO	0.000	0.008	0.000	0.008	0.000
FeO	0.267	0.000	0.000	0.089	0.153
MnO	0.134	0.000	0.081	0.000	0.000
CaO	0.070	1.239	0.060	0.591	0.000
K_2O	15.960	0.076	15.830	0.041	15.360
Na_2O	0.364	10.040	0.630	11.170	0.764
BaO	0.017	0.000	0.150	0.000	0.603
Total	100.07	97.49	99.21	99.87	100.92
Number of ions on the basis of 8O					
Si	2.984	2.938	2.978	2.943	2.982
Al	1.017	1.084	1.024	1.071	1.023
Fe	0.010	0.000	0.000	0.003	0.006
Ti	0.000	0.000	0.000	0.000	0.000
Mg	0.000	0.001	0.000	0.001	0.000
Mn	0.005	0.000	0.003	0.000	0.000
Na	0.033	0.872	0.057	0.948	0.068
Ca	0.003	0.059	0.003	0.028	0.000
K	0.941	0.004	0.942	0.002	0.898
Ba	0.000	0.000	0.003	0.000	0.011
Total	4.99	4.96	5.01	5.00	4.99
Mole percentages					
Albite	2.2	88.4	3.8	94.6	4.7
Anorthite	0.4	10.9	0.4	5.0	0.0
Orthoclase	97.4	0.7	95.8	0.3	95.3

Zone	GRD	GRD	GRD	GRD
Oxide	CC1-1plagcoreL	CC1-1plagrimL	CC1-1plagcoreM	CC1-1plagnearmuscS
SiO_2	65.350	68.940	64.440	65.270
TiO_2	0.008	0.004	0.000	0.000
Al_2O_3	22.460	20.660	22.540	22.240
MgO	0.004	0.000	0.020	0.000
FeO	0.022	0.110	0.044	0.000
MnO	0.000	0.000	0.000	0.026
CaO	3.050	0.530	3.230	3.030
K_2O	0.096	0.153	0.180	0.208
Na_2O	9.950	11.370	9.600	9.820
BaO	0.049	0.041	0.041	0.105
Total	100.99	101.81	100.09	100.70
Number of ions on the basis of 8O				
Si	2.850	2.962	2.837	2.856
Al	1.154	1.046	1.170	1.147
Fe	0.001	0.004	0.002	0.000
Ti	0.000	0.000	0.000	0.000
Mg	0.000	0.000	0.001	0.000
Mn	0.000	0.000	0.000	0.001
Na	0.841	0.947	0.820	0.833
Ca	0.143	0.024	0.152	0.142
K	0.005	0.008	0.010	0.012
Ba	0.001	0.001	0.001	0.002
Total	5.00	4.99	4.99	4.99
Mole percentages				
Albite	76.0	94.3	73.8	75.2
Anorthite	23.3	4.4	24.8	23.2
Orthoclase	0.7	1.3	1.4	1.6

Zone	GRD	GRD	GRD	GRD	GRD
Oxide	CC1-1plagrimM	CC1-1kspar(perth)	CC1-1plag(perth)	CC1-1plag(perth)	CC1-1kspar
SiO_2	64.940	64.650	69.710	68.670	63.860
TiO_2	0.000	0.000	0.000	0.036	0.016
Al_2O_3	22.380	18.860	20.200	19.870	19.230
MgO	0.000	0.004	0.000	0.000	0.000
FeO	0.066	0.153	0.088	0.110	0.022
MnO	0.053	0.026	0.026	0.026	0.026
CaO	2.810	0.013	0.094	0.166	0.000
K_2O	0.044	15.900	0.110	0.210	15.580
Na_2O	9.710	0.382	11.450	11.130	0.105
BaO	0.000	0.343	0.000	0.000	1.149
Total	100.00	100.33	101.68	100.22	99.99
Number of ions on the basis of 8O					
Si	2.855	2.982	2.990	2.990	2.966
Al	1.159	1.025	1.021	1.020	1.053
Fe	0.002	0.006	0.003	0.004	0.001
Ti	0.000	0.000	0.000	0.001	0.001
Mg	0.000	0.000	0.000	0.000	0.000
Mn	0.002	0.001	0.001	0.001	0.001
Na	0.827	0.034	0.953	0.940	0.009
Ca	0.132	0.001	0.004	0.008	0.000
K	0.002	0.936	0.006	0.012	0.923
Ba	0.000	0.006	0.000	0.000	0.021
Total	4.98	4.99	4.98	4.98	4.97
Mole percentages					
Albite	77.3	2.3	98.3	96.7	0.7
Anorthite	22.4	0.1	0.8	1.4	0.0
Orthoclase	0.3	97.6	0.9	1.8	99.3

Zone	GRD	GRD	GRD	GRD	GRD
Oxide	CC2-8kspar(perth)	CC2-8plag(perth)	CC2-8perth(pscan)	CC2-8ksparS	CC2-8ksparS
SiO_2	64.480	68.310	68.170	65.410	63.890
TiO_2	0.000	0.004	0.000	0.093	0.016
Al_2O_3	18.860	20.800	20.400	19.070	19.400
MgO	0.026	0.000	0.016	0.000	0.004
FeO	0.044	0.044	0.000	0.153	0.066
MnO	0.131	0.000	0.000	0.000	0.000
CaO	0.006	0.784	0.508	0.000	0.010
K_2O	15.840	0.081	0.100	15.360	15.390
Na_2O	0.363	11.900	11.310	0.453	0.571
BaO	0.750	0.049	0.130	0.815	0.897
Total	100.50	101.97	100.63	101.35	100.24
Number of ions on the basis of 8O					
Si	2.977	2.940	2.963	2.984	2.956
Al	1.027	1.055	1.045	1.025	1.058
Fe	0.002	0.002	0.000	0.006	0.003
Ti	0.000	0.000	0.000	0.003	0.001
Mg	0.002	0.000	0.001	0.000	0.000
Mn	0.005	0.000	0.000	0.000	0.000
Na	0.032	0.993	0.953	0.040	0.051
Ca	0.000	0.036	0.024	0.000	0.000
K	0.933	0.004	0.006	0.894	0.908
Ba	0.014	0.001	0.002	0.015	0.016
Total	4.99	5.03	4.99	4.97	4.99
Mole percentages					
Albite	2.2	93.2	94.9	2.9	3.6
Anorthite	0.0	6.1	4.3	0.0	0.1
Orthoclase	97.7	0.6	0.8	97.1	96.4

Zone	GRD	GRD	GRD	GRD	GRD
Oxide	CC2-8plagcoreM	CC2-8plagrimM	CC2-8plagcoreL	CC2-8plagcoreL	CC2-8plagrimL
SiO_2	65.060	65.020	65.530	65.510	66.310
TiO_2	0.000	0.000	0.004	0.000	0.000
Al_2O_3	22.610	22.460	22.390	22.250	22.140
MgO	0.000	0.008	0.000	0.000	0.008
FeO	0.110	0.132	0.154	0.044	0.000
MnO	0.053	0.000	0.000	0.053	0.000
CaO	2.890	2.711	2.930	2.980	2.006
K_2O	0.118	0.125	0.137	0.115	0.106
Na_2O	9.490	10.470	9.960	9.730	10.010
BaO	0.146	0.016	0.049	0.114	0.000
Total	100.48	100.94	101.15	100.80	100.58
Number of ions on the basis of 8O					
Si	2.850	2.842	2.854	2.861	2.888
Al	1.167	1.157	1.149	1.145	1.136
Fe	0.004	0.005	0.006	0.002	0.000
Ti	0.000	0.000	0.000	0.000	0.000
Mg	0.000	0.001	0.000	0.000	0.001
Mn	0.002	0.000	0.000	0.002	0.000
Na	0.806	0.887	0.841	0.824	0.846
Ca	0.136	0.127	0.137	0.139	0.094
K	0.007	0.007	0.008	0.006	0.006
Ba	0.003	0.000	0.001	0.002	0.000
Total	4.97	5.03	5.00	4.98	4.97
Mole percentages					
Albite	75.9	78.7	76.5	75.9	82.6
Anorthite	23.1	20.4	22.5	23.2	16.5
Orthoclase	0.9	0.9	1.1	0.9	0.9

Zone	Q-PL	Q-PL	Q-PL	Q-PL	Q-PL
Oxide	CC2-6kspar(antP)3	CC2-6plag(antiP)4	CC2-6plag(antiP)4	CC2-6kspar	CC2-6plagL
SiO_2	65.050	66.840	66.360	64.890	66.390
TiO_2	0.060	0.000	0.032	0.040	0.016
Al_2O_3	18.920	21.340	21.250	18.720	21.550
MgO	0.000	0.000	0.020	0.000	0.000
FeO	0.197	0.000	0.110	0.000	0.000
MnO	0.079	0.000	0.210	0.000	0.157
CaO	0.016	1.835	1.861	0.074	2.025
K_2O	15.730	0.128	0.044	15.920	0.128
Na_2O	0.625	10.570	10.450	0.693	10.550
BaO	0.082	0.000	0.000	0.098	0.000
Total	100.76	100.71	100.34	100.43	100.82
Number of ions on the basis of 8O					
Si	2.981	2.911	2.904	2.985	2.894
Al	1.022	1.095	1.096	1.015	1.107
Fe	0.008	0.000	0.004	0.000	0.000
Ti	0.002	0.000	0.001	0.001	0.001
Mg	0.000	0.000	0.001	0.000	0.000
Mn	0.003	0.000	0.008	0.000	0.006
Na	0.055	0.892	0.887	0.062	0.891
Ca	0.001	0.086	0.087	0.004	0.095
K	0.919	0.007	0.002	0.934	0.007
Ba	0.001	0.000	0.000	0.002	0.000
Total	4.99	4.99	4.99	5.00	5.00
Mole percentages					
Albite	3.8	84.3	84.6	4.2	83.1
Anorthite	0.1	14.6	15.1	0.4	15.9
Orthoclase	96.1	1.0	0.4	95.4	1.0

Zone	Q-PL	Q-PL	Q-PL	Q-PL-M	Q-PL-M
Oxide	CC2-6plagL	CC2-6ksparM	CC2-6plagS	CC1-2plag1L	CC1-2plag1rimL
SiO_2	66.850	65.590	66.790	65.560	66.090
TiO_2	0.044	0.000	0.040	0.000	0.040
Al_2O_3	22.100	18.540	20.900	22.920	22.170
MgO	0.000	0.008	0.004	0.000	0.000
FeO	0.066	0.000	0.066	0.132	0.022
MnO	0.053	0.157	0.000	0.026	0.052
CaO	2.185	0.051	1.928	2.930	2.584
K_2O	0.109	15.450	0.112	0.205	0.149
Na_2O	10.560	0.368	10.810	9.320	10.390
BaO	0.000	0.016	0.024	0.000	0.170
Total	101.97	100.18	100.67	101.09	101.67
Number of ions on the basis of 8O					
Si	2.882	3.009	2.915	2.849	2.866
Al	1.123	1.002	1.075	1.174	1.133
Fe	0.002	0.000	0.002	0.005	0.008
Ti	0.001	0.000	0.001	0.000	0.001
Mg	0.000	0.001	0.000	0.000	0.000
Mn	0.002	0.006	0.000	0.001	0.002
Na	0.883	0.033	0.915	0.785	0.873
Ca	0.101	0.003	0.090	0.137	0.120
K	0.006	0.904	0.006	0.011	0.008
Ba	0.000	0.000	0.000	0.000	0.003
Total	5.00	4.96	5.01	4.96	5.01
Mole percentages					
Albite	82.2	2.3	84.1	74.8	79.2
Anorthite	17.0	0.3	15.0	23.5	19.7
Orthoclase	0.8	97.4	0.9	1.6	1.1

Zone	Q-PL-M	Q-PL-M	Q-PL-M	GRD
Oxide	CC1-2ksparinplagS	CC1-2plag2L	CC1-2ksparinplag	RoanRdplagcoreL
SiO_2	65.010	66.610	65.290	64.980
TiO_2	0.012	0.000	0.040	0.000
Al_2O_3	18.970	21.830	19.090	21.210
MgO	0.000	0.000	0.000	0.000
FeO	0.109	0.110	0.000	0.000
MnO	0.052	0.000	0.000	0.000
CaO	0.000	2.189	0.010	2.340
K_2O	15.690	0.143	16.050	0.209
Na_2O	0.906	9.970	0.381	9.670
BaO	0.082	0.049	0.147	0.000
Total	100.83	100.90	101.01	98.41
Number of ions on the basis of 8O				
Si	2.978	2.896	2.984	2.896
Al	1.024	1.118	1.028	1.114
Fe	0.004	0.004	0.000	0.000
Ti	0.000	0.000	0.001	0.000
Mg	0.000	0.000	0.000	0.000
Mn	0.002	0.000	0.000	0.000
Na	0.081	0.841	0.034	0.836
Ca	0.000	0.102	0.000	0.112
K	0.917	0.008	0.936	0.012
Ba	0.001	0.001	0.003	0.000
Total	5.01	4.97	4.99	4.97
Mole percentages				
Albite	5.5	81.0	2.3	79.1
Anorthite	0.0	17.8	0.1	19.2
Orthoclase	94.5	1.2	97.6	1.7

Zone	GRD	GRD	GRD	GRD	GRD
Oxide	RoanRdplagcoreL	RoanRdplagrimL	RoanRdksparS	RoanRdksparS	RoanRdksparM
SiO_2	65.720	65.800	64.240	65.430	64.870
TiO_2	0.000	0.088	0.024	0.032	0.073
Al_2O_3	21.910	21.660	18.580	18.750	18.600
MgO	0.000	0.008	0.004	0.000	0.000
FeO	0.022	0.022	0.000	0.110	0.088
MnO	0.000	0.000	0.000	0.026	0.000
CaO	2.550	2.352	0.022	0.016	0.000
K_2O	0.271	0.199	15.050	14.950	15.460
Na_2O	9.910	10.590	0.658	0.660	0.472
BaO	0.000	0.000	0.180	0.441	0.294
Total	100.38	100.72	98.76	100.41	99.86
Number of ions on the basis of 8O					
Si	2.878	2.877	2.993	2.999	2.996
Al	1.131	1.116	1.020	1.013	1.012
Fe	0.001	0.001	0.000	0.004	0.003
Ti	0.000	0.003	0.001	0.001	0.003
Mg	0.000	0.001	0.000	0.000	0.000
Mn	0.000	0.000	0.000	0.001	0.000
Na	0.841	0.898	0.059	0.059	0.042
Ca	0.120	0.110	0.001	0.001	0.000
K	0.015	0.011	0.894	0.874	0.911
Ba	0.000	0.000	0.003	0.008	0.005
Total	4.99	5.02	4.97	4.96	4.97
Mole percentages					
Albite	77.8	80.6	4.2	4.2	3.0
Anorthite	20.0	17.9	0.1	0.1	0.0
Orthoclase	2.1	1.5	95.7	95.7	97.0

Zone	GRD	GRD	GRD	GRD
Oxide	RoanRdplagcoreL	RoanRdplagrimL	RoanRdkspar(antiP)S	RoanRdplag(antiP)L
SiO_2	65.300	65.800	62.860	65.250
TiO_2	0.072	0.044	0.040	0.012
Al_2O_3	21.490	22.200	18.860	21.590
MgO	0.024	0.000	0.000	0.004
FeO	0.000	0.176	0.000	0.000
MnO	0.000	0.026	0.000	0.026
CaO	2.561	2.263	0.000	2.673
K_2O	0.305	0.090	15.790	0.411
Na_2O	9.790	10.050	0.250	9.640
BaO	0.170	0.000	0.000	0.000
Total	99.71	100.65	97.80	99.61
Number of ions on the basis of 8O				
Si	2.883	2.872	2.968	2.881
Al	1.118	1.142	1.049	1.124
Fe	0.000	0.006	0.000	0.000
Ti	0.002	0.001	0.001	0.000
Mg	0.002	0.000	0.000	0.000
Mn	0.000	0.001	0.000	0.001
Na	0.838	0.850	0.023	0.825
Ca	0.121	0.106	0.000	0.126
K	0.017	0.005	0.951	0.023
Ba	0.003	0.000	0.000	0.000
Total	4.98	4.98	4.99	4.98
Mole percentages				
Albite	77.4	81.0	1.6	75.8
Anorthite	20.2	18.2	0.0	21.0
Orthoclase	2.4	0.7	98.4	3.2

Zone	GRD
Oxide	RoanRdkspar(antiP)S
SiO_2	64.810
TiO_2	0.000
Al_2O_3	18.790
MgO	0.011
FeO	0.000
MnO	0.000
CaO	0.000
K_2O	15.330
Na_2O	0.541
BaO	0.188
Total	99.67

Number of ions on the basis of 8O

Si	2.993
Al	1.023
Fe	0.000
Ti	0.000
Mg	0.001
Mn	0.000
Na	0.048
Ca	0.000
K	0.903
Ba	0.003
Total	4.97

Mole percentages

Albite	3.4
Anorthite	0.0
Orthoclase	96.6

APPENDIX F

ELECTRON MICROPROBE ANALYSES OF EPIDOTE FROM SPRUCE PINE GRANODIORITES AND PEGMATITES.

Zone Key:

GRD ----------	Host Granodiorite
GG ----------	Graphic Granite
Q-PL-M -	Quartz-Plagioclase-Muscovite Pegmatite
Q-PL-PE -	Quartz-Plagioclase-Perthite Pegmatite
PE-G ----------	Perthite-Garnet Pegmatite
Q-PL ----------	Quartz-Plagioclase Pegmatite
Q-PE-M -	Quartz-Perthite-Muscovite Pegmatite
Q-PE-M-G -	Quartz-Perthite-Muscovite-Garnet Pegmatite
Q-M ----------	Quartz-Muscovite Pegmatite
Q-PL-M-G -	Quartz-Plagioclase-Muscovite-Garnet Pegmatite
PE ----------	Perthite Pegmatite
Q-PL-PE-G -	Quartz-Plagioclase-Perthite-Garnet Pegmatite
Q-PL-PE-M-G	Quartz-Plagioclase-Perthite-Muscovite-Garnet Pegmatite
Q ---------	Quartz

Zone		GRD	GRD	GRD	GRD
Oxide	MDL ox wt %	CC2-1ep-in-musc	CC2-1ep-in-musc2	CC2-1ep3	CC2-2Aep-in-musc
SiO_2	0.052	37.820	38.780	37.840	38.850
TiO_2	0.079	0.072	0.127	0.003	0.054
Al_2O_3	0.048	24.510	28.930	25.700	29.390
MgO	0.051	0.024	0.000	0.000	0.000
FeO	0.165	11.070	2.900	9.890	4.680
CaO	0.041	22.870	24.210	23.000	23.100
MnO	0.142	0.593	0.095	0.422	1.005
K_2O	0.032	0.031	0.000	0.000	0.107
Na_2O	0.072	0.126	0.073	0.000	0.000
Total		97.11	98.13	96.86	97.19
Number of ions on the basis of 12.5O					
Si		2.956	2.910	2.941	2.926
Al		0.044	0.090	0.059	0.074
Al		2.214	2.469	2.295	2.535
Fe		0.724	0.370	0.643	0.295
Ti		0.004	0.007	0.000	0.003
Mn		0.039	0.006	0.028	0.064
Mg		0.003	0.000	0.000	0.000
Ca		1.915	1.947	1.915	1.864
K		0.003	0.000	0.000	0.010
Na		0.019	0.011	0.000	0.000
Total		7.92	7.81	7.88	7.77

Zone	GRD	GRD	Q-PL-PE	Q-PL-PE
Oxide	CC2-2Aepzoned	CC2-2Aepzoned2	CC2-2Bepzoned	CC2-2Bepzoned2
SiO_2	37.660	36.470	38.790	35.430
TiO_2	0.021	0.063	0.186	0.269
Al_2O_3	24.470	23.500	29.520	26.670
MgO	0.000	0.000	0.000	0.000
FeO	11.470	11.060	5.070	9.330
CaO	23.420	20.980	24.060	21.960
MnO	0.318	0.619	0.113	0.190
K_2O	0.009	0.000	0.004	0.034
Na_2O	0.000	0.016	0.010	0.010
Total	97.37	92.71	97.75	93.89
Number of ions on the basis of 12.5O				
Si	2.943	2.980	2.906	2.835
Al	0.057	0.020	0.094	0.165
Al	2.197	2.243	2.513	2.351
Fe	0.749	0.756	0.318	0.625
Ti	0.001	0.004	0.011	0.016
Mn	0.021	0.043	0.007	0.013
Mg	0.000	0.000	0.000	0.000
Ca	1.960	1.837	1.931	1.883
K	0.001	0.000	0.000	0.004
Na	0.000	0.003	0.001	0.002
Total	7.93	7.89	7.78	7.89

Zone	Q-PL-PE	PE-G	Q-PL	Q-PL	BSX	Q-M	Q-M
Oxide	CC2-2Bep	CC2-3ep1	CC2-6ep1	CC2-6ep2	HO1-1ep	HO1-2ep	HO1-2ep2
SiO_2	36.740	36.670	37.620	37.630	37.590	37.800	37.920
TiO_2	0.028	0.024	0.104	0.085	0.033	0.115	0.174
Al_2O_3	24.330	25.300	24.550	24.850	24.320	25.680	26.730
MgO	0.000	0.000	0.000	0.000	0.242	0.000	0.000
FeO	10.340	10.690	11.090	10.050	11.370	9.480	8.020
CaO	22.240	23.760	22.550	23.090	22.360	23.850	23.290
MnO	0.534	0.353	0.488	0.429	0.274	0.343	0.344
K_2O	0.000	0.015	0.001	0.002	0.000	0.000	0.006
Na_2O	0.024	0.008	0.034	0.018	0.000	0.010	0.000
Total	94.24	96.82	96.45	96.15	96.19	97.28	96.48
Number of ions on the basis of 12.5O							
Si	2.949	2.879	2.957	2.954	2.962	2.927	2.930
Al	0.051	0.121	0.043	0.046	0.038	0.073	0.070
Al	2.251	2.221	2.231	2.253	2.221	2.271	2.364
Fe	0.694	0.702	0.729	0.660	0.749	0.614	0.518
Ti	0.002	0.001	0.006	0.005	0.002	0.007	0.010
Mn	0.036	0.023	0.032	0.029	0.018	0.023	0.023
Mg	0.000	0.000	0.000	0.000	0.028	0.000	0.000
Ca	1.913	1.999	1.899	1.942	1.888	1.979	1.928
K	0.000	0.001	0.000	0.000	0.000	0.000	0.001
Na	0.004	0.001	0.005	0.003	0.000	0.002	0.000
Total	7.90	7.95	7.90	7.89	7.91	7.89	7.84

Zone	GG	GRD	GRD	GRD
Oxide	HO1-4ep	HO1-5ep	MCK3-5Aep	Rrep
SiO_2	38.400	37.990	37.840	37.990
TiO_2	0.141	0.196	0.000	0.000
Al_2O_3	28.020	28.220	25.060	24.320
MgO	0.000	0.008	0.000	0.003
FeO	6.560	6.290	10.250	11.280
CaO	23.620	23.840	22.730	21.960
MnO	0.095	0.078	0.306	0.506
K_2O	0.009	0.003	0.011	0.007
Na_2O	0.018	0.065	0.011	0.013
Total	96.86	96.69	96.20	96.07
Number of ions on the basis of 12.5O				
Si	2.927	2.902	2.964	2.992
Al	0.073	0.098	0.036	0.008
Al	2.444	2.442	2.278	2.249
Fe	0.418	0.402	0.672	0.743
Ti	0.008	0.011	0.000	0.000
Mn	0.006	0.005	0.020	0.034
Mg	0.000	0.001	0.000	0.000
Ca	1.929	1.951	1.908	1.853
K	0.001	0.000	0.001	0.001
Na	0.003	0.010	0.002	0.002
Total	7.81	7.82	7.88	7.88